

Vol. 24, no. 4, 2024

eISSN 2687-1653

PEER-REVIEWED SCIENTIFIC AND PRACTICAL JOURNAL

Advanced Engineering Research (Rostov-on-Don)

Mechanics

Machine Building
and Machine Science

Information Technology,
Computer Science
and Management



www.vestnik-donstu.ru
DOI 10.23947/2687-1653



Advanced Engineering Research (Rostov-on-Don)

Peer-reviewed scientific and practical journal

eISSN 2687–1653

Published since 2000

Periodicity – 4 issues per year

DOI: 10.23947/2687–1653

Founder and Publisher — Don State Technical University (DSTU), Rostov-on-Don, Russian Federation

The journal is aimed at informing the readership about the latest achievements and prospects in the field of mechanics, mechanical engineering, computer science and computer technology. The publication is a forum for cooperation between Russian and foreign scientists, it contributes to the convergence of the Russian and world scientific and information space.

The journal is included in the List of the leading peer-reviewed scientific publications (Higher Attestation Commission under the Ministry of Science and Higher Education of the Russian Federation), where basic scientific results of dissertations for the degrees of Doctor and Candidate of Science in scientific specialties and their respective branches of science should be published.

The journal publishes articles in the following fields of science:

- Theoretical Mechanics, Dynamics of Machines (Engineering Sciences)
- Deformable Solid Mechanics (Engineering, Physical and Mathematical Sciences)
- Mechanics of Liquid, Gas and Plasma (Engineering Sciences)
- Mathematical Simulation, Numerical Methods and Program Systems (Engineering Sciences)
- System Analysis, Information Management and Processing, Statistics (Engineering Sciences)
- Automation and Control of Technological Processes and Productions (Engineering Sciences)
- Software and Mathematical Support of Machines, Complexes and Computer Networks (Engineering Sciences)
- Computer Modeling and Design Automation (Engineering, Physical and Mathematical Sciences)
- Computer Science and Information Processes (Engineering Sciences)
- Machine Science (Engineering Sciences)
- Machine Friction and Wear (Engineering Sciences)
- Technology and Equipment of Mechanical and Physicotechnical Processing (Engineering Sciences)
- Engineering Technology (Engineering Sciences)
- Welding, Allied Processes and Technologies (Engineering Sciences)
- Methods and Devices for Monitoring and Diagnostics of Materials, Products, Substances and the Natural Environment (Engineering Sciences)
- Hydraulic Machines, Vacuum, Compressor Equipment, Hydraulic and Pneumatic Systems (Engineering Sciences)

<i>Registration:</i>	Extract from the Register of Registered Mass Media ЭЛ № ФС 77 – 78854 dated August 07, 2020, issued by the Federal Service for Supervision of Communications, Information Technology and Mass Media
<i>Indexing and Archiving:</i>	RISC, CyberLeninka, CrossRef, Dimensions, DOAJ, EBSCO, Index Copernicus, Internet Archive, Google Scholar
<i>Website:</i>	http://vestnik-donstu.ru
<i>Address of the Editorial Office</i>	1, Gagarin sq., Rostov-on-Don, 344003, Russian Federation
<i>E-mail:</i>	vestnik@donstu.ru
<i>Telephone:</i>	+7 (863) 2–738–372
<i>Date of Publication No.4, 2024:</i>	30.12.2024





Advanced Engineering Research (Rostov-on-Don)

Рецензируемый научно-практический журнал

eISSN 2687–1653

Издается с 2000 года

Периодичность – 4 выпуска в год

DOI: 10.23947/2687–1653

Учредитель и издатель — Федеральное государственное бюджетное образовательное учреждение высшего образования «Донской государственный технический университет» (ДГТУ), г. Ростов-на-Дону

Создан в целях информирования читательской аудитории о новейших достижениях и перспективах в области механики, машиностроения, информатики и вычислительной техники. Издание является форумом для сотрудничества российских и иностранных ученых, способствует сближению российского и мирового научно-информационного пространства.

Журнал включен в перечень рецензируемых научных изданий, в котором должны быть опубликованы основные научные результаты диссертаций на соискание ученой степени кандидата наук, на соискание ученой степени доктора наук (Перечень ВАК) по следующим научным специальностям:

- 1.1.7 – Теоретическая механика, динамика машин (технические науки)
- 1.1.8 – Механика деформируемого твердого тела (технические, физико-математические науки)
- 1.1.9 – Механика жидкости, газа и плазмы (технические науки)
- 1.2.2 – Математическое моделирование, численные методы и комплексы программ (технические науки)
- 2.3.1 – Системный анализ, управление и обработка информации, статистика (технические науки)
- 2.3.3 – Автоматизация и управление технологическими процессами и производствами (технические науки)
- 2.3.5 – Математическое и программное обеспечение вычислительных систем, комплексов и компьютерных сетей (технические науки)
- 2.3.7 – Компьютерное моделирование и автоматизация проектирования (технические, физико-математические науки)
- 2.3.8 – Информатика и информационные процессы (технические науки)
- 2.5.2 – Машиноведение (технические науки)
- 2.5.3 – Трение и износ в машинах (технические науки)
- 2.5.5 – Технология и оборудование механической и физико-технической обработки (технические науки)
- 2.5.6 – Технология машиностроения (технические науки)
- 2.5.8 – Сварка, родственные процессы и технологии (технические науки)
- 2.5.9 – Методы и приборы контроля и диагностики материалов, изделий, веществ и природной среды (технические науки)
- 2.5.10 – Гидравлические машины, вакуумная, компрессорная техника, гидро- и пневмосистемы (технические науки)

Регистрация:	Выписка из реестра зарегистрированных средств массовой информации ЭЛ № ФС 77 – 78854 от 07 августа 2020 г., выдано Федеральной службой по надзору в сфере связи, информационных технологий и массовых коммуникаций
Индексация и архивация:	РИНЦ, CyberLeninka, CrossRef, Dimensions, DOAJ, EBSCO, Index Copernicus, Internet Archive, Google Scholar
Сайт:	http://vestnik-donstu.ru
Адрес редакции:	344003, Российская Федерация, г. Ростов-на-Дону, пл. Гагарина, 1
E-mail	vestnik@donstu.ru
Телефон	+7 (863) 2–738–372
Дата выхода №4, 2024 в свет	30.12.2024



Editorial Board

Editor-in-Chief

Alexey N. Beskopylny, Dr.Sci. (Eng.), Professor, Don State Technical University (Rostov-on-Don, Russian Federation)

Deputy Chief Editor

Alexandr I. Sukhinov, Corresponding Member, Russian Academy of Sciences, Dr.Sci. (Phys.-Math.), Professor, Don State Technical University (Rostov-on-Don, Russian Federation)

Executive Editor

Manana G. Komakhidze, Cand.Sci. (Chemistry), Don State Technical University (Rostov-on-Don, Russian Federation)

Executive Secretary

Nadezhda A. Shevchenko, Don State Technical University (Rostov-on-Don, Russian Federation)

Ahilan Appathurai, National Junior Research Fellow, Anna University Chennai (India);

Ahmet Uyumaz, PhD (Eng.), Professor, Burdur Mehmet Akif Ersoy University (Turkey);

Alexander T. Rybak, Dr.Sci. (Eng.), Professor, Don State Technical University (Rostov-on-Don, Russian Federation);

Ali M. Hasan, PhD (Computer Engineering), Al Nahrain University (Baghdad, Iraq);

Andrey V. Nasedkin, Dr.Sci. (Phys.-Math.), Professor, Southern Federal University (Rostov-on-Don, Russian Federation);

Arestak A. Sarukhanyan, Dr.Sci. (Eng.), Professor, National University of Architecture and Construction of Armenia (Armenia);

Arkady N. Solovyev, Dr.Sci. (Phys.-Math.), Professor, Crimean Engineering and Pedagogical University the name of Fevzi Yakubov (Simferopol, Russian Federation);

Batyr M. Yazyev, Dr.Sci. (Eng.), Professor, Don State Technical University (Rostov-on-Don, Russian Federation);

Bertram Torsten, Dr.Sci. (Eng.), Professor, TU Dortmund University (Germany);

Evgenii A. Demekhin, Dr.Sci. (Phys.-Math.), Professor, Financial University under the RF Government, Krasnodar branch (Krasnodar, Russian Federation);

Geny V. Kuznetsov, Dr.Sci. (Phys.-Math.), Professor, Tomsk Polytechnic University (Tomsk, Russian Federation);

Gultekin Basmaci, PhD (Eng.), Professor, Burdur Mehmet Akif Ersoy University (Turkey);

Hamid A. Jalab, PhD (Computer Science & IT), University of Malaya (Malaysia);

Hubert Anysz, PhD (Eng.), Assistant Professor, Warsaw University of Technology (Republic of Poland);

Huchang Liao, Professor, IAAM Fellow, IEEE Business School Senior Fellow, Sichuan University (China);

Igor M. Verner, PhD (Eng.), Professor, Technion — Israel Institute of Technology (Israel);

Ilya I. Kudish, PhD (Phys.-Math.), Kettering University (USA);

Imad R. Antipas, Cand.Sci. (Eng.), Don State Technical University (Rostov-on-Don, Russian Federation);

Janusz Witalis Kozubal, Dr.Sci. (Eng.), Wrocław Polytechnic University (Republic of Poland);

José Carlos Quadrado, PhD (Electrical Engineering and Computers), DSc Habil, Polytechnic Institute of Porto (Portugal);

Kamil S. Akhverdiev, Dr.Sci. (Eng.), Professor, Rostov State Transport University (Rostov-on-Don, Russian Federation);

Karen O. Egiazaryan, Dr.Sci. (Eng.), Professor, Tampere University of Technology (Finland);

Konstantin V. Podmaster'ev, Dr.Sci. (Eng.), Professor, Orel State University named after I.S. Turgenev (Orel, Russian Federation);

LaRoux K. Gillespie, Dr.Sci. (Eng.), Professor, President-Elect of the Society of Manufacturing Engineers (USA);

Mezhlum A. Sumbatyan, Dr.Sci. (Phys.-Math.), Professor, Southern Federal University (Rostov-on-Don, Russian Federation);

Mikhail A. Tamarkin, Dr.Sci. (Eng.), Professor, Don State Technical University (Rostov-on-Don, Russian Federation);

Murat Tezer, Professor, Near East University (Turkey);

Murman A. Mukutadze, Dr.Sci. (Eng.), Professor, Rostov State Transport University (Rostov-on-Don, Russian Federation);

Muzafer H. Saračević, Full Professor, Novi Pazar International University (Serbia);

Nguyen Dong Ahn, Dr.Sci. (Phys.-Math.), Professor, Academy of Sciences and Technologies of Vietnam (Vietnam);

Nguyen Xuan Chiem, Dr.Sci. (Eng.), Le Quy Don Technical University (Vietnam);

Nikolay E. Galushkin, Dr.Sci. (Eng.), Professor, Institute of Service and Business, DSTU branch (Shakhty, Russian Federation);

Nikolay N. Prokopenko, Dr.Sci. (Eng.), Professor, Don State Technical University (Rostov-on-Don, Russian Federation);

Oleg V. Dvornikov, Dr.Sci. (Eng.), Professor, Belarusian State University (Belarus);

Revaz Z. Kavtaradze, Dr.Sci. (Eng.), Professor, Raphael Dvali Institute of Machine Mechanics (Georgia);

Roman N. Polyakov, Dr.Sci. (Eng.), Associate Professor, Orel State University named after I.S. Turgenev (Orel, Russian Federation);

Sergei A. Voronov, Dr.Sci. (Eng.), Associate Professor, Russian Foundation of Fundamental Research (Moscow, Russian Federation);

Sergey G. Parshin, Dr.Sci. (Eng.), Associate Professor, St. Petersburg Polytechnic University (St. Petersburg, Russian Federation);

Sergey M. Aizikovich, Dr.Sci. (Phys.-Math.), Professor, Don State Technical University (Rostov-on-Don, Russian Federation);

Tamaz M. Natriashvili, Academician, Raphael Dvali Institute of Machine Mechanics (Georgia);

Umid M. Turdaliev, Dr.Sci. (Eng.), Professor, Andijan Machine-Building Institute (Uzbekistan);

Valentin L. Popov, Dr.Sci. (Phys.-Math.), Professor, Berlin University of Technology (Germany);

Valery N. Varavka, Dr.Sci. (Eng.), Professor, Don State Technical University (Rostov-on-Don, Russian Federation);

Victor A. Ereemeev, Dr.Sci. (Phys.-Math.), Professor, Southern Scientific Center of RAS (Rostov-on-Don, Russian Federation);

Victor M. Kureychik, Dr.Sci. (Eng.), Professor, Southern Federal University (Rostov-on-Don, Russian Federation);

Vilor L. Zakovorotny, Dr.Sci. (Eng.), Professor, Don State Technical University (Rostov-on-Don, Russian Federation);

Vladimir I. Lysak, Dr.Sci. (Eng.), Professor, Volgograd State Technical University (Volgograd, Russian Federation);

Vladimir I. Marchuk, Dr.Sci. (Eng.), Professor, Institute of Service and Business, DSTU branch (Shakhty, Russian Federation);

Vladimir M. Mladenovic, Dr.Sci. (Eng.), Professor, University of Kragujevac (Serbia);

Vladimir N. Sidorov, Dr.Sci. (Eng.), Russian University of Transport (Moscow, Russian Federation);

Vyacheslav G. Tsybulin, Dr.Sci. (Phys.-Math.), Associate Professor, Southern Federal University (Rostov-on-Don, Russian Federation);

Yuri O. Chernyshev, Dr.Sci. (Eng.), Professor, Don State Technical University (Rostov-on-Don, Russian Federation);

Редакционная коллегия

Главный редактор

Бескопыйный Алексей Николаевич, доктор технических наук, профессор, Донской государственный технический университет (Ростов-на-Дону, Российская Федерация)

Заместитель главного редактора

Сухинов Александр Иванович, член-корреспондент РАН, доктор физико-математических наук, профессор, Донской государственный технический университет (Ростов-на-Дону, Российская Федерация)

Ответственный редактор

Комахидзе Манана Гивиевна, кандидат химических наук, Донской государственный технический университет (Ростов-на-Дону, Российская Федерация)

Ответственный секретарь

Шевченко Надежда Анатольевна, Донской государственный технический университет (Ростов-на-Дону, Российская Федерация)

Айзикович Сергей Михайлович, доктор физико-математических наук, профессор, Донской государственный технический университет (Ростов-на-Дону, Российская Федерация);

Антибас Имад Ризакалла, кандидат технических наук, Донской государственный технический университет (Ростов-на-Дону, Российская Федерация);

Ахилан Аппатурай, младший научный сотрудник, Инженерно-технологический колледж PSN, Университет Анны Ченнаи (Индия);

Ахвердиев Камил Самед Оглы, доктор технических наук, профессор, Ростовский государственный университет путей сообщения (Ростов-на-Дону, Российская Федерация);

Варавка Валерий Николаевич, доктор технических наук, профессор, Донской государственный технический университет (Ростов-на-Дону, Российская Федерация);

Вернер Игорь Михайлович, доктор технических наук, профессор, Технологический институт в Израиле (Израиль);

Воронов Сергей Александрович, доктор технических наук, доцент, Российский фонд фундаментальных исследований (Москва, Российская Федерация);

Галушкин Николай Ефимович, доктор технических наук, профессор, Институт сферы обслуживания и предпринимательства, филиал ДГТУ (Шахты, Российская Федерация);

Лару Гиллесси, доктор технических наук, профессор, Президент Общества машиностроителей (США);

Аныш Губерт, доктор наук, доцент, Варшавский технологический университет (Польша);

Басмачи Гюльтекин, доктор наук, профессор, Университет Бурдура Мехмета Акифа Эрсея (Турция);

Дворников Олег Владимирович, доктор технических наук, профессор, Белорусский государственный университет (Беларусь);

Демехин Евгений Афанасьевич, доктор физико-математических наук, профессор, Краснодарский филиал Финансового университета при Правительстве РФ (Краснодар, Российская Федерация);

Хамид Абдулла Джалаб, доктор наук (информатика и ИТ), университет Малайя (Малайзия);

Егназарян Карен Оникович, доктор технических наук, профессор, Технологический университет Тампере (Финляндия);

Еремеев Виктор Анатольевич, доктор физико-математических наук, профессор, Южный научный центр РАН (Ростов-на-Дону, Российская Федерация);

Заковоротный Вилор Лаврентьевич, доктор технических наук, профессор, Донской государственный технический университет (Ростов-на-Дону, Российская Федерация);

Кавтарадзе Реваз Зурабович, доктор технических наук, профессор, Институт механики машин им. Р. Двали (Грузия);

Козубал Януш Виталис, доктор технических наук, профессор, Вроцлавский технический университет (Польша);

Хосе Карлос Куадрадо, доктор наук (электротехника и компьютеры), Политехнический институт Порту (Португалия);

Кудиш Илья Исидорович, доктор физико-математических наук, Университет Кеттеринга (США);

Кузнецов Гений Владимирович, доктор физико-математических наук, профессор, Томский политехнический университет (Томск, Российская Федерация);

Курейчик Виктор Михайлович, доктор технических наук, профессор, Южный федеральный университет (Ростов-на-Дону, Российская Федерация);

Лысак Владимир Ильич, доктор технических наук, профессор, Волгоградский государственный технический университет (Волгоград, Российская Федерация);

Марчук Владимир Иванович, доктор технических наук, профессор, Институт сферы обслуживания и предпринимательства, филиал ДГТУ (Шахты, Российская Федерация);

Владимир Младенович, доктор технических наук, профессор, Крагуевацкий университет (Сербия);

Мукутадзе Мурман Александрович, доктор технических наук, доцент, Ростовский государственный университет путей сообщения (Ростов-на-Дону, Российская Федерация);

Наседкин Андрей Викторович, доктор физико-математических наук, профессор, Южный федеральный университет (Ростов-на-Дону, Российская Федерация);

Натришвили Тамаз Мамиевич, академик, Институт механики машин им. Р. Двали (Грузия);

Нгуен Донг Ань, доктор физико-математических наук, профессор, Институт механики Академии наук и технологий Вьетнама (Вьетнам);

Нгуен Суан Тьем, доктор технических наук, Вьетнамский государственный технический университет им. Ле Куй Дона (Вьетнам);

Паршин Сергей Георгиевич, доктор технических наук, доцент, Санкт-Петербургский политехнический университет (Санкт-Петербург, Российская Федерация);

Подмастерьев Константин Валентинович, доктор технических наук, профессор, Орловский государственный университет им. И. С. Тургенева (Орел, Российская Федерация);

Поляков Роман Николаевич, доктор технических наук, доцент, Орловский государственный университет им. И. С. Тургенева (Орел, Российская Федерация);

Попов Валентин Леонидович, доктор физико-математических наук, профессор, Институт механики Берлинского технического университета (Германия);

Прокопенко Николай Николаевич, доктор технических наук, профессор, Донской государственный технический университет (Ростов-на-Дону, Российская Федерация);

Рыбак Александр Тимофеевич, доктор технических наук, профессор, Донской государственный технический университет (Ростов-на-Дону, Российская Федерация);

Музафер Сарачевич, доктор наук, профессор, Университет Нови-Пазара (Сербия);

Саруханиян Арестак Арамаисович, доктор технических наук, профессор, Национальный университет архитектуры и строительства Армении (Армения);

Сидоров Владимир Николаевич, доктор технических наук, Российский университет транспорта (Москва, Российская Федерация);

Соловьев Аркадий Николаевич, доктор физико-математических наук, профессор, Крымский инженерно-педагогический университет имени Февзи Якубова (Симферополь, Российская Федерация);

Сумбатян Межлум Альбертович, доктор физико-математических наук, профессор, Южный федеральный университет (Ростов-на-Дону, Российская Федерация);

Тамаркин Михаил Аркадьевич, доктор технических наук, профессор, Донской государственный технический университет (Ростов-на-Дону, Российская Федерация);

Мурат Тезер, профессор, Ближневосточный университет (Турция);

Бертрам Торстен, доктор технических наук, профессор, Технический университет Дортмунда (Германия);

Турдалиев Умид Мухтаралиевич, доктор технических наук, профессор, Андижанский машиностроительный институт (Узбекистан);

Ахмет Умоаз, доктор технических наук, профессор, университет Бурдура Мехмета Акифа Эрсея (Турция);

Али Маджид Хасан Алвазли, доктор наук (компьютерная инженерия), доцент, Университет Аль-Нахрейн (Ирак);

Цибулин Вячеслав Георгиевич, доктор физико-математических наук, доцент, Южный федеральный университет (Ростов-на-Дону, Российская Федерация);

Чернышев Юрий Олегович, доктор технических наук, профессор, Донской государственный технический университет (Ростов-на-Дону, Российская Федерация);

Хуан Ляо, профессор, научный сотрудник ИААМ; Старший член Школы бизнеса IEEE, Университет Сычуань (Китай);

Языев Батыр Меретович, доктор технических наук, профессор, Донской государственный технический университет (Ростов-на-Дону, Российская Федерация).

Contents

MECHANICS

Estimation of Stresses in a Plate with a Concentrator through Ultrasonic Measurements of Acoustic Anisotropy	307
<i>Dmitry A. Tretyakov, Dmitry S. Osovik</i>	
Investigation of Parameters Influencing the Establishment of Hydrostatic Mode in the Crosshead-Guide Assembly of High-Pressure Plunger Pump	316
<i>Marina V. Korchagina, Valentin N. Stepanov, Sergey O. Kireev, Alexey R. Lebedev</i>	
Evaluation of Wear Resistance of a Modified Radial Bearing Design Taking into Account Compressibility and Viscosity of the Lubricant	328
<i>Ekaterina A. Bolgova, Murman A. Mukutadze, Victor M. Prikhodko, Igor A. Kolobov</i>	
Finite Element Modeling of a Flat Cell of Highly Porous Piezocomposite with Inclined Edges Taking into Account Nonuniform Polarization	339
<i>Arkadiy N. Soloviev, Maria S. Germanchuk</i>	

MACHINE BUILDING AND MACHINE SCIENCE

Testing Bench for Reciprocating Hydraulic Cylinders with Energy Recovery: Structure, Simulation, and Calculation	347
<i>Alexander R. Zenin, Alexander T. Rybak, Alexey N. Beskopylny, Alexey Yu. Pelipenko, Yuliya A. Serdyukova</i>	
Experimental Study of the Kinematics of a Double-Row Planetary Mechanism Using Two Elliptical External Gears	360
<i>Alexander A. Prikhodko, Nataliya N. Belina, Andrey V. Novitsky, Maksim M. Shchetinin</i>	
Analysis of Technologies for Applying High-Entropy Coatings by Physical Deposition Method	369
<i>Kirill N. Polityko, Igor V. Kolesnikov, Dmitry S. Manturov</i>	
Development of a Method for Obtaining Nanoscale Magnesium Carbonate Stabilized with Chitosan as the Basis of Scaffold Matrices for Regenerative Medicine.....	392
<i>Andrey V. Blinov, Zafar A. Rekhman, Alexey A. Gvozdenko, Maria A. Yasnaya, Maxim A. Kolodkin, Maxim A. Taravanov</i>	
Selection of the Process of Arc Welding of Sealing Surfaces of Power Valves with a Consumable Electrode in the Shielding Gas.....	402
<i>Dmitrii V. Rogozin, Vyacheslav A. Lenivkin</i>	

INFORMATION TECHNOLOGY, COMPUTER SCIENCE AND MANAGEMENT

Algorithm for Constructing the Hazard Function of the Extended Cox Model and its Application to the Prostate Cancer Patient Database	413
<i>Ilya I. Mikulik, Gennadiy M. Zharinov, Aleksei Y. Kneev</i>	
Optimization Problem for Probabilistic Time Intervals of Quasi-Deterministic Output and Self-Similar Input Data Packet Flow in Telecommunication Networks	424
<i>Gennadii I. Linets, Roman A. Voronkin, Gennadii V. Slyusarev, Svetlana V. Govorova</i>	

Содержание

МЕХАНИКА

- Оценка напряжений в пластине с концентратором посредством ультразвуковых измерений акустической анизотропии 307
Д.А. Третьяков, Д.С. Осовик
- Исследование параметров, влияющих на установление гидростатического режима в узле крейцкопф-направляющие плунжерного насоса высокого давления 316
М.В. Корчагина, В.Н. Степанов, С.О. Киреев, А.Р. Лебедев
- Оценка износостойкости модифицированной конструкции радиального подшипника при учете сжимаемости и вязкости смазочного материала 328
Е.А. Болгова, М.А. Мукутадзе, В.М. Приходько, И.А. Колобов
- Конечно-элементное моделирование плоской ячейки высокопористого пьезокompозита с наклонными ребрами с учетом неоднородной поляризации 339
А.Н. Соловьев, М.С. Германчук

МАШИНОСТРОЕНИЕ И МАШИНОВЕДЕНИЕ

- Стенд испытания поршневых гидравлических цилиндров с рекуперацией энергии: структура, моделирование и расчёт 347
А.Р. Зенин, А.Т. Рыбак, А.Н. Бескопильный, А.Ю. Пелипенко, Ю.А. Сердюкова
- Экспериментальное исследование кинематики двухрядной планетарной передачи эллиптическими зубчатыми колесами с двумя внешними зацеплениями 360
А.А. Приходько, Н.Н. Белина, А.В. Новицкий, М.М. Щетинин
- Анализ технологий нанесения высокoэнтропийных покрытий методом физического осаждения 369
К.Н. Политыко, И.В. Колесников, Д.С. Мантуров
- Разработка метода получения наноразмерного карбоната магния, стабилизированного хитозаном, как основы скаффолд-матриц для регенеративной медицины 392
А.В. Блинов, З.А. Рехман, А.А. Гвозденко, М.А. Ясная, М.А. Колодкин, М.А. Тараванов
- Выбор процесса дуговой наплавки плавящимся электродом в защитном газе уплотнительных поверхностей энергетической арматуры 402
Д.В. Rogozin, В.А. Ленивкин

ИНФОРМАТИКА, ВЫЧИСЛИТЕЛЬНАЯ ТЕХНИКА И УПРАВЛЕНИЕ

- Алгоритм построения функции риска расширенной модели Кокса и его применение на базе данных больных раком предстательной железы 413
И.И. Микулик, Г.М. Жаринов, А.Ю. Кнеев
- Оптимизационная задача для вероятностных временных интервалов квазидетерминированного выходного и самоподобного входного потока пакетов данных в телекоммуникационных сетях 424
Г.И. Линец, Р.А. Воронкин, Г.В. Слюсарев, С.В. Говорова

MECHANICS МЕХАНИКА



UDC 620.179.16

Original Empirical Research

<https://doi.org/10.23947/2687-1653-2024-24-4-307-315>

Estimation of Stresses in a Plate with a Concentrator through Ultrasonic Measurements of Acoustic Anisotropy

Dmitry A. Tretyakov , Dmitry S. Osovik 

Peter the Great St. Petersburg Polytechnic University, St. Petersburg, Russian Federation

✉ dmitry.tretyakov93@yandex.ru

EDN: RMBTZU

Abstract

Introduction. Acoustic anisotropy is measured during ultrasonic nondestructive testing. It estimates the magnitude of stresses by the acoustoelasticity method. The literature describes in detail the application of this approach in the case of a biaxial strength of extended structures: main pipelines, rail strings, steam generators, and others. They assume the presence of a uniform field with zero or weak gradients of stresses and deformations. However, the problem of timely detection and assessment of critical stresses caused by local concentrators through ultrasonic testing has not been solved. The presented material is intended to fill this gap. The work is aimed at determining the possibilities of the acoustoelasticity method to estimate the difference in the main biaxial stresses around the concentrator — a circular cutout in a rectangular plate.

Materials and Methods. A 510×120×15 mm plate with a central hole of 40 mm in diameter was cut from a sheet of commercially pure aluminum of the AMc brand (AW-3003 according to ISO) across the rolling direction, and subjected to uniaxial step loading in an Instron-8850 testing machine. For ultrasonic measurements, an acoustic sensor with a carrier frequency of 5 MHz was used. The stresses were calculated by solving the problem of stretching an isotropic linear-elastic plate in the ANSYS finite element modeling package and by the relations of the plane Kirsch problem obtained in the polar coordinate system.

Results. The research allows us to state that the results of analytical and numerical calculations largely coincide only for points located near the zone of greatest stress concentration. In all other cases, the indicators differ several times in sign and modulus. The difference is explained by the fact that Kirsch's approach assumes the action of compressive stresses in the area of location of some points, but this factor is absent if we are talking about a real plate. It has been established that in the area of material with predominant tensile stresses, the acoustoelasticity method allows for a quantitative estimate of their difference with an error not exceeding the engineering one. The calculations based on the Kirsch relations correlate with the others only at points with the maximum concentration of tensile stresses.

Discussion and Conclusion. The results of the study provide applying the acoustoelasticity method to estimate the magnitude of tensile biaxial stresses in the area around the fabrication holes. They are consistent with well-known scientific results and make it possible to rationally select the measurement points of acoustic anisotropy. The results of this scientific work can be applied in ultrasonic nondestructive testing using the acoustoelasticity method.

Keywords: zone of highest stress concentration, principal stress differences, acoustic anisotropy of initially inhomogeneous material, stress-strain state, ultrasonic nondestructive testing

Acknowledgements. The authors would like to thank the Editorial board and the reviewers for their attentive attitude to the article and for the specified comments that improved the quality of the article.

Funding Information. The research is done with the support of the Ministry of Science and Higher Education of the Russian Federation at the expense of the Russian Presidential Scholarship No. SP–5336.2022.1.

For Citation. Tretyakov DA, Osovik DS. Estimation of Stresses in a Plate with a Concentrator through Ultrasonic Measurements of Acoustic Anisotropy. *Advanced Engineering Research (Rostov-on-Don)*. 2024;24(4):307–315. <https://doi.org/10.23947/2687-1653-2024-24-4-307-315>

Оценка напряжений в пластине с концентратором посредством ультразвуковых измерений акустической анизотропии

Д.А. Третьяков , Д.С. Осовик 

Санкт-Петербургский политехнический университет Петра Великого, г. Санкт-Петербург, Российская Федерация

✉ dmitry.tretyakov93@yandex.ru

Аннотация

Введение. Акустическая анизотропия измеряется при ультразвуковом неразрушающем контроле и позволяет оценить величину напряжений методом акустоупругости. В литературе подробно описано применение такого подхода в случае двухосного напряженного состояния протяженных конструкций: магистральных трубопроводов, рельсовых плетей, парогенераторов и других. Для них предполагается наличие однородного поля с нулевыми либо слабыми градиентами напряжений и деформаций. Однако не решена проблема своевременного обнаружения и оценки критических напряжений, вызванных локальными концентраторами, посредством ультразвукового контроля. Представленный материал призван восполнить этот пробел. Цель работы — определить возможности применения метода акустоупругости для оценки разности главных двухосных напряжений вокруг концентратора — кругового выреза в прямоугольной пластине.

Материалы и методы. Из листа технически чистого алюминия марки АМц поперек направления проката вырезали пластину 510×120×15 мм с центральным отверстием диаметром 40 мм и подвергли ее одноосному ступенчатому нагружению в испытательной машине Instron-8850. Для ультразвуковых измерений задействовали акустический датчик с несущей частотой 5 МГц. Напряжения рассчитывались путем решения задачи о растяжении изотропной линейно-упругой пластины в пакете конечноэлементного моделирования ANSYS и по соотношениям плоской задачи Кирша, полученным в полярной системе координат.

Результаты исследования. Итоги работы позволяют утверждать, что результаты аналитических и численных расчетов во многом совпадут только для точек, расположенных рядом с зоной наибольшей концентрации напряжений. Во всех остальных случаях показатели отличаются в несколько раз по знаку, и по модулю. Разница объясняется тем, что подход Кирша предполагает действие сжимающих напряжений в области расположения некоторых точек, однако этот фактор отсутствует, если речь идет о реальной пластине. Установлено, что в области материала с преобладающими растягивающими напряжениями метод акустоупругости позволяет количественно оценить их разность с погрешностью, не превышающей инженерную. Расчеты по соотношениям Кирша коррелируют с остальными только в точках с максимальной концентрацией растягивающих напряжений.

Обсуждение и заключение. Результаты исследования позволяют применять метод акустоупругости для оценки величины растягивающих двухосных напряжений в области вокруг технологических отверстий. Они согласуются с известными научными результатами и дают возможность рационально выбрать точки измерения акустической анизотропии. Итоги данной научной работы можно применить при ультразвуковом неразрушающем контроле методом акустоупругости.

Ключевые слова: зона наибольшей концентрации напряжений, разности главных напряжений, акустическая анизотропия начально неоднородного материала, напряженно-деформированное состояние, ультразвуковой неразрушающий контроль

Благодарности. Авторы выражают благодарность редакции и рецензентам за внимательное отношение к статье и замечания, которые позволили повысить ее качество.

Финансирование. Исследование выполнено при поддержке Министерства науки и высшего образования РФ за счет стипендии № СП–5336.2022.1 Президента Российской Федерации.

Для цитирования. Третьяков Д.А., Осовик Д.С. Оценка напряжений в пластине с концентратором посредством ультразвуковых измерений акустической анизотропии. *Advanced Engineering Research (Rostov-on-Don)*. 2024;24(4):307–315. <https://doi.org/10.23947/2687-1653-2024-24-4-307-315>

Introduction. In recent decades, domestic nondestructive testing technologies have been developed to determine the stress-strain state of elements of energy systems, railway and pipeline transport [1]. These approaches involve solving inverse problems in the case of a nonuniform stress state [2], noncontact electromagnetic acoustic strain measurement [3], taking

into account the degradation of elastic properties in combined nondestructive testing [4], as well as precision measurement of time delays in the propagation of elastic waves in the material [5]. The technologies have been verified in industrial measurements¹ [6], their application is accompanied by the operation of modern diagnostic equipment [7]. However, the task of testing existing approaches in the diagnostics of anisotropic structural materials, which include industrial rolled products, remains relevant [8].

This work is devoted to the study of acoustic anisotropy [9] of an initially inhomogeneous material. In this case, it is commercially pure aluminum of the AMc brand (AW-3003 according to ISO). Samples cut from a rolled sheet were not prepared to remove the initial internal stresses caused by plastic deformation during rolling [10]. The task is to establish the possibility of estimating the difference in the magnitude of biaxial stresses in a metal with inhomogeneous initial acoustic anisotropy [11].

Materials and Methods. In the experiments, we used the IN-5101A ultrasonic acoustic anisotropy analyzer². This is a certified device for measuring mechanical stresses by the acoustoelasticity method [12]. The stresses were calculated from the formula:

$$\sigma_{\theta\theta} = \sigma_{rr} = D(a_{\sigma} - a_0). \quad (1)$$

Here, $\sigma_{\theta\theta}$ and σ_{rr} — principal components of the stress tensor in polar coordinates, D — coefficient of elastic-acoustic coupling of the material; a_0 — initial acoustic anisotropy at the measurement point; a_{σ} — value of the acoustic anisotropy parameter under the current value of the uniaxial tensile load σ . For the aluminum alloy AMc, coefficient $D = -2.0 \pm 0.3 \cdot 10^{-4} \text{MPa}$ [13].

The current value of the acoustic anisotropy parameter a_{σ} [14] was determined from formula (2) as the relative difference in the propagation time of transverse ultrasonic waves of mutually orthogonal polarization [15]:

$$a_{\sigma} = (t_2 - t_1) / ((t_2 + t_1) / 2). \quad (2)$$

Here, t_1, t_2 — current values of time delays during the passage of transverse wave packets through the thickness of the material after their multiple reflection, whose velocities are directed along and across the line of uniaxial loading.

The measurements were performed using acoustic sensors with a pulse emission frequency of 5 MHz. The accuracy of the measurements of time delays t_1, t_2 was 3 ns.

The low-alloy corrosion-resistant aluminum-manganese alloy of the AMc brand, close in its properties to commercially pure aluminum (97/99% Al in composition), was studied. Aluminum was a model material for ultrasonic research. It was with it that the basic results in the acoustoelasticity were obtained [1].

Mechanical tests were performed on a 510×120×15 mm rectangular plate, cut from a rolled aluminum sheet across the rolling direction. The sample had a stress concentrator in the form of a central circular hole with a diameter of 40 mm (Fig. 1).

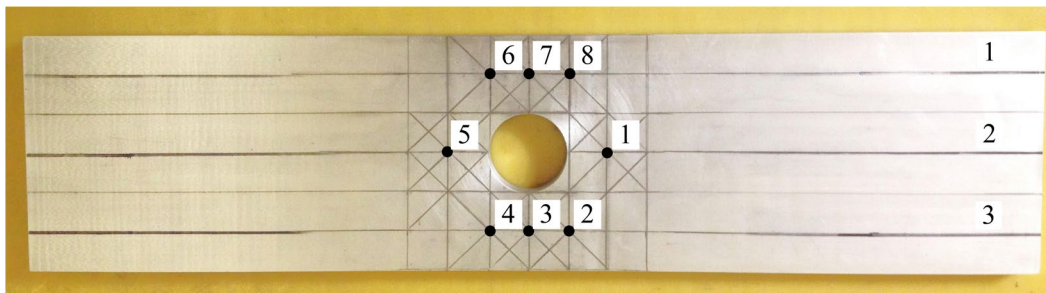


Fig. 1. Diagram of a sample from a sheet of rolled aluminum grade AMc

The direction of rolling affects the sign of the initial acoustic anisotropy a_0 [16]:

$$a_0 = (t_{02} - t_{01}) / ((t_{02} + t_{01}) / 2). \quad (3)$$

Here, t_{01}, t_{02} — initial time delays of transverse waves. In the case of samples cut across the rolled product, the dimensionless parameter of the initial acoustic anisotropy a_0 , calculated from formula (3), is negative: $a_0 < 0$.

For rigid step loading of the plate, uniaxial tension was applied in an Instron-8850 hydraulic machine (Fig. 3). The stress-strain state was considered at three loading stages with tensile load values $F_1 = 30 \text{ kN}$, $F_2 = 50 \text{ kN}$ and $F_3 = 70 \text{ kN}$. For the study, $n = 8$ sections (points) of the sample were selected. The diagram of their location is shown in Figure 2.

¹ GOST R 52731–2007. *Nondestructive Testing. Stress Evaluation by Ultrasound. General Requirements*. Electronic Fund of Legal and Technical Guidance Documents. (In Russ.) URL: <https://docs.cntd.ru/document/1200051032> (accessed: 25.05.2024).

² *Devices for Measuring Mechanical Stresses IN-5101A. Operations Manual. INKO.468160.008 RE*. (In Russ.) URL: https://encotes.ru/system/files/RE-IN-5101A_0.pdf?ysclid=m00rujbqr0495004447 (accessed: 25.05.2024).

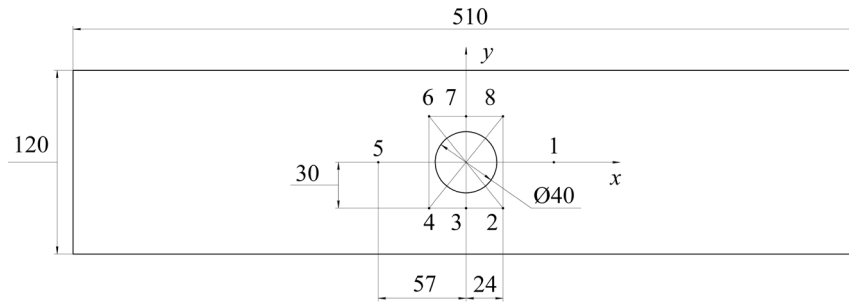


Fig. 2. Layout of the sample points under study

Ultrasonic testing was performed along three rows of points: 1–5, 2–4 and 6–8, symmetrically located relative to each other around the stress concentrator (Fig. 2). The characteristic size of the plates of the piezoelectric elements of the acoustic sensor was 12×12 mm. That means that each point was associated with its own local representative volume of material. The points were selected so that the representative volumes differed significantly in their stress-strain state [17].

Mechanical tensile testing in an Instron-type machine involved different boundary conditions for the sample. Its lower part (points 4–6 in Figure 2) was rigidly fixed in a stationary grip of the testing machine (Fig. 3). In the upper part (points 1, 2 and 8 in Figure 2), the sample, fixed in a movable grip, was stretched at a low constant strain rate (Fig. 3). Points 3 and 7 were located on the central transverse axis of the sample (Fig. 2).

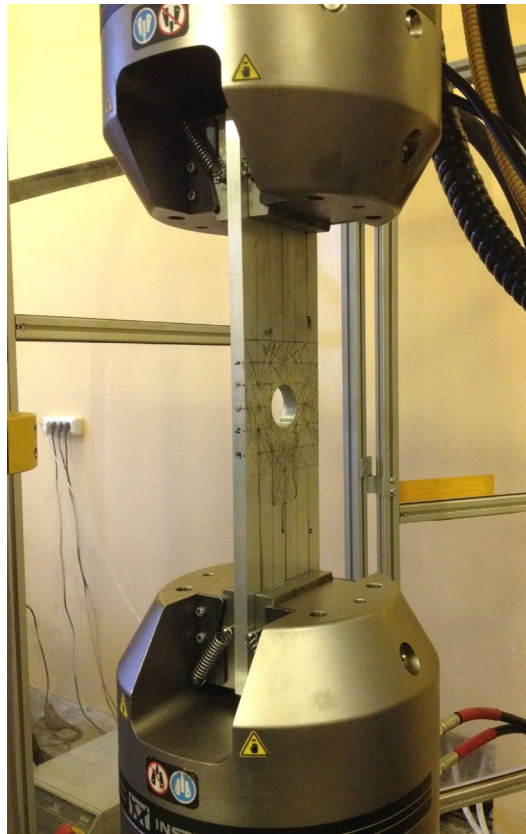


Fig. 3. Sample under load in a testing machine

The asymmetry of the problem conditions was taken into account in numerical modeling using the finite element method. The actual dimensions of the sample, its elastic and mechanical properties obtained during testing of samples from the same batch (Young's modulus E , yield strength σ_y , elasticity modulus H), as well as known data for commercially pure aluminum (density ρ , Poisson's ratio ν) were used. It was taken into account that the sample was fixed in the testing machine over a wide surface, and the tangential tensile load was applied to it, and not to the end of the sample, as in the case of two-dimensional models.

The stress-strain state was calculated in the ANSYS finite element modeling package. Taking into account the area of application of loads F_1 , F_2 , F_3 , the values of tensile stresses were determined: $\sigma_1 = 16.67$ MPa, $\sigma_2 = 27.78$ MPa, and $\sigma_3 = 38.89$ MPa. They were used in the numerical solution. Figure 4 shows a model of the sample with the display of the finite element mesh and boundary conditions. It consists of 936,152 elements and 3,981,073 nodes.

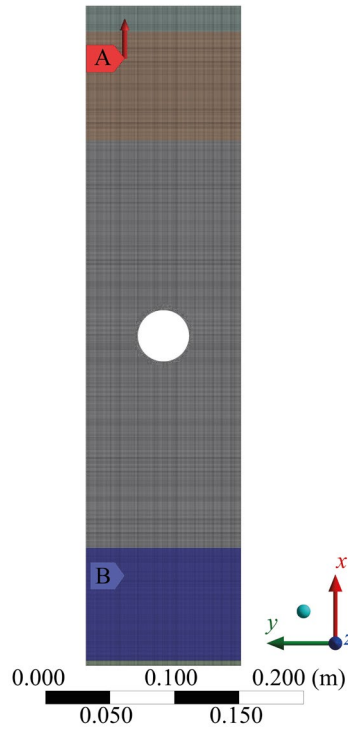


Fig. 4. Finite element model of a sample taking into account boundary conditions

The analytical solution was based on the use of formulas (4) and (5), which are the solution to the Kirsch problem in polar coordinates [18]:

$$\sigma_{\theta\theta} = \frac{S}{2} \left(1 + \frac{a^2}{r^2} \right) - \frac{S}{2} \left(1 + \frac{3a^4}{r^4} \right) \cos 2\theta, \quad (4)$$

$$\sigma_{rr} = \frac{S}{2} \left(1 - \frac{a^2}{r^2} \right) + \frac{S}{2} \left(1 + \frac{3a^4}{r^4} - \frac{4a^2}{r^2} \right) \cos 2\theta, \quad (5)$$

where S — load applied to the plate; a — radius of the hole in the plate; r — distance from the center of the hole to the stress calculation point; θ — angle corresponding to the point being calculated.

The formulation of the problem in this work assumes the presence of only elastic deformations of the sample. Its further development, taking into account the influence of inelastic deformations, is associated with the consideration of the solution to the plane elastic-plastic problem of stretching a plate with a circular hole (an ideal plastic body), obtained by L.A. Galin in 1946 [19].

The principal stresses co-directed with the longitudinal axis x ($\sigma_{\theta\theta}$) and the transverse axis y of the sample (σ_{rr}) were calculated for all $n = 8$ points under study. The components $\sigma_{\theta\theta}$, σ_{rr} — functions of the radial distance to the hole center r and of the angle θ , measured relative to the reference axis. Relations (4) and (5) were obtained under the assumption that the circular hole was located at the center of an infinite isotropic linear elastic plate subjected to uniform plane loading. They were previously used in [20] to determine the stresses in two regions on the boundary of the hole located along ($\theta = 0^\circ$) and across ($\theta = 90^\circ$) the line of action of the load.

Ultrasonic measurements were performed at points 1–3 (Fig. 2) in the sample before loading ($F_0 = 0$ kN), as well as upon reaching elastic deformation levels corresponding to loads F_1 , F_2 , F_3 . The finite size effect of the plate (mainly, in its cross-section) on the discrepancy between the stress values obtained experimentally, numerically and analytically, was investigated. The values of acoustic anisotropy a_0 , % and a_σ , % were calculated using formulas (2) and (3). To take into account the effects associated with stress relaxation, control measurements were performed at the start and end of each stage. A total of 198 time delays (t_{01} , t_{02}) and (t_1 , t_2) were measured during the propagation of transverse waves along and across the sample.

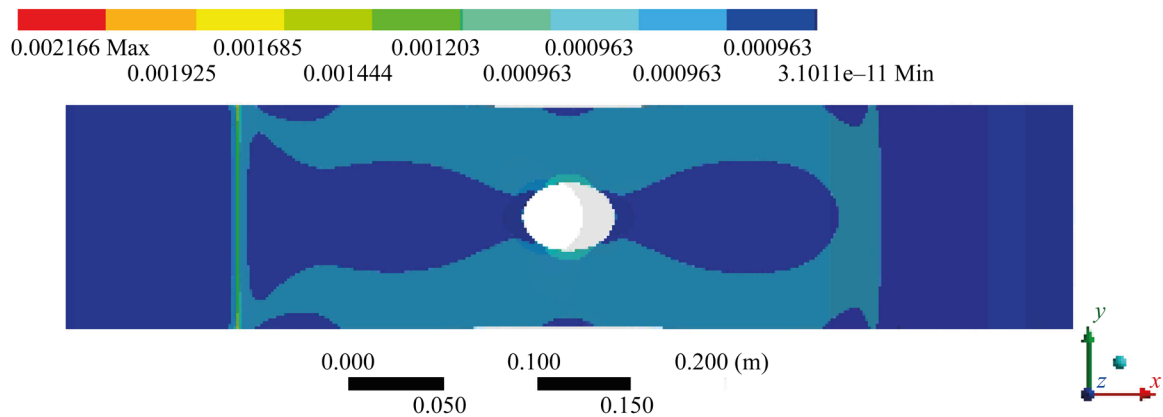
Research Results. Table 1 shows the values of internal stresses σ_{xx} (analog $\sigma_{\theta\theta}$ in the polar coordinate system) and σ_{yy} (analog σ_{rr}) for $n = 8$ points around the plate hole (Fig. 2). They were obtained as a result of finite element modeling and calculations using formulas (4) and (5) with external tensile stresses σ_1 , σ_2 , σ_3 (correspond to loads F_1 , F_2 , F_3).

Table 1

Calculated Stress Values around the Plate Hole, MPa

Load	$F_1 = 30 \text{ kN}$ ($\sigma_1 = 16.67 \text{ MPa}$)		$F_2 = 50 \text{ kN}$ ($\sigma_2 = 27.78 \text{ MPa}$)		$F_3 = 70 \text{ kN}$ ($\sigma_3 = 38.89 \text{ MPa}$)	
N	σ_{xx}, σ_{yy} , Ansys	$\sigma_{\theta\theta}, \sigma_{rr}$, Kirsch	σ_{xx}, σ_{yy} , Ansys	$\sigma_{\theta\theta}, \sigma_{rr}$, Kirsch	σ_{xx}, σ_{yy} , Ansys	$\sigma_{\theta\theta}, \sigma_{rr}$, Kirsch
1	12.120 1.270	0.647 11.920	20.210 2.110	1.078 19.860	28.280 2.960	1.510 27.800
2, 8	22.090 -3.380	13.060 5.800	38.160 -5.640	21.760 9.666	53.420 -7.890	30.460 13.530
3, 7	27.690 6.390	25.310 6.174	46.157 10.650	42.180 10.290	64.610 14.910	59.060 14.400
4, 6	22.890 -3.390	13.060 5.800	38.170 -5.650	21.760 9.666	53.430 -7.920	30.460 13.530
5	12.180 1.230	0.647 11.920	20.310 2.500	1.0780 19.860	28.430 2.870	1.510 27.800

The conditions of fixing the sample are different: the left part is fixed, the right one is movable. Hence the asymmetry in the pattern of the sample deformation field, which is preserved for all values of loads in the elastic region (an example for $F_1 = 30 \text{ kN}$ is shown in Figure 5).

Fig. 5. Calculated deformation field under tensile load $F = 30 \text{ kN}$

Due to the asymmetry noted above, when solving the problem using the finite element method, the stress values in pairs of points:

- coincide if they are obtained through mirroring relative to the central longitudinal axis of the sample;
- differ if they are obtained by the reflection relative to the transverse axis of the sample.

In the first case, pairs 2, 8; 3, 7 and 4, 6 can serve as an example, in the second case — 1, 5; 2, 4 and others. Note that even if there is a difference in stresses, it does not exceed 1 MPa. This corresponds to the engineering error level $\pm 5\%$ (Table 1). The stress values calculated for the specified pairs of points using formulas (4) and (5) are the same.

Finally, close values between the results of analytical and numerical calculations are observed only for points {3, 7}, located near the region with the highest stress concentration (Table 1). At the other points, there is a multiple difference not only to modulo (2, 8 and 4, 6), but also in sign (1, 5). This is due to the fact that calculations using formulas (4) and (5) for a plate of equal (infinite) dimensions assume the presence of a compressive-stress zone in the region of the location of points 1, 5. The situation is different with a real plate (Fig. 1 and 2), whose dimensions are limited and differ from each other in the ratio of length and width by 4.25 times. In this case, there is no compressive-stress zone (Table 1 and Fig. 5).

The comparison of the results suggests that the effect of the finite dimensions of the plate does not allow for the use of relations (4) and (5) to estimate the stresses in this problem. This contradicts the conclusions of [20]. Note that the presence of a correlation for points with the maximum value of the stress concentration coefficient is confirmed by the results for pair 3, 7.

Table 2 shows the initial a_0 and current a_σ values of acoustic anisotropy in the region of the locations of points 1, 2 and 3, calculated from formulas (2) and (3) in the no-load state (F_0) and at three load values F_1, F_2, F_3 .

Table 2

Acoustic Anisotropy and Average Values of Time Delays at Different Stages of Loading

Load	$F_0 = 0 \text{ kN}$ $\sigma_0 = 0 \text{ MPa}$		$F_1 = 30 \text{ kN}$ $\sigma_1 = 16.67 \text{ MPa}$		$F_2 = 50 \text{ kN}$ $\sigma_2 = 27.78 \text{ MPa}$		$F_3 = 70 \text{ kN}$ $\sigma_3 = 38.89 \text{ MPa}$	
N	a_0	$\langle t_{01} \rangle, \langle t_{02} \rangle$, μs	$a_{\sigma 1}$	$\langle t_1 \rangle, \langle t_2 \rangle$, μs	$a_{\sigma 2}$	$\langle t_1 \rangle, \langle t_2 \rangle$, μs	$a_{\sigma 3}$	$\langle t_1 \rangle, \langle t_2 \rangle$, μs
1	– 0.005886	9.4805 9.4248	– 0.006198	9.4765 9.4180	– 0.006379	9.4802 9.4200	– 0.006445	9.4783 9.4174
2	– 0.004508	9.4602 9.4177	– 0.005947	9.5057 9.4494	– 0.006650	9.5107 9.4476	– 0.007636	9.5147 9.4423
3	– 0.005433	9.4730 9.4217	– 0.006461	9.5113 9.4500	– 0.007142	9.5161 9.4484	– 0.007055	9.5158 9.4489

It follows from Table 2 that the difference in the values of the initial acoustic anisotropy parameter a_0 at points 1, 2 and 3 is largely determined by the initial heterogeneity of the material. This is evident from the variation of parameter a_0 before loading. In addition, with the application of an external load, the discrepancy between the values of the acoustic anisotropy parameter a_σ at the points under study increases.

Based on the ultrasonic measurement data (Table 3), the values $(\sigma_{\theta\theta} - \sigma_{rr})$ of the difference in the principal stresses in the polar coordinates were calculated using the acoustoelasticity relations (1) [21]. They are presented in Table 3 in comparison with the results of finite element modeling and calculations using formulas (4) and (5). The stress values that differ for pairs of symmetrically located points obtained by reflection relative to the transverse axis of the sample are given in parentheses.

Table 3

Comparison of Results of Ultrasonic Measurements, Analytical and Numerical Finite Element Calculations, MPa

Load	$F_1 = 30 \text{ kN}$ ($\sigma_1 = 16.67 \text{ MPa}$)	$F_2 = 50 \text{ kN}$ ($\sigma_2 = 27.78 \text{ MPa}$)	$F_3 = 70 \text{ kN}$ ($\sigma_3 = 38.89 \text{ MPa}$)
N	$(\sigma_{xx} - \sigma_{yy})$. Ansys $(\sigma_{\theta\theta} - \sigma_{rr})$. Kirsch $D(a_{\sigma 1} - a_0)$	$(\sigma_{xx} - \sigma_{yy})$. Ansys $(\sigma_{\theta\theta} - \sigma_{rr})$. Kirsch $D(a_{\sigma 2} - a_0)$	$(\sigma_{xx} - \sigma_{yy})$. Ansys $(\sigma_{\theta\theta} - \sigma_{rr})$. Kirsch $D(a_{\sigma 3} - a_0)$
1 (5)	10.850 (10.950) –11.273 6.240	18.100 (17.810) –18.782 9.850	25.320 (25.560) –26.290 11.180
2, 8 (4, 6)	25.470 (26.280) 7.260 28.780	43.800 (43.820) 12.094 42.840	61.310 (61.350) 16.930 62.560
3, 7	21.300 19.136 20.550	35.507 31.890 34.170	49.700 44.660 44.800

Table 3 shows that the data from acoustoelastic measurements and the finite element method solutions correlate qualitatively and quantitatively with each other. Consequently, we can talk about mutual verification of the results of full-scale and numerical experiments. The highest correlation is observed for points 2, 8; (4, 6) and 3, 7, located near the region of maximum tensile stresses.

Different results were obtained for points 1 and (5), where the presence of compressive stresses was assumed according to formulas (4), (5). Here, the differences in the principal values $(\sigma_{\theta\theta} - \sigma_{rr})$, obtained according to the ultrasonic measurements, were on average two times smaller than the predicted numerical values. Thus, calculations based on the acoustic anisotropy values provide a lower estimate of the stresses for the studied sections of the sample.

Discussion and Conclusion. The principal biaxial stresses in an aluminum plate around a concentrator — a central circular hole — were investigated. The values obtained as a result of natural ultrasonic measurements, numerical experiments using the finite element method, and analytical calculations using the Kirsch relations were compared. The effect of the asymmetry of stress and strain fields, arising due to different conditions of sample fixation and reflecting the process of uniaxial elastic deformation under tension in a testing machine, was taken into account.

It was noted that similar results of the analytical and numerical calculations were observed only for points located near the region of the greatest stress concentration. In all other cases, the values differed several times both to modulo and in sign. This is explained by the presence or absence of compressive stresses. The analytical approach assumes that they exist. There are none in a real plate. Thus, the Kirsch relations for stresses of a uniaxially stretched infinite isotropic linear-elastic plate cannot be correctly applied in the case under consideration.

The acoustoelasticity method has established a correlation between the results of numerical modeling and ultrasonic measurements of biaxial stresses. This is specifically noticeable in relation to points located near the zone of maximum tensile stresses.

The research results can be used in industrial nondestructive testing for stress diagnostics in rolled metal objects.

References

1. Belyaev AK, Polyanskiy VA, Tretyakov DA. Estimating of Mechanical Stresses, Plastic Deformations and Damage by means of Acoustic Anisotropy. *PNRPU Mechanics Bulletin*. 2020;(4):130–151. <https://doi.org/10.15593/perm.mech/2020.4.12>
2. Vatul'yan AO. The Theory of Inverse Problems in the Linear Mechanics of a Deformable Solid. *Journal of Applied Mathematics and Mechanics*. 2010;74(6):648–653. <https://doi.org/10.1016/j.jappmathmech.2011.01.004>
3. Murav'ev VV, Strizhak VA, Pryakhin AV. Acousto-Elastic Study of the Internal Stresses in Metal Structures. *Industrial Laboratory. Diagnostics of Materials*. 2016;82(12):52–57. (In Russ.) URL: <https://www.zldm.ru/jour/article/view/349/350> (accessed: 25.05.2024).
4. Kurashkin KV, Gonchar AV, Klyushnikov VA, Mishakin VV. Use of Texture-Dependent Ultrasonic Parameter as Indicator of Degradation of Hot-Rolled Thin-Sheet Steel Under Uniaxial Tension. *Journal of Nondestructive Evaluation*. 2022;41(2):46. <https://doi.org/10.1007/s10921-022-00879-w>
5. Uglov AL, Khlybov AA. On the Inspection of the Stressed State of Anisotropic Steel Pipelines Using the Acoustoelasticity Method. *Russian Journal of Nondestructive Testing*. 2015;51:210–216. <https://doi.org/10.1134/S1061830915040087>
6. Stepanova LN, Beher SA, Kurbatov AN, Tenitilov ES. Mechanical Strains Condition Investigation in Rails by means of Acoustic Elasticity and Strain Measurement. *News of Higher Educational Institutions. Construction*. 2013;655(7):103–109.
7. Ivanova Y, Partalin T, Pashkuleva D. Acoustic Investigations of the Steel Samples Deformation during the Tensile. *Russian Journal of Nondestructive Testing*. 2017;53(1):39–50. <https://doi.org/10.1134/S1061830917010077>
8. Volkova LV, Murav'eva OV, Murav'ev VV. Nonuniformity of Acoustic Anisotropy of Thick-Sheet Steel. *Steel in Translation*. 2021;51:335–341. <https://doi.org/10.3103/S0967091221050120>
9. Belyaev AK, Lobachev AM, Modestov VS, Pivkov AV, Polyanskii VA, Semenov AS, et al. Estimating the Plastic Strain with the Use of Acoustic Anisotropy. *Mechanics of Solids*. 2016;51:606–611. <https://doi.org/10.3103/S0025654416050149>
10. Murav'ev VV, Murav'eva OV, Volkova LV. Influence of the Mechanical Anisotropy of Thin Steel Sheets on the Parameters of Lamb Waves. *Steel in Translation*. 2016;46:752–756. <https://doi.org/10.3103/S0967091216100077>
11. Khlybov AA, Uglov AL. On an Acoustic Testing Method for Monitoring the Spatial Inhomogeneity of Plastic Deformation in Weakly Anisotropic Orthotropic Materials. *Russian Journal of Nondestructive Testing*. 2023;59(1):22–32. <https://doi.org/10.1134/S1061830923700183>
12. Nikitina NYe, Kamyshev AV, Kazachek SV. Application of the Acoustoelasticity Phenomenon in Studying Stress States in Technological Pipelines. *Russian Journal of Nondestructive Testing*. 2009;45:861–866. <https://doi.org/10.1134/S1061830909120043>
13. Nikitina NE. *Acoustoelasticity. Application Experience*. Nizhny Novgorod: TALAM; 2005. 208 p. (In Russ.)
14. Erofeev VI, Ilyakhinsky AV, Nikitina EA, Pakhomov PA, Rodyushkin VM. Ultrasonic Sensing Method for Evaluating the Limit State of Metal Structures Associated with the Onset of Plastic Deformation. *Physical Mesomechanics*. 2020;23:241–245. <https://doi.org/10.1134/S102995992003008X>
15. Murav'eva O, Murav'ev V, Volkova L, Kazantseva N, Nichipuruk A, Stashkov A. Acoustic Properties of Low-Carbon 2% Mn-Doped Steel Manufactured by Laser Powder Bed Fusion Technology. *Additive Manufacturing*. 2022;51:102635. <https://doi.org/10.1016/j.addma.2022.102635>
16. Kurashkin KV. Study of the Acoustoelastic Effect in an Anisotropic Plastically Deformed Material. *Acoustical Physics*. 2019;65(3):316–321. <https://doi.org/10.1134/S1063771019030047>
17. Grishchenko AI, Modestov VS, Polyanskiy VA, Tretyakov DA, Shtukin LV. Experimental Investigation of the Acoustic Anisotropy Field in the Sample with a Stress Concentrator. *St. Petersburg Polytechnical University Journal: Physics and Mathematics*. 2017;3(1):77–82. <https://doi.org/10.1016/j.spjpm.2017.02.005>
18. Kirsch G. Die Theorie der Elastizitat und die Bedurfnisse der Festigkeitslehre. *Zeitschrift des Vereines deutscher Ingenieure*. 1898;42:797–807.
19. Galin LA. Plane Elastico-Plastic Problem. *Journal of Applied Mathematics and Mechanics*. 1946;10(3):367–386. (In Russ.) URL: <https://pmm.ipmnet.ru/ru/get/1946/10-3/367-386> (accessed: 25.05.2024).

20. Nikitina NE, Kazachek SV. Theoretical and Experimental Study of Stress Concentration during Stretching of a Plate with a Cut. *Journal of Machinery Manufacture and Reliability*. 2008;37(1):38–41. URL: <https://link.springer.com/article/10.1007/s12001-008-1009-9> (accessed: 25.05.2024).

21. Nikitina NYe, Kamyshev AV, Kazachek SV. The Application of the Acoustoelasticity Method for the Determination of Stresses in Anisotropic Pipe Steels. *Russian Journal of Nondestructive Testing*. 2015;51:171–178. <https://doi.org/10.1134/S1061830915030079>

About the Authors:

Dmitry A. Tretyakov, Cand.Sci. (Eng.), Associate Professor of the Higher School of Automation and Robotics, Institute of Machinery, Materials, and Transport, Peter the Great St. Petersburg Polytechnic University (29 B, Polytechnicheskaya Str., St. Petersburg, 195251, Russian Federation), [SPIN-code](#), [ORCID](#), [ScopusID](#), [ResearcherID](#), dmitry.tretyakov93@yandex.ru

Dmitry S. Osovik, student of the Higher School of Automation and Robotics, Institute of Machinery, Materials, and Transport, Peter the Great St. Petersburg Polytechnic University (29 B, Polytechnicheskaya Str., St. Petersburg, 195251, Russian Federation), [ORCID](#), osovik.dim@gmail.com

Claimed Contributorship:

DA Tretyakov: academic advising, ultrasonic measurements and calculations by the acoustoelasticity method, preparation of the text.

DS Osovik: numerical finite element calculations, preparation of illustrations with a mesh model and fields of the stress-strain state of the plate.

Conflict of Interest Statement: the authors declare no conflict of interest.

All authors have read and approved the final version of the manuscript.

Об авторах:

Дмитрий Алексеевич Третьяков, кандидат технических наук, доцент Высшей школы автоматизации и робототехники института машиностроения, материалов и транспорта Санкт-Петербургского политехнического университета Петра Великого (195251, Российская Федерация, г. Санкт-Петербург, ул. Политехническая, 29 Б), [SPIN-код](#), [ORCID](#), [ScopusID](#), [ResearcherID](#), dmitry.tretyakov93@yandex.ru

Дмитрий Сергеевич Осовик, студент Высшей школы автоматизации и робототехники института машиностроения, материалов и транспорта Санкт-Петербургского политехнического университета Петра Великого (195251, Российская Федерация, г. Санкт-Петербург, ул. Политехническая, 29 Б), [ORCID](#), osovik.dim@gmail.com

Заявленный вклад авторов:

Д.А. Третьяков: научное руководство, ультразвуковые измерения и расчеты методом акустоупругости, подготовка текста.

Д.С. Осовик: численные конечноэлементные расчеты, подготовка иллюстраций с сеточной моделью и расчетными полями напряжений и деформаций пластины.

Конфликт интересов: авторы заявляют об отсутствии конфликта интересов.

Все авторы прочитали и одобрили окончательный вариант рукописи.

Received / Поступила в редакцию 23.09.2024

Reviewed / Поступила после рецензирования 20.10.2024

Accepted / Принята к публикации 28.10.2024

MECHANICS МЕХАНИКА



UDC 621.836.2; 621.89.012.75


Original Empirical Research

<https://doi.org/10.23947/2687-1653-2024-24-4-316-327>

Investigation of Parameters Influencing the Establishment of Hydrostatic Mode in the Crosshead-Guide Assembly of High-Pressure Plunger Pump

Marina V. Korchagina  , Valentin N. Stepanov Sergey O. Kireev , Alexey R. Lebedev 

Don State Technical University, Rostov-on-Don, Russian Federation

 ms.korchaginamv@mail.ru

EDN: TSFHRJ

Abstract

Introduction. When applying hydraulic fracturing technology to increase the efficiency of formation fluids, high-pressure pumps with a crosshead drive assembly are used. The major problem in the operation of these pumps is the wear of the crosshead guides. The crosshead is a flat sliding friction pair, leading to wear of the plunger seals and a decrease in the basic pump performance indicators. To solve this problem, it was previously proposed to use new materials and antifriction coatings, original designs of friction units, etc. However, a detailed description and solution to the problem under consideration has not been found in the literature at present. The objective of this study is to determine, under maximum load, the influence of the unit design, process temperature and pressure in the lubrication system on the values of the parameters that provide for the hydrostatic mode for a flat thrust bearing in a crosshead-guide unit of a high-pressure plunger pump.

Materials and Methods. The parameters were determined by the simulation technique using modal analysis applicable in the case of high dynamic loads acting on the studied unit. The calculation of the hydrodynamic parameters of the lubricating layer was based on the combination of the Reynolds model and the Stokes model in numerical modeling. The study was conducted using a calculation model representing a section of a plunger pump, considered as “flexible bodies” model, in the field of gravity forces. The mathematical dependences of the parameters under consideration were presented in the form of regression equations obtained from the results of a numerical experiment.

Results. The maximum load on the lower crosshead guide was determined, for which further hydrodynamic studies were conducted. Factors influencing the process were studied — gaps filled with lubricant (depending on the design of the unit), temperature, and pressure in the lubrication system. Mathematical dependences of the influence of the considered factors on the values of the parameters determining the establishment of the hydrostatic mode were obtained.

Discussion and Conclusion. The obtained mathematical models show the degree and influence of the factors under consideration on the studied parameters of the hydrostatic lubrication mode of the unit — the force acting on the crosshead from the lubricating layer, and the mass flow rate of the lubricant at the outlet of the system. It is found that the greatest influence is exerted by the change in the volume of gaps filled with lubricant, the mass flow rate of lubricant at the entrance to the system, which simulates the increase in pressure in the lubrication system of the friction unit. The results obtained do not contradict the conclusions reached in works on similar topics, and can be used in further research.

Keywords: plunger pump, crosshead, hydrostatic friction, flat sliding bearing, lubricating layer, hydrodynamic parameters

Acknowledgements. The authors would like to thank A.V. Efimov, Cand.Sci. (Engineering), Associate Professor, for consultations on crosshead assembly designs. The authors also appreciate the Editorial board of the Journal and anonymous reviewers for constructive comments that allowed improving the article.

Funding Information. The work was done within the framework of the state-financed R&D AAAA–A20–120012190068–8 “Research, Modeling and Development of Innovative Designs of Machinery and Equipment for Oil and Gas Fields”.

For Citation. Korchagina MV, Stepanov VN, Kireev SO, Lebedev AR. Investigation of Parameters Influencing the Establishment of Hydrostatic Mode in the Crosshead-Guide Assembly of High-Pressure Plunger Pump. *Advanced Engineering Research (Rostov-on-Don)*. 2024;24(4):316–327. <https://doi.org/10.23947/2687-1653-2024-24-4-316-327>

Оригинальное эмпирическое исследование

Исследование параметров, влияющих на установление гидростатического режима в узле крейцкопф-направляющие плунжерного насоса высокого давления

М.В. Корчагина  , В.Н. Степанов , С.О. Киреев  , А.Р. Лебедев 

Донской государственный технический университет, г. Ростов-на-Дону, Российская Федерация

 ms.korchaginamv@mail.ru

Аннотация

Введение. При использовании технологии гидроразрыва пласта для повышения эффективности пластовых флюидов используют насосы высокого давления с крейцкопфной компоновкой приводной части. Основная проблема при эксплуатации данных насосов — износ направляющих крейцкопфа, представляющего собой плоскую поступательную пару трения, приводящий к износу уплотнений плунжера и снижению основных показателей насоса. На пути решения данной задачи ранее было предложено применение новых материалов и антифрикционных покрытий, оригинальных конструкций узлов трения и пр. Однако детального описания и решения рассматриваемой проблемы в настоящее время в литературе не найдено. Целью данного исследования является определение при максимальной нагрузке влияния конструкции узла, температуры процесса и давления в системе смазки на значения параметров, обеспечивающих гидростатический режим для плоского подпятника в узле крейцкопф-направляющие плунжерного насоса высокого давления.

Материалы и методы. Определение параметров проводилось методом имитационного моделирования с использованием модального анализа, применимого в случае возникновения высоких динамических нагрузок, действующих на исследуемый узел. Расчет гидродинамических параметров смазочного слоя основан на объединении модели Рейнольдса и модели Стокса в численном моделировании. Исследование проводилось с использованием расчетной модели, представляющей собой секцию плунжерного насоса, рассматриваемой с точки зрения модели «гибких тел», в поле сил гравитации. Математические зависимости рассматриваемых параметров представлены в виде уравнений регрессии, полученных по результатам численного эксперимента.

Результаты исследования. Определено значение максимальной нагрузки на нижнюю направляющую крейцкопфа, для которого проводились дальнейшие гидродинамические исследования. Исследованы факторы, оказывающие влияние на процесс — зазоры, заполняемые смазкой (зависящие от конструкции узла), температура и давление в системе смазки. Получены математические зависимости влияния рассмотренных факторов на значения параметров, определяющих установление гидростатического режима.

Обсуждение и заключение. Полученные математические модели показывают степень и характер влияния рассматриваемых факторов на исследуемые параметры гидростатического режима смазки узла — силу, действующую на крейцкопф от смазочного слоя и массовый расход смазки на выходе системы. Выявлено, что наибольшее влияние оказывают изменение объема зазоров, заполненных смазкой, массовый расход смазки на входе в систему, который моделирует увеличение давления в смазочной системе узла трения. Полученные результаты не противоречат выводам, полученным в работах подобной тематики, и могут быть использованы в дальнейших исследованиях.

Ключевые слова: плунжерный насос, крейцкопф, гидростатическое трение, плоский поступательный подшипник, смазочный слой, гидродинамические параметры

Благодарности. Авторы выражают благодарность кандидату технических наук, доценту Ефимову А.В. за консультации по конструкциям крейцкопфных узлов.

Финансирование. Работа выполнена в рамках госбюджетной НИОКР АААА–А20–120012190068–8 «Исследование, моделирование и разработка инновационных конструкций машин и оборудования нефтегазовых промыслов».

Для цитирования. Корчагина М.В., Степанов В.Н., Киреев С.О., Лебедев А.Р. Исследование параметров, влияющих на установление гидростатического режима в узле крейцкопф-направляющие плунжерного насоса высокого давления. *Advanced Engineering Research (Rostov-on-Don)*. 2024;24(4):316–327. <https://doi.org/10.23947/2687-1653-2024-24-4-316-327>

Introduction. In recent years, hydraulic fracturing (HF) and massive hydraulic fracturing technologies have been widely used for the efficient extraction of formation fluids. The unique properties of the materials used in hydraulic fracturing provide a short production cycle and a small investment compared to the conventional extraction. Energy companies often refuse to participate in long-term projects with an unstable and unknown future. However, the flexible manufacturing process of HF technology avoids the uncertainty that is typical of mineral commodity markets that focus on the short-term [1]. The HF technology requires the use of high-pressure pumps (105 and 138 MPa) with high flow rates (9,000 l/min) and a capacity of more than 5,000 kW. The elastic seals of piston pumps do not withstand the required loads and do not allow adjusting the tightening forces of the seal pack. This has led to the use of plunger pumps under these conditions. With such capacities, the load on the pump rod (plunger) can reach more than 140 tons. With a pressure in the hydraulic part of the pump of 105 (138) MPa (using highly aggressive and highly abrasive media as working fluids), sealing packs operate under extremely difficult conditions, the modeling of which is the subject of papers [2, 3]. To relieve the radial load on the plunger seals, a crosshead arrangement of the drive part is used, when the entire radial load from the connecting rod group is taken up by the crosshead (slider). In high-power pumps (3,500–5,000 kW), the load on the crosshead in the contact zone with the guide can reach tens of tons, which can cause the breakdown of the oil film in the contact zone.

The crosshead, moving along the guides, provides radial fixation of the plunger, taking up significant alternate loads from the connecting rod and the pressure of the pump working medium. The crosshead is made of high-alloy steels and experiences significant loads, unlike the guides, which, in addition to centering, must provide a minimum of friction costs. Wear of the crosshead guides causes wear of the plunger seals and a decrease in pressure and feed. The crosshead guides are a composite structure — a rigid base made of carbon steel and antifriction liners. To reduce wear of the liners, liquid lubricant is supplied to the contact area under pressure by means of an oil hydraulic system. Uniform distribution of lubricant in the contact area is provided by oil distribution grooves on the crosshead. However, these measures ultimately provide a rather short service life (800–1,000 hours) of the crosshead group, which entails a reduction in the service life of the entire pump. This determines the urgency of studying the conditions for the occurrence of a hydrostatic mode in the unit under consideration, which is a flat sliding bearing. Such interaction is a typical example of flat sliding of a solid surface of one part relative to another, which occurs in numerous mechanisms. The friction pair under consideration is an open hydrostatic pair and has the advantages and disadvantages inherent in such systems. The instability of the position of the moving element causes inevitable deviations in the hydrostatic pressure.

Sliding bearings are units that determine the reliability of numerous modern high-speed and highly loaded machines (pumps, turbochargers, internal combustion engines, etc.). Sliding friction units have a number of common disadvantages that cause premature wear and reduce the service life of a machine or unit. These include insufficient load-bearing and damping capacity, leading to intensive wear, increased power losses, and lubricant consumption, as well as increased mechanical wear of the bearing surfaces of the pads (so-called “bearing sagging”), which requires increased clearances.

Due to its high topicality, numerous researchers are working on the problem under consideration. The authors [4] formulate indices for assessing the efficiency of the load by comparing the results to similar ones calculated on a virtual test model. In the area of research conducted for friction units, the use of new materials and antifriction coatings is proposed [5]. The quality of friction units is taken into account in the initial calculations and design. At the same time, modeling methodologies are constantly being developed and improved [6]. The parameters affecting friction units are constantly changing in accordance with operating conditions and materials. There is a need for new methods of modeling and experimental verification of the models obtained. A number of studies are devoted to the problem of developing optimized bearing units. Paper [7] describes an evolutionary optimization approach that enables designing a bearing with exceptional characteristics both under specific and extreme operating conditions. An optimization approach was used in developing a thrust bearing prototype. Some researchers are considering issues of obtaining a protective coating that reduces wear on contact surfaces [8]. The results of studies [9] are devoted to the development of a mathematical model of finite-length radial plain bearings and dampers with porous structural elements on the surface of the bearing bushing.

A number of researchers have noted the significance of selecting a suitable contact force model for analyzing the dynamic response due to the presence of clearance. The closest to the problem under consideration is the study presented in [10]. The conducted modeling and testing have shown that the dynamic characteristics of the mechanism taking into account friction have significant differences at the acceleration level. Considering friction increases energy consumption. The clearance in the prismatic pair of the slider(crosshead)-guides affects the dynamic characteristics and causes a chaotic

response of the mechanism. Based on the experiment conducted by the authors of the paper, a 3D model of a hinge with clearance for a slider-crank mechanism was proposed. This model is a comprehensive description of contact modes, which uses a group of contact force models reflecting various phenomena of contact action. Nonlinear dynamic characteristics of a mechanism with a sliding joint with clearance are established by combining theoretical calculation, modeling and experiment. However, the study does not cover the slider-guide pair, and therefore, does not provide a complete description and solution to the problem under consideration.

All the studies under consideration are to some extent devoted to the problem of increasing the service life of engineering devices, developing new technologies or improving existing technologies and calculation methods that increase the wear resistance of sliding friction units. Most of the papers are devoted to the operation of radial and thrust bearings with linear contact surfaces. The calculations provided in them cannot be fully applied to flat bearings and translational action. All the results obtained can form the basis of the present study, but require verification of applicability for the planar contact of rubbing surfaces considered here. To develop an optimal design of the friction unit power supply system, it is necessary to conduct a multifactorial study based on the Reynolds equation, whose boundary conditions are the conditions of equality of pressure in the forcing and drain planes. This calculation is needed to determine the parameters at which the hydrostatic friction mode is created. This research is aimed at determining, at maximum load, the effect of the unit design, process temperature, and pressure in the lubrication system on the values of the parameters that provide the hydrostatic mode for the flat thrust bearing in the crosshead-guide unit of a high-pressure plunger pump. The research objectives include developing a computational model, performing a numerical experiment, processing its results, identifying the relationship, and establishing mathematical dependences between the parameters that affect the establishment of the hydrostatic operating mode of a flat translational friction unit.

Materials and Methods. Currently, numerous widely known approaches to modeling the motion of deformable structures have been developed and are actively used to study complex engineering systems. The most acceptable research method in the case of impossibility or high cost of conducting an experiment on a real object, due to its high cost and significant mass and dimensional characteristics, is the method of simulation modeling. Among various methods of approximate solution to the problem, the finite element method (FEM) stands out. This is a simple, but at the same time very productive method, allowing for many different formulations oriented to various areas of application. It is well studied and widely used in practice. In the considered case of high dynamic loads acting on the studied unit, when it is required to take into account the inertial coupling between large displacements of the body and elastic deformations, the use of modal analysis is applicable. Modal analysis allows obtaining natural frequencies, shapes and vectors of modes, helps in the assessment of forces and reactions of the system at natural frequencies arising as a result of minimal deformations. The study of force interaction in the system under consideration is assumed on a solid model of the plunger pump section by means of modal analysis taking into account free vibrations and the frequency of natural modes of all elements of the mechanism. This method gives good results in the case of conducting studies on the dynamic characteristics of a structure subject to vibration [11].

Modeling the contact interaction of the crosshead and guides is reduced to solving a dynamic nonlinear problem of the mechanics of a deformable solid body. In this formulation, it represents a system consisting of a crank shaft, connecting rod, and crosshead-plunger. During the pump operating cycle, non-stationary dynamic stresses arise in the structural elements, and the contact interaction is characterized by a time-varying contact area and force. The motion of the mechanical system is described by the Lagrange equation of the second kind:

$$\frac{\partial}{\partial t} \left(\frac{\partial T}{\partial \dot{q}_i} \right) - \frac{\partial T}{\partial q_i} + \frac{\partial U}{\partial q_i} = Q_i, i = 1, n, \quad (1)$$

where T — kinetic energy of the system; U — potential energy; Q_i — generalized force; q_i — generalized speed; i — number of degrees of freedom of the given system.

The formulation of the FEM in terms of absolute coordinates takes into account small elastic deformations and the motion of the body as a whole. This formulation covers the entire spectrum of possible problems in the area under consideration, but it is very complex both for its study and for carrying out practical calculations. Therefore, the application of this approach in problems in which elastic bodies participate in macromotion, but are subject to only small deformations, often turns out to be unjustified from the point of view of efficiency.

The most effective method of model reduction is the Craig-Bampton method, widely known as dynamic reduction or the method of coupled substructures. When deriving the equations of the dynamics of elastic bodies subject to global motion and small deformations, the following additional approximation is introduced: the inertia of the elastic structure is concentrated in the nodes of its FEM model. This approximation makes it possible to derive the equations of dynamics quite simply. These equations themselves turn out to be simple. The Craig-Bampton method determines the matrices of the generalized mass and generalized rigidity through the modal transformation [12].

The study of hydrodynamic parameters of the lubricating layer is based on the combination of the Reynolds model and the Stokes model in numerical simulation.

Continuity equation:

$$\frac{\partial u}{\partial x} + \frac{\partial v}{\partial y} + \frac{\partial w}{\partial z} = 0. \quad (2)$$

Navier-Stokes equations for the model of motion of a viscous incompressible medium [13]:

$$\begin{aligned} \frac{\partial u}{\partial t} + u \cdot \frac{\partial u}{\partial x} + v \cdot \frac{\partial u}{\partial y} + w \cdot \frac{\partial u}{\partial z} &= \frac{-1}{\rho} \cdot \frac{\partial p}{\partial x} + \eta \cdot \Delta u + g_x, \\ \frac{\partial v}{\partial t} + u \cdot \frac{\partial v}{\partial x} + v \cdot \frac{\partial v}{\partial y} + w \cdot \frac{\partial v}{\partial z} &= \frac{-1}{\rho} \cdot \frac{\partial p}{\partial y} + \eta \cdot \Delta v + g_y, \\ \frac{\partial w}{\partial t} + u \cdot \frac{\partial w}{\partial x} + v \cdot \frac{\partial w}{\partial y} + w \cdot \frac{\partial w}{\partial z} &= \frac{-1}{\rho} \cdot \frac{\partial p}{\partial z} + \eta \cdot \Delta w + g_z, \end{aligned} \quad (3)$$

where v, w, u — components of the speed vector in the Cartesian coordinate system x, y, z ; η — kinematic viscosity; g_x, g_y, g_z — components of mass forces; ρ — density of matter.

The Reynolds-Stokes-Galerkin finite element method (R-SGFEM) with sliding boundary conditions was used to model and study the hydrodynamic lubrication. The effects were obtained on the basis of the Stokes equation, which was calculated by the Galerkin finite element method [14]. Among them, the modified Reynolds equation effectively handles the sliding boundary with different degrees of slippage. The Stokes equation solves the problem of recirculation in micro-channels. The Galerkin method with elements can accurately simulate the pressures and speed in the lubricating field with high accuracy and good adaptation to the shape of the boundaries. The motion of a continuous medium is described by a system of hydrodynamic equations.

Mathematical dependences are supposed to be presented in the form of regression equations obtained from the results of a numerical experiment. To construct regression equations, it is supposed to apply multivariate regression analysis using the theory of experimental design [15].

Research Results. As a calculation model for the numerical experiment, a section of a plunger pump was simulated consisting of: crank shaft (1), connecting rod (2), crosshead (3), crosshead guides (4), rod (5), plunger (6), seal pack (7) (Fig. 1). The materials of the elements used in the dynamic calculation were: steel with an elastic modulus of 207 GPa (crank shaft, connecting rod, crosshead-plunger), bronze with an elastic modulus of 106 GPa (guides) and 100 GPa (plunger seals).

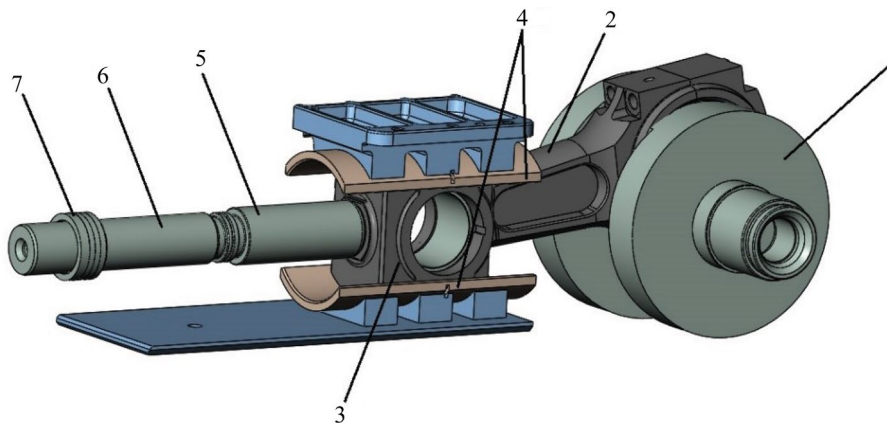


Fig. 1. Plunger pump section

The system was considered from the point of view of the “flexible body” model with six modes. An analysis of the crosshead motion in the field of gravitational forces was performed for each element of the section [16]. The connections (contact, rotation) were redefined, the shaft rotation frequency was set to 80 rpm (480 deg./s). Maximum plunger pressure was 105 MPa, plunger diameter — 80 mm. The pressure from the pumped medium on the plunger during the injection process was modeled by a spring with the appropriate stiffness, taking into account the plunger stroke of 164 mm. At suction, the spring is automatically disconnected. The dynamic model is shown in Figure 2.

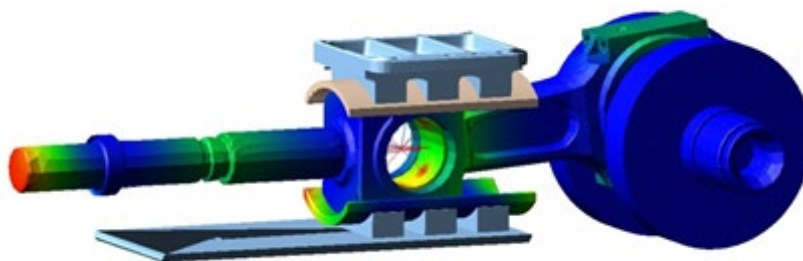


Fig. 2. Dynamic research model

Using this model, the maximum load on the lower crosshead guide was specified to be 43.5 kN, and its position corresponding to this load was determined. All further calculations were performed for this load value. Based on the determined position of the maximum load on the lower crosshead guide, the calculated hydrodynamic model shown in Figure 3 was simulated. The gap between the crosshead and the guide was 0.35 mm. The thickness of one of the six calculated boundary layers of the hydrodynamic calculation was 0.03 mm.

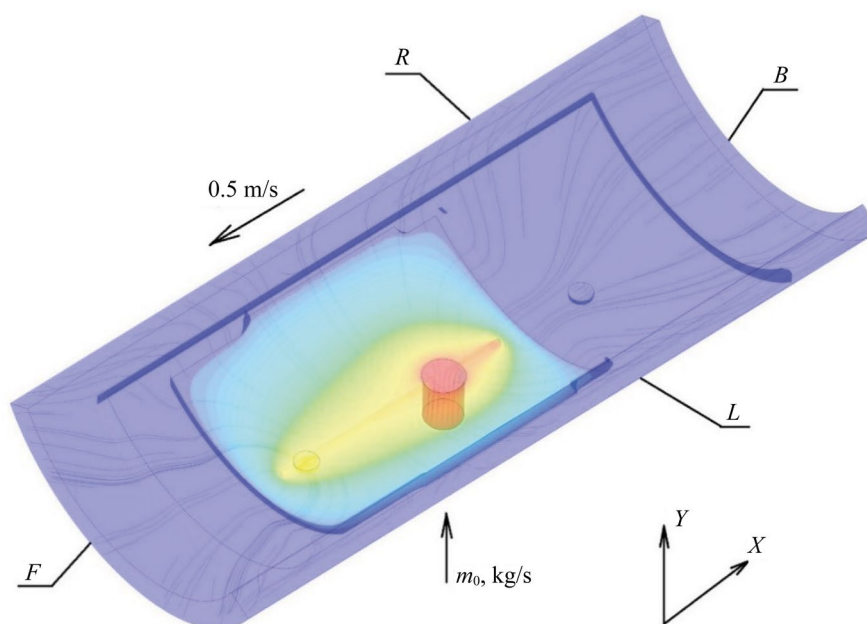


Fig. 3. Computational hydrodynamic model

The study was based on the following hypotheses and assumptions:

1. The friction pair slider — guide is a flat axial sliding bearing (thrust collar pivot-pad).
2. To provide hydrostatic conditions, the lubricant must be supplied under sufficiently high pressure so that the external load is balanced hydrostatically. To calculate, it is necessary to determine the amount and pressure of liquid required to be supplied into the gap to maintain the optimum thickness of the lubricating layer.
3. We make the assumption that the bearing is flat and wedge-shaped, we do not take into account the clearance. The clearance is considered as geometric (the space between the guides and the crosshead, corresponding to the fit in the unit under study).

The following parameters are accepted as factors affecting the provision of hydrostatic conditions for a flat plain bearing, which includes the crosshead-guide assembly under consideration:

- volume of lubricant in the gaps of the assembly under study depends on the design option, cm^3 ;
- lubricant temperature in the contact zone, $^{\circ}\text{C}$;
- pressure in the lubrication system, MPa.

The lubrication pressure was set through the lubrication flow rate at the system input. A preliminary regression analysis was performed to determine the relationship between these parameters. The pressure was measured for a fixed volume of 125 cm^3 and a temperature of 50°C . The results are shown in Figure 4.

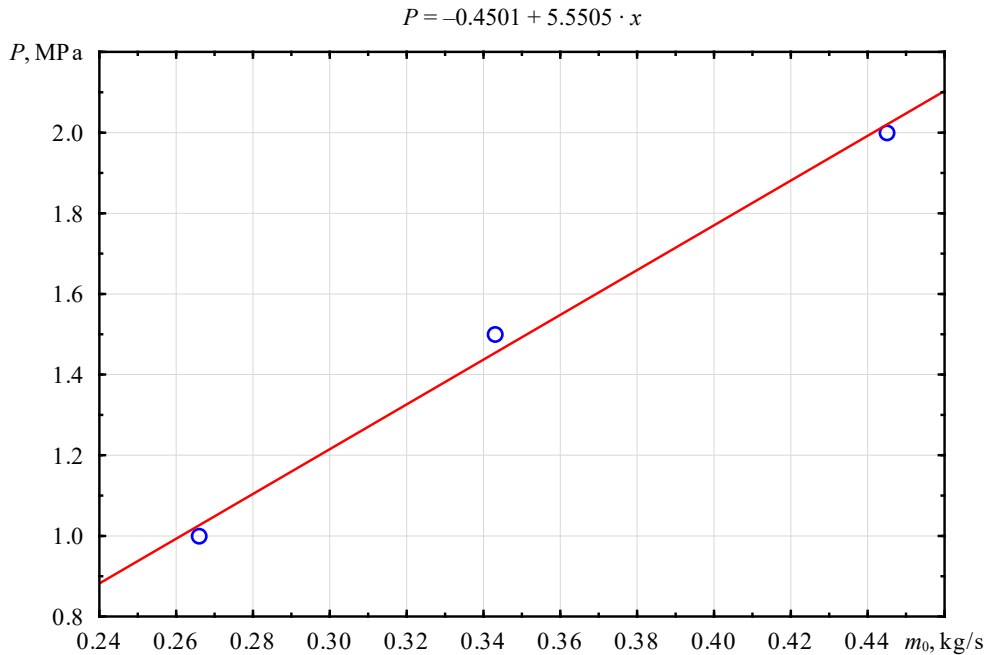


Fig. 4. Relationship between pressure F_{cm} and lubricant flow rate m_0 at the system input

The results presented in Figure 3 show a directly proportional, close to linear dependence and confirm the correctness of using the lubricant flow rate at the input to the system to simulate the process of setting the required pressure.

To conduct a full factorial experiment 2^3 , the variation intervals presented in Table 1 were determined, and the design matrix was compiled (Table 2).

The output parameters were: the force from the lubricating layer acting on crosshead F_{kp} , N and the lubricant flow rate at the outlet of the system, defined as the amount of liquid flowing through the gaps R , B , L , F .

Table 1

Intervals of Variation of Factors

Factor levels	Variation factors		
	x_1	x_2	x_3
	Design option (volume of lubrication system, cm^3)	Temperature, $^{\circ}\text{C}$	Pressure in lubrication system, MPa
Lower level (–)	Option 1 ($V_1 = 1.532$)	20	1.0
Basic level (0)	Option 2 ($V_2 = 4.125$)	50	1.5
Upper level (+)	Option 3 ($V_3 = 5.475$)	90	2.0

The design matrix and the response function values are presented in Table 2.

Table 2

Design Matrix 2^3 of Full Factorial Experiment

Experiment number	Input parameters			Output parameters	
	x_1 Design option (volume of lubrication system, m ³)	x_2 Temperature, °C	x_3 Pressure in lubrication system, MPa	y_1 Force from lubricant layer on crosshead F_{cm} , kN	y_2 Lubricant consumption parameter (rate of flow through gap), m kg/s
1	+ Option 3	+ 90	+ 2.0	15.803	0.3127
2	– Option 1	+ 90	+ 2.0	23.278	0.2104
3	+ Option 3	– 20	+ 2.0	44.940	0.3139
4	– Option 1	– 20	+ 2.0	66.074	0.2091
5	+ Option 3	+ 90	– 1.0	93.14	–0.1689
6	– Option 1	+ 90	– 1.0	14.005	0.1169
7	+ Option 3	– 20	– 1.0	27.310	–0.1661
8	– Option 1	– 20	– 1.0	40.969	0.1155
9	0 Option 2	0 50	0 1.5	18.579	0.2756

After processing the results of the numerical experiment, according to the presented planning matrix, dependences were obtained, describing the influence of the factors under consideration on additional parameters:

$$y_1 = 13.298 + 3.052x_1 + 3.56x_3 - 6.5x_1x_2 + 0.9x_1x_3 - 1.65x_1x_2x_3, \quad (4)$$

$$y_2 = 0.12 + 0.14x_3 + 0.096x_1x_3. \quad (5)$$

After the transition from the standard scale to the natural scale, the regression equations took the following form:

– equation describing the pressure from the lubricating layer on the crosshead, N:

$$F_{kp} = -10.94 + 2.67V - 9.75m_0 - 26.89t - 0.004Vt + 18.46Vm_0 + 1.64m_0t - 0.398m_0Vt. \quad (6)$$

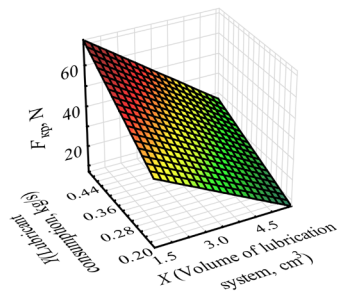
– equation describing lubricant consumption (flow through gaps), kg/s:

$$M = 0.59 - 1.37m_0 + 0.696m_0V. \quad (7)$$

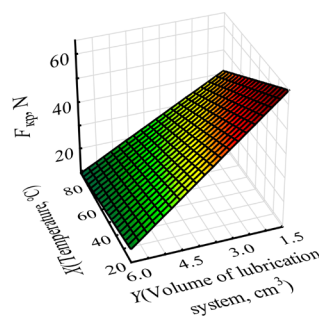
To visualize the results and perform their further analysis, graphs of the force function acting on the crosshead were constructed. When fixing one of the factors at the basic level, the obtained dependences are presented in Figure 5.

$$F_{kp} = 27.908 - 6.153 \cdot x + 12.63 \cdot y + 9.85 \cdot x \cdot y$$

$$F_{kp} = 91.229 - 0.4395 \cdot x - 12.502 \cdot y + 0.06 \cdot x \cdot y$$



a)



b)



$$F_{kp} = -8.692 + 0.224 \cdot x - 142 \cdot y + 1.25 \cdot x \cdot y$$

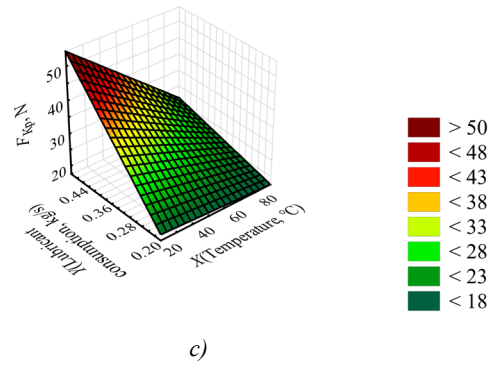


Fig. 5. Dependences of the value of the force acting on the crosshead on the lubricating layer, with different combinations of variation factors: *a* — value of the force at $t = 50^\circ\text{C}$; *b* — value of the force at $m = 0.346 \text{ kg/s}$; *c* — value of the force at $V = 4.125 \text{ cm}^3$

The graph of the dependence describing the lubricant consumption (flow through gaps) is shown in Figure 6.

$$P_{\text{см-вых}} = 0.59 - 0.37 \cdot x - 0.23 \cdot y + 0.649 \cdot x \cdot y$$

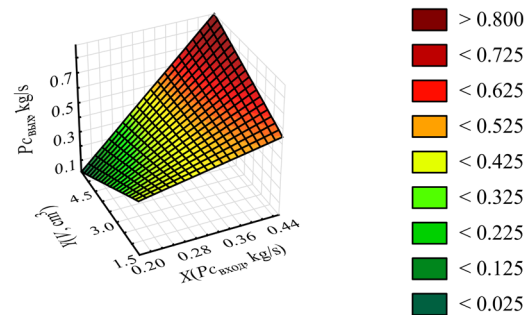


Fig. 6. Lubricant consumption at the system outlet (flow through gaps)

The dependences of the mass flow rate of lubricant at the system outlet (Fig. 6) and the mass flow rate of lubricant supply (Fig. 7) on the volume of gaps filled with lubricant were also determined.

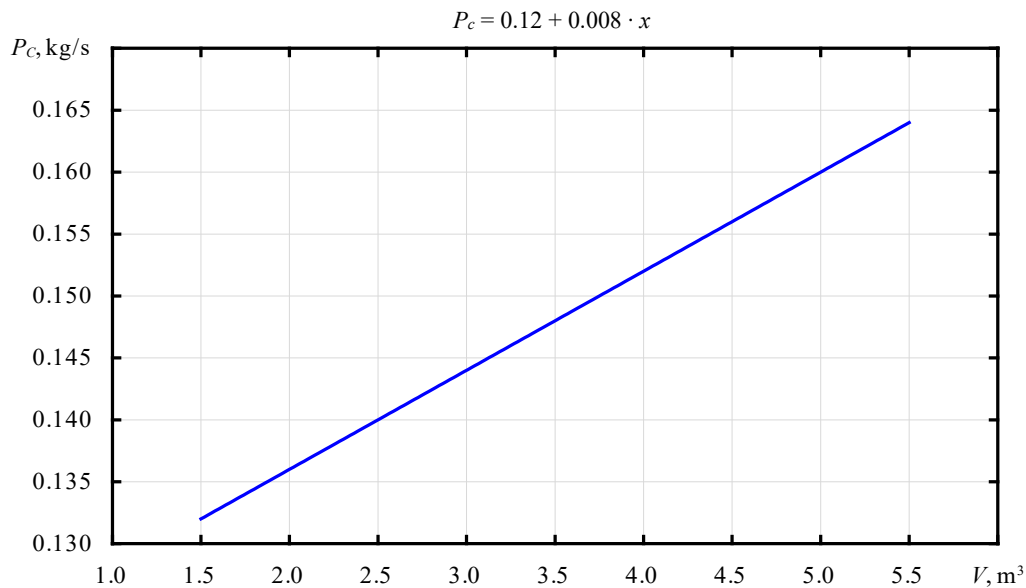


Fig. 7. Dependence of mass flow rate on volume

Discussion and Conclusion. The resulting mathematical model, describing the dependence of the force acting on the crosshead on the lubricating layer, shows that temperature has no great impact on the parameter under consideration, since the coefficient of the regression equation for this factor is recognized as insignificant, and its influence is realized only in pair interaction. This is well illustrated by Figure 4 *b, c*. The change in the volume of gaps

filled with lubricant and the mass flow rate of lubricant at the inlet to the system, simulating the increase in pressure in the lubrication system of the friction unit, have an equal effect. Simultaneous increase of these parameters leads to a decrease in the force acting on the crosshead and maintaining the hydrostatic mode of operation of the unit when the values are equal to the normal force pressing the crosshead against the guides. It is determined that an increase in volume leads to a decrease in pressure in the system, and the desired effect is not achieved (Fig. 4 a). When fixing the pressure in the lubrication system, an increase in the volume of gaps filled with lubricant results in an increase in the force being studied and gives a positive effect (Fig. 4 b). Similarly, fixing the gap with increasing pressure leads to an increase in the force of lubricant pressure on the crosshead (Fig. 4 c). The results of the numerical experiment do not contradict the conclusions made in works that describe basic equations of the hydrodynamic theory of lubrication [9], the rationale for the selection of initial and boundary conditions [10], as well as those papers that consider various methods of supplying lubricant to the friction unit [16]. These results can be used in further research.

The equations obtained for the mass flow rate of lubricant at the system outlet, defined as its outflow through the gaps, show that it depends on the parameters of the mass flow rate at the system inlet (lubricant supply to the unit) and the volume of the gaps. The other factors considered do not affect this parameter. In this case, an increase in volume leads to a decrease in the force acting on the crosshead, and an increase in mass flow leads to an increase in it (Fig. 5). The analysis of the relationship between the mass flow rate of lubricant at the outlet of the system and the volume of the gaps allows us to establish that the ratio of the increase in flow through the gaps to the increase in volume is approximately $\frac{1}{2}$. This shows that to maintain the pressure in the system at the same level with an increase in the volume of the gaps, a twofold increase in the mass flow rate of lubricant when feeding into the system is required.

To determine the extremum for each of the parameters under consideration that affect the process of establishing the hydrostatic mode and identify the optimal value of the initial operating parameters of the unit, it is necessary to conduct a second-order experiment that takes into account the patterns identified in this work.

References

1. Eckhouse G. United States Hydraulic Fracturing's Short-Cycle Revolution and the Global Oil Industry's Uncertain Future. *Geoforum*. 2021;127:246–256. <https://doi.org/10.1016/j.geoforum.2021.07.010>
2. Shaowen Mao, Kan Wu, George Moridis. Integrated Simulation of Three-Dimensional Hydraulic Fracture Propagation and Lagrangian Proppant Transport in Multilayered Reservoirs. *Computer Methods in Applied Mechanics and Engineering*. 2023;410:116037. <https://doi.org/10.1016/j.cma.2023.116037>
3. Huiying Tang, Philip H Winterfeld, Yu-Shu Wu, Zhao-qin Huang, Yuan Di, Zhengfu Pan, et al. Integrated Simulation of Multi-Stage Hydraulic Fracturing in Unconventional Reservoirs. *Journal of Natural Gas Science and Engineering*. 2016;36A:875–892. <https://doi.org/10.1016/j.jngse.2016.11.018>
4. Chen Yang, Xingwen Wu, Maoru Chi, Wubin Cai, Zikui Ma, Xuesong Yao. A Load Estimation Model for Axle Box Bearings of High-Speed Trains Based on Vehicle Dynamic Response. *Mechanical Systems and Signal Processing*. 2024;221:111728. <https://doi.org/10.1016/j.ymssp.2024.111728>
5. Vasilenko VV, Kirishchieva VI, Mukutadze MA, Shvedova VE. Investigation of the Wear Resistance of the Journal Bearing with Polymer-Coated Grooved Support Ring. *Advanced Engineering Research (Rostov-on-Don)*. 2022;22(4):365–372. <https://doi.org/10.23947/2687-1653-2022-22-4-365-372>
6. Polyakov RN, Savin AL. The Method of Long-Life Calculation for a Friction Couple “Rotor – Hybrid Bearing”. In: *Proc. 7th International Conference on Coupled Problems in Science and Engineering*. Barcelona: CIMNE; 2017: P. 433–440. URL: <https://upcommons.upc.edu/bitstream/handle/2117/190572/Coupled-2017-39-The%20method%20of%20long-life.pdf?sequence=1&isAllowed=y> (accessed: 20.07.2024).
7. Novotný P, Jonák M, Vacula J. Evolutionary Optimisation of the Thrust Bearing Considering Multiple Operating Conditions in Turbomachinery. *International Journal of Mechanical Sciences*. 2021;195:106240. <https://doi.org/10.1016/j.ijmecsci.2020.106240>
8. Shutin DV, Polyakov RN. Active Hybrid Bearings as Mean for Improving Stability and Diagnostics of Heavy Rotors of Power Generating Machinery. *IOP Conference Series: Materials Science and Engineering*. 2020;862(3):032098. <https://doi.org/10.1088/1757-899X/862/3/032098>

9. Kolesnikov IV, Mukutadze AM, Avilov VV. Ways of Increasing Wear Resistance and Damping Properties of Radial Bearings with Forced Lubricant Supply. In: Radionov A, Kravchenko O, Guzeev V, Rozhdestvenskiy Y (eds). *Proc. 4th International Conference on Industrial Engineering*. Cham: Springer; 2019. P. 1049–1062. http://doi.org/10.1007/978-3-319-95630-5_110
10. Polyakov R, Majorov S, Kudryavcev I, Krupenin N. Predictive Analysis of Rotor Machines Fluid-Film Bearings Operability. *Vibroengineering Procedia*. 2020;30:61–67. <http://doi.org/10.21595/vp.2020.21379>
11. Hemant Kumar Gurve, Rajesh Kumar Satankar. Modal and Harmonic Analysis of Stiffened Plate Using First-Order Shear Deformation Theory. *Materials Today: Proceedings*. 2022;51(1):325–331. <https://doi.org/10.1016/j.matpr.2021.05.416>
12. Yudakov AA. Principles of Flexible Body General Dynamic Equations Derivation Based on the Craig–Bampton Model and Their Practically Significant Ap-proximations. *Bulletin of the Udmurt University. Mathematics. Mechanics. Computer Science*. 2012;3:126–140. URL: http://vst.ics.org.ru/uploads/vestnik/3_2012/12-03-12.pdf (accessed: 20.07.2024).
13. Radchenko SG, Lapach SN. Basic Concepts of Multiple Regression Analysis. *Mathematical Machines and Systems*. (In Russ.) 2013;(1):150–156.
14. Xia Tao, Jiaxiong Hao, Yu Zhang. The Uniform Convergence of a Weak Galerkin Finite Element Method in the Balanced Norm for Reaction–Diffusion Equation. *Mathematics and Computers in Simulation*. 2024;220:445–461. <https://doi.org/10.1016/j.matcom.2024.02.001>
15. Polyakov RN, Savin LA, Vnukov AV. Mathematical Model of the Non-Contact Finger Seal with Active Management of the Clearance. *Fundamental and Applied Problems of Technics and Technology*. 2018;327(1):66–71.
16. Kornaeva EP, Kornaev AV, Kazakov YuN, Polyakov RN. Application of Artificial Neural Networks to Diagnostics of Fluid-Film Bearing Lubrication. *IOP Conference Series: Materials Science and Engineering*. 2020;734:012154. <http://doi.org/10.1088/1757-899X/734/1/012154>

About the Authors:

Marina V. Korchagina, Cand.Sci. (Eng.), Associate Professor of the Department of Machinery and Equipment of the Oil and Gas Complex, Don State Technical University (1, Gagarin Sq., Rostov-on-Don, 344003, Russian Federation), [SPIN-code](#), [ORCID](#), [ScopusID](#), [ResearcherID](#), ms.korchaginamv@mail.ru

Valentin N. Stepanov, Senior Lecturer of the Department of Machinery and Equipment of the Oil and Gas Complex, Don State Technical University (1, Gagarin Sq., Rostov-on-Don, 344003, Russian Federation), [SPIN-code](#), [ORCID](#), st_fem@bk.ru

Sergey O. Kireev, Dr.Sci. (Eng.), Professor, Head of the Department of Machinery and Equipment of the Oil and Gas Complex, Don State Technical University (1, Gagarin Sq., Rostov-on-Don, 344003, Russian Federation), [SPIN-code](#), [ORCID](#), [ScopusID](#), [ResearcherID](#), kireevso@yandex.ru

Alexey R. Lebedev, Cand.Sci. (Eng.), Associate Professor of the Department of Machinery and Equipment of the Oil and Gas Complex, Don State Technical University (1, Gagarin Sq., Rostov-on-Don, 344003, Russian Federation), [SPIN-code](#), [ScopusID](#), [ORCID](#), alex-diplom@mail.ru

Claimed Contributorship:

MV Korchagina: basic concept formulation, research objectives and tasks, preparation of the text, analysis of the research results, formulation of conclusions.

VN Stepanov: computational analysis.

SO Kireev: academic advising.

AR Lebedev: revision of drawings and the text, correction of the conclusions.

Conflict of Interest Statement: the authors claimed no conflict of interest.

All authors have read and approved the final manuscript.

Об авторах:

Марина Валерьевна Корчагина, кандидат технических наук, доцент кафедры машин и оборудования нефтегазового комплекса Донского государственного технического университета (344003, Российская Федерация, г. Ростов-на-Дону, пл. Гагарина, 1), [SPIN-код](#), [ORCID](#), [ScopusID](#), [ResearcherID](#), ms.korchaginamv@mail.ru

Валентин Николаевич Степанов, старший преподаватель кафедры машин и оборудования нефтегазового комплекса Донского государственного технического университета (344003, Российская Федерация, г. Ростов-на-Дону, пл. Гагарина, 1), [SPIN-код](#), [ORCID](#), st_fem@bk.ru

Сергей Олегович Киреев, доктор технических наук, профессор, заведующий кафедрой машин и оборудования нефтегазового комплекса Донского государственного технического университета (344003, Российская Федерация, г. Ростов-на-Дону, пл. Гагарина, 1), [SPIN-код](#), [ORCID](#), [ScopusID](#), [ResearcherID](#), kireevso@yandex.ru

Алексей Романович Лебедев, кандидат технических наук, доцент, доцент кафедры машин и оборудования нефтегазового комплекса Донского государственного технического университета (344003, Российская Федерация, г. Ростов-на-Дону, пл. Гагарина, 1), [SPIN-код](#), [ORCID](#), [ScopusID](#), alex-diplom@mail.ru

Заявленный вклад авторов:

М.В. Корчагина: формирование основной концепции, цели и задачи исследования, подготовка текста, анализ результатов исследований, формирование выводов.

В.Н. Степанов: проведение расчетов.

С.О. Киреев: научное руководство.

А.Р. Лебедев: доработка рисунков и текста, корректировка выводов.

Конфликт интересов: авторы заявляют об отсутствии конфликта интересов.

Все авторы прочитали и одобрили окончательный вариант рукописи.

Received / Поступила в редакцию 27.09.2024

Reviewed / Поступила после рецензирования 23.10.2024

Accepted / Принята к публикации 31.10.2024

MECHANICS МЕХАНИКА



UDC 621.822.17

Original Empirical Research

<https://doi.org/10.23947/2687-1653-2024-24-4-328-338>

Evaluation of Wear Resistance of a Modified Radial Bearing Design Taking into Account Compressibility and Viscosity of the Lubricant

Ekaterina A. Bolgova , Murman A. Mukutadze ✉,

Victor M. Prikhodko , Igor A. Kolobov

Rostov State Transport University, Rostov-on-Don, Russian Federation

✉ murman1963@yandex.ru

EDN: USPXOX

Abstract

Introduction. The challenge problem of the quality of lubricants has led to both large-scale and narrow-focused theoretical and applied studies that relate to the operational properties of lubricants. In particular, the authors of the publications are interested in the interaction of bearing and lubrication, since numerous types of machinery and equipment contain these elements. In the literature, the composites used to strengthen the bearing surface are compared, the most effective compositions are determined, and the advantages and disadvantages of the components are analyzed. Mathematical models have been proposed and tested for some of the processes of the interaction under consideration, and acceptable adequacy has been proved for some of them. However, the improvement of such solutions requires taking into account the specifics of the tribosystem. This issue has been poorly worked out, and the presented article is intended to fill this gap. When evaluating the wear resistance of a radial bearing, the compressibility of a high viscosity lubricant is taken into account.

Materials and Methods. The study was based on the tribocontact scheme, which included the radius of the polymer-coated shaft, the radius of the bearing sleeve, the height of the lubrication groove, and the thickness of the lubricating layer. To create new mathematical models that took into account the compressibility of the lubricant, the authors used three equations: motion of the liquid lubricant, continuity, and state. To verify the model, the results of calculations and laboratory tests were compared. In the experiments, a bearing with a groove to preserve lubrication was used. Its rotation speed, loads and temperature conditions were changed. Friction was measured using traditional methods and modern instruments.

Results. The bearing design was modified to take into account an additional factor — the compressibility of the lubricant. The new model predicted the bearing capacity of the part by 8–10% more accurately, and the coefficient of friction — by 7–9%. Fluctuations in the coefficient of friction up to 45 MPa (equivalent to a five-fold increase in load) were detected and explained. This was due to dynamic changes in the surface contact conditions and the effects of external parameters. Optimal applications of antifriction coatings based on hybrid composite materials were determined. The possibilities of practical use of calculation models of a journal bearing were expanded. Its critically important operational characteristics were evaluated in practice.

Discussion and Conclusion. The scientific research results described in this article make it possible to establish the performance characteristics of the bearing at the design stage. The significant potential of this approach has been identified in terms of increasing the reliability and durability of the studied part, and this seems to be an important step in the development of bearing and lubricant technologies. In the future, the authors intend to study such factors as temperature conditions, dynamic loads, and interaction with various lubricants. This will allow us to improve bearing designs and expand their application areas.

Keywords: journal plain bearing, lubricant compressibility, high viscosity lubricant, wear resistance assessment, tribosystem specificity, hybrid composite

Acknowledgements. The authors would like to thank Vladimir Ivanovich Kolesnikov, Academician of the Russian Academy of Sciences, Head of the Laboratory of the Theoretical Mechanics Department, for his assistance in conducting the experimental research.

For Citation. Bolgova EA, Mukutadze MA, Prikhodko VM, Kolobov IA. Evaluation of Wear Resistance of a Modified Radial Bearing Design Taking into Account Compressibility and Viscosity of the Lubricant. *Advanced Engineering Research (Rostov-on-Don)*. 2024;24(4):328–338. <https://doi.org/10.23947/2687-1653-2024-24-4-328-338>

Оригинальное эмпирическое исследование

Оценка износостойкости модифицированной конструкции радиального подшипника при учете сжимаемости и вязкости смазочного материала

Е.А. Болгова^{id}, М.А. Мукутадзе^{id}✉, В.М. Приходько^{id}, И.А. Колобов^{id}

Ростовский государственный университет путей сообщения, г. Ростов-на-Дону, Российская Федерация

✉ murman1963@yandex.ru

Аннотация

Введение. Актуальная проблема качества смазочных материалов обусловила как масштабные, так и узкопрофильные теоретические и прикладные исследования, которые касаются эксплуатационных свойств смазок. В частности, авторов публикаций интересует взаимодействие подшипника и смазки, так как эти элементы присутствуют во многих видах машин и оборудования. В литературе сопоставляются композиты, которыми упрочняют поверхность подшипников, определяются наиболее эффективные составы, анализируются достоинства и недостатки компонентов. По некоторым процессам рассматриваемого взаимодействия предложены и протестированы математические модели, и для некоторых из них доказана приемлемая адекватность. Однако совершенствование таких решений требует учитывать специфику трибосистемы. Данный вопрос проработан слабо, и представленная статья призвана восполнить этот пробел. При оценке износостойкости радиального подшипника принимается во внимание сжимаемость истинно вязкого смазочного материала.

Материалы и методы. Исследование базируется на схеме трибоконтакта, в которую включаются радиус вала с полимерным покрытием, радиус подшипниковой втулки, высота канавки для смазки и толщина смазочного слоя. Для создания новых математических моделей, учитывающих сжимаемость смазочного материала, авторы задеиствовали три уравнения: движения жидкого смазочного материала, неразрывности и состояния. Для верификации модели сопоставили итоги расчетов и лабораторных испытаний. В экспериментах использовали подшипник с канавкой для сохранения смазки. Меняли скорость его вращения, нагрузки и температурные условия. Трение измеряли традиционными методами и современными инструментами.

Результаты исследования. Конструкция подшипника модифицирована с учетом дополнительного фактора — сжимаемости смазочного материала. Новая модель на 8–10 % точнее прогнозирует несущую способность детали и на 7–9 % — коэффициент трения. Обнаружены и получили объяснение колебания коэффициента трения до 45 МПа (эквивалент пятикратного роста нагрузки). Это связано с динамическими изменениями в условиях контакта поверхностей и воздействиями внешних параметров. Определены оптимальные области применения антифрикционных покрытий на основе гибридных композиционных материалов. Расширены возможности практического использования расчетных моделей радиального подшипника скольжения. Оценены на практике его критически важные эксплуатационные характеристики.

Обсуждение и заключение. Результаты научных изысканий, описанных в данной статье, дают возможность на этапе проектирования устанавливать эксплуатационные характеристики подшипника. Выявлен значимый потенциал данного подхода в плане повышения надежности и долговечности исследованной детали, и это представляется важным шагом в развитии технологий подшипников и смазочных материалов. В перспективе авторы намерены изучить такие факторы, как температурные условия, динамические нагрузки и взаимодействие с различными смазочными материалами. Это позволит совершенствовать конструкции подшипников и расширять области их применения.

Ключевые слова: радиальный подшипник скольжения, сжимаемость смазочного материала, истинно вязкий смазочный материал, оценка износостойкости, специфика трибосистемы, гибридный композит

Благодарности. Авторы выражают благодарность руководителю лаборатории кафедры «Теоретическая механика» академику Российской академии наук Колесникову Владимиру Ивановичу за помощь в проведении экспериментальных исследований.

Для цитирования. Болгова Е.А., Мукутадзе М.А., Приходько В.М., Колобов И.А. Оценка износостойкости модифицированной конструкции радиального подшипника при учете сжимаемости и вязкости смазочного материала. *Advanced Engineering Research (Rostov-on-Don)*. 2024;24(4):328–338. <https://doi.org/10.23947/2687-1653-2024-24-4-328-338>

Introduction. In all sectors of the economy, the efficient functioning of mechanisms requires working with high-quality lubricants. The relevance of this issue stimulates scientific research that concerns the operational properties of lubricants. In particular, the authors of the publications are interested in the interaction of two elements that are present in many types of machines and equipment. It concerns, specifically, bearings and lubricants. Researchers often focus on such a lubricant parameter as compressibility. Mathematical models are built to determine the potential efficiency of lubrication in various bearing operating modes.

When studying lubricants, working oils are considered incompressible, but their volume still varies slightly. The compressibility factor depends on the chemical composition of the oil, its temperature, its pressure level, and contamination with air foam, which can cause cavitation, loss of efficiency, drop of oil pressure, origination of noise and erosion.

Modern lubricants play a significant role in increasing the service life of sliding bearings. Advances in chemistry and materials science have made it possible to create new types of lubricants that significantly reduce friction and wear on the working surfaces of bearing supports, and therefore increase the performance of the mechanism. The effect is provided by hydrocarbons and molybdenum disulfide in the lubricant. The use of such lubricants not only increases the reliability and durability of the supports, but also reduces the costs of maintenance and routine repairs.

Among modern developments in the field of polymer coatings, there are modifications of base materials to improve their tribological characteristics. For this purpose, fillers are introduced into polymers [1], including such solid lubricants as graphite, molybdenum disulfide, or carbon nanotubes [2]. These composites have significantly higher wear resistance and can withstand the effects typical of industrial tribosystems [3]. Such coatings can function without special lubricants, which significantly simplifies the operation of mechanisms and reduces operating costs.

At the design stage, it is critically important to take into account the interaction of various materials and coatings [4], to analyze their operation under the influence of high temperatures and speeds. At the same time, the accuracy of calculating the parameters of wear and interaction of surfaces allows for a significant increase of the reliability and durability of friction units [5]. Paper [6] describes the composite structure, friction and wear characteristics of the antifriction polymer fluoroplastic-containing coating.

Article [7] confirms that the use of rubber powder as a filler for epoxy polymers opens up new possibilities for the creation of highly effective vibration-absorbing composites. The flexibility of the process allows changing the type, content and combination of organomineral ingredients and epoxy compounds. This enables the material properties to be adapted to specific requirements and operating conditions, which in turn helps improve the performance and durability of equipment.

In [8], the problem of determining the nature of defects in fiberglass is considered. The solution [9] is based on the analysis of the Fourier spectra of acoustic emission signals. It is found that interlayer damage to matrices appears and develops in the frequency range of 160–240 kHz. This allows for early diagnostics and prompt elimination of such defects.

The fourfold increase in Young's modulus confirms the significance of using a soft template with modified polydopamine and a dispersion coating [10]. Higher mechanical strength combined with improved thermal conductivity opens up new prospects for the creation of materials capable of withstanding extreme operating conditions.

In [11], the capabilities of polyethylene oxide (PEO) solutions in chloroform are described. A multiple increase in relaxation and stretching time indicates a qualitative change in the behavior of PEO and opens up new prospects for its industrial application. Such changes can improve the mechanical stability of polymer products, expand the range of their use and increase the efficiency of production processes.

As experiment [12] has shown, metal powders in the coating composition improve adhesion with the base material. This helps to avoid peeling and cracking of the coating, which is critical for the durability and reliability of the brake transmission. In [13], it is established that combined coatings can become a mechanical engineering standard — they will be used in highly loaded and critical units.

Based on the results of research [14], it can be concluded that the introduction of antifriction polymer composite coatings with a cold-curing matrix is promising in terms of increasing the reliability and efficiency of industrial equipment.

In [15], a mathematical model for assessing electrophoretic mobility is proposed. It assumes that the presence of a scalable structure of the adsorbed permeable polymer layer does not affect the Poisson-Boltzmann distribution of ions in the double electrical layer.

One of the key approaches is the introduction of various fillers into polymers, including solid lubricants. Such fillers as graphite [16], molybdenum disulfide [17] and carbon nanotubes increase significantly the wear resistance of polymeric materials [18].

In [19], the aging of plasma-polymerized hexamethyldisiloxane coatings was investigated. They were activated by helium or dry air plasma and compared to the aging of plasma-activated silicone elastomer.

Experimental data [20] indicate that the operational properties of the material are determined by the nature of the acoustic emission. And this indicator depends on such variables as the filler concentration and curing temperature.

The theoretical calculation models [21] were visualized. Their accuracy was estimated. For this purpose, the following tribological parameters were compared:

- determined by the results of numerical analysis;
- calculated by adequate regression models obtained experimentally.

The comparison proved the high accuracy of the models — within 9–13%.

For successful application of the above methods, it is necessary to take into account the specifics of each tribosystem. Ignoring these features can lead to unreliable results or a decrease in the effectiveness of the proposed approaches.

It is noted in the literature that the liquid lubricant moving in the working gap contains atmospheric gases, on which compressibility depends. This means that its introduction into the model allows us to more accurately predict the behavior of the lubricant and the efficiency of lubrication in various bearing operating modes. This issue is not described in sufficient detail in the available sources, and the presented research is intended to fill this gap. The authors created and analyzed a mathematical model of a viscous lubricant in a bearing. Moreover, on the surface of the bearing bushing there was a composite coating with fluoroplastic. The modified design of the bearing provided for the presence of a polymer coating with a groove for better distribution of the lubricant, which, in turn, increased the durability of the system. Thus, a method for engineering calculations of the design of a radial plain bearing with a groove in a polymer coating has been developed for the first time. The new solution takes into account the compressibility of the lubricant and allows determining the basic tribotechnical parameters. The research objective is to evaluate the wear resistance of a modified design of a radial plain bearing taking into account the compressibility of a high viscosity lubricant. A high viscosity lubricant is a medium that obeys Newton's law. This dependence describes the flow of numerous oils at temperatures far from the freezing point quite well.

Materials and Methods. The wear resistance of a modified radial bearing design is estimated. Parameter Ω specifies the shaft speed. The surface of the modified bushing remains stationary.

A polar coordinate system is adopted to solve the problem. Its pole is the center of the bushing (Fig. 1).

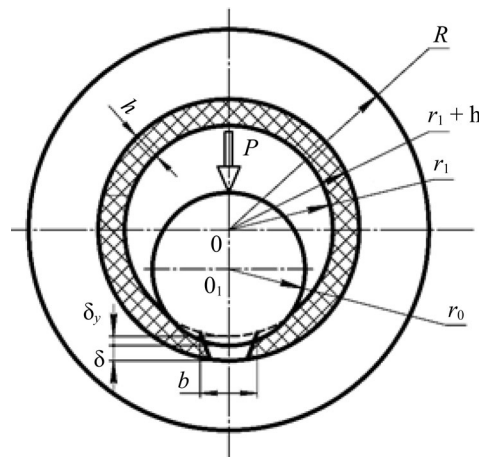


Fig. 1. Triboccontact diagram

In this case, the contours of the shaft, bushing and modified bushing are described in the form:

$$r' = r_0(1 + H), r' = r_1, r' = r_1 - \tilde{h}, \quad (1)$$

where r_0 — radius of the shaft with a polymer coating; r_1 — radius of the bearing bushing; \tilde{h} — groove height; H — thickness of the lubricating layer.

The viscosity of the lubricant depends on the pressure:

$$\mu' = \mu_0 e^{\alpha' p'}. \quad (2)$$

Here, μ' — coefficient of dynamic viscosity of the lubricant; μ_0 — characteristic viscosity; α' — constant; p' — hydrodynamic pressure in the lubricating layer; e — eccentricity.

The solution to this problem is based on the equation of liquid lubricant motion, the equation of continuity, and the equation of state:

$$\frac{\partial p'_i}{\partial r'} = 0, \mu' \frac{\partial^2 v_{\theta_i}}{\partial r'^2} = \frac{dp'_i}{d\theta}, \frac{\partial(\rho' v_{r'_i})}{\partial r'} + \frac{\rho' v_{r'_i}}{r'} + \frac{1}{r'} \frac{\partial(\rho' v_{\theta_i})}{\partial \theta} = 0, p' = \frac{\lambda \Omega^2 r^2}{2} \rho'. \quad (3)$$

Here, θ — angular coordinate; v_{θ_i} , $v_{r'_i}$ — components of the velocity vector of the lubricating medium; ρ' — density (dimensionless quantity).

Boundary conditions for system (3):

$$\begin{aligned} v_{\theta} &= 0, v_{r'} = 0 \text{ at } r' = r_1, \\ v_{\theta} &= v^*(\theta), v_{r'} = u^*(\theta) \text{ at } r' = r_1 - \tilde{h}, \\ v_{\theta} &= r_0 \Omega, v_{r'} = -\Omega e \sin \theta \text{ at } r' = r_0 + e \cos \theta, \\ p'(0) &= p'(\theta) = p_g. \end{aligned} \quad (4)$$

Here, p_g — lubrication supply pressure; Ω — shaft angular velocity.

We use formula (5) to move to dimensionless variables:

$$\begin{aligned} r' &= r_1 - \delta r, \delta = r_1 - r_0, v_{\theta_i} = \Omega r_0 v_i, v_{r'} = \Omega \delta u_i, \\ p' &= p^* p, p^* = \frac{\mu_0 \Omega r_0^2}{\delta^2}, \mu' = \mu_0 \mu, \alpha' = \frac{\alpha}{p^*}, \\ \rho^* &= \frac{2 p_g}{\lambda \Omega^2 r_0^2}, \rho' = \rho^* \rho. \end{aligned} \quad (5)$$

Here, u — horizontal component of the velocity; v — vertical component of the velocity.

As a result of transformations (5) taking into account (3) and (4), we obtain:

$$\frac{\partial p_i}{\partial r} = 0, \frac{\partial^2 v_i}{\partial r^2} = \frac{1}{\Lambda} e^{-\alpha p} \frac{dp_i}{d\theta}, \frac{\partial(\rho u_i)}{\partial r} + \frac{\partial(\rho v_i)}{\partial \theta} = 0, p = \rho, \quad (6)$$

$$\begin{aligned} v &= 1, u = -\eta \sin \theta \text{ at } r = 1 - \eta \cos \theta = h(\theta), \\ v &= 0, u = 0 \text{ at } r = 0, \theta_1 \leq \theta \leq \theta_2, \\ v &= v^*(\theta), u = u^*(\theta) \text{ at } r = \eta_2, 0 \leq \theta \leq \theta_1, \theta_2 \leq \theta \leq 2\pi, \end{aligned} \quad (7)$$

$$p(0) = p(\theta_1) = p(\theta_2) = p(2\pi) = \frac{p_g}{p^*},$$

$$p_3(\theta_2) = p_2(\theta_2), p_1(\theta_1) = p_2(\theta_1), Q = \text{const.}$$

Here, $\eta = e / \delta$ — design parameter of a bearing with a standard support profile; $\eta_1 = a' / \delta$ — design parameter of a bearing with an adapted support profile; $\Lambda = r_0^2 \mu \Omega / p_g \delta^2$ — compressibility parameter.

We introduce $z = e^{-\alpha p}$. After a series of transformations, we obtain:

$$\frac{\partial^2 v_i}{\partial r^2} = -\frac{1}{\Lambda} \frac{1}{\alpha} \frac{\partial z_i}{\partial \theta}, \frac{\partial(\rho u_i)}{\partial r} + \frac{\partial(\rho v_i)}{\partial \theta} = 0, p = \rho. \quad (8)$$

Boundary conditions for (8):

$$\begin{aligned} v &= 1, u = -\eta \sin \theta \text{ at } r = h(\theta), \\ v &= 0, u = 0 \text{ at } r = 0, \theta_1 \leq \theta \leq \theta_2, \\ v &= \frac{1}{h(\theta) - \eta_2}, u = \frac{\eta \sin \theta}{h(\theta) - \eta_2} \text{ at } r = \eta_2, 0 \leq \theta \leq \theta_1, \theta_2 \leq \theta \leq 2\pi, \end{aligned} \quad (9)$$

$$z(0) = z(\theta_1) = z(\theta_2) = z(2\pi) = e^{-\alpha \frac{p_g}{p^*}}.$$

Using method [22], we found a self-similar solution to problem (8) taking into account parameters (9):

$$\begin{aligned}\rho v_i &= \frac{\partial \psi_i}{\partial r} + V_i(r, \theta), \rho u_i = -\frac{\partial \psi_i}{\partial \theta} + U_i(r, \theta), \\ \psi_i(r, \theta) &= \tilde{\psi}_i(\xi_i), V_i(r, \theta) = p\tilde{v}_i(\xi_i), U_i(r, \theta) = -p\tilde{u}_i(\xi_i) \cdot h'(\theta), \\ \xi_i &= \frac{r_i}{h(\theta)} \text{ at } \theta_1 \leq \theta \leq \theta_2, \\ \xi_i &= \frac{r - \eta_2}{h(\theta) - \eta_2} \text{ at } 0 \leq \theta \leq \theta_1 \text{ и } \theta_2 \leq \theta \leq 2\pi.\end{aligned}\quad (10)$$

Here, ψ — function depending on self-similar variable ξ ; V , U — components of the velocity field; θ_2 — design parameter characterizing the groove depth.

Taking into account (10), equations (8) and boundary conditions (9) take the form:

$$\tilde{\psi}_i'''(\xi_i) = a_i, \tilde{v}_i''(\xi_i) = b_i, \tilde{u}_i'(\xi_i) + \frac{h(\theta)}{h'(\theta)} \frac{1}{p} \frac{dp}{d\theta} - \xi_i \tilde{v}_i'(\xi_i) = 0, \quad (11)$$

$$e^{-ap_i} \frac{p_i}{\Lambda} \frac{dp_i}{d\theta} = \frac{b_i p_i}{h^2(\theta)} + \frac{a_i}{h^3(\theta)}, \quad i = 1, 3,$$

$$e^{-ap_2} \frac{p_2}{\Lambda} \frac{dp_2}{d\theta} = \frac{b_2 p_2}{(h(\theta) + \tilde{h})^2} + \frac{a_2}{(h(\theta) + \tilde{h})^3},$$

$$\tilde{\psi}'_{\xi} = 0 \text{ at } \xi = 0, \xi = 1, \tilde{v}_i(\xi, \theta) = p, \tilde{u}_i = 0 \text{ at } \xi = 0,$$

$$\tilde{v}_i(\xi, \theta) = 0, \tilde{u}_i = -\eta \sin \theta \text{ at } \xi = 1, \int_0^1 \tilde{v}_i(\xi) d\xi = 0,$$

$$p(0) = p(\theta_1) = p(\theta_2) = p(2\pi) = 1. \quad (12)$$

Taking into account (12) and (13), we obtain the following systems of equations.

For the velocity field:

$$\begin{aligned}\tilde{\psi}'_1(\xi_1) &= a_1 \frac{\xi_1^2}{2} (\xi_1 - 1), \quad \tilde{v}_1(\xi_1) = b_1 \frac{\xi_1^2}{2} - \left(1 + \frac{b_1}{2}\right) \xi_1 + 1, \\ \tilde{\psi}'_2(\xi_2) &= a_2 \frac{\xi_2^2}{2} (\xi_2 - 1), \quad \tilde{v}_2(\xi_2) = b_2 \frac{\xi_2^2}{2} - \left(1 + \frac{b_2}{2}\right) \xi_2 + 1, \\ \tilde{\psi}'_3(\xi_3) &= a_3 \frac{\xi_3^2}{2} (\xi_3 - 1), \quad \tilde{v}_3(\xi_3) = b_3 \frac{\xi_3^2}{2} - \left(1 + \frac{b_3}{2}\right) \xi_3 + 1.\end{aligned}\quad (13)$$

For hydrodynamic pressure:

$$\begin{aligned}p_1 &= 1 + \frac{6\Lambda}{(1 - \eta_2)^2} \left(\theta + 2\tilde{\eta} \sin \theta - 2 \frac{1 - \tilde{\eta}^2}{2 + \tilde{\eta}^2} \frac{1}{p} (\theta + 3\tilde{\eta} \sin \theta) \right) \times \left(1 + \alpha \frac{p_g}{p^*} - \frac{\alpha^2}{2} \left(\frac{p_g}{p^*} \right)^2 \right), \\ \tilde{\psi}'_2(\xi_2) &= a_2 \frac{\xi_2^2}{2} - a_2 \frac{\xi_2}{2}, \tilde{v}_2(\xi_2) = b_2 \frac{\xi_2^2}{2} + \left(1 - \frac{b_2}{2}\right) \xi_2 + 1, u_2(\xi_2) = \int_0^{\xi_2} \xi_2 \tilde{v}'_2(\xi_2) d\xi_2, \\ p_2 &= 1 + 6\Lambda(\theta - \theta_1) \left(1 + \alpha \frac{p_g}{p^*} - \frac{\alpha^2}{2} \left(\frac{p_g}{p^*} \right)^2 \right) \left[1 + \frac{2\eta}{\theta - \theta_1} (\sin \theta - \sin \theta_1) - \frac{1}{p} \left(1 - \frac{\eta}{\theta_1} \sin \theta_1 \right) \left(1 + \frac{3\eta}{\theta - \theta_1} (\sin \theta - \sin \theta_1) \right) \right], \\ \tilde{\psi}'_3(\xi_3) &= a_3 \frac{\xi_3^2}{2} - a_3 \frac{\xi_3}{2}, \tilde{v}_3(\xi_3) = b_3 \frac{\xi_3^2}{2} + \left(1 - \frac{b_3}{2}\right) \xi_3 + 1, u_3(\xi_3) = \int_0^{\xi_3} \xi_3 \tilde{v}'_3(\xi_3) d\xi_3,\end{aligned}$$

$$p_3 = 1 + \frac{6\Lambda(\theta - \theta_2)}{(1 - \eta_2)^2} \left(1 + \alpha \frac{p_g}{p^*} - \frac{\alpha^2}{2} \left(\frac{p_g}{p^*} \right)^2 \right) \left[1 + \frac{2\tilde{\eta}}{\theta - \theta_2} (\sin \theta - \sin \theta_2) - \frac{1}{p} \left(1 - \frac{\tilde{\eta}}{\theta_2} \sin \theta_2 \right) \left(1 + \frac{3\tilde{\eta}}{\theta - \theta_2} (\sin \theta - \sin \theta_2) \right) \right]. \quad (14)$$

We solve equation (14) using the method of successive approximations, limiting ourselves to two approximations:

$$\begin{aligned} p_{11} = 1, \quad p_{21} = 1, \quad p_{31} = 1, \quad p_{12} = 6\Lambda \left(1 + \alpha \frac{p_g}{p^*} - \frac{\alpha^2}{2} \left(\frac{p_g}{p^*} \right)^2 \right) \frac{6\Lambda}{(1 - \eta_2)^2} \left(\theta + 2\tilde{\eta} \sin \theta - 2 \frac{1 - \tilde{\eta}^2}{2 + \tilde{\eta}^2} (\theta + 3\tilde{\eta} \sin \theta) \right), \\ p_{22} = +6\Lambda (\theta - \theta_1) \left(1 + \alpha \frac{p_g}{p^*} - \frac{\alpha^2}{2} \left(\frac{p_g}{p^*} \right)^2 \right) \left[1 + \frac{2\eta}{\theta - \theta_1} (\sin \theta - \sin \theta_1) - \left(1 - \frac{\eta}{\theta_1} \sin \theta_1 \right) \left(1 + \frac{3\eta}{\theta - \theta_1} (\sin \theta - \sin \theta_1) \right) \right], \\ p_{32} = \frac{6\Lambda(\theta - \theta_2)}{(1 - \eta_2)^2} \left(1 + \alpha \frac{p_g}{p^*} - \frac{\alpha^2}{2} \left(\frac{p_g}{p^*} \right)^2 \right) \left[1 + \frac{2\tilde{\eta}}{\theta - \theta_2} (\sin \theta - \sin \theta_2) - \left(1 - \frac{\tilde{\eta}}{\theta_2} \sin \theta_2 \right) \left(1 + \frac{3\tilde{\eta}}{\theta - \theta_2} (\sin \theta - \sin \theta_2) \right) \right]. \end{aligned} \quad (15)$$

To determine the bearing capacity and friction force, we use formula (15):

$$\begin{aligned} R_x &= \frac{6\mu_0 r_0^3 \Omega}{2\delta^2} \left[\int_0^{\theta_1} p_{12} \cos \theta d\theta + \int_{\theta_1}^{\theta_2} p_{22} \cos \theta d\theta + \int_{\theta_2}^{2\pi} p_{32} \cos \theta d\theta \right], \\ R_y &= \frac{6\mu_0 \omega r_0^3}{2\delta^2} \left[\int_0^{\theta_1} p_{12} \sin \theta d\theta + \int_{\theta_1}^{\theta_2} p_{22} \sin \theta d\theta + \int_{\theta_2}^{2\pi} p_{32} \sin \theta d\theta \right], \\ L_{TP} &= \mu \left(1 + \alpha p - \frac{\alpha^2}{2} p^2 \right) \left[\int_0^{\theta_1} \frac{1}{p} \left(\frac{\tilde{\psi}_1''(0)}{h^2(\theta)} + \frac{\tilde{v}_1'(0)}{h(\theta)} \right) d\theta + \right. \\ &\quad \left. + \int_{\theta_1}^{\theta_2} \frac{1}{p} \left(\frac{\tilde{\psi}_2''(0)}{(h(\theta) + \tilde{h})^2} + \frac{\tilde{v}_2'(0)}{(h(\theta) + \tilde{h})^3} \right) d\theta + \int_{\theta_2}^{2\pi} \frac{1}{p} \left(\frac{\tilde{\psi}_3''(0)}{h(\theta)} + \frac{\tilde{v}_3'(0)}{h(\theta)} \right) d\theta \right]. \end{aligned} \quad (16)$$

These studies established the effectiveness of the proposed theoretical model in the specified parameter ranges. The values of compressibility parameter $\Lambda = 0.1\text{--}0.9$ and stress σ in the range of 9–45 MPa were thoroughly tested to provide the accuracy of the model and the possibility of its wide application.

Experimental Conditions. The research started with the verification of the developed calculation model. For this purpose, numerical calculations were performed, which allowed us to estimate the basic parameters of the bearing operation. The verification included a comparison of these calculation data with the results of laboratory tests. The analysis showed that the calculation model predicted the behavior of the structure with a high degree of accuracy. At the same time, the identified deviations were within the permissible error limits.

Experiments for a bearing with an oil-supporting groove contour were conducted under various operating conditions. In particular, the rotation speed, loads and temperature conditions were changed. The correct selection of mode ensured reduced wear and increased heat generation. This approach allowed for increased reliability and reduced downtime in the operation of mechanisms.

The tests involved traditional methods of measuring friction and wear, as well as modern instrumental approaches. This maintained high measurement accuracy and helped to better understand the mechanisms of friction and wear in the new design.

Research Results. The study allowed us to more accurately represent the performance characteristics of polymer-coated bearings (Table 1). This is of great importance for their effective use in various engineering systems. With the new model, the forecast of data on the bearing capacity turned out to be 8–10% more accurate, and on the friction coefficient — 7–9%.

Table 1

Results of Theoretical Research

No	σ , MPa	Compressibility parameter				
		0.5	0.4	0.3	0.2	0.1
		Friction factor				
1	9	0.00479000	0.00711300	0.00310000	0.00100000	0.00023000
2	18	0.00149000	0.00149100	0.00165300	0.00008500	0.00049350
3	27	0.00017300	0.00009200	0.00000600	0.00005050	0.00002700
4	36	0.00007500	0.00014130	0.00000400	0.00001160	0.00000793
5	45	0.00000100	0.00001070	0.00000100	0.00002700	0.00000687

The experiment showed the presence of fluctuations in the friction factor. This was due to dynamic changes under the conditions of surface contact and the effects of external parameters. Such behavior of the friction factor with increasing load indicated the complexity of interactions in the system, especially considering the maximum recorded load indicator. It reached 45 MPa, which was equivalent to a step increase in load by 5 times (Table 2).

Table 2

Comparison of the Results of Theoretical Research and Experiment

No	Mode		Friction factor		
			Theoretical research		Experiment
	σ , MPa	V , m/s	Coating	Considering compressibility	
1	9	0.3	0.0105	0.0103	0.0104
2	18	0.3	0.0095	0.0093	0.0094
3	27	0.3	0.0090	0.0088	0.0090
4	36	0.3	0.0085	0.0080	0.0082
5	45	0.3	0.0075	0.0071	0.0074

The research results confirm the effectiveness of the developed theoretical models. Their implementation opens up the possibility to significantly increase the load capacity of parts and to considerably reduce the friction factor. The results of the work can be presented as follows.

1. The studies of radial plain bearings taking into account the compressibility of liquid lubricant, firstly, showed a significant improvement in their operational characteristics. Secondly, the accuracy of engineering calculations for the bearing capacity increased by 8–10%, and for the friction coefficient — by 7–9%.

2. The possibilities of practical use of calculation models of radial plain bearings were significantly expanded. Its critical operational characteristics were assessed in practice.

Discussion and Conclusion. The results of the research described in this article establish the main operational characteristics of the bearing at the design stage. The ability to increase the reliability and durability of the studied part is an important step in the development of bearing and lubricant technologies.

The new method is premised on a theoretical background and has been experimentally confirmed. It is intended for the development of calculation models of radial plain bearings. An important characteristic of the part is an antifriction

polymer coating with a groove for retaining the lubricating fluid. The compressibility and rheological properties of the lubricant are taken into account. Considering the previously established parameters of such grooves, a calculation model that describes in detail the behavior of the bearing in the hydrodynamic mode, has been developed. Particular attention is paid to the compressibility of a high viscosity lubricant, whose viscosity parameters depend on the pressure and friction conditions. Recommendations for the use of bearings with optimal grooves have been formulated.

The scope of application of the research results is engineering design and verification calculations when it is necessary to maintain a hydrodynamic lubrication mode. The method is potentially in demand in mechanical engineering, aircraft manufacturing, instrument making, and other industries.

In further research, it seems appropriate to study such factors as temperature conditions, dynamic loads, and interaction with various lubricants. This will allow for the improvement of bearing designs and expansion of their application areas.

References

1. Glushko SP. Investigation of the Electrospark Coating, Alloying and Strengthening Technology. *Advanced Engineering Research (Rostov-on-Don)*. 2021;21(3):253–259. <https://doi.org/10.23947/2687-1653-2021-21-3-253-259>
2. Tamarkin MA, Tishchenko EhEh, Verchenko AV, Troitskii VM. Formation of Surface Layer Quality under Abrasive Treatment of Polymer-Composite Materials. *Advanced Engineering Research (Rostov-on-Don)*. 2020;20(3):235–242. <https://doi.org/10.23947/2687-1653-2020-20-3-235-242>
3. Negmatov SS, Abed NS, Saidakhmedov RKh, Ulmasov TU, Grigoriev AY, Sergienko VP, et al. Research of Viscoelastic and Adhesion-Strength Property and Development of Effective Vibration Absorbing Composite Polymeric Materials and Coatings of Mechanical Engineering Purpose. *Plasticheskie massy*. 2020;(7–8):32–36. <https://doi.org/10.35164/0554-2901-2020-7-8-32-36>
4. Pavlycheva EA. Development of Polymer Composition for Obtaining a Protective Coating on Metal Surfaces. *International Journal of Applied and Fundamental Research*. 2022;(2):33–36. <https://doi.org/10.17513/mjpf.13355>
5. Kharlamov PV. Application of the Physico-Chemical Approach to Study the Mechanism of Formation of Secondary Frictional Transfer Structures on the Control Surface. *Vestnik RGUPS*. 2021;83(3):37–45.
6. Kohanovsky VA, Petroff IA. Friction and Wear of Composites with Polytetrafluorethylene. *Vestnik of DSTU*. 2009;9(1):30–35.
7. Petukhov DS, Adamov AA, Keller IE. Selection and Identification of a Model of Elasto-Viscoplasticity of the Filled Fluorocomposite according to Free and Constrained Compression Tests. *Advanced Engineering Research (Rostov-on-Don)*. 2022;22(3):180–192. <https://doi.org/10.23947/2687-1653-2022-22-3-180-192>
8. Bryansky AA, Bashkov OV, Belova IV, Bashkova TI. Investigation of Damages Formed in Polymer Composite Materials under Bending Loading and Their Identification by the Acoustic Emission Technique. *Frontier Materials and Technologies*. 2022;(2):7–16. <https://doi.org/10.18323/2782-4039-2022-2-7-16>
9. Shizheng Wen, Si-Dan Zhong, Wei-Qiu Kan, Pu-Su Zhao, Yuan-Chun He. Experimental and Theoretical Investigation on the Hydrochromic Property of Ni(II)-Containing Coordination Polymer with an Inclined 2D→3D Polycatenation Architecture. *Journal of Molecular Structure*. 2022;1269(12):133753. <https://doi.org/10.1016/j.molstruc.2022.133753>
10. Liyuan Jin, Wenjing Cao, Pei Wang, Na Song, Peng Ding. Interconnected MXene/Graphene Network Constructed by Soft Template for Multi-Performance Improvement of Polymer Composites. *Nano-Micro Letters*. 2022;14:133. <https://doi.org/10.1007/s40820-022-00877-7>
11. Robertson BP, Calabrese MA. Evaporation-Controlled Dripping-onto-Substrate (DoS) Extensional Rheology of Viscoelastic Polymer Solutions. *Scientific Reports*. 2022;12(1):4697. [10.1038/s41598-022-08448-x](https://doi.org/10.1038/s41598-022-08448-x)
12. Ivanochkin PG, Bolshikh IV, Talakhadze TZ, Bolshikh EP. Application of Antifriction Polymer Composite Coatings in the Brake Lever Transmission of Locomotive. *Vestnik RGUPS*. 2022;85(1):16–22. https://doi.org/10.46973/0201-727X_2022_1_16
13. Ivanochkin PG, Manturov DS, Danilchenko SA, Karpenko KI. Study on the Effect of the Sealers on the Steel Surface Layer Modified by Electrical Discharge Machining. *Solid State Phenomena*. 2021;316:713–719. <https://doi.org/10.4028/www.scientific.net/SSP.316.713>
14. Bryansky AA, Bashkov OV. Identification of Acoustic Emission Sources in a Polymer Composite Material under the Cycle Tension Loading. *Frontier Materials and Technologies*. 2021;(3):19–27. <https://doi.org/10.18323/2073-5073-2021-3-19-27>

15. Santanu Saha, Yasuhisa Adachi. Shielding Behavior of Electrokinetic Properties of Polystyrene Latex Particle by the Adsorption of Neutral Poly(ethylene Oxide). *Journal of Colloid and Interface Science*. 2022;626:930–938. <https://doi.org/10.1016/j.jcis.2022.06.154>
16. Kohanovsky VA, Kamerova EA. Composites Cover Content Fluor Ethylene in the Liquid Lubricants. *Friction and Lubrication in Machines and Mechanisms*. 2014;(1):34–37.
17. Kohanovsky VA, Kamerova EA. Friction of the Polymeric Cover in the Liquid Lubricants. *Friction and Lubrication in Machines and Mechanisms*. 2014;(4):17–20.
18. Kamerova EA, Vlasenko IB, Snezhina NG, Oganessian PA. Methodology for Studying the Effect of Liquid Media on Fluoroplastic-Containing Antifriction Coatings. *Ural'skii nauchnyi vestnik*. 2014;100(21);137–142. (In Russ.)
19. Egghe T, Ghobeira R, Morent R, Hoogen-Boom R, De Geyter N. Comparative Study of the Aging Behavior of Plasma Activated Hexamethyldisiloxane-Based Plasma Polymers and Silicone Elastomer Thin Films. *Progress in Organic Coatings*. 2022;172:107091. <https://doi.org/10.1016/j.porgcoat.2022.107091>
20. Peng Hu, Ru Xie, Qingyi Xie, Chunfeng Ma, Guangzhao Zhang. Simultaneous Realization of Antifouling, Self-Healing, and Strong Substrate Adhesion via a Bioinspired Self-Stratification Strategy. *Chemical Engineering Journal*. 2022;449:137875. <https://doi.org/10.1016/j.cej.2022.137875>
21. Khasyanova DU, Mukutadze MA. The Regularity of Increasing the Wear Resistance of a Modified Radial Slide Bearing. *Journal of Machinery Manufacture and Reliability*. 2023;(2):71–81. <https://doi.org/10.31857/S0235711923010066>
22. Kirishchieva VI, Lagunova EO, Mukutadze MA. Increasing the Wear Resistance of the Radial Bearing with a Non-Standard Support Profile and Polymer Coating on the Shaft Surface. *Vestnik UGATU*. 2023;27(2):15–23. https://doi.org/10.54708/19926502_2023_27210015

About the Authors:

Ekaterina A. Bolgova, Postgraduate student of the Higher Mathematics Department, Rostov State Transport University (2, Rostovskogo Strelkovogo Polka Narodnogo Opolchenia Sq., Rostov-on-Don, 344038, Russian Federation), [SPIN-code](#), [ORCID](#), [ScopusID](#), bolgova_katya6@mail.ru

Murman A. Mukutadze, Dr.Sci. (Eng.), Professor, Head of the Higher Mathematics Department, Rostov State Transport University (2, Rostovskogo Strelkovogo Polka Narodnogo Opolchenia Sq., Rostov-on-Don, 344038, Russian Federation), [SPIN-code](#), [ORCID](#), [ScopusID](#), [ResearcherID](#), murman1963@yandex.ru

Victor M. Prikhodko, Dr.Sci. (Eng.), Professor, Head of the Descriptive Geometry and Engineering Graphics Department, Rostov State Transport University (2, Rostovskogo Strelkovogo Polka Narodnogo Opolchenia Sq., Rostov-on-Don, 344038, Russian Federation), [SPIN-code](#), [ORCID](#), [ScopusID](#), [ResearcherID](#), v.m.prihodko@yandex.ru

Igor A. Kolobov, Cand.Sci. (Eng.), Associate Professor, Dean of the Transportation Management Faculty, Rostov State Transport University (2, Rostovskogo Strelkovogo Polka Narodnogo Opolchenia Sq., Rostov-on-Don, 344038, Russian Federation), [SPIN-code](#), [ORCID](#), [ScopusID](#), upp@rgups.ru

Claimed Contributorship:

EA Bolgova: computational analysis, text preparation, correction of the conclusions.

MA Mukutadze: academic advising, analysis of the research results, revision of the text.

VM Prikhodko: basic concept formulation, research objectives and tasks.

IA Kolobov: testing, formulation of conclusions.

Conflict of Interest Statement: the authors declare no conflict of interest.

All authors have read and approved the final version of the manuscript.

Об авторах:

Екатерина Александровна Болгова, аспирант кафедры высшей математики Ростовского государственного университета путей сообщения (344038, Российская Федерация, г. Ростов-на-Дону, пл. Ростовского Стрелкового Полка Народного Ополчения, 2), [SPIN-код](#), [ORCID](#), [ScopusID](#), bolgova_katya6@mail.ru

Мурман Александрович Мукутадзе, доктор технических наук, профессор, заведующий кафедрой высшей математики Ростовского государственного университета путей сообщения (344038, Российская Федерация, г. Ростов-на-Дону, пл. Ростовского Стрелкового Полка Народного Ополчения, 2), [SPIN-код](#), [ORCID](#), [ScopusID](#), [ResearcherID](#), murman1963@yandex.ru

Виктор Маркович Приходько, доктор технических наук, профессор, заведующий кафедрой начертательной геометрии и графики Ростовского государственного университета путей сообщения (344038, Российская Федерация, г. Ростов-на-Дону, пл. Ростовского Стрелкового Полка Народного Ополчения, 2), [SPIN-код](#), [ORCID](#), [ScopusID](#), [ResearcherID](#), v.m.prikhodko@yandex.ru

Игорь Анатольевич Колобов, кандидат технических наук, доцент, декан факультета управления процессами перевозок Ростовского государственного университета путей сообщения (344038, Российская Федерация, г. Ростов-на-Дону, пл. Ростовского Стрелкового Полка Народного Ополчения, 2), [SPIN-код](#), [ORCID](#), [ScopusID](#), upp@rgups.ru

Заявленный вклад авторов:

Е.А. Болгова: расчеты, подготовка текста, корректировка выводов;

М.А. Мукутадзе: научное руководство, анализ результатов исследований, доработка текста;

В.М. Приходько: формирование основной концепции, цели и задачи исследования.

И.А. Колобов: проведение эксперимента, формирование выводов.

Конфликт интересов: авторы заявляют об отсутствии конфликта интересов.

Все авторы прочитали и одобрили окончательный вариант рукописи.

Received / Поступила в редакцию / 01.10.2024

Reviewed / Поступила после рецензирования / 23.10.2024

Accepted / Принята к публикации / 31.10.2024

MECHANICS МЕХАНИКА




UDC 534.1, 539.3, 539.5

Original Theoretical Research

<https://doi.org/10.23947/2687-1653-2024-24-4-339-346>

Finite Element Modeling of a Flat Cell of Highly Porous Piezocomposite with Inclined Edges Taking into Account Nonuniform Polarization

Arkadiy N. Soloviev^{1,2}  , Maria S. Germanchuk^{2,3} ¹ Southern Federal University, Rostov-on-Don, Russian Federation² Crimean Engineering and Pedagogical University named after Fevzi Yakubov, Simferopol, Republic of Crimea³ V.I. Vernadsky Crimean Federal University, Simferopol, Republic of Crimea solovievare@gmail.com

EDN: BNDEOI

Abstract

Introduction. Highly porous composites — metal foams — are widely used due to their mechanical properties. The literature presents various methods for their mathematical modeling, including those based on periodic Gibson-Ashby cells. Piezoactive composites have a number of properties, such as high sensor sensitivity and a large bandwidth. This is the reason for the interest in their modeling. However, when constructing such models from piezoceramic materials, a certain difficulty, associated with the selection of the distribution of preliminary polarization, arises. It should be noted that this issue, specifically for highly porous piezoceramics, has not been sufficiently studied in the literature. Therefore, the objective of this work was to establish the effect of the polarization model on the characteristics of the piezoactive composite.

Materials and Methods. The design material was PZT-4 piezoceramics, whose polarization depended significantly on the conditions of its guidance (model geometry, electrode arrangement). The study was divided into two steps: in the first, the residual polarization was calculated based on the theory known in the literature, the implementation of which was performed in the ACELAN package; in the second, a number of problems for a composite cell were solved, and the dependence of its properties on the polarization model was found. The finite element method implemented in the ACELAN package was used as a method for solving the corresponding boundary value problems of electroelasticity for piecewise inhomogeneous bodies.

Results. The problem of determining nonuniform polarization for two types of flat cell designs of highly porous piezoceramics was solved. Some features of the obtained polarization distribution were noted, in particular, its nonuniformity and the presence of counter polarization in some edges. The problems of determining natural frequencies and vibration modes “intra cell” and their dependence on the polarization model (homogeneous and nonhomogeneous) were solved. It was noted that some frequencies differed by 10%, while the vibration modes coincided qualitatively. The dependence of the stress-strain state and output characteristics on polarization, whose difference in some values reached 15%, was analyzed.

Discussion and Conclusion. The process of polarization of highly porous piezoceramics has a number of features that must be taken into account to obtain reliable information about its mechanical and electrical behavior. Auxetic properties, the difference in the mechanical and electrical response of the cell in question are directly related to these features. Thus, the polarization model has a significant impact on the characteristics of the piezoactive composite, which determines the importance of its correct selection. The results obtained should be taken into account when modeling representative volumes of highly porous piezoelectric composites to determine their effective properties, on the basis of which models of piezoelectric devices are constructed, and their output characteristics are calculated.

Keywords: highly porous piezoceramics, nonuniform polarization, flat cell, finite element method

Acknowledgements. The authors would like to thank the Editorial board and the reviewers for their attentive attitude towards the article.

Funding Information. The research was done with the financial support from the Russian Science Foundation (no. 22–11–00302) at the Southern Federal University, <https://rscf.ru/project/22-11-00302/>

For Citation. Soloviev AN, Germanchuk MS. Finite Element Modeling of a Flat Cell of Highly Porous Piezocomposite with Inclined Edges Taking into Account Nonuniform Polarization. *Advanced Engineering Research (Rostov-on-Don)*. 2024;24(4):339–346. <https://doi.org/10.23947/2687-1653-2024-24-4-339-346>

Оригинальное теоретическое исследование

Конечно-элементное моделирование плоской ячейки высокопористого пьезокompозита с наклонными ребрами с учетом неоднородной поляризации

А.Н. Соловьев^{1,2} , М.С. Германчук^{2,3} 

¹ Южный Федеральный Университет, г. Ростов-на-Дону, Российская Федерация

² Крымский инженерно-педагогический университет имени Февзи Якубова, г. Симферополь, Республика Крым

³ Крымский федеральный университет им. В.И. Вернадского, г. Симферополь, Республика Крым

 solovievare@gmail.com

Аннотация

Введение. Высокопористые композиты — металлические пены — находят широкое применение в силу своих механических свойств. В литературе представлены различные методы их математического моделирования, в том числе, на основе периодических ячеек Гибсона-Эшби. Пьезоактивные композиты обладают рядом свойств, таких как высокая чувствительность сенсоров и широкая полоса пропускания. Этим обусловлен интерес к их моделированию. Однако при построении таких моделей из пьезокерамических материалов возникает определенная трудность, связанная с выбором распределения предварительной поляризации. Следует отметить, что этот вопрос, особенно для высокопористой пьезокерамики, недостаточно изучен в литературе. Поэтому целью данной работы являлось установление влияния модели поляризации на характеристики пьезоактивного композита.

Материалы и методы. Материал конструкции — пьезокерамика PZT-4, поляризация которой существенно зависит от условий ее наведения (геометрии модели, расположения электродов). Исследование разделено на два шага: в первом проводится расчет остаточной поляризации на основе теории известной в литературе, реализация которой осуществлена в пакете ACELAN; на втором решается ряд задач для ячейки композита и находится зависимость ее свойств от модели поляризации. В качестве метода решения соответствующих краевых задач электроупругости для кусочно-неоднородных тел используется метод конечных элементов, реализованный в пакете ACELAN.

Результаты исследования. Решена задача определения неоднородной поляризации для двух видов конструкций плоских ячеек высокопористой пьезокерамики. Отмечены некоторые особенности полученного распределения поляризации, в частности, ее неоднородность и наличие встречной поляризации в некоторых ребрах. Решены задачи определения собственных частот и форм колебаний «внутри ячейки» и их зависимость от модели поляризации (однородной и неоднородной). Отмечается, что некоторые частоты отличаются на 10 %, а формы колебаний качественно совпадают. Проанализирована зависимость напряженно деформированного состояния и выходных характеристик от поляризации, разница некоторых значений которых достигала 15 %.

Обсуждение и заключение. Процесс поляризации высокопористых пьезокерамик имеет ряд особенностей, которые необходимо учитывать для получения достоверных сведений о ее механическом и электрическом поведении. Ауксесктивные свойства, разница в механическом и электрическом отклике рассматриваемой ячейки напрямую связаны с этими особенностями. Таким образом модель поляризации оказывает существенное влияние на характеристики пьезоактивного композита, что определяет важность ее правильного выбора. Полученные результаты надо учитывать при моделировании представительных объемов высокопористых пьезоэлектрических композитов для определения их эффективных свойств, на основе которых строятся модели пьезоэлектрических устройств и рассчитываются их выходные характеристики.

Ключевые слова: высокопористая пьезокерамика, неоднородная поляризация, плоская ячейка, метод конечных элементов

Благодарности. Авторы выражают благодарность редакции журнала и рецензентам за внимательное отношение к статье.

Финансирование. Исследование выполнено при финансовой поддержке гранта РНФ (№ 22–11–00302) в Южном федеральном университете, <https://rscf.ru/project/22-11-00302/>

Для цитирования. Соловьев А.Н., Германчук М.С. Конечноэлементное моделирование плоской ячейки высокопористого пьезокомпозита с наклонными ребрами с учетом неоднородной поляризации. *Advanced Engineering Research (Rostov-on-Don)*. 2024;24(4):339–346. <https://doi.org/10.23947/2687-1653-2024-24-4-339-346>

Introduction. One type of highly porous composite is a material constructed on the basis of Gibson-Ashby cells [1]. In [2], an assessment of the effective Young's modulus of porous titanium with open pores was performed on the basis of a three-dimensional array of such cells. A comparison of the mechanical behavior of foam models composed of regular and irregular arrays of open Gibson-Ashby cells is carried out in [3]. Figure 1 *a* shows an open cell, Figures 1 *b* and 1 *c* show modified Gibson-Ashby models with inclined edges for functionally graded lattice structures [4].

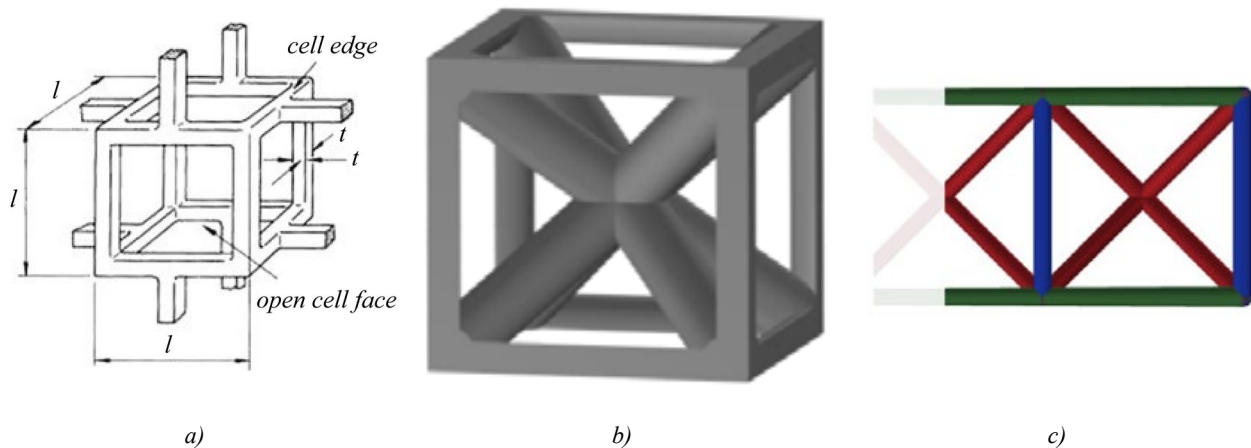


Fig. 1. Schemes of cells of highly porous composite: *a* — Gibson-Ashby cell; *b* — cell with inclined edges; *c* — flat cell with inclined edges [4]

Homogenization methods used in modeling the effective properties of composites are considered in monographs [5, 6]. Studies on highly porous structures, such as foamy, cellular, honeycomb and cell structures are presented in monographs [7, 8], in reviews [9–12], etc. In [13], the polarization of porous piezoceramics is considered experimentally and theoretically and, based on a model example, features of some of its effective properties are theoretically explained, as mentioned above. The issue of the effective properties of highly porous piezoelectric composites has not been sufficiently studied in the scientific literature. This is primarily due to the fact that the process of describing the polarization of such structures is a certain difficulty. This research is aimed at studying the influence of the polarization model on the stress-strain state of the cell and on the effective properties of such composites. Two models are considered: the first model assumes uniform polarization; in the second, the polarization distribution is calculated using methods and software known from the literature, among the developers of which is one of the authors of this work. The work shows that the selection of the polarization model affects significantly the mechanical properties of highly porous piezoelectric composites.

Materials and Methods

Mathematical Formulation of the Problem. We consider flat cells, which are elements of the structures shown in Figure 1. The cell material is PZT-4 piezoelectric ceramics, described within the framework of the linear theory of electroelasticity [14]. In the homogeneous case, it is polarized along the vertical axis, in the inhomogeneous case — the polarization distribution is found according to the theory proposed in [15] and implemented in the finite element package ACELAN [16].

Materials. Figure 2 *a* shows the geometry of a flat cell corresponding to the diagram in Figure 1 *a* with inclined edges, the edge thickness is 1 mm, the external size is 10×10 mm. Figure 2 *b* shows a diagram of nonuniform polarization for such a design, when the electrodes are located on the outer ends of the upper and lower vertical edges. The characteristic feature of this polarization is its nonuniformity on inclined edges and the presence of its opposite directions on the upper and lower horizontal edges. Figure 2 *c* shows the polarization scheme for a composite element, whose periodicity is realized through vertical and horizontal edges. The characteristic feature of the polarization of this element is the practically unpolarized horizontal edges.

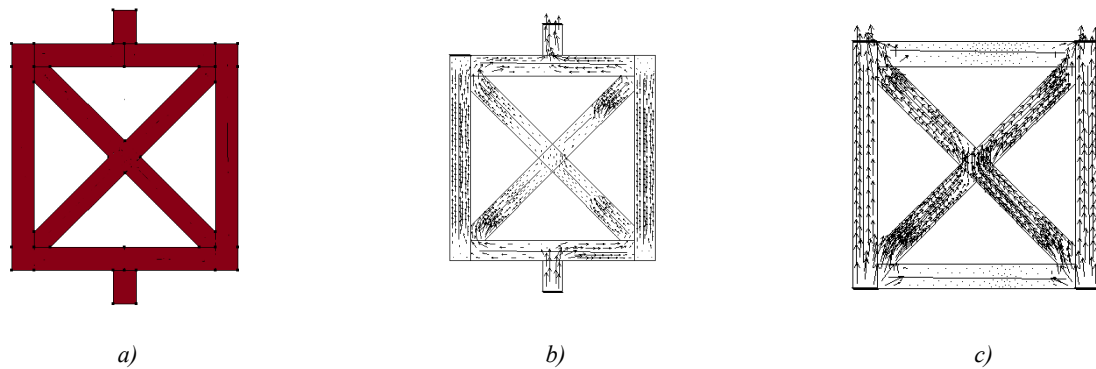


Fig. 2. Schemes of cells and polarization of highly porous composite:
a — uniform polarization; *b* — nonuniform with electrodes on the lower and upper edges;
c — nonuniform with electrodes at the bottom and top on vertical edges

Methods. The finite element method (FEM) implemented in the ACELAN package is used as a method for calculating the stress-strain state of cells [16].

Research Results. First, the natural frequencies and modes of vibrations “inside” the cell shown in Figures 1 *c* and 2 *c* are investigated. In this case, the cell is fixed in the corners along the normal to the thickness of the horizontal and vertical edges, which corresponds to the periodicity of the composite structure. Table 1 shows the natural resonance frequencies for uniform and nonuniform polarization (Fig. 2 *c*), and Figures 3–5 show eigenvibrations at these frequencies.

Table 1

Eigenvibrations for Uniform and Nonuniform Polarization

Frequency number \ Polarization	Eigenvibrations in Hz	
	Uniform	Nonuniform
1	0.43455×10^5	0.41271×10^5
2	0.47277×10^5	0.47249×10^5
3	0.54538×10^5	0.49562×10^5
4	0.61497×10^5	0.58611×10^5
5	0.67255×10^5	0.67607×10^5

For nonuniform polarization 1, 3 and 4, the natural frequencies are lower than for uniform polarization, but the vibration modes 1–5 are qualitatively the same. Therefore, Figures 3–5 show the natural modes for a cell with uniform polarization. Figures 3 *a*, *b* show the distribution of horizontal displacements and vertical displacements for the first vibration mode. In Figures 4 *a*, *b* the distributions for the second mode of vibrations of horizontal displacements and for the third mode of vibrations of vertical displacements are presented, respectively. In Figures 5 *a*, *b* the distribution of the displacement modulus is presented for the fourth and fifth modes, respectively.

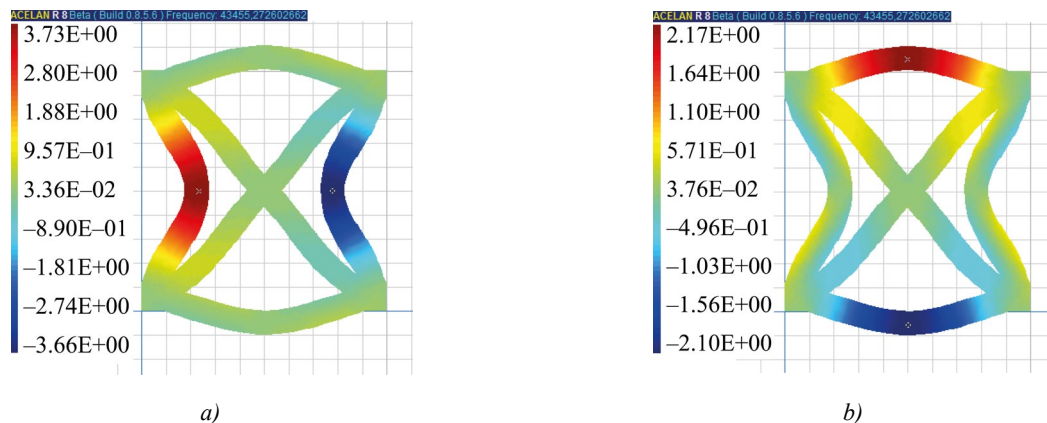


Fig. 3. The first form of vibrations is uniform polarization:
a — distribution of horizontal displacements;
b — distribution of vertical displacements

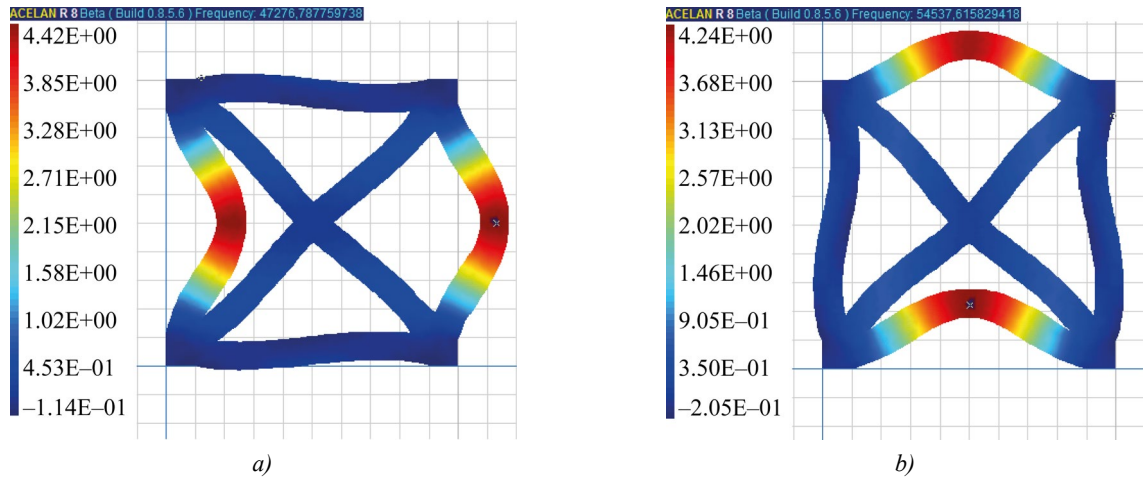


Fig. 4. Forms of vibrations of uniform polarization:
a — the second, distribution of horizontal displacements;
b — the third, distribution of vertical displacements

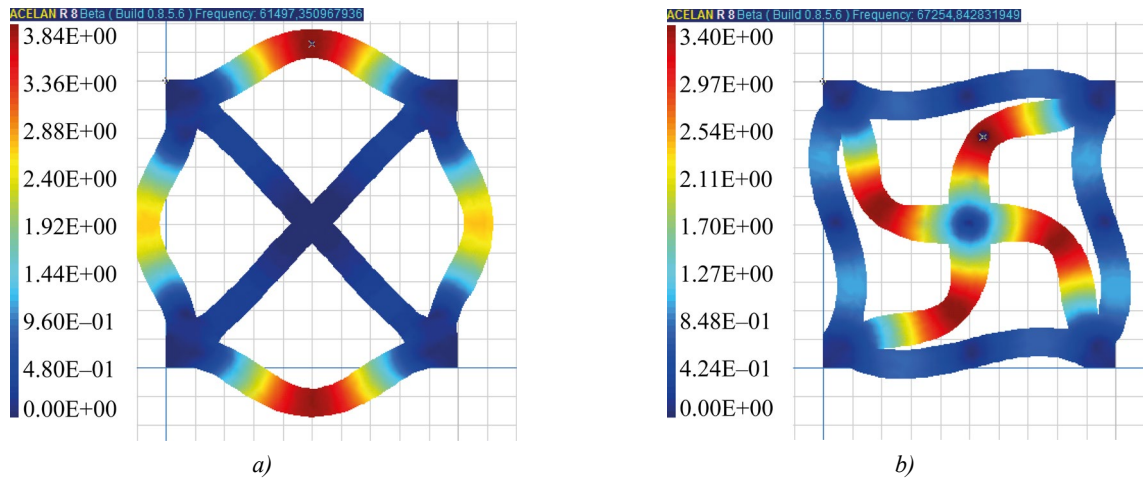


Fig. 5. Forms of vibrations with the distribution of the displacement modulus for uniform polarization: *a* — the fourth mode; *b* — the fifth mode

With longitudinal tension-compression of this cell in the vertical direction in the composite structure (modeled by the free entire upper surface and the application of uniform pressure to the upper end of the vertical edges), the displacement in the case of uniform polarization is 15% greater (Fig. 6 *a*). The potential on free electrodes is 3% higher in the case of nonuniform polarization. It should be noted that the shear stresses (Fig. 6 *b*) are 10% higher in the case of nonuniform polarization. The electromechanical coupling coefficient for the 7th oscillation mode (Fig. 6 *c*) is 14% higher for uniform polarization of the cell.

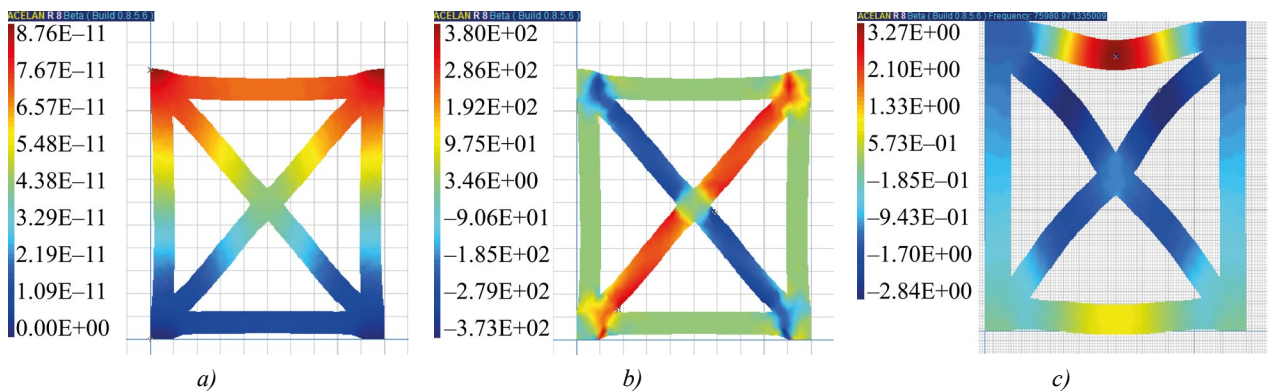


Fig. 6. Under the action of vertical pressure, the distribution of:
a — vertical displacement; *b* — shear stresses;
c — distribution of vertical displacement on the 7th oscillation mode

Calculations for the cell presented in Figures 2 *a* and *b* show that the vertical displacement (Fig. 7 *a*) under the action of pressure on the end of the upper rod in the case of nonuniform polarization is 11% greater. In statics, under the action of the potential difference at the lower and upper ends, the cell exhibits auxetic properties, which is associated with the opposite polarization (Fig. 2 *b*) of the horizontal edges. Figures 7 *b* and *c* show the distributions of vertical and horizontal displacements. It is evident that when stretched vertically, the cell also expands horizontally.

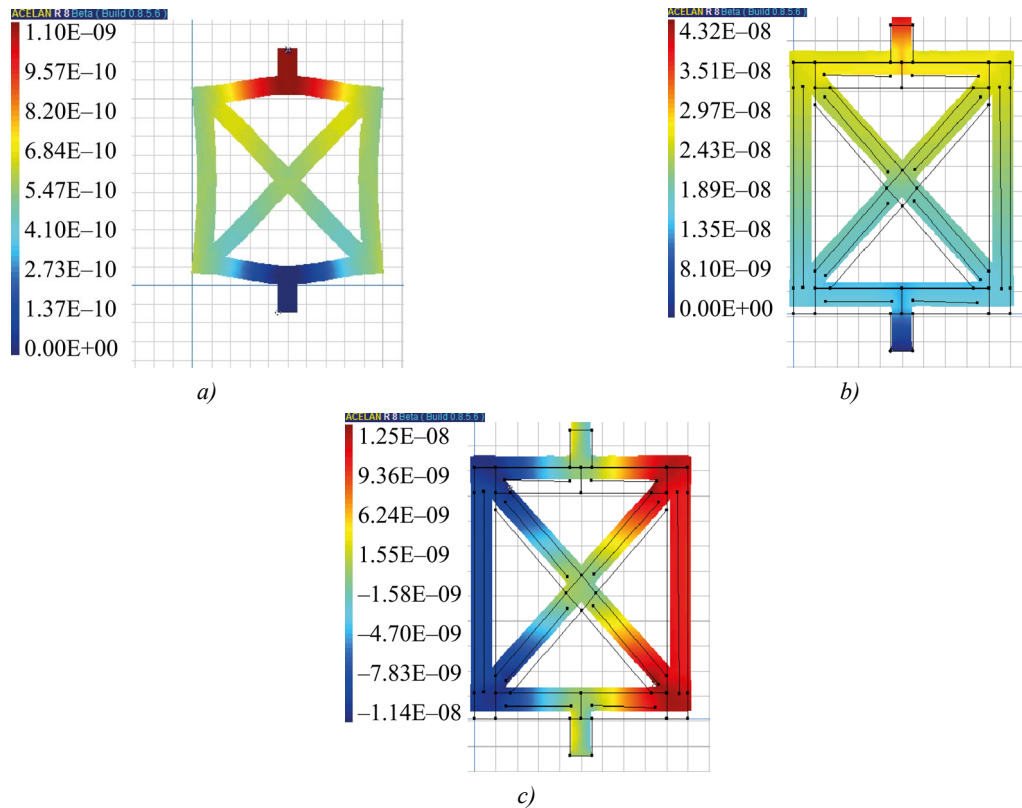


Fig. 7. Distribution: *a* — vertical displacement under the action of vertical pressure;
b — vertical displacement under the action of potential difference;
c — horizontal displacement under the action of potential difference

Discussion and Conclusion. Thus, on the basis of this stress-strain state (SSS), the effective properties of composites, which are used in modeling piezoelectric devices, are found. Therefore, the study of the influence of the type of polarization on the SSS of a highly porous piezoelectric material is urgent.

The calculation of the preliminary polarization field in a cell of a highly porous material has shown that it depends significantly on its geometry and the arrangement of the electrodes. These features include the fact that some edges are practically not polarized, others are polarized in one direction, but nonuniformly, and, finally, edges with opposite polarization may appear. The calculation of the mechanical and electrical response of the cell and its natural resonance frequencies have proven that taking into account the nonuniformity of polarization leads to the fact that the magnitude of the discrepancy between these results and the results for the model with uniform polarization reaches 15% and 10%, respectively. And the cell with edges on which there is counter polarization exhibits auxetic properties. The paper shows that in problems of determining the effective properties of highly porous piezoelectric composites based on the construction of representative volumes from its cells, it is essential to take into account the inhomogeneous polarization corresponding to their structure.

The practical relevance of the results obtained is due to the fact that the effective properties of composites allow for modeling, calculation and optimization of various piezoelectric devices (sensors, emitters and receivers of acoustic waves, piezoelectric generators, etc.) at the design stage.

References

1. Gibson LJ, Ashby MF. The Mechanics of Three-Dimensional Cellular Materials. *Proceedings of the Royal Society A: Mathematical, Physical and Engineering Sciences*. 1982;382:43–59. <https://doi.org/10.1098/rspa.1982.0088>

2. Nikitin AV, Mikhasev FI. Estimation of the Effective Young's Modulus for Open Cell Porous Titanium Based on 3D Gibson-Ashby Cell Array. *Journal of the Belarusian State University. Mathematics and Informatics*. 2022;(1):75–82. <https://doi.org/10.33581/2520-6508-2022-1-75-82>
3. Kornievsky AS, Nasedkin AV. Comparison of Foam Models from Regular and Irregular Arrays of Gibson-Ashby Open-Cells. *PNPRU Mechanics Bulletin*. 2021;(3):70–83. <https://doi.org/10.15593/perm.mech/2021.3.07>
4. Seyed Kamal Jalali, Mohammad Javad Beigrezaee, Diego Misseroni, Nicola Maria Pugno. A Modified Gibson-Ashby Model for Functionally Graded Lattice Structures. *Mechanics of Materials*. 2024;188:104822. <https://doi.org/10.1016/j.mechmat.2023.104822>
5. Kachanov M, Sevostianov I. *Micromechanics of Materials, with Applications*. Cham: Springer; 2018. 712 p. <https://doi.org/10.1007/978-3-319-76204-3>
6. Milton GW. *The Theory of Composites*. Cambridge: Cambridge University Press; 2002. 568 p. <https://doi.org/10.1017/CBO9780511613357>
7. Scheffler M, Colombo P. (eds) *Cellular Ceramics: Structure, Manufacturing, Properties and Applications*. Hoboken, NJ: John Wiley & Sons; 2005. 645 p. <http://doi.org/10.1002/3527606696>
8. Gibson LJ, Ashby MF. *Cellular Solids: Structure and Properties*. 2nd ed. Cambridge: Cambridge University Press; 1997. 510 p. <https://doi.org/10.1017/CBO9781139878326>
9. Hössinger-Kalteis A, Reiter M, Jerabek M, Major Z. Overview and Comparison of Modelling Methods for Foams. *Journal of Cellular Plastics*. 2021;57(6):951–1001. <https://doi.org/10.1177/0021955X20966329>
10. Chen Pan, Yafeng Han, Jiping Lu. Design and Optimization of Lattice Structures: A Review. *Applied Sciences*. 2020;10(18):6374. <https://doi.org/10.3390/app10186374>
11. Srivastava V, Srivastava R. On the Polymeric Foams: Modeling and Properties. *Journal of Materials Science*. 2014;49:2681–2692. <https://doi.org/10.1007/s10853-013-7974-5>
12. Firooz S, Steinmann P, Javili A. Homogenization of Composites with Extended General Interfaces: Comprehensive Review and Unified Modeling. *Applied Mechanics Reviews*. 2021;73(4):040802. <https://doi.org/10.1115/1.4051481>
13. Vernigora GD, Lupeiko TG, Skaliukh AS, Solovyev AN. On Polarization and Identification of Porous Piezoceramics Effective Characteristics. *Vestnik of Don State Technical University*. 2011;11(4):462–469. URL: <https://www.vestnik-donstu.ru/jour/article/view/746/745> (accessed: 28.08.2024).
14. Belokon' AV, Eremeyev VA, Nasedkin AV, Solovyev AN. Partitioned Schemes of the Finite-Element Method for the Dynamic Problems of Acoustoelectroelasticity. *Journal of Applied Mathematics and Mechanics*. 2000;64(3):381–393.
15. Belokon AV, Skaliukh AS. *Mathematical Modeling of Irreversible Polarization Processes*. Moscow: Fizmatlit; 2010. 328 p. (In Russ.)
16. Skaliukh AS, Oganessian PA, Soloviev AN. Modeling of Piezoelectric Elements with Inhomogeneous Polarization in ACELAN. *Ferroelectrics*. 2015;483(1):95–101. <https://doi.org/10.1080/00150193.2015.1059138>

About the Authors:

Arkadiy N. Soloviev, Dr.Sci. (Phys.-Math.), Professor of the Mathematics and Physics Department, Crimean Engineering and Pedagogical University named after Fevzi Yakubov (8, Uchebnyi Lane, Simferopol, 295015, Republic of Crimea), Chief Researcher, Southern Federal University (105/42, Bolshaya Sadovaya Str., Rostov-on-Don, 344006, Russian Federation), [SPIN-code](#), [ORCID](#), [ScopusID](#) [ResearcherID](#), solovievarc@gmail.com

Maria S. Germanchuk, Cand.Sci. (Phys.-Math.), Associate Professor of the Informatics Department, V.I. Vernadsky Crimean Federal University (4, Prospect Vernadskogo, Simferopol, 295007, Republic of Crimea), Associate Professor of the Mathematics and Physics Department, Crimean Engineering and Pedagogical University named after Fevzi Yakubov (8, Uchebnyi Lane, Simferopol, 295015, Republic of Crimea), [SPIN-code](#), [ORCID](#), [ScopusID](#), [ResearcherID](#), m.german4uk@yandex.ru

Claimed Contributorship:

AN Soloviev: formulation of the idea and research objectives and tasks, application of mathematical methods of analysis and synthesis of research data, development of auxiliary algorithms.

MS Germanchuk: conducting the research process, namely, performing a numerical experiment in the ACELAN package, preparing and creating a draft manuscript, finalizing the text.

Conflict of Interest Statement: the authors declare no conflict of interest.

All authors have read and approved the final version of the manuscript.

Об авторах:

Аркадий Николаевич Соловьев, доктор физико-математических наук, профессор кафедры математики и физики Крымского инженерно-педагогического университета имени Февзи Якубова (295015, Республика Крым, г. Симферополь, пер. Учебный, д. 8), главный научный сотрудник Южного федерального университета (344006, Российская Федерация, г. Ростов-на-Дону, ул. Большая Садовая, 105/42), [SPIN-код](#), [ORCID](#), [ScopusID](#), [ResearcherID](#), solovievare@gmail.com

Мария Сергеевна Германчук, кандидат физико-математических наук, доцент кафедры информатики Крымского федерального университета им. В.И. Вернадского, (295007, Республика Крым, г. Симферополь, пр. Вернадского, д. 4), доцент кафедры математики и физики Крымского инженерно-педагогического университета имени Февзи Якубова (295015, Республика Крым, г. Симферополь, пер. Учебный, д. 8), [SPIN-код](#), [ORCID](#), [ScopusID](#), [ResearcherID](#), m.german4uk@yandex.ru

Заявленный вклад авторов:

А.Н. Соловьев: формулировка идеи и исследовательских целей и задач, применение математических методов анализа и синтеза данных исследования, разработка вспомогательных алгоритмов.

М.С. Германчук: проведение исследовательского процесса, а именно, проведение численного эксперимента в пакете ACELAN, подготовка и создание черновика рукописи, доработка текста.

Конфликт интересов: авторы заявляют об отсутствии конфликта интересов.

Все авторы прочитали и одобрили окончательный вариант рукописи.

Received / Поступила в редакцию 14.10.2024

Reviewed / Поступила после рецензирования 30.10.2024

Accepted / Принята к публикации 08.11.2024

MACHINE BUILDING AND MACHINE SCIENCE МАШИНОСТРОЕНИЕ И МАШИНОВЕДЕНИЕ



UDC 621.018.2

Original Empirical Research

<https://doi.org/10.23947/2687-1653-2024-24-4-347-359>

Test Bench for Reciprocating Hydraulic Cylinders with Energy Recovery: Structure, Simulation, and Calculation

Alexander R. Zenin^{ID}, Alexander T. Rybak^{ID}✉, Alexey N. Beskopylny^{ID},
Alexey Yu. Pelipenko^{ID}, Yuliya A. Serdyukova

Don State Technical University, Rostov-on-Don, Russian Federation

✉ 2130373@mail.ru



EDN: BQOJNU

Abstract

Introduction. Energy conservation is an urgent topic of research in the mechanical engineering all over the world. A particular direction in these studies is the search for energy-efficient methods of testing technical systems, which provide the most accurate prediction of the reliability of the designed equipment. The duration of resource tests, established by technical conditions and GOST standards, causes an irreversible loss of energy, amounting to more than 1.5 of the resource of the tested machine, and the energy lost in the form of “harmful heat” is released into the environment. Therefore, the problem of energy saving during testing is given special attention. One of the ways of energy saving under testing of hydraulic machines is energy recovery. However, in papers devoted to energy recovery during testing of hydraulic machines, the problems of energy recovery during testing of rotary hydraulic machines were solved, and for reciprocating hydraulic machines, the problem of energy recovery during testing of plunger hydraulic cylinders was solved. The results of these studies cannot be directly used for testing reciprocating hydraulic cylinders. In this regard, the objective of this work has been formulated — to develop the structure and basic scheme of a test bench for reciprocating hydraulic cylinders, providing the recovery of part of the energy spent on testing, due to which the energy efficiency of the testing process is significantly increased.

Materials and Methods. The paper used simulation techniques for the stand functioning based on the application of the theory of volumetric rigidity. To perform preliminary calculations of the stand operation process, a computer program based on the SimInTech software package was developed.

Results. A structural and schematic diagram of a test bench for reciprocating hydraulic cylinders has been developed. A mathematical expression has been obtained that provides a preliminary assessment of the test efficiency coefficient. A computer program based on the SimInTech software package has been created, which allows the design parameters of the stand affect its operational characteristics, including the coefficient of energy efficiency of the test process.

Discussion and Conclusion. The preliminary calculations of the operating characteristics of the stand showed that the efficiency coefficient of the proposed stand was 1.7. It can be increased by conducting additional studies aimed at obtaining rational design parameters of the stand. The proposed stand provides testing of reciprocating hydraulic cylinders with recovery of part of the expended energy, and its mathematical model allows using the numerical methods in calculations. This significantly simplifies the calculation process and increases the accuracy of the calculations. At the same time, it is possible to obtain rational parameters of the stand already at the design stage, without resorting to expensive and labor-intensive field studies.

Keywords: mathematic simulation, reciprocating hydraulic cylinders, test bench, energy recovery, test efficiency coefficient

Acknowledgements. The authors would like to thank the Editors and reviewers for their attentive attitude to the article and the comments indicated, the elimination of which allowed us to improve the quality of the paper.

For Citation. Zenin AR, Rybak AT, Beskopylny AN, Pelipenko AYU, Serdyukova YUA. Test Bench for Piston Hydraulic Cylinders with Energy Recovery: Structure, Simulation, and Calculation. *Advanced Engineering Research (Rostov-on-Don)*. 2024;24(4):347–360. <https://doi.org/10.23947/2687-1653-2024-24-4-347-360>

Стенд испытания поршневых гидравлических цилиндров с рекуперацией энергии: структура, моделирование и расчёт

А.Р. Зенин , А.Т. Рыбак ✉, А.Н. Бескопыльный , А.Ю. Пелипенко , Ю.А. Сердюкова

Донской государственный технический университет, г. Ростов-на-Дону, Российская Федерация

✉ 2130373@mail.ru

Аннотация

Введение. Во всем мире энергосбережение является актуальной проблемой для исследований в области машиностроения. Особое направление в этих исследованиях — поиск энергоэффективных методов испытаний технических систем, которые позволяют наиболее точно прогнозировать надёжность проектируемого оборудования. Установленная техническими условиями и ГОСТами длительность ресурсных испытаний приводит к безвозвратной потере энергии, составляющей более чем 1,5 ресурса испытуемой машины, теряемая же при этом энергия в виде «вредного тепла» выделяется в окружающую среду. Поэтому проблеме энергосбережения в процессе испытаний уделяется особое внимание. Одним из путей энергосбережения при испытаниях гидравлических машин является рекуперация энергии. Однако в работах, посвящённых рекуперации энергии при испытаниях гидравлических машин, решались задачи рекуперации энергии при испытаниях гидромашин вращательного действия, а для гидромашин возвратно-поступательного действия была решена задача рекуперации энергии при испытаниях плунжерных гидравлических цилиндров. Результаты этих исследований не могут напрямую использоваться для испытаний поршневых гидроцилиндров. В связи с этим сформулирована цель настоящей работы — разработка структуры и принципиальной схемы стенда испытаний поршневых гидроцилиндров, обеспечивающего рекуперацию части энергии, затрачиваемой на испытания, за счёт чего энергетическая эффективность процесса испытаний значительно повышается.

Материалы и методы. В работе использовались методы моделирования процесса функционирования стенда на основе применения теории объёмной жёсткости. Для проведения предварительных расчётов процесса функционирования стенда разработана компьютерная программа на базе программного комплекса SimInTech.

Результаты исследования. Разработаны структурная и принципиальная схемы стенда испытания поршневых гидравлических цилиндров. Получено математическое выражение, позволяющее дать предварительную оценку коэффициенту эффективности испытаний. Создана компьютерная программа на базе программного комплекса SimInTech, дающая возможность конструктивным параметрам стенда влиять на его эксплуатационные характеристики, включая коэффициент энергетической эффективности процесса испытания.

Обсуждение и заключение. Проведенные предварительные расчёты характеристик функционирования стенда показали, что коэффициент эффективности предлагаемого стенда составляет 1,7. Его можно повысить за счёт проведения дополнительных исследований, направленных на получение рациональных конструктивных параметров стенда. Предложенный стенд обеспечивает испытания поршневых гидравлических цилиндров с рекуперацией части затраченной энергии, а его математическая модель позволяет использовать при расчётах численные методы. Это значительно упрощает процесс расчётов и повышает их точность. При этом получать рациональные параметры стенда можно уже на стадии его проектирования, не прибегая к дорогостоящим и трудозатратным натурным исследованиям.

Ключевые слова: математическое моделирование, поршневые гидравлические цилиндры, стенд для испытания, рекуперация энергии, коэффициент эффективности испытания

Благодарности. Авторы выражают благодарность редакции и рецензентам за внимательное отношение к статье и указанные замечания, устранение которых позволило повысить ее качество.

Для цитирования. Зенин А.Р., Рыбак А.Т., Бескопыльный А.Н., Пелипенко А.Ю., Сердюкова Ю.А. Стенд испытания поршневых гидравлических цилиндров с рекуперацией энергии: структура, моделирование и расчёт. *Advanced Engineering Research (Rostov-on-Don)*. 2024;24(4):347–359. <https://doi.org/10.23947/2687-1653-2024-24-4-347-359>

Introduction. Most critical criteria of the quality of modern engineering products are their reliability and energy efficiency. Reliability is maintained at various stages of the product life cycle [1]: at the stages of theoretical research [2], development [3], production [4], and operation [5]. Energy efficiency is of great importance in the running of continuously operating drives of technological [6], transport [7], loading-and-unloading machines [8], hydraulic excavators [9], and other machines and mechanisms. Energy saving acquires special interest in the operation of highly loaded machines [10], their testing [11], and diagnostics [12].

At present, when testing hydraulic machines, loading systems are often used in the form of loading devices that consume a significant amount of hydraulic or mechanical energy resources, which are inefficiently used and eventually irretrievably lost.

One of the most important areas of improvement and development of new testing systems for hydraulic machines is moving away from traditional hydraulic motor loading systems (mechanical, hydraulic, electrical and other braking systems), which cause significant unproductive energy losses, to systems with energy recovery.

Therefore, the issue of maintaining energy recovery during testing is a relevant area for increasing energy saving of hydraulic machines. A very promising design in this case is the test bench for rotary hydraulic machines [13], which can be used as a loading system for a recuperative system of the “pump – motor – pump” type when testing reciprocating hydraulic machines.

The diagram of the recuperative system of the “pump – motor – pump” type is shown in Figure 1. In this recuperative system, the test energy transferred from the hydraulic pump to the hydraulic motor is returned from the motor to the pump shaft through mechanical transmission II, which reduces significantly its unproductive losses during the test. In this case, the load for the pump is the motor, and the load for the motor is the pump. The energy lost to overcome the internal resistances of the test system is compensated by the electric motor through mechanical transmission I.

Based on the use of a recuperative system of the “pump – motor – pump” type [14], a test stand for hydraulic machines with reciprocating motion (plunger hydraulic cylinders) [15] has been developed, which allows for significant energy saving during the testing of plunger hydraulic cylinders.

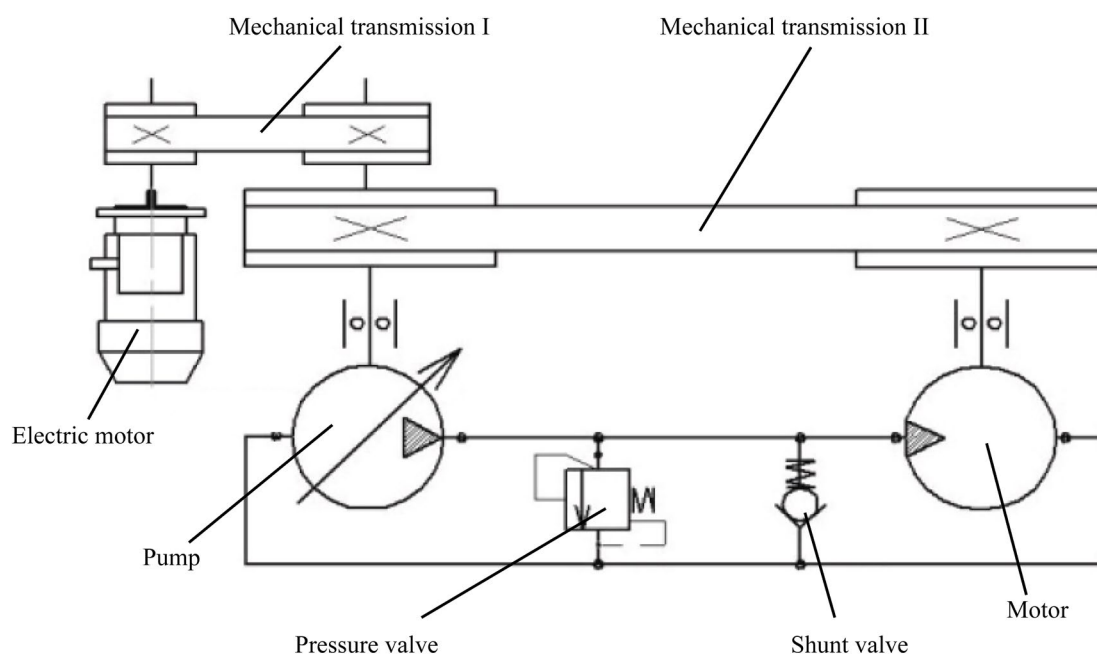


Fig. 1. Scheme of recuperative system of “pump-motor-pump” type

However, the said stand does not allow testing hydraulic piston cylinders. This research objective is to develop the structure and basic diagram of a stand for testing piston hydraulic cylinders, which would provide the recovery of part of the energy spent on testing, as well as its modeling and preliminary calculation of operational characteristics.

Materials and Methods. Based on previously known testing methods, a test stand for checking piston hydraulic cylinders with energy recovery was developed [16]. The structural diagram of the proposed experimental stand is shown in Figure 2.

The stand system includes four hydromechanical subsystems and a system for monitoring and controlling the testing process:

- 1) primary energy source, which includes an electric motor EM and a hydraulic pump P and is designed to compensate for the energy lost by the system during testing;
- 2) hydraulic cylinder testing mechanism, including the tested hydraulic cylinders HC1 and HC2, mechanical transmission MT and hydraulic distributor HD;
- 3) guiding system consisting of check valves CV1, CV2, CV3 and CV4 and designed to control fluid flows when changing the direction of movement of the working parts of hydraulic cylinders;

4) energy recovery system, including hydraulic motor M, pressure hydraulic valve PV and mechanical transmission MT, designed to create a load on the tested hydraulic cylinders and return part of the energy from the shaft of hydraulic motor M to the shaft of hydraulic pump P and implement energy recovery during testing;

5) control and management subsystem “Automatic Control and Management System” (ACMS), designed to monitor the basic technological parameters of the hydraulic cylinder testing process and manage this process. It includes pressure sensors PS1...PS4; speed sensors SS1 and SS2; rotation sensor RS and kilowatt meter KM, designed to measure pressure at characteristic points of the system, the rotation speed of the shafts of the hydraulic pump P and hydraulic motor M, the angle of rotation of the rocker arm RA, the power consumed by the electric motor EM, and further processing of information. For this purpose, the ACMS has an electronic system for processing, displaying on the screen and printing the received information about the progress of the test.

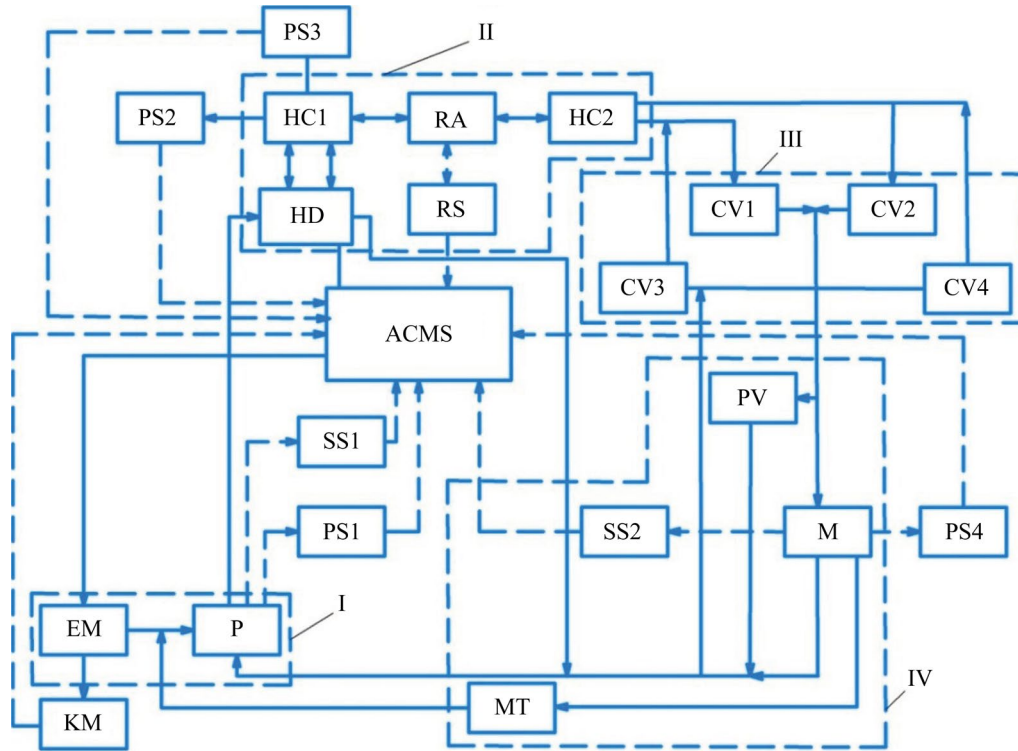


Fig. 2. Structural diagram of the experimental test stand for piston hydraulic cylinders with energy recovery

In the structural diagram (Fig. 2), solid lines show the hydraulic and mechanical connections of the system elements, and dashed lines show the connections of the ACMS elements.

According to the proposed structural diagram, the energy conversion model on the experimental stand will be implemented as follows.

The energy that arises at the output of the primary energy source *I* as a result of its operation N_{BxI} , is transmitted with some losses to the input of the hydraulic cylinder testing mechanism *II* N_{BxII} :

$$N_{\text{BxII}} = N_{\text{BxI}} \cdot \eta_{I-II}, \quad (1)$$

where η_{I-II} — efficiency factor taking into account the corresponding energy losses.

The output power of the hydraulic cylinder test mechanism *II* after its double conversion within the second subsystem, taking into account the corresponding losses, can be determined from equation:

$$N_{\text{BxII}} = N_{\text{BxII}} \cdot \eta_{II}, \quad (2)$$

where N_{BxII} — output power of the hydraulic cylinder testing mechanism *II*; η_{II} — efficiency factor of the hydraulic cylinder testing mechanism *II*, taking into account energy losses arising in the second subsystem as a result of its double conversion — from hydraulic to mechanical and vice versa. They consist of losses of hydraulic energy in the internal hydraulic lines of the system and losses of mechanical energy during the movement of the pistons of the hydraulic cylinders HC1, HC2, and energy in the mechanical transmission MT from the leading hydraulic cylinder HC1 to the slave hydraulic cylinder HC2.

The power supplied to the input of the third subsystem of the guide system *III* will be determined taking into account the losses of hydraulic energy between the testing mechanism of hydraulic cylinders *II* and subsystem *III*, which is lost to overcome the hydraulic resistance of the corresponding hydraulic lines:

$$N_{\text{BXIII}} = N_{\text{БЫХII}} \cdot \eta_{\text{II-III}}, \quad (3)$$

where N_{BXIII} — capacity of the hydraulic flow at the input of guide system *III*; $\eta_{\text{II-III}}$ — efficiency of the hydraulic transmission (hydraulic system) between the second and third subsystems, taking into account energy losses in the corresponding hydraulic lines.

The capacity of the fluid flow at the outlet of the third subsystem is determined from equation:

$$N_{\text{БЫХIII}} = N_{\text{BXIII}} \cdot \eta_{\text{III}}, \quad (4)$$

where $N_{\text{БЫХIII}}$ — capacity of the fluid flow at the outlet of subsystem *III*; η_{III} — efficiency of the third subsystem, taking into account energy losses during the operation of the guide system.

The capacity of the fluid flow at the inlet of the energy recovery system is determined from equation:

$$N_{\text{BXIV}} = N_{\text{БЫХIII}} \cdot \eta_{\text{III-IV}}, \quad (5)$$

where N_{BXIV} — capacity of the fluid flow at the outlet of the fourth subsystem; $\eta_{\text{III-IV}}$ — efficiency factor, taking into account the corresponding energy losses.

The output power of the energy recovery system consists of two components: the power of the hydraulic flow transmitted from the drain of the energy recovery system to the input of the hydraulic pump *P*, and the mechanical energy transmitted from the hydraulic motor shaft to the hydraulic pump shaft through the mechanical transmission *MT*.

In this case, the total power given by the energy recovery system $N_{\text{БЫХIV}}$ to the primary energy source can be determined from formula:

$$N_{\text{БЫХIV}} = N_{\text{BXIV}} \cdot \eta_{\text{IV}}, \quad (6)$$

where η_{IV} — total efficiency of the energy recovery system *IV*.

The total power supplied to the input of the primary energy source N_{BXI} from the energy recovery system, taking into account the total efficiency factor, which considers both mechanical and hydraulic energy losses during its transfer from the output of the energy recovery system to the input of the primary energy source $\eta_{\text{IV-I}}$ can be determined from formula:

$$N_{\text{BXI}} = N_{\text{БЫХIV}} \cdot \eta_{\text{IV-I}}. \quad (7)$$

Power N_{BXI} , received at the input of the primary energy source from the output of the energy recovery system is added to power $N_{\text{ЭДБЫХ}}$, received from the output of the electric motor *EM*, and is converted by the pump *P* into power $N_{\text{БЫХI}}$ of the working fluid flow at the output of the primary energy source, which can be determined from formula:

$$N_{\text{БЫХI}} = (N_{\text{ЭДБЫХ}} \cdot \eta_{\text{ЭД-H}} + N_{\text{BXI}}) \cdot \eta_{\text{H}}, \quad (8)$$

where $\eta_{\text{ЭД-H}}$ — efficiency of the mechanical transmission between the electric motor *EM* and the pump *P*; η_{H} — total efficiency of the pump.

$$N_{\text{ЭДБЫХ}} = N_{\text{ЭДБХ}} \cdot \eta_{\text{ЭД}}, \quad (9)$$

where $N_{\text{ЭДБХ}}$ — power at the input of the electric motor *EM* (power consumed by the electric motor from the power supply network); $\eta_{\text{ЭД}}$ — efficiency of the electric motor.

The joint solution to equations (1)–(9) allows us to obtain equation:

$$N_{\text{ЭДБЫХ}} \cdot \eta_{\text{ЭД-H}} \cdot \eta_{\text{ЭД}} \cdot \eta_{\text{H}} = N_{\text{BXII}} \left(\frac{1}{\eta_{\text{I-II}}} - \eta_{\text{II}} \cdot \eta_{\text{II-III}} \cdot \eta_{\text{III}} \cdot \eta_{\text{III-IV}} \cdot \eta_{\text{IV}} \cdot \eta_{\text{IV-I}} \right), \quad (10)$$

or

$$\frac{N_{\text{BXII}}}{N_{\text{ЭДБЫХ}}} = \frac{\eta_{\text{ЭД-H}} \cdot \eta_{\text{ЭД}} \cdot \eta_{\text{H}} \cdot \eta_{\text{I-II}}}{1 - \eta_{\text{II}} \cdot \eta_{\text{II-III}} \cdot \eta_{\text{III}} \cdot \eta_{\text{III-IV}} \cdot \eta_{\text{IV}} \cdot \eta_{\text{IV-I}}}. \quad (11)$$

In the right part of equation (11), we see the ratio of the power supplied to the tested hydraulic machines (*HC1*, *HC2*), to the power consumed by the electric motor of the power source of the test system *I*. This is nothing more than the efficiency factor of the test system $k_{\text{эфф}}$. Thus, the efficiency factor of the recuperative system under consideration is generally determined from formula:

$$k_{\text{эфф}} = \frac{\eta_{\text{ЭД-H}} \cdot \eta_{\text{ЭД}} \cdot \eta_{\text{H}} \cdot \eta_{\text{I-II}}}{1 - \eta_{\text{II}} \cdot \eta_{\text{II-III}} \cdot \eta_{\text{III}} \cdot \eta_{\text{III-IV}} \cdot \eta_{\text{IV}} \cdot \eta_{\text{IV-I}}}. \quad (12)$$

From equation (12), it is evident that in the general case, efficiency factor $k_{\text{эфф}}$ of the proposed piston hydraulic cylinder testing system is determined by the efficiency factors of the subsystems and elements that make up the testing system. In the numerator of equation (12), there is the product of the efficiency factors of all energy transmission elements — from the primary source of electrical energy to the hydraulic cylinder testing mechanism, and in the denominator, there is the difference between the unit and the product of the efficiency factors of the remaining elements of the system. Thus, to increase the efficiency factor of the testing system, it is required, first of all, to increase the efficiency factors of all the elements that make up the system.

Theoretically, if the efficiency of all elements that make up the hydraulic cylinder testing system are equal to 1, then the efficiency factor of the testing system becomes equal to infinity.

In accordance with the considered structural diagram, presented in Figure 2, a basic diagram of the experimental stand has been developed (Fig. 3). In it, as a hydraulic recuperation system, a hydraulic transmission HST-90 is used, including an adjustable hydraulic pump P1 and a nonadjustable hydraulic motor HM, kinematically connected by mechanical transmission MT2.

The primary energy source *I* on the experimental stand has a hydraulic connection with the hydraulic cylinder testing mechanism *II* through hydraulic line *l1*, which, in turn, is connected through hydraulic lines *l13* and *l14* to the guide system *III*, and then through hydraulic line *l16* to energy recovery system *IV* and through hydraulic lines *l6*, *l9* and *l10* — to the primary energy source *I*.

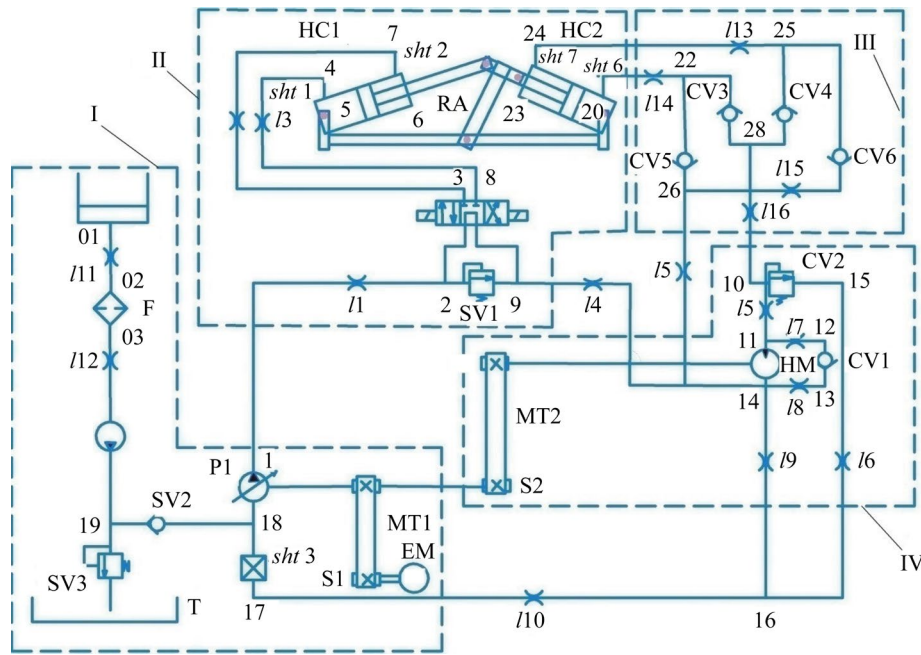


Fig. 3. Hydro-kinematic diagram of the test stand for piston hydraulic cylinders

Thus, the hydraulic system of the stand, like its energy system, is a closed circuit.

The most effective method of preliminary study of the properties of the technical systems being developed is its modeling with subsequent research [17]; therefore, to confirm the correctness of the previously considered method of modeling the test stand for piston hydraulic cylinders, its mathematical model has been developed using the theory of volume rigidity [18]. For this purpose, the hydraulic system of the stand is divided into sections by characteristic points (a total of 32 points, including points 01, 02, 03 and 04 of the feed system).

In accordance with the theory of volume rigidity of hydraulic systems, the time derivative of pressure, taking into account the reduced coefficient of volume rigidity of the section under consideration $C_{\pi pi}$, can be determined depending on the values of incoming Q_{bxi} and outgoing liquid flow rates Q_{bxi} using formula:

$$\frac{dp_i}{dt} = C_{\pi pi} \left(\sum Q_{bxi} - \sum Q_{bxi} \right). \quad (13)$$

The flow rates of the working fluid for substitution into equation (13) are determined in accordance with the actual operating conditions of the system using known dependences [19].

The feed rates of hydraulic pumps P1 and P2 and the flow rate of the hydraulic motor HM are determined taking into account their volume efficiency factors.

Since the shafts of the hydraulic pump S2 and the hydraulic motor S3 are connected through a mechanical transmission, the following dependence is satisfied:

$$\omega_{B3} = \omega_{B2} i_{3,2}, \quad (14)$$

where $i_{3,2}$ — gear ratio of mechanical transmission MT2 of rotation from the shaft of hydraulic motor S3 to the shaft of hydraulic pump S2.

The rotation speed of the hydraulic pump shaft is set by the angular speed of the electric motor shaft S1 ω_{B1} and is determined from the ratio:

$$\omega_{B1} = \omega_{B2} i_{1,2}, \quad (15)$$

where $i_{1,2}$ — gear ratio of mechanical transmission MT1 of rotation from the shaft of hydraulic motor S1 to the shaft of hydraulic pump S2.

The flow rates through the valves (pressure valves PV1...PV3 and check valves CV1...CV6) are determined by their flow characteristics from the ratio:

$$\begin{aligned} \text{if } p_{\text{кл}} < p_{\text{кл.откр}}, \text{ then } Q_{\text{кл}} &= 0; \\ \text{if } p_{\text{кл}} \geq p_{\text{кл.откр}}, \text{ then } Q_{\text{кл}} &= Q_{\text{кл.ном}} \cdot \frac{p_{\text{кл}} - p_{\text{кл.откр}}}{\Delta p_{\text{кл.ном}}}, \end{aligned} \quad (16)$$

where $p_{\text{кл}}$ — pressure at the valve inlet; $p_{\text{кл.откр}}$ — valve start-to-open pressure; $\Delta p_{\text{кл.ном}}$ — difference between the full valve open pressure at the nominal flow rate and the start-to-open valve pressure; $Q_{\text{кл}}$ — actual flow rate of the working fluid through the valve; $Q_{\text{кл.ном}}$ — nominal flow rate of the valve.

Figure 4 shows the kinematic diagram of the hydraulic cylinder testing mechanism. When modeling its operation, it should be borne in mind that the speed of piston movement of the hydraulic cylinder HC1 is determined by the flow rate of the working fluid supplied to its piston cavity:

$$v_{\text{п1}} = \frac{Q_{4.5}}{S_{\text{п}}}. \quad (17)$$

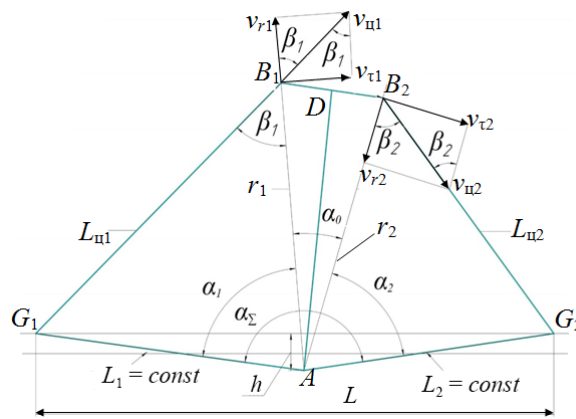


Fig. 4. Kinematic diagram of the hydraulic cylinder testing mechanism

The movement of hydraulic cylinder $L_{\text{п1}}$ is transmitted to the mechanical transmission MT, which performs a rotational movement around point A.

The angular rotational speed of mechanical transmission MT is determined by the tangential component $v_{\tau 1}$ of the movement speed of the piston of hydraulic cylinder HC1. It depends on angle β_1 between the direction of its movement and radius r_1 , that connects the point of rotation of the mechanical transmission MT and point B_1 that joins the rod of the hydraulic cylinder HC1 with it:

$$\omega_{\text{AD}} = \frac{v_{\tau 1}}{r_1},$$

or

$$\omega_{\text{AD}} = \frac{v_{\text{п1}} \cdot \sin \beta_1}{r_1}. \quad (18)$$

Rotating around point A, mechanical transmission MT transmits movement to the piston of the slave hydraulic cylinder HC2, whose speed $v_{\text{п2}}$ also depends on angle β_2 between the direction of its movement and radius r_2 , that connects the point of rotation of the mechanical transmission MT and point B_2 that joins the rod of the hydraulic cylinder HC2 with it:

$$v_{\text{п2}} = \frac{r_2 \omega_{\text{AD}}}{\sin \beta_2}. \quad (19)$$

Having solved equations (18) and (19) simultaneously, we obtain a formula that determines the relationship between the speed of movement of the pistons of the leading hydraulic cylinder HC1 and the slave hydraulic cylinder HC2:

$$v_{\text{п2}} = v_{\text{п1}} \frac{r_2 \sin \beta_1}{r_1 \sin \beta_2}. \quad (20)$$

From the analysis of triangles (according to the law of cosines) AG_1B_1 and AG_2B_2 , angles β_1 and β_2 are determined:

$$\begin{aligned} \cos \beta_1 &= \frac{L_{c1}^2 + r_1^2 - L_1^2}{2L_{\text{п1}}r_1}, \\ \cos \beta_2 &= \frac{L_{c2}^2 + r_2^2 - L_2^2}{2L_{\text{п2}}r_2}, \end{aligned}$$

where L_{u1} and L_{u2} — distances between the axes of the connection of the housings of the corresponding hydraulic cylinders to the stand frame and their rods with the mechanical transmission MT; L_1 and L_2 — distances from the axis of rotation of the mechanical transmission MT and points G_1 and G_2 of connection with the stand frame of the housings of hydraulic cylinders HC1 and HC2, respectively.

During the return piston stroke of the slave hydraulic cylinder HC1, the working fluid is supplied to its rod cavity, and then the rest of the calculation formulas remain unchanged.

$$v_{u1} = \frac{Q_{7-6}}{S_{n.шрт}}. \quad (21)$$

In dynamic calculations, the movement of the piston of the leading cylinder HC1 is described by the equation of motion:

$$\frac{dv_{u1}}{dt} = \frac{1}{M_{np1}} (S_n \cdot p_5 - S_{n.шрт} \cdot p_6 - v_1 \cdot k_{tp1} - F_1), \quad (22)$$

$$\frac{dx_{u1}}{dt} = v_1, \quad (23)$$

where v_{u1} and x_{u1} — speed and displacement of the piston of the hydraulic cylinder HC1; M_{np1} — reduced mass; S_n and $S_{n.шрт}$ — working areas of the pistons of the hydraulic cylinders; p_5 and p_6 — pressure in the corresponding cavities of the hydraulic cylinder HC1; k_{tp1} — friction factor during movement of the working element of the first hydraulic cylinder HC1, taking into account friction in the transmission mechanism RA; F_1 — force of impact on the working body of the leading hydraulic cylinder from the side of the hydraulic cylinder HC2.

Force F_1 is determined by formula:

$$F_1 = (S_n \cdot p_{20} - S_{n.шрт} \cdot p_{23} + v_{u2} \cdot k_{tp2}) \cdot \frac{\sin \beta_2}{\sin \beta_1}, \quad (24)$$

where p_{20} and p_{23} — pressure in the piston and rod cavities of the slave hydraulic cylinder HC2, respectively; v_{u2} and k_{tp2} — speed of movement of the working body of the slave hydraulic cylinder HC2 and friction factor during its movement.

Research Results. Figures 5–9 show the results of the preliminary calculation of the proposed mathematical model of the test stand. The calculations were performed using a special program developed in the SimInTech environment [20]. The calculations allowed us to determine the functional parameters of the stand already at the design stage and take meaningful measures to improve them.

Having analyzed the graphs of the piston motion parameters of the tested hydraulic cylinders (Fig. 5), it can be concluded that the test cycle of the piston hydraulic cylinders HC63.500.16.000 on the proposed stand will last about four seconds. The piston motion speed, when the rod is extended, will be 0.24 m/s, and when it is retracted — 0.32 m/s.

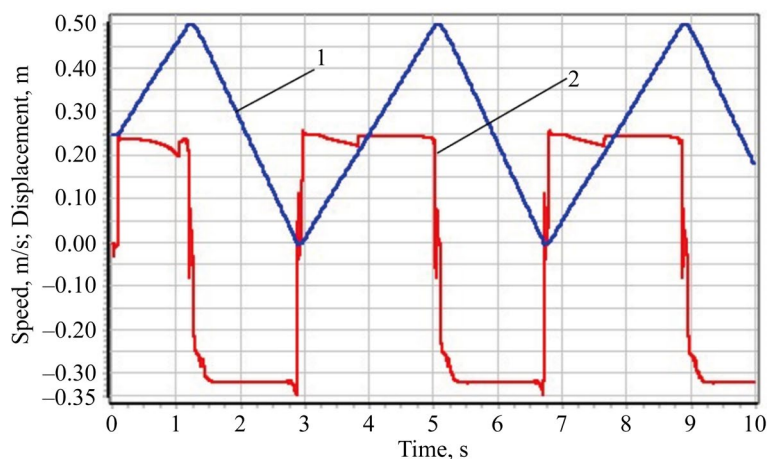


Fig. 5. Change in the parameters of the piston movement of the leading hydraulic cylinder under testing:
1 — displacement; 2 — speed

The graphs (Fig. 5) show that the hydraulic cylinders are exposed to working fluid pressures of 120 to 130 atmospheres under testing. Of particular interest is the fact that during testing, at the moment of reversing the direction of movement of the piston, the pressure at all considered points becomes the same — about 70 atmospheres.

Figure 6 shows data on the pressure at the nodal points of the hydraulic system of the stand under testing.

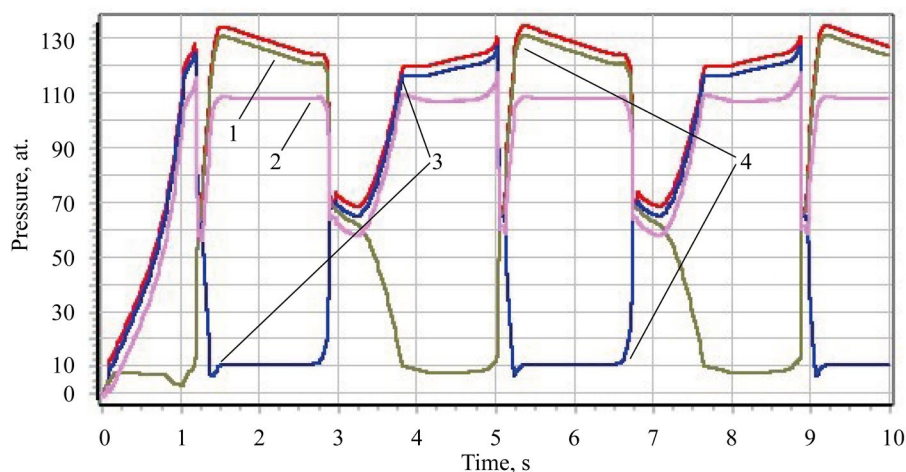


Fig. 6. Pressure change at characteristic points of the hydraulic system of the stand under testing of hydraulic cylinders:
1 — hydraulic pump outlet; 2 — hydraulic motor inlet; 3 — piston cavity of HC1; 4 — rod cavity of HC1

The graphs of pressure variations in low-pressure hydraulic lines, which are shown in Figure 7, allow us to estimate the magnitude and nature of the pressure change at the input to the feed hydraulic pump of the stand. It can be seen that at the moment of reversal of the piston movement of the tested hydraulic cylinders, the pressure in the suction branch of the main hydraulic pump of the stand increases sharply to 70 atmospheres. Particularly noteworthy is the fact that when the direction of the piston movement of the leading hydraulic cylinder changes from extension to retraction, the pressure at the outlet of the feed pump grows less than the setting pressure of its pressure valve. To explain this effect, it should be recalled that the hydraulic system of the stand is essentially a closed system, i.e., the working fluid from the drain of the recovery system enters the suction branch of the main pump of the stand. At some point during the operation of the stand, this fluid is not enough, the main pump receives additional fluid flow from the feed pump. This fact is very important to remember when designing a test stand.

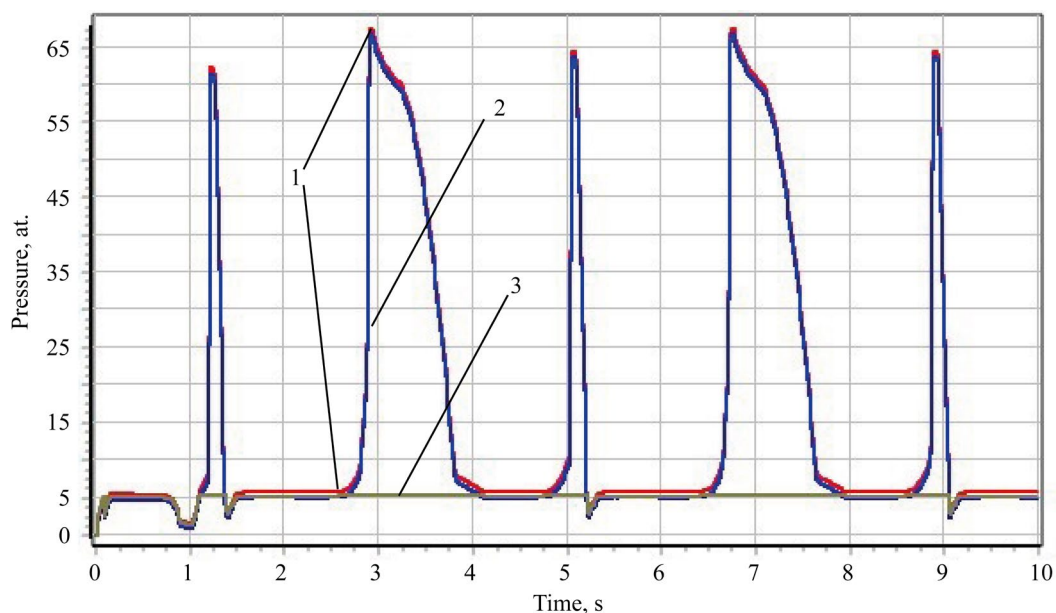


Fig. 7. Change in pressure at characteristic points of the low-pressure hydraulic system under testing of hydraulic cylinders:
1 — output of the hydraulic system of the hydraulic cylinder testing mechanism; 2 — input of the main hydraulic pump;
3 — output of the feed hydraulic pump

The graphs of power variations on the hydraulic machines of the test stand during testing (Fig. 8) show that the highest power during testing of hydraulic cylinders occurs at the output of the hydraulic pump, and the lowest — at the input of the main energy source of the bench — the electric motor. This is the main objective that the authors were trying to achieve by creating a stand with a recuperative system: the recuperative system returns part of the energy spent on testing

hydraulic cylinders back to the hydraulic pump, which reduces the overall energy consumption of the primary source, and this provides an increase in the energy efficiency of the testing process. It should also be noted that when the direction of movement of the pistons of the tested hydraulic cylinders is reversed, the power on some elements of the stand takes on a negative value. Obviously, this is the effect of the release of energy accumulated in the system during its elastic deformation, volume compression in the hydraulic system.

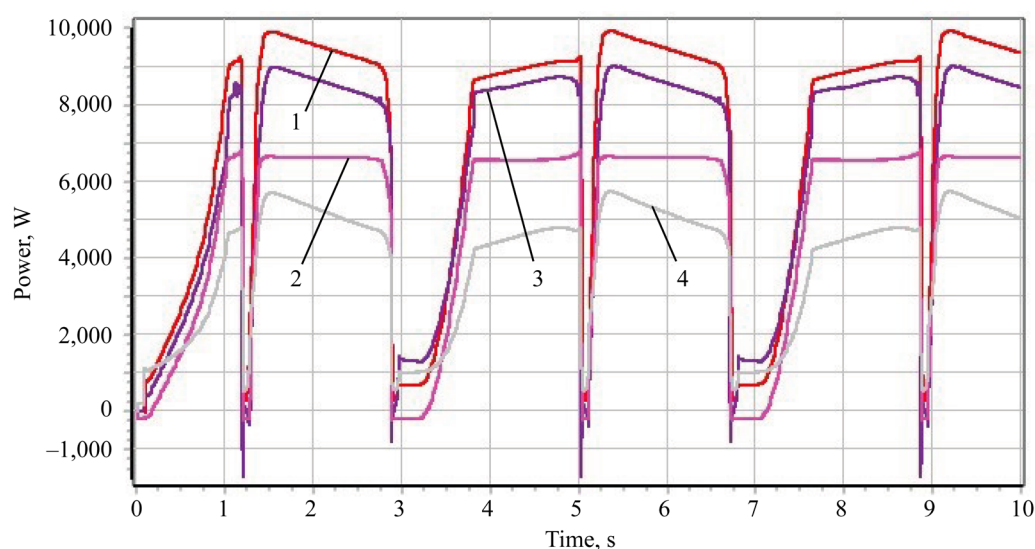


Fig. 8. Change in power on the hydraulic machines of the stand under testing of hydraulic cylinders:

- 1 — hydraulic pump output; 2 — hydraulic motor shaft;
3 — in the hydraulic cylinder testing system; 4 — electric motor input

The graphs (Fig. 9) show that the instantaneous efficiency coefficient takes on a zero value when the direction of movement of the pistons of the tested hydraulic cylinders is reversed. This is explained by the fact that at this moment, the piston of the hydraulic cylinder stops, and therefore, the power on the tested hydraulic cylinders also goes to zero.

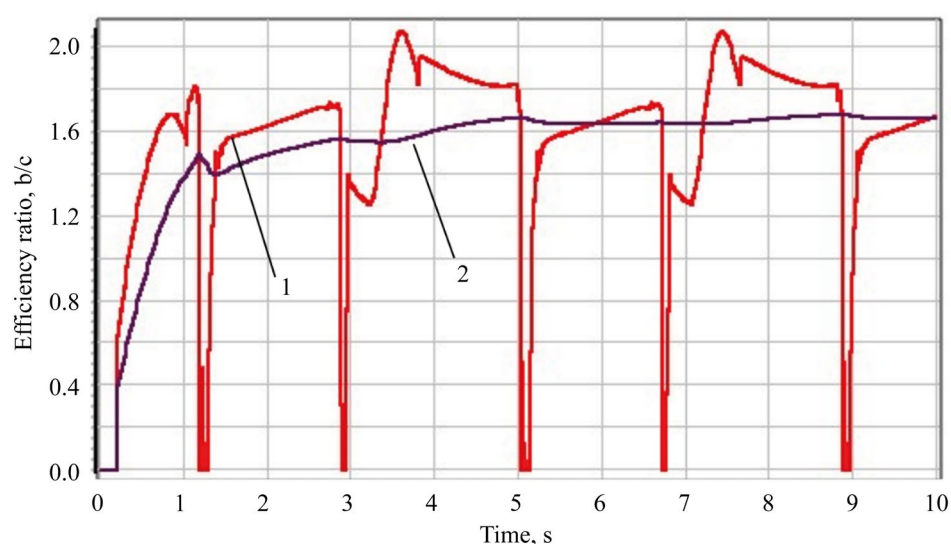


Fig. 9. Test efficiency factors: 1 — instantaneous value; 2 — average value

It is also seen that the value of the average test efficiency ratio approaches the value of 1.7. This indicates that the power of the hydraulic cylinder test is 70% greater than the power expended during this test.

Discussion and Conclusion. The results of the research done by the authors and presented in this article show that the proposed stand scheme allows testing piston hydraulic cylinders with a test efficiency factor of 1.7. Considering that tests performed using classical loading methods have an efficiency factor of no more than 0.8–0.9, it can be concluded that the proposed energy recovery scheme is two times more efficient than classical loading methods. That is, when testing the same hydraulic cylinders, the energy consumed is more than two times less than when testing through special loading means (mechanical, hydraulic, etc.) without energy recovery.

The maximum (highest) value of the efficiency coefficient for testing piston hydraulic cylinders using the proposed stand can be determined by equation (12). The proposed mathematical model of the stand and the program developed for its study allow for a preliminary study of the influence of various design and functional parameters of the stand on the test efficiency factor, as a result of which rational values of the design parameters of the stand can be obtained.

Список литературы / References

1. Suslov AG, Fedorov VP, Gorlenko OA, Il'itsky VB, Totai AV, Khandozhko AV, et al. *Fundamental Principles of Technological Support and Increasing the Reliability of Mechanical Engineering Products*. Moscow: Innovatsionnoe mashinostroenie; 2022. 552 p. (In Russ.)
2. Teplyakova SV. Justification of the Concept of Creating Practically Trouble-Free Machines. *Bulletin of Higher Educational Institutions. North Caucasus Region. Technical Sciences*. 2021;210(2):41–45. <https://doi.org/10.17213/1560-3644-2021-2-41-45>
3. Kuznetsova VN, Savinkin VV. Development of Hybrid Drive's Construction of a Traversing Platform of an Earthmoving Machine for Implementing Construction Works. *The Russian Automobile and Highway Industry Journal*. 2015;41(1):17–23. URL: <https://vestnik.sibadi.org/jour/article/view/95> (accessed: 20.08 2024).
4. Deryushev VV, Teplyakova SV, Zaitseva MM. Production Facilities Safety Assessment according to the Maximum Values of Machines Reliability. *Safety of Technogenic and Natural Systems*. 2023;7(2):58–69. <https://doi.org/10.23947/2541-9129-2023-7-2-58-69>
5. Antipas IR. Modeling the Dynamic Loads Affecting a Bridge Crane during Start-Up. *Advanced Engineering Research (Rostov-on-Don)*. 2024;24(2):190–197. <https://doi.org/10.23947/2687-1653-2024-24-2-190-197>
6. Nikonov VO, Posmetev VI, Kozlov EV, Borodkin VO. Analysis of Constructive Peculiarities of Hydroficated Technological Machines with Recovery of the Potential Energy of the Working Body with Cargo. *Voronezh Scientific-Technical Bulletin*. 2019;27(1):4–19.
7. Chmil VP. Reconcilitive Transmission as Means of Improving the Operational Properties of Cars. *Mechanization of Construction*. 2017;78(8):55–59.
8. Chmil VP. Energy Recovery in Hydraulic Mechanism of Turning Excavator Platform. *Mechanization of Construction*. 2017;78(2):5–8.
9. Lianpeng Xia, Long Quan, Lei Ge, Yunxiao Hao. Energy Efficiency Analysis of Integrated Drive and Energy Recuperation System for Hydraulic Excavator Boom. *Energy Conversion and Management*. 2018;156:680–687. <http://doi.org/10.1016/j.enconman.2017.11.074>
10. Popikov PI, Derpasko IV, Khomenko KG, Rudoy DV, Olshevskaya AV, Rybak AT, et al. Analysis of Studies of Work Processes of Energy-Saving Hydraulic Drives and Devices of Highly Loaded Technological Machines and Equipment. *E3S Web of Conferences*. 2023;462:01039. <https://doi.org/10.1051/e3sconf/202346201039>
11. Ustyantsev MV. *Improving the Efficiency of the Drive of the Test Stand for Rotary Hydraulic Machines*. Cand.Sci. (Eng.), diss., author's abstract. Rostov-on-Don; 2012. 18 p. (In Russ.)
12. Fominykh AM. Application of Energy-Efficient Diagnostic Method for Hydraulic Drives. *Eurasian Union of Scientists*. 2014;3(6):46–48. (In Russ.)
13. Rybak AT, Tsybriy IK, Pelipenko AY. *Test Bench for Hydraulic Motors and Pumps with Energy Recovery*. RF Patent, no. 204153. 2021. 7 p. (In Russ.)
14. Rybak A, Meskhi B, Rudoy D, Olshevskaya A, Serdyukova Yu, Teplyakova S, et al. Improving the Efficiency of the Drive of the Test Bench of Rotary Hydraulic Machines. *Actuators*. 2024;13(2):63. <https://doi.org/10.3390/act13020063>
15. Pelipenko A, Rybak A, Vyborova N, Zubtsov V, Lugantsev D. Energy Saving in Hydraulic Testing Systems. In book: A Guda (ed). *Networked Control Systems for Connected and Automated Vehicles*. Cham: Springer; 2022. P. 1889–1896. http://doi.org/10.1007/978-3-031-11051-1_194
16. Rybak AT, Zenin AR, Pelipenko AY. *Test Bench for Piston Hydraulic Cylinders with Energy Recovery*. RF Patent, no. 2796721. 2022. 9 p. (In Russ.)
17. Yudin RV, Popikov PI, Uskov VI, Platonov AA, Popikov VP, Kanishchev DA. Mathematical Model of Working Processes of a Chokerless Hauling Grip with an Energy-Saving Hydraulic Drive. *Resources and Technology*. 2022;19(1):72–86. <http://doi.org/10.15393/j2.art.2022.6023>
18. Rybak AT, Boguslavskiy IV. Improvement of the Scientific-Methodological Design Principles of the Production Machines Drive Systems. *Vestnik of Don State Technical University*. 2010;10(2):249–257. <https://www.vestnik-donstu.ru/jour/article/view/971/966> (accessed: 20.08.2024).

19. Boguslavskiy IV, Rybak AT, Chernavskiy VA. *Scientific-Methodological Foundations for Designing Drives for Technological Machines*. Monograph. Rostov-on-Don: Institute of Management and Innovation of the Aviation Industry; 2010. 276 p. (In Russ.)

20. Abalov AA, Nosachev SV, Zharov VP, Minko VA. Using the SimInTech Dynamic Modeling Environment to Build and Check the Operation of Automation Systems. *MATEC Web of Conferences*. 2018;226:04003. <https://doi.org/10.1051/mateconf/201822604003>

About the Authors:

Alexander R. Zenin, Head of the Department of Capital Construction and Capital Repairs, Acting Vice-Rector for Capital Construction and Development of the Property Complex, Teacher of the Department of Life Safety and Environmental Protection, Don State Technical University (1, Gagarin sq., Rostov-on-Don, 344003, Russian Federation), [SPIN-code](#), [ORCID](#), [ScopusID](#), [ResearcherID](#)

Alexander T. Rybak, Dr.Sci. (Eng.), Professor of the Department of Technologies and Equipment for Processing Agricultural Products, Don State Technical University (1, Gagarin sq., Rostov-on-Don, 344003, Russian Federation), [SPIN-code](#), [ORCID](#), [ScopusID](#), [ResearcherID](#), 2130373@mail.ru

Alexey N. Beskopylny, Dr.Sci. (Eng.), Professor, Vice-Rector for Academic and International Affairs, Professor of the Organization of Transportation and Road Traffic Department, Don State Technical University (1, Gagarin sq., Rostov-on-Don, 344003, Russian Federation), [SPIN-code](#), [ORCID](#), [ScopusID](#), [ResearcherID](#)

Alexey Yu. Pelipenko, Cand.Sci. (Eng.), Associate Professor of the Hydraulics, Hydropneumodynamics and Heat Management Department, Don State Technical University (1, Gagarin sq., Rostov-on-Don, 344003, Russian Federation), [SPIN-code](#), [ORCID](#), [ScopusID](#), pelipenko16a@mail.ru

Yuliya A. Serdyukova, Postgraduate student of Life Safety and Environment Protection Department, Don State Technical University (1, Gagarin sq., Rostov-on-Don, 344003, Russian Federation), [SPIN-code](#), [ScopusID](#), serdyukova.ya@gs.donstu.ru

Claimed Contributorship:

AR Zenin: development and design of research methodology, creation of a research model.

AT Rybak: academic advising, analysis of the research results.

AN Beskopylny: analysis of the research results, correction of the conclusions, formulation of the conclusions.

AYu Pelipenko: basic concept formulation, research objectives and tasks.

YuA Serdyukova: development of software, calculations, participation in the analysis of their results.

Conflict of Interest Statement: the authors claimed no conflict of interest.

All authors have read and approved the final version of the manuscript.

Об авторах:

Александр Романович Зенин, начальник управления капитального строительства и капитального ремонта, и. о. проректора по капитальному строительству и развитию имущественного комплекса, преподаватель кафедры безопасности жизнедеятельности и защиты окружающей среды Донского государственного технического университета (344003, Российская Федерация, г. Ростов-на-Дону, пл. Гагарина, 1), [SPIN-код](#), [ORCID](#), [ScopusID](#), [ResearcherID](#)

Александр Тимофеевич Рыбак, доктор технических наук, профессор кафедры технологии оборудования и переработки продукции агропромышленного комплекса Донского государственного технического университета (344003, Российская Федерация, г. Ростов-на-Дону, пл. Гагарина, 1), [SPIN-код](#), [ORCID](#), [ScopusID](#), [ResearcherID](#), 2130373@mail.ru

Алексей Николаевич Бескопыйный, доктор технических наук, профессор, проректор по учебной работе и международной деятельности, профессор кафедры организации перевозок и дорожного движения Донского государственного технического университета (344003, Российская Федерация, г. Ростов-на-Дону, пл. Гагарина, 1), [SPIN-код](#), [ORCID](#), [ScopusID](#), [ResearcherID](#)

Алексей Юрьевич Пелипенко, кандидат технических наук, доцент кафедры гидравлики, гидропневмоавтоматики и тепловых процессов Донского государственного технического университета (344003, Российская Федерация, г. Ростов-на-Дону, пл. Гагарина, 1), [SPIN-код](#), [ORCID](#), [ScopusID](#), pelipenko16a@mail.ru

Юлия Александровна Сердюкова, аспирант кафедры безопасности жизнедеятельности и защиты окружающей среды Донского государственного технического университета (344003, Российская Федерация, г. Ростов-на-Дону, пл. Гагарина, 1), [SPIN-код](#), [ScopusID](#), serdyukova.ya@gs.donstu.ru

Заявленный вклад авторов:

А.Р. Зенин: разработка и проектирование методологии исследования, создание модели исследования.

А.Т. Рыбак: научное руководство, анализ результатов исследований.

А.Н. Бескопыйный: анализ результатов исследований, корректировка выводов, формирование выводов.

А.Ю. Пелипенко: формирование основной концепции, цели и задачи исследования.

Ю.А. Сердюкова: разработка программного обеспечения, проведение расчётов и участие в анализе их результатов.

Конфликт интересов: авторы заявляют об отсутствии конфликта интересов.

Все авторы прочитали и одобрили окончательный вариант рукописи.

Received / Поступила в редакцию 03.09.2024

Reviewed / Поступила после рецензирования 24.09.2024

Accepted / Принята к публикации 05.10.2024

MACHINE BUILDING AND MACHINE SCIENCE МАШИНОСТРОЕНИЕ И МАШИНОВЕДЕНИЕ



UDC 621.833.51

Original Empirical Research

<https://doi.org/10.23947/2687-1653-2024-24-4-360-368>

Experimental Study of the Kinematics of a Double-Row Planetary Mechanism Using Two Elliptical External Gears

Alexander A. Prikhodko , Nataliya N. Belina , Andrey V. Novitsky ,
Maksim M. Shchetinin

Kuban State Technological University, Krasnodar, Russian Federation

✉ sannic92@gmail.com



EDN: BSOKNM

Abstract

Introduction. Mechanisms with non-circular gears are of wide interest to researchers and inventors due to their compactness and the implementation of a wide range of transfer functions. The development of this area is stimulated by the advancements and reduction in cost of mechanical processing and additive manufacturing technologies, as well as the use of applied mathematical modeling packages for the analysis and synthesis of non-circular gears. Traditionally, non-circular gears are used to transmit rotational motion between parallel axes with a variable ratio of angular velocities. However, their use in planetary gear schemes provides implementing various types of output link motion. The analysis of the papers on the research area shows that gears with movable rotation axes have not been sufficiently studied from the point of view of kinematics and dynamics. Most research papers reveal the theory of such mechanisms without verifying the results obtained in practice. This work is aimed at the experimental verification of the kinematics of a planetary mechanism with two external engagements, which contains elliptical gears.

Materials and Methods. The kinematic model of the mechanism under study is built on the basis of the velocity diagram of its links, which made it possible to obtain expressions for finding an analogue of the angular velocity and the position function of the output shaft. The experimental study of kinematics was performed on a laboratory stand containing a model of a planetary mechanism with a set of replaceable gear wheels, absolute encoders on the input and output shafts of the mechanism, a controller, and a PC for recording and processing the signal. The analysis of the obtained results was performed on a computer using statistical analysis methods.

Results. As a result of kinematic analysis, position functions were constructed for three alternative planetary mechanisms, which had different geometric parameters of the gears and made it possible to implement various types of motion of the output shaft: swinging motion, discontinuous motion, and unilateral uneven rotation.

Discussion and Conclusion. The analysis of the experimental results showed the adequacy of the constructed mathematical model of kinematics to real mechanisms. The confidence interval of measuring errors at a reliability level of 95% was $0.16 \pm 0.08^\circ$ for the first version of the mechanism, $0.57 \pm 0.22^\circ$ — for the second version, and $0.08 \pm 0.26^\circ$ — for the third. The proposed planetary mechanism with elliptical gears for implementing various types of motion can be used in drives of process equipment in numerous industries: chemical and food (mixers), oil refining (pumping units for crude production), mechanical engineering (compressors, pumps, automated machines), and others. The conducted kinematic studies of the planetary mechanism and their experimental analysis are needed for further dynamic and force investigations, as well as for the design of drives based on the proposed transmission.

Keywords: planetary mechanism, elliptical gears, kinematic analysis, position function, statistical analysis, uncertainty of measurement, confidence interval

Acknowledgements. The authors would like to thank the Editorial board and the reviewers for their attentive attitude to the article and for the specified comments that improved its quality.

Funding Information. The work was done with the financial support from the Kuban Science Foundation within the framework of the research and innovative project no. NIP-20.1/135 “Design and Study of a Planetary Transmission with Elliptical Gears as Part of a Piston Compressor Drive”.

For citation. Prikhodko AA, Belina NA, Novitsky AV, Shchetinin MM. Experimental Study of the Kinematics of a Double-Row Planetary Mechanism Using Two Elliptical External Gears. *Advanced Engineering Research (Rostov-on-Don)*. 2024;24(4):360–368. <https://doi.org/10.23947/2687-1653-2024-24-4-360-368>

Оригинальное эмпирическое исследование

Экспериментальное исследование кинематики двухрядной планетарной передачи эллиптическими зубчатыми колесами с двумя внешними зацеплениями

А.А. Приходько , Н.Н. Белина , А.В. Новицкий , М.М. Щетинин 

Кубанский государственный технологический университет, г. Краснодар, Российская Федерация

✉ sannic92@gmail.com

Аннотация

Введение. Механизмы с некруглыми зубчатыми колесами вызывают широкий интерес исследователей и изобретателей вследствие их компактности и реализации широкого спектра передаточных функций. Развитие данной области стимулируется развитием и удешевлением технологий механической обработки и аддитивного производства, а также применением прикладных пакетов математического моделирования для анализа и синтеза некруглых зубчатых колес. Некруглые зубчатые колеса традиционно служат для передачи вращательного движения между параллельными осями с переменным отношением угловых скоростей. Однако их применение в схемах планетарных передач позволяет реализовать различные виды движения выходного звена. Анализ работ по тематике исследования показывает, что передачи с подвижными осями вращения недостаточно исследованы с точки зрения кинематики и динамики. Большинство научных работ раскрывают теорию таких механизмов, не проводя верификации полученных результатов на практике. Целью настоящей работы является экспериментальная верификация кинематики планетарного механизма с двумя внешними зацеплениями, имеющего в своем составе эллиптические зубчатые колеса.

Материалы и методы. Кинематическая модель исследуемого механизма построена на базе плана скоростей его звеньев, который позволил получить выражения для нахождения аналога угловой скорости и функции положения выходного вала. Экспериментальное исследование кинематики выполнено на лабораторном стенде, содержащем макет планетарного механизма с набором сменных зубчатых колес, абсолютные энкодеры на входном и выходном валах механизма, контроллер и ПК для регистрации и обработки сигнала. Анализ полученных результатов проведен на ЭВМ с использованием методов статистического анализа.

Результаты исследования. В результате кинематического анализа построены функции положения для трех вариантов планетарного механизма, имеющих различные геометрические параметры зубчатых колес и позволяющих реализовать различные виды движения выходного вала: возвратно-вращательное движение, движение с остановками и одностороннее неравномерное вращение.

Обсуждение и заключение. Анализ результатов эксперимента показал адекватность построенной математической модели кинематики реальным механизмам. Доверительный интервал ошибок измерения при уровне достоверности 95 % составил для первого варианта механизма $0,16 \pm 0,08$, для второго варианта — $0,57 \pm 0,22$ и для третьего — $0,08 \pm 0,26$. Предложенный планетарный механизм с эллиптическими зубчатыми колесами для реализации различных видов движения может быть применен в приводах технологического оборудования многих отраслей промышленности: химической и пищевой (перемешивающие устройства), нефтеперерабатывающей (станки-качалки для добычи нефти), машиностроительной (компрессоры, насосы, станки-автоматы) и других. Проведенные кинематические исследования планетарного механизма и их экспериментальный анализ необходимы при дальнейшем динамическом и силовом исследованиях, а также при проектировании приводов на базе предложенной передачи.

Ключевые слова: планетарный механизм, эллиптические зубчатые колеса, кинематический анализ, функция положения, статистический анализ, неопределенность измерения, доверительный интервал

Благодарности. Авторы выражают благодарность редакции и рецензентам за внимательное отношение к статье и указанные замечания, которые позволили повысить ее качество.

Финансирование. Исследование выполнено при финансовой поддержке Кубанского научного фонда в рамках научно-инновационного проекта № НИП-20.1/135 «Конструирование и исследование планетарной передачи эллиптическими зубчатыми колесами в составе привода поршневого компрессора».

Для цитирования. Приходько А.А., Белина Н.Н., Новицкий А.В., Щетинин М.М. Экспериментальное исследование кинематики двухрядной планетарной передачи эллиптическими зубчатыми колесами с двумя внешними зацеплениями. *Advanced Engineering Research (Rostov-on-Don)*. 2024;24(4):360–368. <https://doi.org/10.23947/2687-1653-2024-24-4-360-368>

Introduction. Mechanisms with non-circular gears have been known for a long time, but their experimental research and practical implementation have long been difficult due to the focused specialization of such mechanisms, the complexity and high cost of their manufacture. Nowadays, there is an increase in the interest of researchers in this topic. At the same time, most scientific papers on designing non-circular gearing are based on the analysis of geometry [1] and kinematics [2] to obtain the required transfer function for practical application [3]. In [4] and [5], mechanisms for synthesizing angular velocity functions were developed and studied. Researchers proposed robotics with non-circular gears, for example, a jumping robot [6], a hexapod robot [7], an exoskeleton mechanism for knee joint rehabilitation [8]. More efficient planting machines for the agricultural industry were studied from the point of view of kinematics [9] and dynamics [10]. Other numerous devices were developed and designed.

A review of sources has shown that the most common gears are those with an elliptical centrode [11, 12]. Machines [10] and devices [4] with elliptical gears are created, the geometry [13] is studied, and some design [14] and manufacturing issues are resolved [15].

Elliptical gears are mainly used to transmit rotary movement between parallel fixed axes [16]. However, such use of non-circular gears allows for only one-way nonuniform rotary movement, which limits the scope of their application. Planetary gears have broader capabilities for implementing complex types of movement of working bodies. The creation of drives based on them will provide the development and implementation of more efficient and compact machines for various technological purposes.

Based on the results of the analysis of scientific literature in the field of transmissions with non-circular gears, a planetary mechanism with elliptical wheels is proposed as an object of study. The objective of the work is an experimental kinematic analysis of a planetary transmission. It is justified by the need to verify theoretical provisions for their correct use at the following stages of design — in dynamic, force analysis and strength calculations.

Materials and Methods. The kinematic model of the mechanism is constructed on the basis of the velocity diagram of its links (Fig. 1).

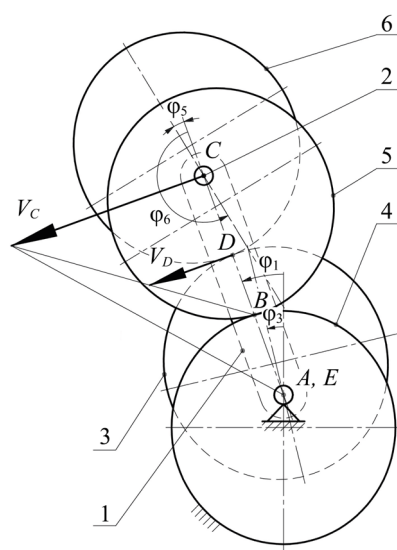


Fig. 1. Velocity diagram for the mechanism under consideration:
1 — carrier; 2 — satellite shaft; 3 — elliptical gear on the output shaft;
4 — sun elliptical wheel; 5, 6 — elliptical wheels of the satellite

The analog of the angular velocity of the output shaft is determined as follows [17]:

$$\phi'_3 = \frac{\omega_3}{\omega_1} = \frac{V_D \cdot AC}{V_C \cdot DE} = \frac{BD \cdot AC}{BC \cdot DE}. \quad (1)$$

Segments BD , BC and DE are determined through the polar equation of the ellipse [17]:

$$\rho(\varphi) = \frac{a(1-e^2)}{1-e \cdot \cos \varphi}, \quad (2)$$

where φ — rotation angle, e and a — eccentricity and semi-major axis of an ellipse.

We determine the engagement radii of gears 5 and 6:

$$BC = \rho_5 = \frac{a(1-e_1^2)}{1-e_1 \cdot \cos \varphi_5}, \quad (3)$$

$$CD = \rho_6 = \frac{a(1-e_2^2)}{1-e_2 \cdot \cos \varphi_6}, \quad (4)$$

where e_1 and e_2 — eccentricities for each pair of elliptical gears, whose rotation angles φ_5 and φ_6 are obtained as follows:

$$\varphi_5 = \int \frac{1-e_1^2}{1+e_1^2+2e_1 \cdot \cos \varphi_1} d\varphi_1. \quad (5)$$

$$\varphi_6 = \pi + \varphi_5. \quad (6)$$

Based on the velocity plan and taking into account equations (3), (4), we define the required segments as:

$$BD = \rho_6 - \rho_5, \quad (7)$$

$$AC = EC = 2a, \quad (8)$$

$$DE = 2a - \rho_6. \quad (9)$$

Based on (2)–(9), we obtain an expression for determining the analogue of the angular velocity of the output shaft:

$$\varphi_3' = \frac{(\rho_6 - \rho_5) \cdot 2a}{\rho_5 (2a - \rho_6)}. \quad (10)$$

The rotation angle is determined by integrating equation (10) over joint coordinate φ_1 :

$$\varphi_3 = \int \varphi_3' d\varphi_1. \quad (11)$$

Variations of the kinematic scheme of the mechanism include replacing elliptical gears with cylindrical ones in one of the pairs, for the study of which it is required to replace the radius functions with fixed values in the resulting mathematical model.

We consider mechanisms with a pair of elliptical gears 3–6 ($e=0.28$), and cylindrical wheels 4 and 5 of the following sizes:

- option 1: $R_5=25$ mm, $R_4=25$ mm;
- option 2: $R_5=18$ mm, $R_4=32$ mm;
- option 3: $R_5=16$ mm, $R_4=34$ mm.

Figure 2 shows the graphs of the position functions obtained using (11).

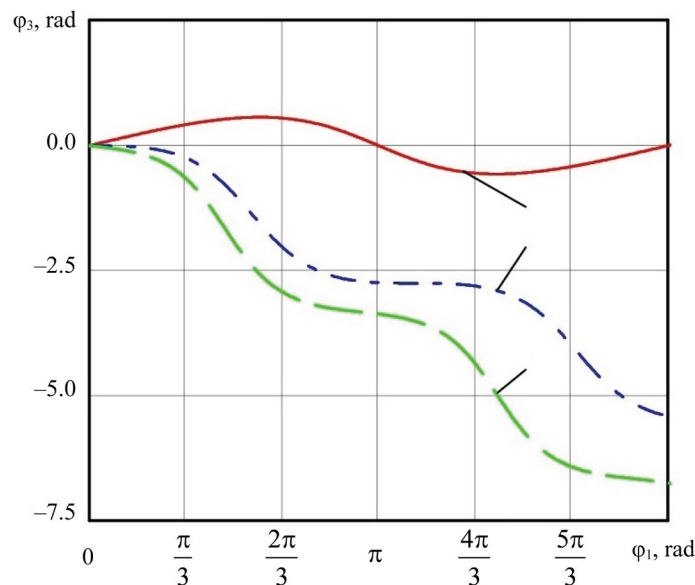


Fig. 2. Dependence graphs for the studied mechanism configurations

The analysis of the graphs shows (in Fig. 2, numbers indicate studied options) that changing the sizes of the gear wheels allows obtaining different types of output shaft movement: reciprocating-rotational (option 1), discontinuous (option 2) and one-way nonuniform rotational movement (option 3).

Research Results. The kinematic analysis confirmed the implementation of various transfer functions, and changing the sizes of gear wheels allows for the kinematic synthesis of new mechanisms.

The object of the experimental study is a prototype, whose details are shown in Figure 3.



Fig. 3. Details of the prototype under study

Rotation angles are measured by absolute encoders (Table 1).

Table 1

Encoder Characteristics

Diameter	Output signal	Resolution	Linearity	Reading speed
22 mm	0–5 V	$360^\circ/4096 \approx 0.088^\circ$	0.3%	0.6 ms

The signal is registered by the Arduino controller and processed on the PC (Fig. 4).

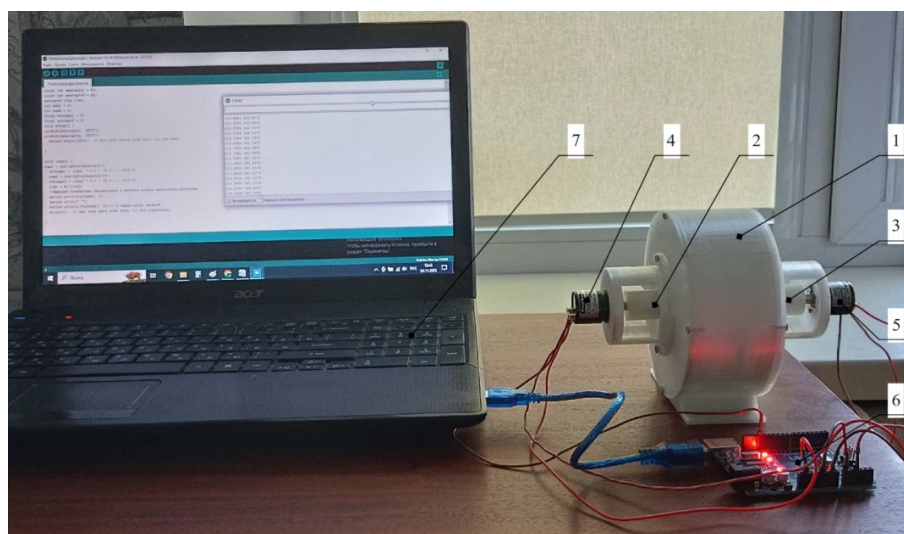
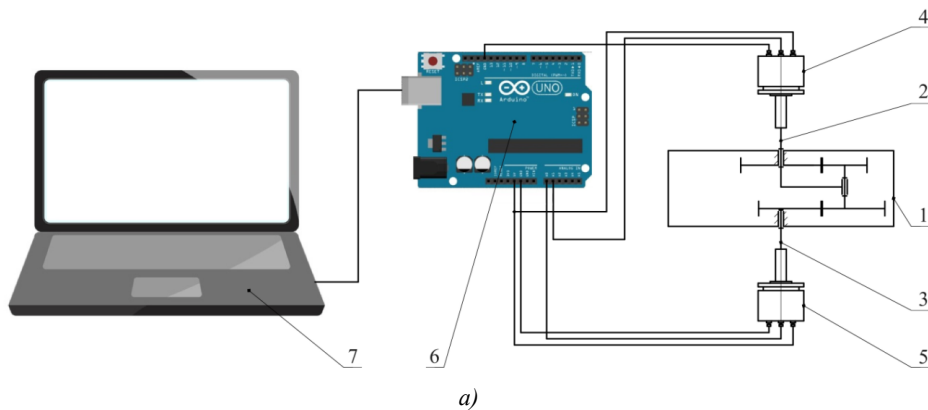


Fig. 4. Schematic diagram (a) and external view (b) of the experimental stand: 1 — housing; 2 — input shaft; 3 — output shaft; 4, 5 — encoders; 6 — Arduino controller; 7 — personal computer

The processing and analysis of the measurement results were performed in the MathCAD application package. The schemes of the studied options and the experiment results are shown in Figure 5.

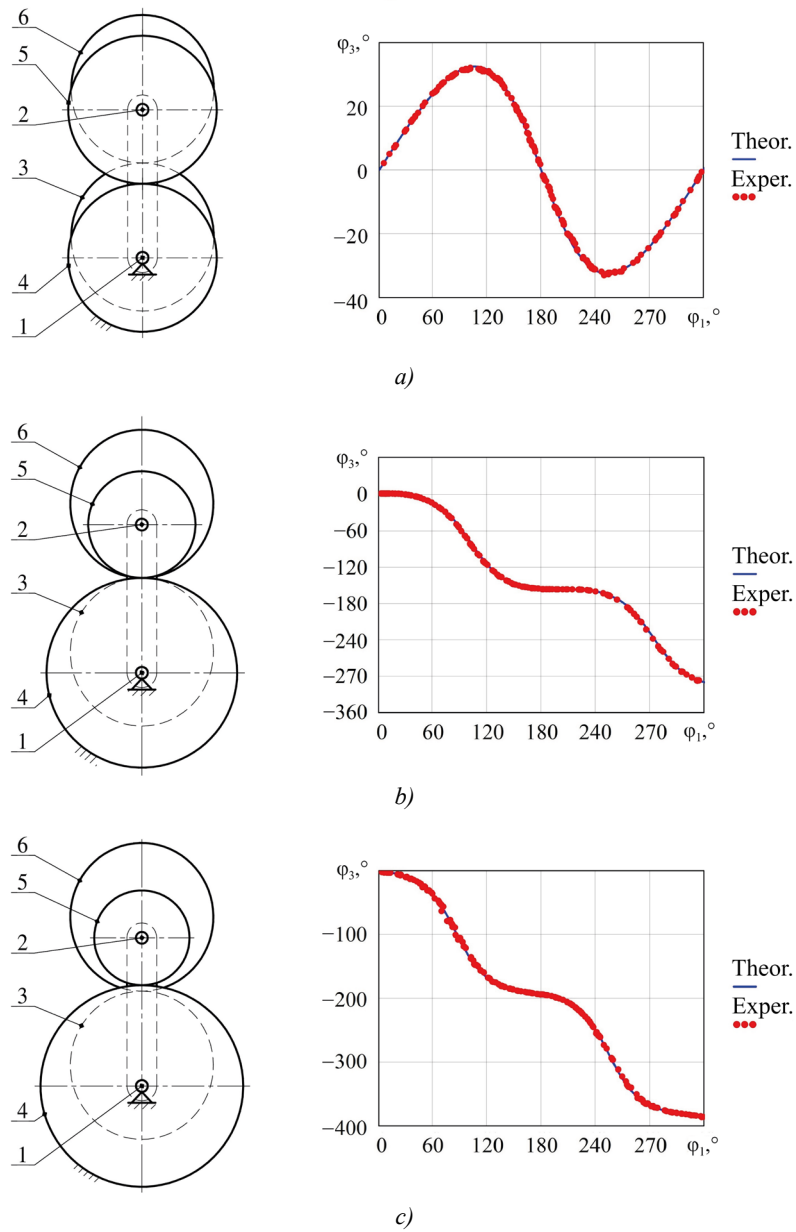


Fig. 5. Research results: *a* — option 1; *b* — option 2; *c* — option 3

As can be seen from the graphs, the measured values of the output shaft rotation angles are adequate to the constructed model. Let us evaluate the results of the experiment using statistical analysis tools.

We determine the average value of measurement errors [18]:

$$\bar{q} = \frac{1}{n} \sum_{k=1}^n q_k, \quad (12)$$

where n — number of independent observations q_k .

Let us calculate the sample variance:

$$s^2(q_k) = \frac{1}{n-1} \sum_{k=1}^n (q_k - \bar{q})^2. \quad (13)$$

An estimate of the dispersion of the mean value is obtained as follows:

$$s^2(q) = \frac{s^2(q_k)}{n}. \quad (14)$$

The standard uncertainty of Type A measurements is determined [19]:

$$u(q) = \sqrt{s^2(q)}. \quad (15)$$

Taking the measurement errors as values q_k and processing them according to (12)–(15), we calculate the measurement uncertainty. The results of the statistical analysis are given in Table 2.

Table 2

Statistical Analysis of Measurement Errors

Mechanism number	Number of measured values	Mean error value	Uncertainty of measurement
1	195	-0.16°	0.04°
2	168	0.57°	0.11°
3	192	0.08°	0.13°

The confidence interval is defined as $\bar{q} \pm 2u$ for a level of certainty of 95% and is $-0.16 \pm 0.08^\circ$ (option 1), $0.57 \pm 0.22^\circ$ (option 2), $0.08 \pm 0.26^\circ$ (option 3). Thus, the constructed mathematical model of kinematics is adequate to the physical prototypes.

Discussion and Conclusion. A planetary gear with elliptical wheels is presented, providing the implementation of nonuniform, discontinuous and reciprocating-rotational movement of the output shaft. The type of movement is determined by the parameters of the gear wheels.

A kinematic model of the transmission was constructed, and the law of movement of the output shaft was obtained. The analysis of mechanisms with different parameters of gear wheels showed the feasibility of a wide range of transmission functions and types of movement of the output shaft.

The correspondence of the results of the conducted kinematic analysis to real mechanisms is confirmed by an experimental study of the output shaft position functions for three options of the physical prototype. The performed assessment of the adequacy of the mathematical model provides its using in dynamic and force analysis of machines based on the proposed transmissions. The studied options of the mechanism can be used in drives of compact and easy-to-balance technological machines.

References

1. Lozzi A. Non-Circular Gears — Graphic Generation of Involute and Base Outlines. *Proceedings of the Institution of Mechanical Engineers, Part C: Journal of Mechanical Engineering Science*. 2000;214(3):411–422. <https://doi.org/10.1243/0954406001523074>
2. Qifeng Gao, Jun Ye, Can Liu. Design and Modeling of Noncircular Gear with Curvature Radius Function. *Journal of Computational Methods in Sciences and Engineering*. 2018;18(3):683–693. <https://doi.org/10.3233/JCM-180819>
3. Čavić D, Čavić M, Penčić M, Dorić J, Rackov M. IC Engine: Increasing Efficiency by Using Epicyclic Non-Circular Gear Train. In book: Lovasz EC, Maniu I, Doroftei I, Ivanescu M, Gruescu CM (eds). *New Advances in Mechanisms, Mechanical Transmissions and Robotics*. Cham: Springer; 2020. P. 391–402. https://doi.org/10.1007/978-3-030-60076-1_36
4. JY Liu, SL Chang, D Mundo. Study on the Use of a Non-Circular Gear Train for the Generation of Figure-8 Patterns. *Proceedings of the Institution of Mechanical Engineers, Part C: Journal of Mechanical Engineering Science*. 2006;220(8):1229–1236. <https://doi.org/10.1243/09544062JMES268>
5. Ottaviano E, Mundo D, Danieli GA, Ceccarelli M. Numerical and Experimental Analysis of Non-Circular Gears and Cam-Follower Systems as Function Generators. *Mechanism and Machine Theory*. 2008;43(8):996–1008. <https://doi.org/10.1016/j.mechmachtheory.2007.07.004>
6. Okada M, Takeda Y. Synthesis and Evaluation of Non-Circular Gear that Realizes Optimal Gear Ratio for Jumping Robot. In: *Proc. IEEE/RSJ International Conference on Intelligent Robots and Systems*. New York City: IEEE; 2013. P. 5524–5529. <https://doi.org/10.1109/IROS.2013.6697157>
7. Ke-Jung Huang, Shen-Chiang Chen, Haldun Komsuoglu, Gabriel Lopes, Jonathan Clark, Pei-Chun Lin. Design and Performance Evaluation of a Bio-Inspired and Single-Motor-Driven Hexapod Robot with Dynamical Gaits. *Journal of Mechanisms and Robotics*. 2015;7(3):031017. <https://doi.org/10.1115/1.4029975>
8. Terada H, Zhu Y, Suzuki M, Cheng C, Takahashi R. Developments of a Knee Motion Assist Mechanism for Wearable Robot with a Non-Circular Gear and Grooved Cams. In book: Lovasz EC, Corves B (eds). *Mechanisms, Transmissions and Applications*. Dordrecht: Springer; 2012. P. 69–76. https://doi.org/10.1007/978-94-007-2727-4_6
9. Guo LS, Zhang WJ. Kinematic Analysis of a Rice Transplanting Mechanism with Eccentric Planetary Gear Trains. *Mechanism and Machine Theory*. 2001;36(11–12):1175–1188. [https://doi.org/10.1016/S0094-114X\(01\)00052-0](https://doi.org/10.1016/S0094-114X(01)00052-0)
10. Zhao Y, Yu GH, Wu CY. Circuit Simulation and Dynamic Analysis of a Transplanting Mechanism with Planetary Elliptical Gears. *Transactions of the ASABE*. 2011;54(4):1179–1188. <https://doi.org/10.13031/2013.39016>

11. Wunderlich W. Contribution to the Geometry of Elliptic Gears. *Mechanism and Machine Theory*. 1975;10(4):273–278. [https://doi.org/10.1016/0094-114X\(75\)90072-5](https://doi.org/10.1016/0094-114X(75)90072-5)
12. Shinn-Liang Chang, Chung-Biau Tsay, Long-Iong Wu. Mathematical Model and Undercutting Analysis of Elliptical Gears Generated by Rack Cutters. *Mechanism and Machine Theory*. 1996;31(7):879–890. [https://doi.org/10.1016/0094-114X\(95\)00121-E](https://doi.org/10.1016/0094-114X(95)00121-E)
13. Biing-Wen Bair. Computerized Tooth Profile Generation of Elliptical Gears Manufactured by Shaper Cutters. *Journal of Materials Processing Technology*. 2002;122(2–3):139–147. [https://doi.org/10.1016/S0924-0136\(01\)01242-0](https://doi.org/10.1016/S0924-0136(01)01242-0)
14. Yazar M. Design, Manufacturing and Operational Analysis of Elliptical Gears. *International Journal of Precision Engineering and Manufacturing*. 2021;22(8):1441–1451. <https://doi.org/10.1007/s12541-021-00549-3>
15. Thai Hong Nguyen. Shaping the Tooth Profile of Elliptical Gear with the Involute Ellipse Curve. *VNUHCM Journal of Engineering and Technology*. 2021;4(3):1048–1056. <https://doi.org/10.32508/stdjet.v4i3.820>
16. Litvin FL. *Non-Circular Gears*. Moscow-Leningrad: MASHGIZ; 1956. 218 p. (In Russ.).
17. Prikhod'ko AA, Smelyagin AI. Kinematics of a Planetary Train with Elliptical Gears with Internal Gearing. *Journal of Machinery Manufacture and Reliability*. 2021;50(5):412–418. <https://doi.org/10.3103/S1052618821050095>
18. Hall BD, White DR. *An Introduction to Measurement Uncertainty*. Lower Hutt: Measurement Standards Laboratory of New Zealand; 2020. 50 p. <https://doi.org/10.5281/zenodo.3872590>
19. Barash VYa. Uncertainty and Error in Modern Metrology. *Legal and Applied Metrology*. 2009;105(5):15–20. (In Russ.)

About the Authors:

Alexander A. Prikhodko, Cand.Sci. (Eng.), Associate Professor of the Department of Technical Mechanics and Special Machines named after Professor A.A. Petrik, Kuban State Technological University (2, Moskovskaya Str., Krasnodar, 350072, Russian Federation), [SPIN-code](#), [ORCID](#), [ResearcherID](#), sannic92@gmail.com

Nataliya N. Belina, Cand.Sci. (Eng.), Associate Professor of the Department of Technical Mechanics and Special Machines named after Professor A.A. Petrik, Kuban State Technological University (2, Moskovskaya Str., Krasnodar, 350072, Russian Federation), [SPIN-code](#), [ORCID](#), belinann@mail.ru

Andrey V. Novitskiy, postgraduate student of the Department of Technical Mechanics and Special Machines named after Professor A.A. Petrik, Kuban State Technological University (2, Moskovskaya Str., Krasnodar, 350072, Russian Federation), [SPIN-code](#), [ORCID](#), novitskiy_19@mail.ru

Maksim M. Shchetinin, student of the Department of Technical Mechanics and Special Machines named after Professor A.A. Petrik, Kuban State Technological University (2, Moskovskaya Str., Krasnodar, 350072, Russian Federation), [ORCID](#), maks.shchetinin202@mail.ru

Claimed Contributorship:

AA Prikhodko: academic advising, basic concept, research objectives and tasks formulation, revision of the text, correction of the conclusions.

NN Belina: computational analysis, text preparation, formulation of conclusions.

AV Novitskiy: development and making of an experimental stand, design of the calculation part of the paper.

MM Shchetinin: processing of the experimental data, preparation of the experimental part of the paper.

Conflict of Interest Statement: the authors claimed no conflict of interest.

All authors have read and approved the final manuscript.

Об авторах:

Александр Александрович Приходько, кандидат технических наук, доцент кафедры технической механики и специальных машин имени профессора А.А. Петрика Кубанского государственного технологического университета (350072, Российская Федерация, г. Краснодар, ул. Московская, 2), [SPIN-код](#), [ORCID](#), [ResearcherID](#), sannic92@gmail.com

Наталья Николаевна Белина, кандидат технических наук, доцент кафедры технической механики и специальных машин имени профессора А.А. Петрика Кубанского государственного технологического университета (350072, Российская Федерация, г. Краснодар, ул. Московская, 2), [SPIN-код](#), [ORCID](#), belinann@mail.ru

Андрей Владимирович Новицкий, аспирант кафедры технической механики и специальных машин имени профессора А.А. Петрика Кубанского государственного технологического университета (350072, Российская Федерация, г. Краснодар, ул. Московская, 2), [SPIN-код](#), [ORCID](#), novitskiy_19@mail.ru

Максим Максимович Щетинин, студент кафедры технической механики и специальных машин имени профессора А.А. Петрика Кубанского государственного технологического университета (350072, Российская Федерация, г. Краснодар, ул. Московская, 2), [ORCID](#), maks.shchetinin202@mail.ru

Заявленный вклад авторов:

А.А. Приходько: научное руководство, формирование основной концепции, цели и задачи исследования, доработка текста, корректировка выводов.

Н.Н. Белина: проведение расчетов, подготовка текста, формирование выводов.

А.В. Новицкий: разработка и изготовление экспериментального стенда, оформление расчетной части научной статьи.

М.М. Щетинин: обработка экспериментальных данных, оформление экспериментальной части научной статьи.

Конфликт интересов: авторы заявляют об отсутствии конфликта интересов.

Все авторы прочитали и одобрили окончательный вариант рукописи.

Received / Поступила в редакцию 25.09.2024

Reviewed / Поступила после рецензирования 20.10.2024

Accepted / Принята к публикации 29.10.2024

MACHINE BUILDING AND MACHINE SCIENCE МАШИНОСТРОЕНИЕ И МАШИНОВЕДЕНИЕ



UDC 621.793 + 06

Systematic Review

<https://doi.org/10.23947/2687-1653-2024-24-4-369-391>

Analysis of Technologies for Applying High-Entropy Coatings by Physical Deposition Method

Kirill N. Polityko , Igor V. Kolesnikov , Dmitry S. Manturov

Rostov State Transport University, Rostov-on-Don, Russian Federation

✉ politykokirill@yandex.ru

EDN: JQMJHZ

Abstract

Introduction. Modern tribology solves the problems of increasing the reliability of friction units through applying vacuum wear-resistant coatings by the physical vapor deposition (PVD) method. More than five thousand scientific papers are devoted to high-entropy alloys (HEA). However, an urgent question about the possibility of obtaining wear-resistant and antifriction high-entropy coatings (HEC) using the PVD method remains unsolved. Its solution opens up the possibility of using HEC in mechanical engineering. The presented article is intended to fill this gap. Research objectives are as follows: to identify the key results on the creation of HEC by such PVD methods as vacuum arc evaporation and magnetron sputtering, to establish tribological characteristics of PVD coatings.

Materials and Methods. From November 2023 to February 2024, the authors analyzed materials published in the Web of Science, Elibrary, Scopus, Medline, CINAHL databases in the Russian and English languages.

Results. At the first stage, the literature on the vacuum arc coating method was considered. The issues of creating a vacuum arc discharge, its technological features, disadvantages, as well as processes in the cathode region of the arc were studied. The conditions of existence of cathode spots, the influence of temperature on the erosion coefficient, and processes on the anode and substrate were noted. The dependence of the deposition rate on the value of the potential on the substrate was shown. Nitride and combined coatings obtained by vacuum-arc method were analyzed: TiN, TiCN, TiAlN, TiMoS, TiSiN, TiN/VN, TiAlN/DLC-Ti.

At the second stage, the history of the magnetron sputtering method was presented; technological features, types of magnetrons and nitride coatings obtained in this way were described.

The third stage was devoted to the five-stage process of forming the coating structure. Island, layer-by-layer, and mixed growth modes of coating were considered. A schematic representation of the fundamental processes of structure formation was given. Defects in vacuum coatings were noted.

At the fourth stage, the HEC based on the HEA were presented. Parameters predicting the formation of a HEA solid solution were indicated. Six families of high-entropy alloys were considered. Modern high-entropy coatings obtained by vacuum arc and magnetron methods were evaluated. The results of studies of structural-phase and physico-mechanical properties were summarized in the form of a table. The data of tribological studies of high-entropy coatings was presented.

Discussion and Conclusion. The literature on HEC describes the coating structure, physical and mechanical properties, and thermal stability. The authors of the presented article found a gap in the research of tribology of high-entropy coatings. From the known results, it can be concluded that these coatings are frictional. However, due to their high hardness and ductility, they exhibit high wear resistance. In addition, it is difficult to talk about their tribological purpose. To solve the issue of the possibility of using PVD coatings in mechanical engineering, attention should be paid to the development of compositions with high hardness, wear resistance, and low coefficient of friction. They can be operated in tribo-loaded nodes.

Keywords: high-entropy coatings, high-entropy alloys, PVD coatings, vacuum arc method, magnetron method

Acknowledgements. The authors would like to thank O.V. Kudryakov, Dr.Sci. (Engineering), Professor, as well as the Editorial board and reviewers for their attentive attitude to the article, and for the above comments, which made it possible to improve its quality.

Funding Information. The research was done at Rostov State Transport University with the financial support from the Russian Science Foundation within the project “Creation of Tribotechnical Materials and Coatings of a New Generation Based on Intelligent (Digital) Synthesis Technology”, State Reg. No. 121052000109-9 (Grant No. 21–79–30007).

For Citation. Polityko KN, Kolesnikov IV, Manturov DS. Analysis of Technologies for Applying High-Entropy Coatings by Physical Deposition Method. *Advanced Engineering Research (Rostov-on-Don)*. 2024;24(4):369–391. <https://doi.org/10.23947/2687-1653-2024-24-4-369-391>

Систематический обзор

Анализ технологий нанесения высокоэнтروпийных покрытий методом физического осаждения

К.Н. Политыко , И.В. Колесников , Д.С. Мантуров 

Ростовский государственный университет путей сообщения, г. Ростов-на-Дону, Российская Федерация

✉ politykokirill@yandex.ru

Аннотация

Введение. Современная трибология решает задачи повышение надежности узлов трения с помощью нанесения вакуумных износостойких покрытий методом физического осаждения (англ. physical vapor deposition, PVD). Высокоэнтропийным сплавам (ВЭС) посвящены более 5 тыс. научных трудов. Однако оставался открытым актуальный вопрос о возможности получения износостойких и антифрикционных высокоэнтропийных покрытий (ВЭП) PVD-методом. Его решение открывает возможность применения ВЭП в машиностроении. Представленная статья призвана восполнить указанный пробел. Задачи исследования: обозначить основные результаты работ по созданию ВЭП такими PVD-методами, как вакуумно-дуговое испарение и магнетронное распыление; установить трибологические характеристики PVD-покрытий.

Материалы и методы. С ноября 2023 года по февраль 2024-го авторы проанализировали материалы на русском и английском языках, опубликованные в базах Web of Science, Elibrary, Scopus, Medline, CINAHL.

Результаты исследования. На первом этапе рассматривалась литература о вакуумно-дуговом методе нанесения покрытий. Изучались вопросы создания вакуумно-дугового разряда, его технологические особенности, недостатки, а также процессы в катодной области дуги. Отмечены условия существования катодных пятен, влияние температуры на коэффициент эрозии, процессы на аноде и подложке. Показана зависимость скорости осаждения от значения потенциала на подложке. Анализируются нитридные и комбинированные покрытия, полученные вакуумно-дуговым методом: TiN, TiCN, TiAlN, TiMoS, TiSiN, TiN/VN, TiAlN/DLC-Ti.

На втором этапе представлена история магнетронного метода распыления, описываются технологические особенности, виды магнетронов и полученные таким образом нитридные покрытия.

Третий этап посвящается пятиэтапному процессу формирования структуры покрытия. Рассматриваются механизмы роста покрытий: островковый, послойный, смешанный. Дается схематическое изображение фундаментальных процессов структурообразования. Отмечаются дефекты в вакуумных покрытиях.

На четвертом этапе представлено ВЭП на базе ВЭС. Указаны параметры, предсказывающие образование твердого раствора ВЭС. Рассматриваются шесть семейств высокоэнтропийных сплавов. Оцениваются современные высокоэнтропийные покрытия, полученные вакуумно-дуговым и магнетронным методами. Обобщаются в виде таблицы результаты исследований структурно-фазовых и физико-механических свойств. Приводятся данные трибологических исследований высокоэнтропийных покрытий.

Обсуждение и заключение. В литературе о ВЭП описываются структура покрытия, физико-механические свойства, термическая устойчивость. Авторы представленной статьи обнаружили пробел в исследованиях трибологии высокоэнтропийных покрытий. Из известных результатов можно сделать вывод, что данные покрытия относятся к фрикционными. Однако из-за высокой твердости и пластичности они демонстрируют высокую износостойкость. К тому же сложно говорить об их трибологическом назначении. Для решения вопроса о возможности применения PVD-покрытий в машиностроении следует уделить внимание разработке составов с высокой твердостью, износостойкостью и низким коэффициентом трения. Их можно будет эксплуатировать в трибонагруженных узлах.

Ключевые слова: высокоэнтропийные покрытия, высокоэнтропийные сплавы, PVD-покрытия, вакуумно-дуговой метод, магнетронный метод

Благодарности. Авторы благодарят О.В. Кудрякова, д.т.н., профессора, а также редакционную коллегию журнала и анонимных рецензентов за конструктивные замечания, позволившие улучшить статью.

Финансирование. Исследование выполнено в Ростовском государственном университете путей сообщения за счет гранта Российского научного фонда в рамках проекта № 21–79–30007 «Создание триботехнических материалов и покрытий нового поколения на основе интеллектуальной (цифровой) технологии синтеза». № гос. рег. — 121052000109-9.

Для цитирования. Политыко К.Н., Колесников И.В., Мантуров Д.С. Анализ технологий нанесения высокоэнтропийных покрытий физическим методом осаждения. *Advanced Engineering Research (Rostov-on-Don)*. 2024;24(4):369–391. <https://doi.org/10.23947/2687-1653-2024-24-4-369-391>

Introduction. In modern tribology, the issues of increasing the reliability, wear resistance and durability of friction units are relevant. Often, the stated tasks are solved by applying thin wear-resistant coatings to the tribocontact. Various approaches to strengthening friction surfaces are known, and they are discussed in the presented review. Particular attention is paid to the physical vapor deposition (PVD) method. The high level of PVD technologies allows applying coatings to the friction surface with such a structure and properties that can “adapt” to friction conditions in a wide range of loads and speeds. At the same time, a systematic approach to the selection of materials and modes of PVD application technology has not yet been formed. This piece of research is intended to partially fill this gap. The article presents a review of the literature on methods for applying PVD coatings to the tribocontact surface of modified and multicomponent layers.

The first PVD coatings appeared early last century and have been widely used in various industries. The method is based on the evaporation of the cathode material in high vacuum (up to 10^{-4} Pa). The vacuum facilitates the transition of the material from a solid state to a plasma state in an inert gas environment (Ar, N₂, O₂, C₂H₂, H₂, etc.). With the help of plasma, the evaporated material is transferred to the sample, on which the coating structure is formed and grows. For the physical implementation of the deposition method, various equipment, methods and technologies can be used. Let us name some, with their own heating sources and methods of particle acceleration: thermal evaporation, molecular-beam epitaxy, ion implantation, vacuum-arc deposition, magnetron sputtering. The latter two methods are particularly widely used [1].

The requirements for the substrate surface are due to the fact that the PVD coating accurately reproduces its relief. With a branched relief and high surface roughness, internal stresses accumulate fast in the growing (in thickness) coating — the causes of cracks and delamination. Therefore, the roughness value of the substrate surface must be at least class 10 ($R_a \leq 0.12 \mu\text{m}$; $R_z \leq 0.6 \mu\text{m}$) according to GOST 2789–73¹. This corresponds to the polished surface of steel.

A significant contribution to the development of technology for applying wear-resistant coatings using the physical deposition method was made by S.N. Grigoriev, S.V. Fedorov, A.K. Sinelshchikov, V.P. Zhed, V.I. Kolesnikov, A.I. Grigorov, Yu.G. Kabaldin, A.V. Bely, G.D. Karpenko, I.P. Tretyakov, L.S. Sablev, I.I. Aksenov, A.A. Andreev, V.G. Padalka [2].

The process under study goes through several stages [3].

1. Evaporation of a material (transition from a solid to a vaporous state).
2. Transfer of material vapors to the sample using inert gases.
3. Bombardment of the substrate surface by particles of material in the vapor phase to form an adhesive bond.
4. Origin and growth of the coating.

In mechanical engineering, solutions from leading global companies developing PVD coatings are widely used. Their innovations are applied to harden, reduce the coefficient of friction, and protect parts from corrosion.

Materials and Methods. In the framework of the presented research, materials in Russian and English, published in the Web of Science, eLibrary, Scopus, Medline, and CINAHL databases, were studied and reviewed. When forming queries by keywords, the authors abandoned the random selection of sources in favor of a systematic approach and were guided by a structured list of questions that they intended to consider. Exemplarily, having received a full understanding of how the initial stages of the coating process are described in the theoretical and applied literature, the authors entered new queries to obtain materials on the following stages. This method allowed us to create a representative sample of sources to solve the problems of this study. The collected data were processed using the funneling technique. The first narrowing of the funnel formed the structure of this article, discovered the basic topics of the review:

- vacuum-arc method of coating deposition;
- processes in the cathode region of the arc;

¹ GOST 2789–73. *Surface Roughness. Parameters and Characteristics*. Moscow: Standartinform; 2006. 8 p. (In Russ.) URL: <http://www.omegамет-аll.ru/Data2/1/4294847/4294847701.pdf> (accessed: 29.07.2024).

- processes on the anode and substrate;
- coatings obtained by the vacuum-arc method;
- magnetron sputtering technique;
- coating growth and structure formation mechanisms;
- properties of high-entropy alloys;
- composition of high-entropy alloys and coatings;
- research techniques for studying high-entropy coatings.

The following steps in narrowing the funnel allowed us to focus on the parameters of processes and materials that affect the qualities of coatings potentially suitable for use in mechanical engineering (e.g., heat resistance, hardness, adhesive strength). Numerical data were summarized in tables. Illustrations were used to visualize the basic processes, including those created by the authors of this article. At a certain stage of this work, the authors received a sufficient idea of the number and volume of studies devoted to this or that technology. They turned out to be different. Calculations, comparison and additional targeted search allowed us to conclude that there was a shortage of works considering this problem from the point of view of tribology.

Research Results

Vacuum-Arc Method of Coating Deposition. Vacuum-arc discharge is a self-sustained discharge [4]. It develops in the vapors of the cathode material. In this case, cathode spots (CS) of 10^{-6} – 10^{-3} m in size are formed on the surface of the cathode itself [5]. In them, due to explosive emission of electrons, the boiling point of the material is quickly reached, and it evaporates [6]. Figure 1 shows a diagram of the vacuum-arc method of coating deposition.

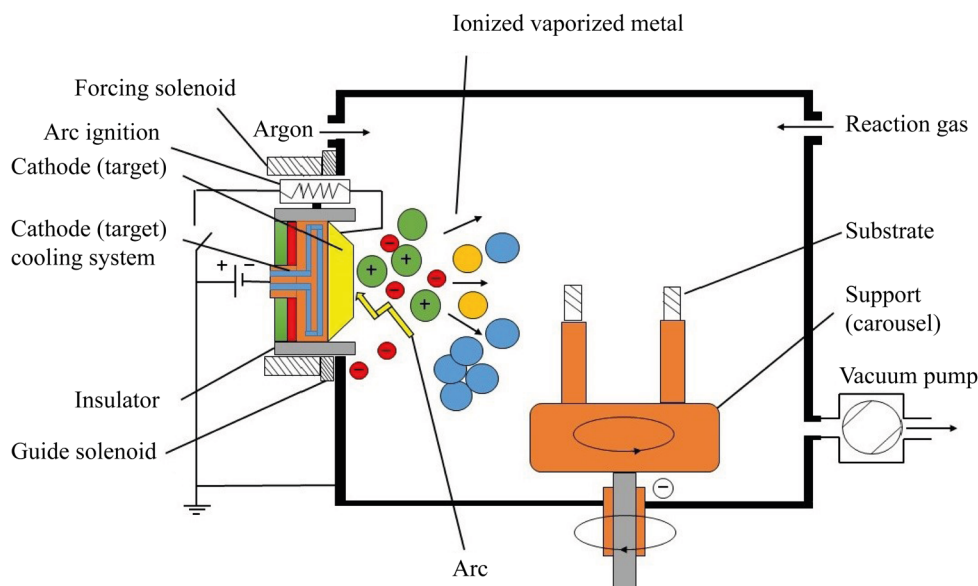


Fig. 1. Scheme of vacuum-arc coating method

The cooperation of academic institutes and universities in Russia has significantly influenced the development of the theory and practice of the new direction. Vacuum-arc technologies are also actively developing in foreign research centers: Lawrence Berkeley National Laboratory (USA), Sydney University of Technology (Australia), Cambridge University (Great Britain), Fraunhofer Institute for Material and Beam Technology (Germany), Wuhan University of Science and Technology (China), etc. [2].

The main unit of vacuum-arc installations is an electric arc evaporator. For uninterrupted operation during coating application, a reliable starting of the evaporator, a stable arc discharge at a given current value, and localization of cathode spots are required. It is also important to have a simple design for quick replacement of ignitions and cathodes, and not to exceed the minimum droplet phase in plasma flows [2].

The authors analyzed this coating application method and noted a disadvantage — the formation of a droplet phase with a size of 0.1–40 μm . Due to this, surface heterogeneity is formed, which causes:

- increased roughness;
- low adhesion of the coating to the substrate;
- formation of internal stresses.

The above-mentioned disadvantages contribute to the formation of structural defects. To reduce the droplet phase, plasma flow separation using a magnetic field, and optimization of the electrical parameters of the vacuum coating installation are used.

Processes in the Cathode Region of the Arc. CS contain erosion products, which are characterized by three phases: microdroplet, vapor, and ionized [7]. The latter predominates when it comes to evaporation in cathodes made of refractory materials [8]. In cathodes made of low-melting metals, the ionized phase accounts for up to 10% [9]. Note that in the plasma flow of a molybdenum arc, the ionized phase accounts for 80–90% of all phases [10].

G.A. Mesyats et al. [8] developed an ectonic theory that described processes in the cathode region of a vacuum arc. According to this theory, the beginning of the CS cycle is the explosive emission of electrons (EEE), which contributes to the appearance of plasma. The potential difference between the electric discharge and the plasma is called the cathode fall potential (CFP). Its value is close to the value of the ionization potential of the metal — and this is the key feature of the phenomenon described. To determine the currents transferred through the CS, two of their characteristics are used — the minimum current and the average value. The minimum (threshold) current is the current at which the CS and arc exist. The parameters of the CS and the threshold current are the major characteristics of the cathode region and the arc discharge [11].

There are three types of cathode spots. The first is observed at the beginning of the arc discharge and moves at a speed of 100–150 m/s [12]. The second is characterized by a more than twofold increase in evaporation and movement at a speed of 50–75 m/s [13]. The third type of CS is considered the most harmful and affects the formation of the droplet phase in vacuum-arc installations. The size of the CS cells depends on the cathode material. For example, the authors [14], studying the formation of CS, have come to the conclusion that for a copper cathode, the size of the CS is about 50–80 μm . It consists of fragments of 5–30 μm and brings current of 10–30 A. The life cycle of the CS is approximately 10^{-7} – 10^{-9} s in craters with a diameter of 1 μm . At the same time, at a distance from the cathode of $2 \cdot 10^{-4}$ cm, the multiplicity and acceleration of ions increase.

The authors [15] have determined that when some cells in the CS disintegrate, others are generated. The process can also occur outside the boundaries of a given CS, but within its plasma halo. This is how other cells are formed and, consequently, a new CS. In [15], it is concluded that CS move a distance of up to 300 μm . As the discharge current increases, the number and size of CP cells grow. Then, the CS is divided into fragments that repel each other [10].

In the early 20th century, J. Stark established that in the presence of a magnetic field perpendicular to the movement of the CS, it moved against the action of the Ampere force [16]. In the case of the CS of the 1st type, a strong plasma flow with a speed of 5–10 km/s will arise. The halo formed in the CS of the 2nd type has a plasma glow and moves in the opposite direction.

From [17], the conditions for changing the speed of the CS movement are known. It grows if the magnetic field induction and the discharge current passing through the cathode increase. It falls with an increase in temperature and arc current.

R. Tanberg has found that the CS cells emit plasma jets at a speed of $(1-2) \cdot 10^6$ cm/s. The speed depends on the cathode material and the electrical parameters of the vacuum installation. Tanberg determined the composition of the plasma jets: electrons, ions, drops of cathode material, and neutral atoms [18].

Considering the operation of the CS cells, we note that the consumption of the cathode mass directly depends on the erosion products and phase. In the ionized phase, the consumption is constant, but when the drop phase appears, it grows in accordance with the increase in the discharge that passes through the CS [2]. The erosion coefficient depends on the current, temperature and material of the cathode (in low-melting materials, destruction occurs faster than in refractory materials).

In [19], the dependence of the erosion coefficient (K_3) on the evaporation temperature for Al, Cu, stainless steel and titanium carbide is considered. It has been found that K_3 for Al, Cu and stainless steel depends on the evaporation temperature, and for titanium carbide in a given range of evaporation temperatures, K_3 does not practically increase. This can be explained by the fact that erosion in this case is a process of intensive evaporation of the cathode due to the uneven magnetic field of refractory materials.

To reduce the erosion coefficient, it is required to apply the coating with an increase in pressure of 10^{-3} – 10^1 Pa. In this case, the 1st type of CS will be actively formed, which will lead to a greater return of evaporated particles to the cathode surface. This phenomenon is less often observed in the 2nd type of CS. From this, we can conclude that the erosion coefficient of the 1st type of CS is less than that of the 2nd. If we consider the “gas – metal” pair, the maximum reduction in cathode mass consumption occurs with an increase in the discharge current and depends on the formed gas compounds with the evaporated material [20].

Thus, having considered the features of the formation of a vacuum-arc discharge and cathode spots, we can conclude that for stable implementation of vacuum-arc deposition, cathode materials with close values of the threshold current of the vacuum-arc discharge should be selected.

Processes on the Anode and Substrate. When the anode is applied, the vapor evaporating from the cathode surface condenses. The anode receives plasma energy. At the same time, its surface must have heat removal to the anode and perform reverse radiation into the plasma with subsequent evaporation of the anode material [21].

It is necessary to reduce the size of the anode to heat it to the melting and evaporation temperature. In this case, it is possible to apply coatings from the anode material with relatively high adhesion. When the anode is cooled to room temperature, brittle porous coatings with a high concentration of internal stresses are formed on its surface.

The energy of ions bombarding the substrate consists of their initial energy and the energy acquired in the Debye layer adjacent to the substrate when a negative potential is applied to it [1]:

$$E_i = E_0 + ezU_n, \quad (1)$$

where E_i — ion energy; E_0 — initial energy; Z — ion charge multiplicity; U_n — substrate potential.

The authors [22] revealed the dependence of the deposition rate on the substrate potential when applying plasma flows of chromium, molybdenum, zirconium and titanium (Fig. 2).

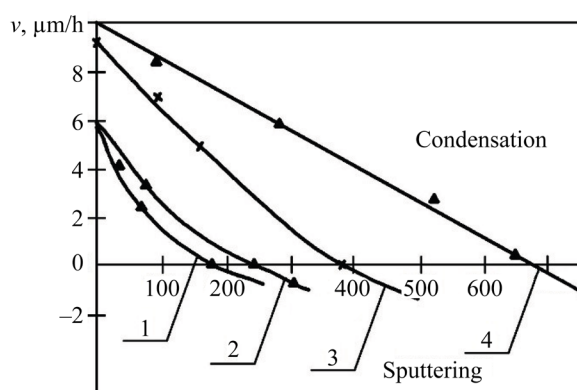


Fig. 2. Dependence of the deposition (sputtering) rate on the substrate potential under interaction with plasma flows of chromium (1), molybdenum (2), zirconium (3) and titanium (4).

Substrate material — steel 30, nitrogen pressure — $2.66 \cdot 10^{-3}$ Pa [22]

From Figure 2, it can be concluded that the potential value at which the processes of condensation and sputtering come into equilibrium depends on the nature of the evaporated material. As the potential value of the substrate increases, its material and the deposited particles are sputtered. Removal of substrate atoms (contaminants) leads to an increase in its temperature. Bombardment of hard alloy plates by chromium and titanium ions in a high vacuum at a potential of 1,000 V increases their average bending strength by 10–15% and reduces strength variation by 40–80% in a few minutes [23]. When the coating is subsequently applied, a diffusion zone up to 2–2.5 μm wide is formed. This treatment provides high adhesion of the coating to the substrate and makes it possible to harden steel with vacuum-arc coatings without losing their physical and mechanical characteristics [14]. With increasing gas pressure, the rate of discharge and speed decrease. This occurs when the active gas is released, which forms compounds with the evaporated gas.

Coatings Obtained Using the Vacuum-Arc Method. The vacuum-arc method (VAM) is used to obtain wear-resistant protective coatings with high physical and mechanical characteristics and a low friction factor. Over the years of developing vacuum technologies, scientists have produced numerous types of coatings for various branches of mechanical engineering. The most famous coatings are nitride (TiN, TiCN, TiAlN, TiMoN, TiSiN) and nanolayer composite (TiN/NbN, TiN/AlN, CrN/TiN, TiN/AlTiN) ones. Recently, the development of multicomponent high-entropy coatings has become a challenge.

Coatings obtained by VAM based on TiN with a nitrogen content of 37.5–52 at.% have been widely studied. Their main feature is a cellular microrelief with a cell size of 0.5–3 μm . The coating can contain two phases: Ti_2N with a hexagonal close-packed (hcp) lattice, and TiN with a face-centered cubic (fcc) lattice. Another characteristic of the coating is a columnar structure. The diameter of the columns is 200 nm, grains with a diameter of 25–75 nm are elongated in the direction of growth [2].

In nitride coatings, nitrogen affects microhardness. With increasing nitrogen pressure in the chamber, microhardness increases to 35–53 GPa, and with further growth, it decreases to 20–24 GPa. This is explained by a decrease in the activation of nitrogen particles at a pressure of more than 1 Pa [2]. Note that the electrical conductivity of the coatings in question depends on the nitrogen content. The friction factor is determined by humidity. If it is low (10%), then the friction factor for chromium steel reaches 0.8, at 50% humidity — about 0.6, and during running-in — about 0.2.

TiCN (titanium carbonitrides) coatings are formed through mixing N_2 with C_2H_2 or CH_4 . They have a columnar structure with a column width of 260 nm. When acetylene is added, the microhardness increases to 50 GPa. Titanium carbonitrides are almost twice as resistant to erosion (compared to TiN coatings) [24].

Coatings $Ti_{1-x}Al_xN$ are substitution solid solutions with a cubic lattice of the B1 TiN type at $0 \leq x \leq 0.6$. They are highly resistant to oxidation at extensive temperatures. Microhardness grows to 30 GPa with an increase in aluminum in the coating composition and the formation of aluminum nitride [25]. The authors [26] found that when applying $Ti_{50}Al_{50}N$ coating with a decrease in reference voltage from -300 V to -150 V, the concentration of aluminum in the coating composition decreased, and this affected the microhardness. With a decrease in reference voltage by 30 V, the microhardness value increased from 29.1 to 34.5 GPa.

The authors [27] applied a TiN coating by the vacuum-arc method and introduced MoS_2 into it through spraying molybdenum disulfide using the magnetron method. It was found that when introducing MoS_x , the hardness increased significantly (up to 30 GPa). The friction factor decreased to 0.15, and the wear rate decreased by 20 times.

Coatings TiSiN have attracted the interest of scientists because Si is an alloying element of transition metal nitrides. It is chemically related to nitrogen and has a minor atomic radius (if we are talking about transition metals). This is why TiSiN coatings have a high microhardness value (30–45 GPa) and a low elastic modulus (200–250 GPa). During tribological tests, silicon forms SiO_2 compound, and this solid lubricant reduces the friction factor to 0.5 [28].

When creating nanolayer composite coatings, layers of metals with different physical-mechanical properties, but close thermal expansion coefficients, alternate. The authors [29] studied nanolayer composite coatings made of materials with nanohardness of ~ 20 GPa. The TiN/NbN coating was found to have high nanohardness. The nanohardness of the TiN/VN coating was 55 GPa, and this is a very high figure for a nanolayer coating.

The use of the VAM is important in the creation of combined MeC(MeN)/a-C:H coatings with alternating nitride and carbon layers. Thus, in [30], TiAlN/DLC-Ti coatings were compared to DLC-Ti. The wear resistance of the combined coatings turned out to be twice as high as that of DLC-Ti, due to an increase in nanohardness to 24 GPa and Young's modulus — to 230 GPa.

In [31], the effect of ion implantation on the adhesive strength of TiN and Ti coatings was studied. Before applying TiN coating with Ti sublayer, U8A steel substrate was irradiated by argon ions with doses from 0 to 10^{17} ion/cm². For TiN obtained on an irradiated substrate up to 10^{17} ion/cm², the adhesive strength increased to 11.3 N. This is twice as much as the adhesive strength of TiN on a non-irradiated substrate. In the case of Ti monocoating, it was found that on a sample without implantation, peeling occurs at minimal indenter loads, and with irradiation of $3 \cdot 10^{16}$ and $1.5 \cdot 10^{17}$ ion/cm², the adhesive strength increases by 1.8–2.5 N. These values are typical for soft coatings, which include titanium. Thus, ion implantation of the substrate increases the adhesive strength of TiN and Ti coatings.

In [32], MoTiN and MoCuN coatings were obtained by the vacuum-arc method, and the adhesive strength was determined using scratch testing. It was found that MoTiN coatings had hardness of up to 40 GPa and an adhesive strength — up to 22 N. This is significantly higher than that of MoCuN. Its hardness did not exceed 22 GPa, and the adhesive strength was no more than 4 N. The authors [32] explained the results by the structure of the coatings being formed. In the first case, a solid solution based on titanium nitride TiN was formed, in the second — a mixture of molybdenum nitride Mo_2N and free copper.

Thus, a review of the literature on coatings obtained by the vacuum-arc method allowed us to draw certain conclusions. Such coatings are used to protect the surface of various tools. If we are talking about heavily loaded friction units, wear-resistant and antifriction coatings are used. It is possible to use different materials and combine application technologies to obtain combined coatings, such as $TiMoS_xN$, MeC(MeN)/a-C:H.

Magnetron Sputtering Method. Magnetron sputtering involves bombarding the target surface by high-energy ions of the working gas (Ar , N_2 , O_2 , CH_4) in glow discharge in vacuum of 10^{-3} – 10^{-2} Pa at a temperature of 100–250°C. This is one of the most common techniques for producing thin films. When sputtering target atoms, secondary electrons are emitted, which maintains the existence of plasma. High sputtering speed is achieved through increasing the ion current density due to a strong magnetic field [33].

The first magnetron sputtering systems (MSS) appeared in the early 1970s. At that time, cylindrical coaxial MSS of normal and inverse type were used. Their main problem was nonregular sputtering of the material due to the escape of electrons along the magnetic field lines. In this regard, the installations were modernized [34], technologies were developed, new types of magnetrons were created and introduced into production. Let us name some of them:

- magnetron with a flat cathode;
- magnetron with a balanced magnetic field;
- magnetron with an unbalanced magnetic field;

- unbalanced magnetrons with a vertical component of the magnetic field to the substrate;
- unbalanced magnetrons with magnetic field dispersion away from the substrate;
- unbalanced MSS with two magnetrons;
- magnetrons with devices for additional gas ionization;
- MSS with bipolar power supply.

The diagram of an unbalanced magnetron is shown in Figure 3.

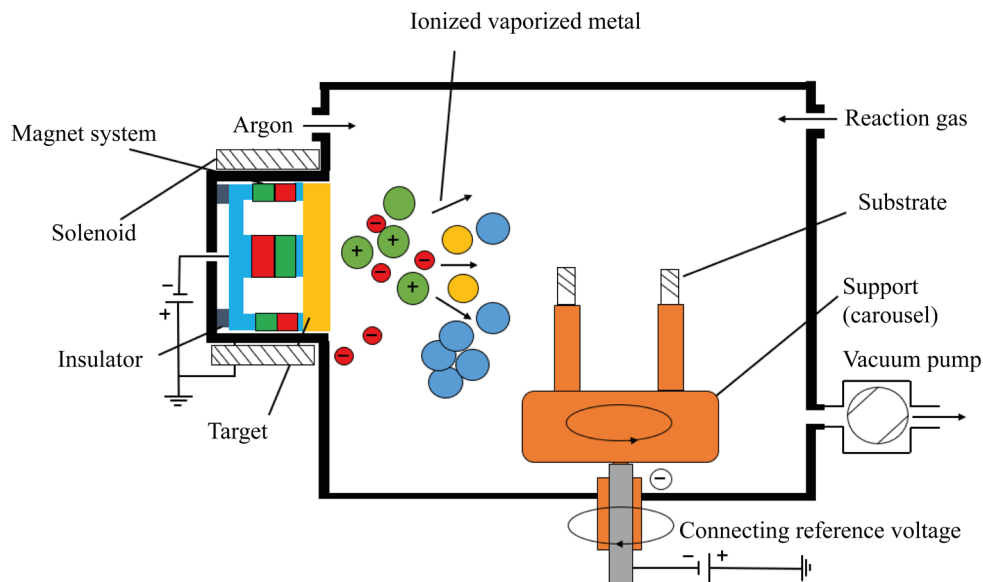


Fig. 3. Unbalanced magnetron circuit

The main elements of the device are: a cathode-target, an anode, and a magnetic system. Magnetrons are made so that a magnetic field is induced in parallel in the near-surface region of the target. As a result, secondary electrons are accelerated towards the targets. One magnetic pole is located in the center, and the second is at the edges of the cathode. This provides capturing the electrons that do not bombard the substrate itself. Thereby, the heating temperature of the target is reduced, but the degree of plasma ionization is increased [35].

The main advantages of this approach [36]:

- repetition of the exact composition of the target in a coating with a high-density structure;
- using any material for application to the substrate;
- applying coatings at low temperatures;
- controlling the quality of coatings through changing the parameters of the application process.

Among the most noticeable disadvantages are:

- low sputtering speed;
- low efficiency;
- weak adhesion of the coating to the substrate;
- instability of the phase components of the coating;
- cost of equipment.

Currently, it is required to obtain nitride and high-entropy coatings using magnetron sputtering. These include combined coatings, high-entropy coatings (HEC), as well as:

- cermet (TiN, ZrN, CrN, TiC, TiCN, TiAlN, AlCrN, TiBN, CrAlTiYN, Al₂O₃, SiO₂);
- metal (Al, Ag, Au, Cu, Zn, Ti, Zr, Hf, Cr, Ta, Ni, Co, Si);
- nanocomposites (TiAlN/Si₃N₄, ZrN/Cu, TiN/CrN, TiN/AlN, CrN/AlN, TiN/CN).

Let us consider the main results of studies on coatings obtained by magnetron deposition method.

The authors [37] have determined that the magnetron type is suitable for depositing titanium nitride coatings with a thickness of 1 nm to 1 μm. For this purpose, they used a facility with pulsed sputtering on silicon substrates [38]. To maintain process stability, they varied the distance between the target and the substrate in the range of 50–100 mm and changed the nitrogen feed rate into the working chamber. Analysis of the obtained titanium nitride (TiN) coating has shown that with a decrease in the distance between the target and the substrate, the mechanical properties of the coating

deteriorate, its quality decrease. This is explained by the fact that due to the close distance, the thermal effect increases, and the effect of thermal annealing occurs.

The authors [39] studied the growth rate of coatings on semiconductor substrates at room temperature. The feed rate and operating power of the magnetron control unit were varied.

Using the magnetron deposition method, superhard $\text{Ti}_{1-x}\text{Al}_x\text{N}$ coatings were obtained at $0.5 > x > 0.6$ with microhardness of 40 GPa. It is worth noting that the lattice parameter for TiN decreased from 0.4255 nm to 0.417 nm [40].

Coating TiMo(SN) alternated layers of molybdenum disulfide MoS_2 with TiN, so the microhardness increased from 4 GPa to 15–35 GPa with a friction factor of 0.02–0.1. MoS_2 was evaporated using a magnetron, and TiN was deposited using vacuum arc deposition. MoS_2Ti with nanohardness of 10 GPa and Young's modulus of 142–169 GPa was applied to a CrN coating with nanohardness of 24–30 GPa and Young's modulus of 352–418 GPa. Due to molybdenum disulfide in the coating composition, the friction factor decreased by 91–95%, wear — by 50–95% [41]. Pure molybdenum disulfide was applied using a magnetron and studied without removing it from the chamber. Its friction factor was 0.002 [42]. Thus, adding MoS_2 to the coating composition reduces significantly the friction factor.

Nanostructured multilayer TiN/AlN coatings obtained by magnetron method showed high results in micro drilling and turning in comparison to TiN coatings. When drilling fiberglass, the durability of drills with TiN/AlN coating was 40% higher than without it, and 25% higher than with TiN coating [43].

An important property of coatings obtained by the magnetron method is adhesive strength. It provides evaluating the resistance of the surface to delamination. In [44], the adhesive strength of nitride coatings CrN, TiN on carbon steel S235 is evaluated. It is found that the application of a multilayer structure (sublayer + coating) provides for the adhesion improvement. Thus, for CrN coating, the value of adhesion strength without a sublayer is 37 N, with a Cr sublayer — 40 N. The indicators for TiN coating are 16 N (without a sublayer) and up to 24 N (with Ti sublayer). Adhesion strength increases when applying coatings to a harder base in the form of pure metals, close in composition to the basic coating.

The authors [45] studied the adhesive strength of AlTiNiAg and NiAg coatings obtained by the magnetron method. The coatings were applied to silicon structures and molybdenum thermocompensators of power semiconductor devices with annealing in vacuum, hydrogen, and without it. The adhesive strength was studied by scratch testing. The maximum adhesive strength was found in samples of a silicon structure with a four-layer AlTiNiAg coating (21.7 N) after annealing in vacuum. For molybdenum thermocompensators, the two-layer NiAg coatings annealed in vacuum turned out to be the strongest (13.5 N).

The review of the literature has established that magnetron sputtering is characterized by:

- ability to work with numerous materials;
- high accuracy of target composition repetition (at. %).

The method is widely used for applying thin layers to semiconductors, glass, and obtaining self-lubricating coatings with a low friction factor.

Coating Growth and Structure Formation Mechanisms. When coatings are applied, the structure formation occurs in several stages (Fig. 4). At the first stage, atoms are adsorbed from the plasma flow. The atom continues to move until a chemical bond with the surface atoms is formed. At this stage, the atom may not form a chemical bond with the substrate surface, depending on the material being applied and the method of application. After the atom is fixed to the surface, chemical bonds are formed with the newly arrived atoms — this is how the coating is formed. Diffusion processes may occur between the substrate and the film.

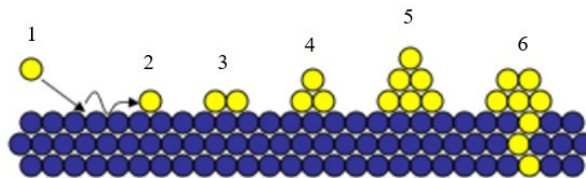


Fig. 4. Scheme of formation of coating structure: 1 — deposition of atom from plasma flow; 2 — movement of atom; 3 — formation of adsorption chemical bond of deposited atoms from plasma with substrate; 4, 5 — formation of coating cells; 6 — penetration of plasma atoms into substrate material

When an atom is adsorbed on a substrate, surface tension arises. The bonds between the atoms of the substrate and the coating are lengthened, therefore, the energy depends on the type of bond formation. The achievement of energy equilibrium is facilitated by the force of surface diffusion, which is determined by the temperature of the substrate and the energy of the atoms.

Figure 5 schematically shows three mechanisms of coating growth.

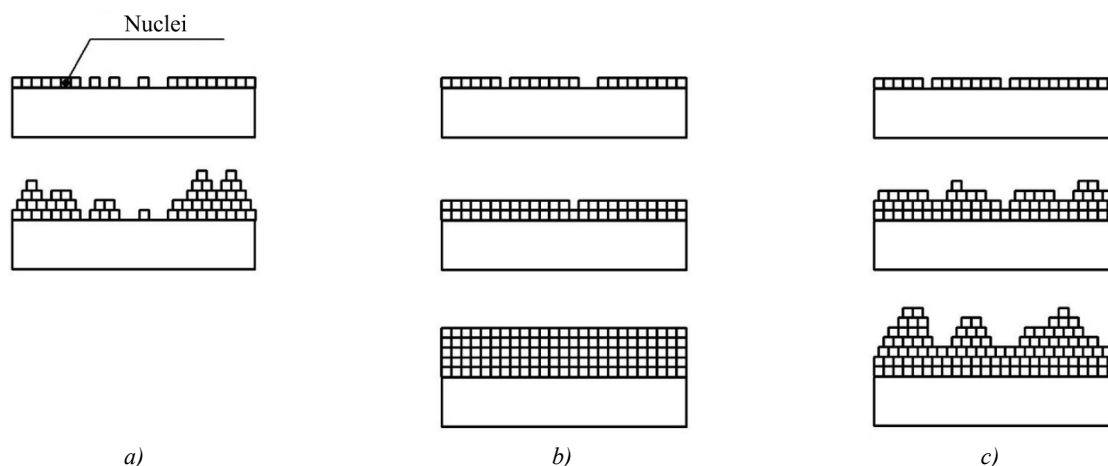


Fig. 5. Schematic representation of three mechanisms of coating growth:
a — island, Volmer-Weber; *b* — layered, Frank-van der Merwe;
c — mixed, Stranski-Krastanov

The layer-by-layer mechanism operates if the bond strength between the coating atoms is less than the bond strength between the coating and substrate atoms, and also if these forces are equal. In this case, the mismatch of the crystal lattices should be minimal. The condition for the island mode to be realized is that the bond between the coating atoms should be stronger than the bond between the coating and substrate atoms. The mixed mode occurs when the crystal lattice parameters of the coating and substrate are mismatched [1].

B.A. Movchan and A.V. Demchishin [46] were the authors of the first significant works on the mechanism of coating growth. In parallel, they developed physical deposition methods and proposed a diagram of the zone structure of coatings depending on the substrate temperature. The researchers have clearly shown that the microstructure of PVD coatings is conditionally divided into three zones with different homologous process temperatures (T_{hm} — ratio of the melting temperature of the coating to the substrate temperature $T_{пл}/T_{под}$).

This model was improved by J.A. Thornton [47]. He introduced the partial pressure of argon in the chamber and the intermediate zone T (between the first and second) into the diagram. The coating density in zone T is higher than in the neighboring zones, the surface roughness is less.

During the formation of the microstructure at different stages [48], nuclei are formed, islands increase in size and coalesce, polycrystalline islands and channels appear, and films grow (Fig. 6).

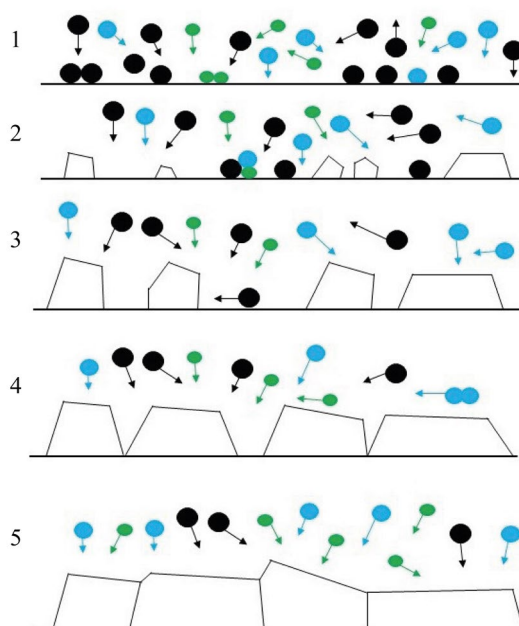


Fig. 6. Schematic representation of structure formation processes: 1 — formation of nuclei; 2 — growth of islands; 3 — contact and coalescence of islands; 4 — coarsening of grains, formation of polycrystalline islands and channels; 5 — development of structure and growth of coating [48]

The formation of nuclei begins with the growth of isolated islands on the surface of the substrate. The size of the islands is 20–30 Å [49].

During the process of island coalescence, a driving force for grain coarsening is created due to the surface diffusion of atoms and grain boundary movement. The resulting low-energy islands absorb others. As a result, the new single-crystal island contributes to a decrease in the energy of the entire surface. The coarsening of the structure under coalescence depends on the temperature, the size of the islands, and determines their orientation [50]. At low temperatures and large island sizes, coarsening occurs more slowly due to grain boundary migration. During the coalescence of crystals, the grains coarsen until their boundaries become large and immobile.

It should be noted that vacuum technologies require preparation of the substrate for coating application. This is important because during coating growth, defects, such as porosity, internal stress, deformation of crystallites and the crystal lattice, may appear. They occur both in the vacuum-arc method and in the magnetron method.

If there is macro-roughness on the sample surface, high internal stresses are formed in the coating, which lead to delamination. Micro-roughness causes porosity of the coating and worsens its physical and mechanical properties. Defects appear on the surface and increase with the growth of the structure. The formation of a droplet phase is possible not only in vacuum-arc coatings, but also in magnetron sputtering of refractory materials [50]. Droplets on the surface are formed rather quickly and stochastically. The result is screw dislocations, which cause spiral growth of crystals. As shown in [51], during the coating process, the “craters” formed due to the separation of large particles are quickly filled with ions of the applied material. Therefore, defects due to the droplet phase are substructural and do not greatly affect the structure and properties of the coating.

Properties of High-Entropy Alloys. Research into HEA and coatings based on them has begun relatively recently. In 2002, Professor Jien-Wei Yeh (National Tsing Hua University, Taiwan) developed a new class of materials [52]. Physical and mechanical properties of HEA have attracted the attention of scientists. Over 20 years, about 5,000 papers on HEA have been published [53]. A characteristic feature of HEA is the mixing of 5 or more elements (each accounts for 5–35% at.). In this case, a substitution solid solution is formed. It is single-phase. A phase with a bcc-, fcc-, or bcc+fcc lattice is formed [54].

The key feature of HEA is the high entropy of mixing. It promotes the formation of solid solutions, which reduces the likelihood of intermetallic compounds. As a result, HEA are characterized by thermal stability, corrosion and wear resistance, increased plasticity at low temperatures, and resistance to ionizing radiation [55]. The average atomic concentration (el/at.) is often used to characterize the atomic-crystalline structure of multicomponent systems. In high-entropy alloys:

- at a concentration of up to 4 el/at., hcp lattice is formed;
- in the range from 4.25 to 7.2 el/at. — a bcc lattice;
- at a concentration from 7.2 to 8.3 el/at. — a two-phase structure with bcc and fcc lattices;
- a level above 8.4 el/at. corresponds to an fcc lattice [56].

The properties of the HEA are described by 5 parameters [57]:

- 1) mixing entropy ΔS_{mix} ;
- 2) mixing enthalpy ΔH_{mix} ;
- 3) difference in atomic sizes δ ;
- 4) electronegative difference $\Delta\chi$;
- 5) concentration of valence electrons VEC .

All criteria are calculated using expressions taking into account the atomic concentration of each i -th component of alloy c_i .

The entropy of the HEA consists of:

- entropy of electron motion (ΔS_B);
- entropy of atomic oscillation (ΔS_v);
- configurational entropy of mixing (ΔS_k);
- entropy of magnetic moments (ΔS_m) [58].

In a high-entropy alloy, configurational entropy (ΔS_k) is higher than that of the components ΔS_B , ΔS_v , ΔS_m . But this is not typical for common metals. Therefore, in high-entropy alloys, a single-phase solid solution is formed due to ΔS_k . With

an increase in the number of elements (n), ΔS_k grows. This reduces the Gibbs energy $\Delta G = \Delta H - T \Delta S$ (ΔH — enthalpy, T — absolute temperature, ΔS — entropy) and maintains thermodynamic stability [59]. The entropy and enthalpy of high-entropy alloys are determined from the expressions:

$$\Delta S_{mix} = -R \sum_{i=1}^n c_i \cdot \ln(c_i), \quad (2)$$

$$\Delta H_{mix} = \sum 4c_i c_j \Delta H_{mix}^{AB}, \quad (3)$$

where R — absolute gas constant, $R = 8.314 \text{ J/(K}\cdot\text{mol)}$; c_i — atomic concentration of element i (at.%); ΔH_{mix}^{AB} — enthalpy of binary alloys near the melting point of elements AB, which are part of HEA.

At equiatomic concentration of components, the atomic concentration of an element is defined as $c_i = 1/n$. This means that the entropy level is $\Delta S_{mix} = R \cdot \ln(n)$. At $n \geq 5$, the configurational entropy is: $\Delta S_{mix} \geq 13.4 \text{ J/(K}\cdot\text{mol)}$, and the alloy is considered high-entropy.

Figure 7 shows the dependence of the mixing entropy on the number of elements [60].

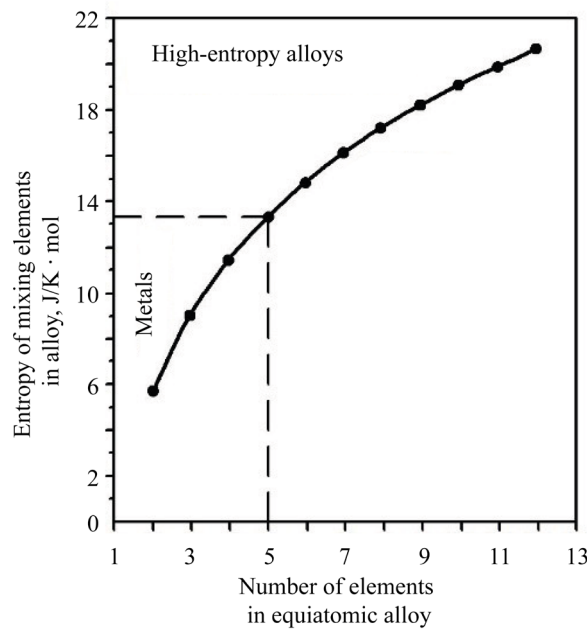


Fig. 7. Dependence of mixing entropy on the number of elements [60]

In metals and simple alloys, atoms can occupy a place in the crystal lattice with equal probability. This is how they differ from high-energy alloys, in which the crystal lattice is distorted due to the substitution of several elements with different atomic sizes. If the sizes of atoms in the alloy structure differ significantly, then internal stresses are formed, which cause an increase in the strength properties of the coatings [58].

The distortion of the crystal lattice determines the strength of the HEA and reduces diffusion. Slowing down the diffusion enhances the formation and stabilization of the solid solution of the HEA, and also reduces the rate of crystal growth. The possibility of forming an amorphous structure is opened up, but the thermal and chemical stability increases [61].

To predict the formation of solid solutions, the difference in atomic radii (in %) is used. This parameter is denoted by δ . The formation of a structural phase in HEA is determined by:

$$\delta = 100 \sqrt{\sum_{i=1}^n c_i \left(1 - \frac{r_i}{\bar{r}}\right)^2}, \quad (4)$$

where n — number of components in the alloy; c_i — content of the i -th component (at. %); r_i — atomic radius of the i -th component; \bar{r} — average atomic radius $\bar{r} = \sum_{i=1}^n c_i r_i$.

To describe the difference in atomic sizes, paper [62] proposes to classify the elements of the HEA. Table 1 shows the classification and elements depending on the atomic size δ .

Table 1

Classification of Elements by Atomic Size [62]

Atomic size (radius) group	Group elements
Minimum	Si — 0.117 nm
Small (about 0.125 nm)	Cr, Co — 0.125 nm, Fe — 0.126 nm, Cu — 0.128 nm, V — 0.132 nm
Medium (about 0.145 nm)	Al — 0.143 nm, Ti — 0.145 nm, Nb — 0.159 nm
Large (about 0.160 nm)	Hf — 0.159 nm, Zr — 0.160 nm
Out size (about 0.180 nm)	Y — 0.180 nm

To exclude the formation of Laves phases, intermetalles, and amorphous phases, theoretical parameter Ω is proposed, which takes into account the melting temperature of the components:

$$\Omega = \frac{T_m \Delta S_{mix}}{|\Delta H_{mix}|}, \quad (5)$$

where T_m — average melting point of the components.

The average melting point is estimated together with the difference in atomic radii. High value $\Omega > 1.1$ and small value $\delta < 6.6$ predict the formation of solid solutions.

The authors [57] proposed a variant of predicting the formation of solid solutions by electronegativity:

$$\Delta\chi_{Allen} = \sum_{i=1}^N c_i \left(1 - \frac{\chi_i}{\chi_a} \right), \quad (6)$$

where χ_i — Pauling electronegativity for the i -th element; χ_a — average electronegativity.

In this case, electronegativity is the average ionization energy of the valence electrons of free atoms. The authors [63] determined that solid solutions were formed in the ranges $3 < \Delta\chi < 6$ and $1 < \delta < 6\%$. It was also established that solid solutions with a bcc lattice exist with a greater mismatch of atomic radii and lower electronegativity (in comparison to the conditions for the fcc lattice).

The valence electron concentration (VEC) affects the stability of the structure of solid solutions and is defined as a weighted average value:

$$VEC = \sum_{i=1}^n c_i (VEC)_i, \quad (7)$$

where $c_i(VEC)_i$ — VEC for the i -th element.

When determining the electron concentration, special attention is paid to the stabilization of the solution due to the accumulation of electrons at low-energy levels [59]. The density of the structure and bonds per atom are estimated. At $VEC \geq 8$, one fcc phase is formed. At $6.87 \leq VEC \leq 8$, the bcc and fcc phases are mixed. At $VEC \leq 6.87$, the alloy contains only the bcc phase. In [64], the influence of VEC on the formation of AlCoCuFeNi alloy lattice is analyzed. The bcc lattice was formed at low values of the valence electron concentration, and the fcc lattice — at high values.

The theoretical analysis allows us to determine the conditions for the formation of a solid solution:

- mixing enthalpy — $7 \leq \Delta H_{mix} \leq 22$ kJ/mol;
- mixing entropy — $11 \leq \Delta S_{mix} \leq 19.5$ J/(K·mol);
- difference in atomic sizes — $0 \leq \delta \leq 8.5\%$.

Composition of High-Entropy Alloys and Coatings. About 40 elements are known, from which approximately 500 materials can be obtained that meet all the criteria of high-entropy alloys [56].

In the literature, the elements of the HEA are divided into families. The first one is the most studied, it is based on 3d-transition elements: Fe, Co, Cr, Ni, Mn, Al, Ti, Cu, V. These are elements with high hardness, corrosion and wear resistance. One of the first and well-studied high-energy alloys is CoCrFeMnNi. This is the so-called Cantor alloy, proposed in 2004. The second family of HEA is based on refractory metals (Hf, Ta, Mo, Nb, V, W, Cr, Zr, Ti). The third includes low-melting elements (Al, Sn, Be, Li, Mg, Ti, Sc, Si, Zn). The fourth includes rare earth elements (Gd, Dy, Lu, Tm, Tb, Y). The fifth consists of high-entropy bronzes and brasses (Zn, Cu, Ni, Mn, Al, Sn). The sixth, the youngest, unites Au, Ag, Cu, Co, Cr, Ni, Pt, Pd, Ru, Rh [57]. Some elements belong to different families.

To reach high values of hardness and strength in modern nitride HEA, transition d-metals with negative enthalpy (ΔH) are used. The composition of nitride HEA and their hardness values are given in Table 2.

Table 2

Hardness Values of High Entropy Alloys [59]

Composition	Hardness (GPa)
(AlCrNiSiTi)N	15
(TiVCrZrY)N	18
(AlCrMoSiTi)N	25
(TiAlCrSiV)N	31
(AlCrTaTiZr)N	35
(AlMoNbSiTsTiVZr)N	37
(AlCrNbSiTiV)N	41
(TiHfZrVNb)N	43

The authors [64] have found that the strength properties of high-entropy alloys are higher than those of numerous metallic alloys. The yield strength and Vickers hardness values of HEA are high — at the level of metallic glass, titanium and nickel alloys. NbCrMo_{0.5}Ta_{0.5}TiZr and Al_{2.0}CoCrCuFeNi occupy a special place. Their Vickers hardness is close to 1000, and the elastic limit exceeds this value.

Heat-resistant HEA are widely used and could be applied in the aerospace industry. The first such alloys based on Mo, Nb, Ta, W, V, had serious drawbacks — high density and low corrosion resistance. The problem is solved by replacing the specified elements with others — Cr, Ti, Zr, Al [65].

An important characteristic of heat-protective alloys and coatings is the thermal coefficient of linear expansion (TCLE). It affects the adhesion between the coating and the substrate, since in coatings with a low TCLE, thermal transformations occur at high temperatures, which cause “peeling”, delamination, and further destruction of the coating:

- diffusion processes between the coating and the substrate;
- phase transformations;
- plastic deformations;
- oxidations;
- compressive stresses.

To solve the problem of coating destruction under the influence of temperature, it is proposed to use a thermal barrier layer of high-entropy NiAlCrW-TaY-SiHf coating with a thickness of 20–30 μm [66]. This allows reducing the diffusion exchange, which causes an increase in the TCLE and adhesion between the combined coating and the substrate. It should be noted that for tribological coatings, this criterion is not relevant due to the small thickness of coatings.

The authors [67] performed annealing of two coatings:

- (Al_{23.1}Cr_{30.8}Nb_{7.7}Si_{7.7}Ti_{30.7})₅₀N₅₀ at bias potential (–100) V;
- (Al_{29.1}Cr_{30.8}Nb_{11.2}Si_{7.7}Ti_{21.2})₅₀N₅₀ at bias potential (–150) V.

The annealing was carried out at a temperature of 900°C for two hours. The study of the microstructure showed that oxide particles were formed on the surface of the coating. Their thickness for the coating (Al_{23.1}Cr_{30.8}Nb_{7.7}Si_{7.7}Ti_{30.7})₅₀N₅₀ was 100 ± 12 nm, for the coating (Al_{29.1}Cr_{30.8}Nb_{11.2}Si_{7.7}Ti_{21.2})₅₀N₅₀ — 80 ± 7 nm. Under the oxide films, the structure of the coating did not change. The study confirmed that high-entropy coatings have high oxidation resistance and, in that indicator, surpassed most of the coatings in use.

To obtain high-entropy coatings, PVD deposition methods are widely used: vacuum arc and magnetron. The properties of several types of coatings from high-entropy alloys have been studied in detail: (AlCrTaTiZr)N, (TiAlCrNbY)C, (FeCoNiCrCuAl)N, (AlCrMoSiTi)N, (AlCrNbSiTiV)N, (TiAlCrSiV)N, (AlMoNbSiTaTiVZr)N, (TiVCrZrY)N, (TiHfZrVNb)N, (TiVCrZrHf)N.

The authors [68] obtained high-entropy nitride coatings using vacuum-arc deposition and magnetron sputtering. It has been found that metals of groups IV–V tend to form nitrides with a stable structure. The microstructure and hardness of high-entropy nitride coatings depend on the parameters of the deposition process. In processes with the same parameters,

expansion in the number of components leads to an increase in the hardness of the coatings. Improved tribological properties are achieved by adding Mo or W elements, which reduce the friction factors. The addition of Al and Si increases oxidation resistance due to the formation of protective oxide layers.

In [69], the production of a CoCrFeNi film with a thickness of about 1 μm using ion-beam sputtering is shown. A film of similar composition and thickness was also obtained using the high-pressure torsion (HPT) technique. In the comparative analysis of the films, the textures and sizes of the crystallites were determined by X-ray diffraction, and the hardness was measured through nanoindentation. The hardness of the film obtained by PVD was 9.8 ± 0.3 GPa. This was greater than that of the HPT sample (7.3 ± 0.3 GPa). The grain size of the crystallites was about 20 nm.

The authors [70] obtained a CuTiZrCrNi coating on a substrate made of AISI 201 steel using magnetron sputtering. It was found that after tribological tests, the coating wear was $3 \cdot 10^{-4}$ g/min. The friction factor of the CuTiZrCrNi coating on copper was 0.041, on aluminum — 0.066.

In [71], a CrTiNiZrCu coating on an AISI 201 steel substrate obtained through magnetron sputtering is described. Atomic force microscopy showed a cellular nanostructure of the high-entropy coating. Several models of its formation are described, and the main reasons for the formation of such nanostructures are established.

The authors [72] used a magnetron to form a CrNbTiMoZr coating with a nanohardness of 9.7 GPa and high tribological properties. In [73], multicomponent coatings based on AlCrTiV with the addition of Cu and Mo were considered. The researchers concluded that the corrosion properties of the coatings significantly exceeded the properties of the steel substrate AISI 304. This was explained by the formation of stable oxides.

In [74], the creation of a TiTaHfNbZr coating with a thickness of 800 nm on a substrate of Ti-6Al-4V alloy was described. It was obtained using magnetron sputtering. The tribological research showed that with an increase in load from 1 N to 3 N, the wear of the substrate without a coating increased significantly, whereas for samples with a TiTaHfNbZr coating the wear was insignificant.

In [75], vacuum arc and magnetron methods were used to obtain a (TiAlSiCrNiCuOC)N coating with a B1-type lattice, identical to TiN, with a superhardness of 47 GPa and a thermal stability of 900–1,000°C.

In [76], the production of a high-entropy nitride coating (TiZrHfVNB)N using the vacuum-arc method is shown. The reference voltage changed from –40 to (–200) V. The coating thickness was 4.78 μm . The results of nanoindentation showed that with a growth of the reference voltage, the following parameters increased:

- microhardness (from 19.34 GPa to 29.94 GPa);
- elasticity modulus (from 281 GPa to 384.1 GPa).

Tribological tests allowed us to establish the friction factor (1.193). The coating had low wear of $0.039 \cdot 10^{-5}$ ($\text{mm}^3/\text{N}/\text{mm}$).

Several works are devoted to the study of the structural-phase state and physical-mechanical properties of high-entropy coatings. The main results of the studies are presented in Table 3.

Table 3

Results of Studies on Structural-Phase State and Physical-Mechanical Properties of HEA

Name of coating	Process variables	Hardness H , GPa	Young's modulus, GPa	Structure	Link
$(\text{Al}_{23,1}\text{Cr}_{30,8}\text{Nb}_{7,7}\text{Si}_{7,7}\text{Ti}_{30,7})_{50}\text{N}_{50}$	$U_c = -50$ V	16.00	305	fcc	[77]
	$U_c = -100$ V	36.10	440		
	$U_c = -150$ V	34.10	400		
$(\text{Al}_{29,1}\text{Cr}_{30,8}\text{Nb}_{11,2}\text{Si}_{7,7}\text{Ti}_{21,2})_{50}\text{N}_{50}$	$U_c = -50$ V	25.00	330	fcc	[77]
	$U_c = -100$ V	35.00	390		
	$U_c = -150$ V	37.00	395		
(AlCrTaTiZr)N	–	34.00–35.00	340–355	fcc	[78]
(AlCrMoTaTiZr)N	N = 40%	40.20	370	fcc	[79]
	N = 50%	37.00	420		

(AlCrMnMoNiZrB _{0.1})N	R _N = N ₂ /Ar = 0	7.10	163	Amorphous	[80]
	R _N = N ₂ /Ar = 0.5	~10.00	~180	fcc	
	R _N = N ₂ /Ar = 1	10.20	~180	fcc	
(TiZrNbHfTa)N	U _c = -50 V	22.50	170	fcc	[81]
	U _c = -100 V	33.00	276		
	U _c = -150 V	32.90	268		
(TiZrNbHfTa)N	U _c = -50 V	22.50	170	fcc	[81]
	U _c = -100 V	33.00	276		
	U _c = -150 V	32.90	268		
(TiZrNbHfTa)C	–	27.50	–	fcc	[81]
TiZrNbHfTa		5.40	–	fcc + double (triple) bonds	[81]
(TiVCrZrHf)N	T _{подложки} = 250°C	41.00	~300	fcc	[82]
	T _{подложки} = 350°C	45.00	~310		
	T _{подложки} = 450°C	49.00	~320		
	T _{отжига} = 300°C	31.24	300		[83]
	T _{отжига} = 500°C	11.85	250		
	T _{отжига} = 700°C	2.30	~60		
(TiHfZrVNb)N	U _c = -50 V	21.00	337	fcc	[59]
	U _c = -100 V	28.70	361		
	U _c = -200 V	29.50	373		
(TiVCrZrY)N	N = 0%	20.90	–	hcp	[84]
	N = 100%	18.90	–		

The data in Table 3 allow us to conclude that to obtain high-strength coatings, it is required to introduce transition metals into their composition. The addition of nitrogen strengthens covalent bonds in the coating and significantly increases the hardness. Coatings based on HEA are multi-parameter; therefore, to change the values of nanohardness and Young's modulus, it is necessary to vary the process parameters during application: nitrogen supply, substrate temperature, reference voltage.

Research on high-entropy coatings is based on the study of the coating structure, physical-mechanical properties, and thermal stability. Less attention is paid to tribological studies. Table 4 summarizes their key known results.

Table 4

Results of Tribological Studies on High-Entropy Coatings

Name of coating	Friction factor	Wear intensity I 10 ⁻⁶ (mm ³ /N/m)	Link
(AlCrTaTiZr)N	0.760	3.66	[85]
(AlCrMoTaTiZr)N	0.800	2.90	[86]
(TiZrNbHfTa)N	0.960	2.90±0.20	[81]
(TiZrNbHfTa)C	0.150	0.80±0.05	[81]
TiZrNbHfTa	0.870	17.00±1.00	[81]
(TiZrHfVNb)N	1.193	390.00	[59]

Table 4 shows that high-entropy coatings have a high friction factor. Note that (TiZrNbHfTa)C has an extremely low coefficient (0.15). This is explained by the formation of a free carbon phase, which acts as a solid lubricant and reduces the friction factor. The high wear resistance of HEA is associated with an increase in hardness when alloying transition metals, nitrogen, and greater resistance to plastic deformation.

Research Methods for High-Entropy Coatings. The microstructure of the HEC is examined using optical metallography. Scanning electron microscopy (SEM) is used to study fine details. Its major advantages are high resolution and clarity. In addition, SEM works with several types of induced radiation. In addition to X-rays, reflected and absorbed electrons, as well as cathodoluminescence, are used. In this way, it is possible to study the surface relief, phase and

orientation contrasts, and conduct micro-X-ray spectral and energy-dispersive analysis. In some cases, the capabilities of electron microscopy and cross-sectional research are combined.

The chemical composition of the coatings is determined by an energy-dispersive X-ray detector. It allows point probing or scanning of a section by the area of the figure or by the distribution map of chemical elements. To increase the accuracy of determining the elemental and phase composition of the coatings, X-ray photoelectron spectroscopy and Auger electron spectroscopy methods are used. Survey spectra are recorded from the surface of the coatings. They are used to study the qualitative and quantitative composition of the surface. In addition, the spectra are used to determine the electron lines of the chemical elements of the surface, which makes it possible to effectively determine the chemical bond. This allows us to judge the phase in which the element is included.

X-ray structural analysis is used to determine the crystalline structure of high-entropy coatings. For this purpose, reflections with maximum intensity are identified on the X-ray diffraction pattern. Based on them, conclusions are made about the phase composition, the size of the coherent scattering regions, the parameters of the crystal lattice, and the deformation of the crystal lattice of the coating [87].

Such stress-strain properties of the coating as hardness (H) and elastic modulus (E) are measured through nanoindentation. In this case, the load curves are analyzed using the Oliver-Farr method [88]. For indentation in continuous measurement mode, Berkovich diamond indenter is used. In addition to hardness and elastic modulus, it is possible to determine:

- H/E ratio, i.e., resistance to elastic deformation (the ability of a material to change its shape and size when deformed);

- H^3/E^2 , i.e., resistance to plastic deformation.

H/E — indicator of tribological properties. The higher it is, the higher the wear resistance. Materials with $H/E < 0.04$ belong to the coarse-crystalline group (metals and alloys), and materials with $H/E \approx 0.05 - 0.09$ belong to the group of fine-crystalline and nanomaterials (ceramics, coatings).

The tribological properties of the coatings are determined using friction machines by the “ball — disk” or “pin — plate” scheme. Based on the test results, such coating characteristics as wear and friction factor are assessed.

Discussion and Conclusion. The literature analysis performed by the authors of the presented article makes it possible to:

- consider widely used methods of applying PVD coatings;
- grasp the principle of creating cathode spots using explosive electron emission in the vacuum arc method;
- track the effect of discharge current in the process of forming cathode spots on the cathode;
- assess the importance of processes occurring on the anode and substrate.

One of the advantages of coatings obtained by vacuum-arc and magnetron methods is a wide range of materials for synthesizing coatings with high physical, mechanical and tribological characteristics.

Three classes of growth of coating formation are distinguished. The essence of the process is determined. This is nucleation with the growth of islands of 20–30 Å in size. We emphasize that any coating may have defects: porosity, internal stresses, deformation of crystallites and crystal lattice.

High-entropy alloys are formed by mixing five or more elements. High entropy promotes the formation of solid solutions. This feature determines thermal stability, wear resistance, increased plasticity at low temperatures, corrosion resistance, resistance to ionizing radiation. There are about 40 known elements that are included in high-entropy alloys; therefore, special criteria (parameters) have been developed for the precise selection of materials, prediction of stability and structural-phase state of high-entropy alloys:

- difference in atomic sizes of components δ ;
- mixing enthalpy ΔH_{mix} ;
- mixing entropy ΔS_{mix} ;
- difference in electronegativity of components $\Delta\chi$;
- valence electron concentration VEC .

Within the framework of this research, it is established that the issues related to nitride coatings obtained by vacuum-arc and magnetron methods are sufficiently explored in the literature. There are fundamental studies on the structure of coatings, their physical and mechanical properties, thermal stability. It is also known that high-entropy coatings are

distinguished by high hardness with a face-centered cubic lattice, high thermal stability. Transition metals with the addition of nitrogen are widely used in the compositions of the coatings under consideration. The main type of high-entropy coatings is nitride. The coatings studied in this paper are characterized by a significant friction factor. However, due to their hardness and plasticity, they demonstrate high wear resistance.

It is difficult to say that high-entropy coatings can already replace traditional ones in mechanical engineering. However, over time, they will be widely used for elements that operate under high-temperature conditions.

Based on the literature analysis results, it should be noted that there is a limited number of papers considering this issue from the point of view of tribology. For further research, it is necessary to develop high-entropy coatings that will provide high hardness, wear resistance, and a low friction factor. This will make it possible to create coatings suitable for use in tribo-loaded units, and therefore, in the mechanical engineering production processes. Thus, it is expected to receive promising materials that will compete with traditional coatings.

References

1. Polityko KN, Manturov DS. Formation of PVD Coatings for Tribological Purposes. *Trudy RGUPS – Transaction of RSTU*. 2023;64(3): 81–93.
2. Andreev AA. *Vacuum-Arc Coatings*. Kharkov: NSC KIPT; 2010. 318 p. (In Russ.)
3. Anders A. *Cathodic Arcs*. New York: Springer; 2008. 540 p. <https://doi.org/10.1007/978-0-387-79108-1>
4. Boxman RL. Early History of Vacuum-Arc Deposition. *IEEE Transactions on Plasma Science*. 2001;29(5):759–761. <https://doi.org/10.1109/27.964470>
5. Mattox DM. *The History of Vacuum Coating Technology*. Albuquerque, NM: Management Plus Inc.; 2002. 51 p. URL: http://www.astrosurf.com/astroptics/files/histoire_des_couches_anti-reflet.pdf (accessed: 03.09.2024).
6. Aksenov II, Andreev AA. Vacuum-Arc Ion-Plasma Coating Technologies in KIPT. *Problems of Atomic Science and Technology. Series “Vacuum, Pure Materials, Superconductors”*. 1998;2(3)/3(4):3–11. (In Russ.)
7. Zimin AM, Ivanov VA, Juttner B. Dynamics of Cathode Spots on the Beryllium Surface in Vacuum Arc Discharge. *Problems of Atomic Science and Technology. Series “Thermonuclear Fusion”*. 2001;(2):44–50.
8. Mesyats GA. *Ectons in a Vacuum Discharge: Breakdown, Spark, Arc*. Moscow: Nauka; 2000. 424 p. (In Russ.)
9. Cobine J, Ecker G, Farrall J, Greenwood A, Harris L. *Vacuum Arcs: Theory and Application*. Moscow: Mir; 1982. 432 p. (In Russ.)
10. Lunev VM, Ovcharenko VD, Khoroshikh VM. Investigation of Some Characteristics of Vacuum Metal Arc Plasma. *Technical Physics*. 1977;47(7):1486–1490. (In Russ.)
11. Zabello KK, Logatchev AA, Chaly AM, Shkolnik SM. Characteristics of the Statistical Distribution of the Current Transmitted by the Cathode Spot of a Vacuum Arc in Various Oriented Magnetic Fields. *Technical Physics*. 2009;79(6):58–66.
12. Fortov VE, Alexandrov AF, Asinovsky EI, Gribkov VA, Didenko AN, Dykhne AM, et al. *Encyclopedia of Low Temperature Plasma. Introductory Volume 1*. Moscow: Nauka; 2000. 634 p. (In Russ.)
13. Juttner B, Puchkarev VF, Hantzsch E, Beilis I. Cathode Spots. In book: Boxman RL, Sanders DM, Martin PJ. (eds) *Handbook of Vacuum Arc Science and Technology*. Park Ridge: Noyes Publications; 1995. P. 73–281.
14. Raizer YuP. *Physics of Gas Discharge*. Moscow: Nauka; 1987. 592 p. (In Russ.)
15. Mattox MD. *Handbook of Physical Vapor Deposition (PVD) Processing*. Norwich, NY: William Andrew Publ.; 2010. 746 p.
16. Tsventukh MM, Barenholts SA, Mesyats VG, Shmelev DL. Reverse Motion of Cathode Spots of the First Type in a Tangential Magnetic Field. *Technical Physics Letters*. 2013;39(21):1–9. (In Russ.) URL: <https://journals.ioffe.ru/articles/viewPDF/14640> (accessed: 03.09.2024).
17. Fang DY, Nürnberg A, Bauder UH, Behrisch R. Arc Velocity and Erosion for Stainless Steel and Aluminum Cathodes. *Journal of Nuclear Materials*. 1982;111–112:517–521. [https://doi.org/10.1016/0022-3115\(82\)90258-6](https://doi.org/10.1016/0022-3115(82)90258-6)
18. Granovsky VL. *Electric Current in Gases. Steady State Current*. Moscow: Nauka; 1971. 543 p. (In Russ.)
19. Nürnberg AW, Fang DY, Bauder UH, Behrisch R, Brossa F. Temperature Dependence of the Erosion of Al and TiC by Vacuum Arcs in a Magnetic Field. *Journal of Nuclear Materials*. 1981;103:305–308. [https://doi.org/10.1016/0022-3115\(82\)90614-6](https://doi.org/10.1016/0022-3115(82)90614-6)

20. Aksenov II, Kononov II, Padalka VG, Khoroshikh VM, Bren VG. *Investigation of Cathode Erosion of a Stationary Vacuum Arc*. Moscow: Atominform; 1984. 23 p. (In Russ.)
21. Borisov DP, Goncharenko IM, Koval NN, Schani PM. Plasma-Assisted Deposition of a Three-Layer Structure by Vacuum and Gas Arcs. *IEEE Transactions on Plasma Science*. 1998;26(6):1680–1684. <https://doi.org/10.1109/27.747886>
22. Aksenov II, Andreev AA, Bren VG, Gavrilko IV, Kudryavtseva EE, Kunchenko VV, et al. Coatings Obtained by Condensation of Plasma Streams in Vacuum (Ion Bombardment Condensation Method). *Ukrainian Journal of Physics*. 1979;24(4):515–525. (In Russ.)
23. Budilov VV, Shekhtman SR, Izmailova NF. Deposition of Vacuum Ion-Plasma Coatings on Turbine Blades of a Gas Turbine Engine with the Use of Discharge and the Hollow Cathode Effect. *Russian Aeronautics*. 2001;(1):76–78.
24. Kunchenko VV, Andreev AA. Titanium Carbonitrides Obtained by Vacuum Arc Deposition. *Problems of Atomic Science and Technology. Series “Physics of Radiation Damage and Radiation Materials Science”*. 2001;(2):116–120. (In Russ.)
25. Roos JR, Selis JP, Vancoille E, Veltrop H, Boelens S, Jungblut F, et al. Interrelationship between Processing, Coating Properties and Functional Properties of Steered Arc Physically Vapour Deposited (TiAl)N and (TiNb)N Coatings. *Thin Solid Films*. 1990;193–194(1):547–556. [https://doi.org/10.1016/S0040-6090\(05\)80064-1](https://doi.org/10.1016/S0040-6090(05)80064-1)
26. Da-Yung Wang, Yen-Way Li, Chi-Long Chang, Wei-Yu Ho. Deposition of High Quality (Ti,Al)N Hard Coatings by Vacuum Arc Evaporation Process. *Surface and Coatings Technology*. 1999;114(2–3):109–113. [https://doi.org/10.1016/S0257-8972\(99\)00020-1](https://doi.org/10.1016/S0257-8972(99)00020-1)
27. Goller R, Torri P, Baker MA, Gilmore R, Gissler W. The Deposition of Low-Friction TiN-MoS_x Hard Coatings by a Combined Arc Evaporation and Magnetron Sputter Process. *Surface and Coatings Technology*. 1999;120–121:453–457. [https://doi.org/10.1016/S0257-8972\(99\)00466-1](https://doi.org/10.1016/S0257-8972(99)00466-1)
28. Kiryukhantsev-Korneev FV, Shtanskii DV, Sheveiko AN, Levashov EA, Lyasotskii IV, Dyakonova NB. Structure and Properties of Ti-Si-N Coatings Produced by Magnetron Sputtering of SHS Targets. *Physics of Metals and Metallography*. 2004;97(3):314–321.
29. PalDey S, Deevi SC. Single Layer and Multilayer Wear Resistant Coatings of (Ti,Al)N: A Review. *Materials Science and Engineering: A*. 2003;342(1–2):58–79. [https://doi.org/10.1016/S0921-5093\(02\)00259-9](https://doi.org/10.1016/S0921-5093(02)00259-9)
30. Xiaolu Pang, Huisheng Yang, Kewei Gao, Yanbin Wang, Alex A Volinsky. AlTiN Layer Effect on Mechanical Properties of Ti-Doped Diamond-like Carbon Composite Coatings. *Thin Solid Films*. 2011;519(16):5353–5357. <https://doi.org/10.1016/j.tsf.2011.02.040>
31. Solodukhin IA, Khodasevich VV, Uglov VV, Prikhodko ZhL. The Change of Adhesion and Tribological Properties of TiN and Ti Coatings in the Case of Their Deposition on Substrates Subjected to Ion Implantation. In: *Proc. IV International Scientific Conference “Interaction of Radiation with Solids”*. Minsk: BSU; 2001. P. 294–296. (In Russ.)
32. Anischik VM, Kuleshov AK, Uglov VV, Rusalsky DP, Syshchenko AF. Measurement of Adhesion Strength of Mo-Ti-N and Mo-Cu-N Coatings Using “Scratch-Tester” Device. *Devices and Methods of Measurements*. 2015;1(10):81–86. URL: <https://rep.bntu.by/handle/data/18005?ysclid=m0ns044q9y49469251> (accessed: 03.02.2024).
33. Filatov MS, Stognei OV. Preparation of Ni-ZrO₂ Composites with Different Concentrations of the Metal Phase by RF Magnetron Sputtering. In: *Proc. 13th International Conference “Films and Coatings”*. St. Petersburg: Peter the Great St. Petersburg Polytechnic University; 2017. P. 106–109. (In Russ.)
34. Yeom GY, Thornton JA, Penfold AS. Magnetic Field Designs for Cylindrical-Post Magnetron Discharge Sources. *Journal of Vacuum Science and Technology A*. 1988;6(6):3156–3158. <https://doi.org/10.1116/1.575048>
35. Larhlmi H, Ghailane A, Makha M. Magnetron Sputtered Titanium Carbide-Based Coatings: A Review of Science and Technology. *Vacuum*. 2022;197:110853. <http://doi.org/10.1016/j.vacuum.2021.110853>
36. Loktev D, Yamashin E. Methods and Equipment for Applying Wear-Resistant Coatings. *Nanoindustry*. 2007;(4):18–24.
37. Yuryev YuN, Mikhnevich KS, Krivobokov VP, Sidelyov DV, Kiselyova DV, Novikov VA. Properties of Titanium Nitride Films Obtained by Magnetron Sputtering. *Proceedings of the Samara Scientific Center of the Russian Academy of Sciences*. 2014;16(4):672–676.
38. Yurjev YuN, Sidelev DV. Technological Peculiarities of Deposition Anti-Reflective Layers in Low-E Coatings. *Journal of Physics: Conference Series*. 2013;479(1):1–4. <http://doi.org/10.1088/1742-6596/479/1/012018>

39. Yerofeev EV, Fedin IV, Kazimirov AI. Investigation of the Electrical Properties of Tin Thin Films Obtained by Magnetron Sputtering. *Herald of the Siberian State University of Telecommunications and Information Science*. 2015;31(3):29–34.
40. Tanaka Y, Gur TM, Kelly M, Hagstrom SB, Ikeda T, Wakihira K, et al. Properties of $(\text{Ti}_{1-x}\text{Al}_x)\text{N}$ Coatings for Cutting Tools Prepared by the Cathodic Arc Ion Plating Method. *Journal of Vacuum Science and Technology A*. 1992;10(4):1749–1756. <http://doi.org/10.1116/1.577742>
41. Carrera S, Salas O, Moore JJ, Woolverton A, Sutter E. Performance of $\text{CrN}/\text{MoS}_2(\text{Ti})$ Coatings for High Wear Low Friction Applications. *Surface and Coatings Technology*. 2003;167(1):25–32. [http://doi.org/10.1016/S0257-8972\(02\)00885-X](http://doi.org/10.1016/S0257-8972(02)00885-X)
42. Donnet C, Le Mogne Th, Martin JM. Superlow Friction of Oxygen-Free MoS_2 Coatings in Ultrahigh Vacuum. *Surface and Coatings Technology*. 1993;62(1–3):406–411. [http://doi.org/10.1016/0257-8972\(93\)90275-S](http://doi.org/10.1016/0257-8972(93)90275-S)
43. Polcar T, Kubart T, Novák R, Kopecký L, Široký P. Comparison of Tribological Behaviour of TiN, TiCN and CrN at Elevated Temperatures. *Surface and Coatings Technology*. 2005;193(1–3):192–199. <http://doi.org/10.1016/j.surfcoat.2004.07.098>
44. Horník J, Krum S, Tondl D, Puchnin M, Sachr P, Cvrček L. Multilayer Coatings Ti/TiN, Cr/CrN and W/WN Deposited by Magnetron Sputtering for Improvement of Adhesion to Base Materials. *Acta Polytechnica*. 2015;55(6):388–392. <http://doi.org/10.14311/AP.2015.55.0388>
45. Nishchev KN, Martynenko VA, Beglov VI, Grishanin AV, Eliseev VV, Malygin MYu, et al. Research of the Properties of Multilayer Metallization of the Structures “Silicon on Molybdenum” obtained by Magnetron Sputtering. *University Proceedings. Volga Region. Physical and Mathematical Sciences*. 2013;27(3):248–260.
46. Movchan BA, Demchishin AV. Structure and Properties of Thick Condensates of Nickel, Titanium, Tungsten, Aluminum Oxides, and Zirconium Dioxide in Vacuum. *Physics of Metals and Metallography*. 1969;28:653–660.
47. Thornton JA. Influence of Apparatus Geometry and Deposition Condition on the Structure and Topography of Thick Sputtered Coatings. *Journal of Vacuum Science and Technology*. 1974;11:666–670. <http://doi.org/10.1116/1.1312732>
48. Barna PB, Adamik M. Fundamental Structure Forming Phenomena of Polycrystalline Films and the Structure Zone Models. *Thin Solid Films*. 1998;317(1/2):27–33. [http://doi.org/10.1016/S0040-6090\(97\)00503-8](http://doi.org/10.1016/S0040-6090(97)00503-8)
49. Petrov I, Hultman L, Barna P, Greene JE. Microstructural Evolution during Film Growth. *Journal of Vacuum Science and Technology A*. 2003;21(5):117–128. <http://doi.org/10.1116/1.1601610>
50. Varavka VN, Kudryakov OV, Ryzhenkov AV. Multilayered Nanocomposite Coatings for Anti-Erosive Protection. Chapter 5. In book: Ivan A Parinov. (ed) *Piezoelectrics and Nanomaterials: Fundamentals, Developments and Applications*. New York: Nova Science Publishers, Inc.; 2015. P. 105–132.
51. Kudryakov OV, Varavka VN, Zabiya IY, Yadrets EA, Karavaev PV. Morphology and Genealogy of Structural Defects in Vacuum Ion-Plasma Coatings. *Advanced Engineering Research (Rostov-on-Don)*. 2020;20(3):269–279. <https://doi.org/10.23947/2687-1653-2020-20-3-269-279>
52. Jien-Wei Yeh, Chen S-K, Su-Jien Lin, Jon-Yiew Gan, Tsung-Shune Chin, Tian Shun, et al. Nanostructured High-Entropy Alloys with Multiple Principal Elements: Novel Alloy Design Concepts and Outcomes. *Advanced Engineering Materials*. 2004;6(5):299–303. <http://doi.org/10.1002/adem.200300567>
53. Rogachev AS. Structure, Stability, and Properties of High-Entropy Alloys. *Physics of Metals and Metallography*. 2020;121(8):807–841. <https://doi.org/10.31857/2687-1653-2020-20-3-269-279>
54. Bashev VF, Kushnerev AI. Structure and Properties of the High-Entropy Alloy CoCrCuFeNiSn_x . *Physics of Metals and Metallography*. 2014;115(7):737–741. <http://doi.org/10.7868/S0015323014040020>
55. Kuzminova YO, Firsov DG, Dagesyan SA, Konev SD, Sergeev SN, Zhilyaev AP, et al. Fatigue Behavior of Additive Manufactured CrFeCoNi Medium-Entropy Alloy. *Journal of Alloys and Compounds*. 2021;863:158609. <http://doi.org/10.1016/j.jallcom.2021.158609>
56. Cantor B. Multicomponent and High Entropy Alloys. *Entropy*. 2014;16(9):4749–4768. <http://doi.org/10.3390/e16094749>

57. Shou-Yi Chang, Chen-Yuan Wang, Chen-En Li, Yi-Chung Huang. 5-nm- Thick (AlCrTaTiZrRu)N_{0.5} Multi-Component Barrier Layer with High Diffusion Resistance for Cu Interconnects. *Nanoscience and Nanotechnology Letters*. 2011;3(2):289–293. <http://doi.org/10.1166/nnl.2011.1155>
58. Miracle DB, Senkov ON. A Critical Review of High Entropy Alloys and Related Concepts. *Acta Materialia*. 2017;122:448–511. <http://doi.org/10.1016/j.actamat.2016.08.081>
59. Pogrebnnyak AD, Komarov FF, Beresnev VM, Konstantinov SV, Salishchev GA. *Multicomponent and High-Entropy Alloys and Nitride Coatings Based on Them*. Moscow: LENAND; 2021. 336 p. (In Russ.)
60. Cantor B, Chang ITH, Knight P, Vincent AJB. Microstructural Development in Equiatomic Multicomponent Alloys. *Materials Science and Engineering: A*. 2004;375–377:213–218. <http://doi.org/10.1016/j.msea.2003.10.257>
61. Chin-You Hsu, Chien-Chang Juan, Woei-Ren Wang, Tsing-Shien Sheu, Jien-Wei Yeh, Swe-Kai Chen. On the Superior Hot Hardness and Softening Resistance of AlCoCr_xFeMo_{0.5}Ni High-Entropy Alloys. *Materials Science and Engineering: A*. 2011;528(10/11):3581–3588. <http://doi.org/10.1016/j.msea.2011.01.072>
62. Chen TK, Shun TT, Yeh JW, Wong MS. Nanostructured Nitride Films of Multi-Element High-Entropy Alloys by Reactive DC Sputtering. *Surface and Coatings Technology*. 2004;188–189:193–200. <http://doi.org/10.1016/j.surfcoat.2004.08.023>
63. Mann JB, Meek TL, Allen L C. Configuration Energies of the Main Group Elements. *Journal of the American Chemical Society*. 2000;122(12):2780–2783. <http://doi.org/10.1021/ja992866e>
64. Pogrebnjak AD, Bagdasaryan AA, Yakushchenko IV, Beresnev VM. The Structure and Properties of High-Entropy Alloys and Nitride Coatings Based on them. *Russian Chemical Reviews*. 2014;83(11):1027–1061. <http://doi.org/10.1070/RC2014v083n11ABEH004407>
65. Senkov ON, Woodward C, Miracle DB. Microstructure of Aluminum-Containing Refractory High-Entropy Alloys. *JOM*. 2014;66(10):2030–2042. <http://doi.org/10.1007/s11837-014-1066-0>
66. Pankov VP, Babayan AL, Kulikov MV, Kosoy VA, Varlamov BS. Heat-Protection Coatings for Turbine Blades of Aircraft Gas Turbine Engines. *Polzunovskiy Vestnik*. 2021;(1):161–172.
67. Milošev I, Strehblow HH, Navinšek B. Comparison of TiN, ZrN and CrN Hard Nitride Coatings: Electrochemical and Thermal Oxidation. *Thin Solid Films*. 1997;303(1-2):264–254. [http://doi.org/10.1016/S0040-6090\(97\)00069-2](http://doi.org/10.1016/S0040-6090(97)00069-2)
68. Novikov V, Stepanov N, Zharebtsov S, Salishchev G. Structure and Properties of High-Entropy Nitride Coatings. *Metals*. 2022;12(5):847. <https://doi.org/10.3390/met12050847>
69. Nagya P, Rohbeck N, Roussely G, Sortais P, Lábár JL, Gubicza J, et al. Processing and Characterization of a Multibeam Sputtered Nanocrystalline CoCrFeNi High-Entropy Alloy Film. *Surface and Coatings Technology*. 2020;386:125465. <http://doi.org/10.1016/j.surfcoat.2020.125465>
70. Yurov VM, Platonova ES, Baltabekov A. High Entropy Coatings CuTiZrCrNi. *Norwegian Journal of Development of the International Science*. 2019;36:25–29.
71. Yurov VM, Guchenko SA, Makhanov KM. Atomic-Power Microscopy of High-Entropy Coatings. *International Journal of Applied and Fundamental Research*. 2020;(4):62–67. URL: <https://s.applied-research.ru/pdf/2020/4/13056.pdf> (accessed: 03.09.2024).
72. Junjun Wang, Shaofu Kuang, Xu Yu, Linqing Wang, Weijiu Huang. Tribo-Mechanical Properties of CrNbTiMoZr High-Entropy Alloy Film Synthesized by Direct Current Magnetron Sputtering. *Surface and Coating Technology*. 2020;403:126374. <http://doi.org/10.1016/j.surfcoat.2020.126374>
73. Wu H, Zhang S, Wang ZY, Zhang CH, Chen HT, Chen J. New Studies on Wear and Corrosion Behavior of Laser Cladding FeNiCoCrMo_x High-Entropy Alloy Coating: The Role of Mo. *International Journal of Refractory Metals and Hard Materials*. 2022;102:105721. <http://doi.org/10.1016/j.ijrmhm.2021.105721>
74. Tüten N, Canadinc D, Motallebzadeh A, Bal B. Microstructure and Tribological Properties of TiTaHfNbZr High Entropy Alloy Coatings Deposited on Ti-6Al-4V Substrates. *Intermetallics*. 2019;105:99–106. <http://doi.org/10.1016/j.intermet.2018.11.015>
75. Korotaev AD, Borisov DP, Moshkov VYu, Ovchinnikov SV, Tyumentsev AN, Pribytkov GA. Peculiarities of the Structural-Phase and Elastic Stress States of Superhard TiN-Based Nanocomposite Coatings. *Physical Mesomechanics*. 2011;14(5):87–97.

76. Pogrebniyak AD, Yakushchenko IV, Bondar OV, Beresnev VM, Sobol OV, Andreev AA, et al. Influence of Nitride Deposition Parameters of High-Entropy Alloys (Ti-Zr-Hf-V-Nb)N on Their Structure, Composition, Mechanical and Tribological Properties. *Journal of Superhard Materials*. 2013;(6):4–19. (In Russ.)
77. Milošev I, Strehblow HH, Navinšek B. Comparison of TiN, ZrN and CrN Hard Nitride Coatings: Electrochemical and Thermal Oxidation. *Thin Solid Films*. 1997;303(1–2):246–254. [http://doi.org/10.1016/S0040-6090\(97\)00069-2](http://doi.org/10.1016/S0040-6090(97)00069-2)
78. Veprek S. The Search for Novel, Superhard Materials. *Journal of Vacuum Science and Technology A*. 1999;17:2401–2420. <http://doi.org/10.1116/1.581977>
79. Jien-Wei Yeh. Recent Progress in High-Entropy Alloy. *Annales de Chimie. Science des Matériaux*. 2006;31(6):633–648. <http://doi.org/10.3166/acsm.31.633-648>
80. Jen-Hao Song, Sheng-Chang Wang, James C Sung, Jow-Lay Huang, Ding-Fwu Lii. Characterization of Reactively Sputtered C-Axis Orientation (Al, B)N Films on Diamond. *Thin Solid Films*. 2009;517(17):4753–4757. <http://doi.org/10.1016/j.tsf.2009.03.125>
81. Braic V, Vladescu A, Balaceanu M, Luculescu CR, Braic M. Nanostructured Multi-Element (TiZrNbHfTa)N and (TiZrNbHfTa)C Hard Coatings. *Surface and Coating Technology*. 2012;211:117–121. <http://doi.org/10.1016/j.surfcoat.2011.09.033>
82. Shih-Chang Liang, Du-Cheng Tsai, Zue-Chin Chang, Huan-Shin Sung, Yi-Chen Lin, Yi-Jung Yeh, et al. Structural and Mechanical Properties of Multi-Element (TiVCrZrHf)N Coatings by Reactive Magnetron Sputtering. *Applied Surface Science*. 2011;258(1):399–403. <http://doi.org/10.1016/j.apsusc.2011.09.006>
83. Du-Cheng Tsai, Zue-Chin Chang, Li-Yu Kuo, Tien-Jen Lin, Tai-Nan Lin, Fuh-Sheng Shieu. Solid Solution Coating of (TiVCrZrHf)N with Unusual Structural Evolution. *Surface and Coatings Technology*. 2013;217:84–87. <http://doi.org/10.1016/j.surfcoat.2012.11.077>
84. Du-Cheng Tsai, Fuh-Sheng Shieu, Shou-Yi Chang, Hsiao-Chiang Yao, Min-Jen Deng. Structures and Characterizations of TiVCr and TiVCrZrY Films Deposited by Magnetron Sputtering under Different Bias Powers. *Journal of The Electrochemical Society*. 2010;157(3):52–58. <http://doi.org/10.1149/1.3285047>
85. Ma C-H, Huang J-H, Haydn Chen. Nanohardness of Nanocrystalline TiN Thin Films. *Surface and Coatings Technology*. 2006;200(12–13):3868–3875. <http://doi.org/10.1016/j.surfcoat.2004.10.098>
86. Hsiao-Chiang Yao, Ming-Chieh Chiu, Wen-Tang Wu, Fuh-Sheng Shieu. Influence of Radio Frequency Bias on the Characteristics of TiO₂ Thin Films Prepared by DC Sputtering. *Journal of The Electrochemical Society*. 2006;153(10):237–243. <http://doi.org/10.1149/1.2221866>
87. Voroshilov YuV, Pavlishin VI. *Fundamentals of Crystallography and Crystal Chemistry. Crystal Radiography*. Kiev: KNT; 2011. 568 p. (In Russ.)
88. Golovin YuI. *Nanoindentation and Its Capabilities*. Moscow: Mashinostroenie; 2009. 312 p. (In Russ.)

About the Authors:

Kirill N. Polityko, postgraduate student, Junior Research Fellow of the Engineering Mechanics Department, Rostov State Transport University (2, Rostovskogo Strelkovogo Polka Narodnogo Opolcheniya Sq., Rostov-on-Don, 344038, Russian Federation), [SPIN-code](#), [ORCID](#), politykokirill@yandex.ru

Igor V. Kolesnikov, Dr.Sci. (Eng.), Corresponding Member of RAS, Professor of the Engineering Mechanics Department, Rostov State Transport University (2, Rostovskogo Strelkovogo Polka Narodnogo Opolcheniya Sq., Rostov-on-Don, 344038, Russian Federation), [SPIN-code](#), [ORCID](#), [ScopusID](#), ivkolesnikov@bk.ru

Dmitry S. Manturov, Cand.Sci. (Eng.), Head of the Laboratory of the Engineering Mechanics Department, Rostov State Transport University (2, Rostovskogo Strelkovogo Polka Narodnogo Opolcheniya Sq., Rostov-on-Don, 344038, Russian Federation), [SPIN-code](#), [ORCID](#), [ScopusID](#), [ResearcherID](#), manturovds@rgups.ru

Claimed Contributorship:

KN Polityko: analysis of literature sources, preparation of the text.

IV Kolesnikov: academic advising, research objectives and tasks formulation.

DS Manturov: finalization of the text, correction of the conclusions.

Conflict of Interest Statement: the authors claimed no conflict of interest.

All authors have read and approved the final manuscript.

Об авторах:

Кирилл Николаевич Политыко, аспирант, младший научный сотрудник кафедры теоретической механики Ростовского государственного университета путей сообщения (344038, Российская Федерация, г. Ростов-на-Дону, пл. им. Ростовского стрелкового полка народного ополчения, 2), [SPIN-код](#), [ORCID](#), polityko856@gmail.com

Игорь Владимирович Колесников, доктор технических наук, член-корреспондент РАН, профессор кафедры теоретической механики Ростовского государственного университета путей сообщения (344038, Российская Федерация, г. Ростов-на-Дону, пл. им. Ростовского стрелкового полка народного ополчения, 2), [SPIN-код](#), [ORCID](#), [ScopusID](#), ivkolesnikov@bk.ru

Дмитрий Сергеевич Мантуров, кандидат технических наук, заведующий лабораторией кафедры теоретической механики Ростовского государственного университета путей сообщения (344038, Российская Федерация, г. Ростов-на-Дону, пл. им. Ростовского стрелкового полка народного ополчения, 2), [SPIN-код](#), [ORCID](#), [ScopusID](#), [ResearcherID](#), manturovds@rgups.ru

Заявленный вклад авторов:

К.Н. Политыко: анализ литературных источников, подготовка текста.

И.В. Колесников: научное руководство, формирование целей и задач исследования.

Д.С. Мантуров: доработка текста, корректировка выводов.

Конфликт интересов: авторы заявляют об отсутствии конфликта интересов.

Все авторы прочитали и одобрили окончательный вариант рукописи.

Received / Поступила в редакцию 10.09.2024

Reviewed / Поступила после рецензирования 29.09.2024

Accepted / Принята к публикации 14.10.2024

MACHINE BUILDING AND MACHINE SCIENCE МАШИНОСТРОЕНИЕ И МАШИНОВЕДЕНИЕ



UDC 661.846

Original Empirical Research

<https://doi.org/10.23947/2687-1653-2024-24-4-392-401>

Development of a Method for Obtaining Nanoscale Magnesium Carbonate Stabilized with Chitosan as the Basis of Scaffold Matrices for Regenerative Medicine

Andrey V. Blinov , Zafar A. Rekhman ✉, Alexey A. Gvozdenko ,

Maria A. Yasnaya , Maxim A. Kolodkin, Maxim A. Taravanov

North-Caucasus Federal University, Stavropol, Russian Federation

✉ zafrehman1027@gmail.com

EDN: KXALAI

Abstract

Introduction. In the public domain there is enough literature on methods of treating the musculoskeletal system. The possibilities of eliminating bone defects using patients' own (autologous) bones are described. The authors of theoretical and applied studies also suggest using synthetic bioinert materials made of polymers, calcium phosphates, plastics, and metals. The creation of three-dimensional matrices based on scaffolds for the formation of systems that are as close as possible to bone tissue in structure has been studied. It is known that the active substances of the scaffold matrix can be hydroxyapatite, tricalcium phosphate, as well as silicates, carbonates of magnesium, calcium, copper, zinc, and manganese. The issue requires detailed study. In light of the stated problem, the features of the listed materials should be considered separately. There are no such publications. The presented work is intended to fill this gap. Its objective is to create a synthesis method and study the properties of nanoscale magnesium carbonate.

Materials and Methods. The materials for the research were samples of magnesium carbonate nanoparticles obtained by chemical precipitation in water. They were studied using X-ray diffractometry, scanning electron microscopy, infrared spectroscopy, and dynamic light scattering. Quantum chemical modeling was performed using the QChem program and the IQmol molecular editor.

Results. It has been established that magnesium carbonate particles are rod-shaped, 2 to 10 μm in length. They consist of nanoparticles from 30 to 60 nm. The quantum chemical modeling elucidated the energy features of the interaction of the basic magnesium carbonate, firstly, with chitosan with carbonate, and secondly, with a separate chitosan molecule. In the first case, the energy value was lower, in the second, it was higher. That indicated the chemical and energetic advantage of forming such complexes. The corresponding indices for the optimal coordination of magnesium carbonate with chitosan were determined. In this case, the interaction was provided by the hydroxyl group of chitosan attached to the C₆ residue of glucosamine. For this process, the lowest energy $\Delta E = 462.387$ kcal/mol and chemical hardness $\eta = 0.062$ eV were noted. Magnesium carbonate nanoparticles had optimal radius and zeta potential with the following parameters of the initial reagents: 0.018 mol of ammonium carbonate, 0.03 mol of magnesium acetate, 0.15 g of chitosan.

Discussion and Conclusion. The obtained data indicate that nanoscale basic magnesium carbonate is a promising material with a wide range of possibilities of practical application. From this point of view, its role in metabolic processes, namely in the assimilation of macronutrients, is of particular interest. Nanoscale osteotropic magnesium micronutrient synthesized in a biopolymer environment can be used as a biologically active filler for three-dimensional scaffold matrices. Implementation of this solution in medical practice will improve the efficiency of bone tissue restoration.

Keywords: musculoskeletal injuries, bone defect repair, bone tissue analogue, nanoscale magnesium carbonate, osteotropic magnesium micronutrient, scaffold matrix

Acknowledgements. The authors would like to thank Irina Mikhailovna Shevchenko, Cand.Sci. (Engineering), Associate Professor of the Department of Physics and Technology of Nanostructures and Materials, Physics and Technology Faculty, North-Caucasus Federal University, for her assistance in writing and correcting this paper.

Funding Information. The research was done with the financial support from the Ministry of Science and Higher Education of the Russian Federation within the framework of the government task under the Agreement on the provision of a subsidy from the federal budget No. 075–03–2024–239/7 on the topic “Three-Dimensional Biopolymer Scaffold Matrices Enriched with Nanoparticles of Osteotropic Micronutrients for Bone Tissue Regeneration” (project FSRN–2023–0037).

For citation. Blinov AV, Rekhman ZA, Gvozdenko AA, Yasnaya MA, Kolodkin MA, Taravanov MA. Development of a Method for Obtaining Nanoscale Magnesium Carbonate Stabilized with Chitosan as the Basis of Scaffold Matrices for Regenerative Medicine. *Advanced Engineering Research (Rostov-on-Don)*. 2024;24(4):392–401. <https://doi.org/10.23947/2687-1653-2024-24-4-392-401>

Оригинальное эмпирическое исследование

Разработка метода получения наноразмерного карбоната магния, стабилизированного хитозаном, как основы скаффолд-матриц для регенеративной медицины

А.В. Блинов , З.А. Рехман ✉, А.А. Гвозденко , М.А. Ясная ,

М.А. Колодкин, М.А. Тараванов 

Северо-Кавказский федеральный университет, г. Ставрополь, Российская Федерация

✉ zafrehman1027@gmail.com

Аннотация

Введение. В открытом доступе достаточно литературы о методах лечения опорно-двигательного аппарата. Описаны возможности устранения дефектов кости с использованием собственных (аутологичных) костей пациентов. Авторы теоретических и прикладных исследований предлагают применять также синтетические биоинертные материалы из полимеров, фосфатов кальция, пластмасс, металлов. Изучено создание на основе скаффолдов трехмерных матриц для формирования систем, по структуре максимально близких костной ткани. Известно, что действующими веществами скаффолд-матрицы могут быть гидроксиапатит, трикальций фосфат, а также силикаты, карбонаты магния, кальция, меди, цинка и марганца. Вопрос нуждается в детальной проработке. В свете заявленной проблемы особенности перечисленных материалов следует изучать по отдельности. Таких публикаций нет. Представленная работа призвана восполнить данный пробел. Ее цель — создание метода синтеза и исследование свойств наноразмерного карбоната магния.

Материалы и методы. Материалами для исследования послужили образцы наночастиц карбоната магния, полученные химическим осаждением в воде. Их изучали методами рентгеновской дифрактометрии, сканирующей электронной микроскопии, инфракрасной спектроскопии и динамического рассеяния света. Квантово-химическое моделирование проводили при помощи программы QChem и молекулярного редактора IQmol.

Результаты исследования. Установлено, что частицы карбоната магния — стержнеобразные, длиной от 2 до 10 мкм. Они состоят из наночастиц от 30 до 60 нм. Благодаря квантово-химическому моделированию выявлены энергетические особенности взаимодействия основного карбоната магния, во-первых, с хитозаном с карбонатом, а во-вторых, с отдельной молекулой хитозана. В первом случае значение энергии ниже, во втором — выше. Это указывает на химическую и энергетическую выгоду образования таких комплексов. Определены соответствующие показатели для оптимального варианта координирования карбоната магния с хитозаном. В этом случае взаимодействие обеспечивает гидроксильная группа хитозана, присоединенная к C₆ остатку глюкозамина. Для данного процесса отмечена самая низкая энергия $\Delta E = 462,387$ ккал/моль и химическая жесткость $\eta = 0,062$ эВ. Наночастицы карбоната магния обладают оптимальными радиусом и дзета-потенциалом при следующих параметрах исходных реагентов: 0,018 моль карбоната аммония, 0,03 моль ацетата магния, 0,15 г хитозана.

Обсуждение и заключение. Полученные данные свидетельствуют о том, что наноразмерный основной карбонат магния — это перспективный материал с широкими возможностями практического применения. С этой точки зрения особый интерес представляет его роль в процессах обмена, а именно в усвоении макронутриентов. Синтезированный в среде биополимера наноразмерный остеотропный микро-нутриент магния можно использовать как биологически активный наполнитель трехмерных скаффолд-матриц. Реализация данного решения в медицинской практике позволит повысить эффективность восстановления костной ткани.

Ключевые слова: травмы опорно-двигательного аппарата, устранение дефектов кости, аналог костной ткани, наноразмерный карбонат магния, остеотропный микро-нутриент магния, скаффолд-матрикс

Благодарности. Коллектив авторов выражает благодарность Ирине Михайловне Шевченко, кандидату технических наук, доценту кафедры физики и технологии наноструктур и материалов физико-технического факультета Северо-Кавказского федерального университета, за помощь в написании и корректировке данной работы.

Финансирование. Работа выполнена при финансовой поддержке Министерства науки и высшего образования Российской Федерации в рамках государственного задания по Соглашению о предоставлении субсидии из федерального бюджета № 075–03–2024–239/7 на тему «Трехмерные биополимерные скаффолд-матрицы, обогащенные наночастицами остеотропных микронутриентов, для регенерации костных тканей» (проект FSRN–2023–0037).

Для цитирования. Блинов А.В., Рехман З.А., Гвозденко А.А., Ясная М.А., Колодкин М.А., Тараванов М.А. Разработка метода получения наноразмерного карбоната магния, стабилизированного хитозаном, как основы скаффолд-матриц для регенеративной медицины. *Advanced Engineering Research (Rostov-on-Don)*. 2024;24(4):392–401. <https://doi.org/10.23947/2687-1653-2024-24-4-392-401>

Introduction. Regenerative medicine constantly requires materials that help accelerate osteogenesis [1]. Even with the emergence of new solutions, the problem remains urgent, since fractures are a very common type of injury [2]. It should be noted that patients fully recover in only 16% of cases. According to the World Health Organization, there are about 50 million severe injuries worldwide that cause the loss of labor capacity and invalidity. Therefore, the treatment of bone tissue defects is a pressing medical and social problem [3]. To help the patient, three-dimensional biopolymer matrices based on scaffolds are used. They contain elements that are close in structure to connective bone tissue. One of such materials for regenerative medicine is nanoscale forms of magnesium carbonate [4]. Magnesium is an essential microelement [5]. It is responsible for the strength of bones [6] and participates in their formation [7]. Orthopedic implants are created on its basis [8]. In nanoscale form, magnesium carbonate has the following properties:

- low toxicity;
- good biocompatibility;
- permeability for drugs [9].

In biological interactions, the roughness and chemical composition of the surface of the elements play an important role [10]. Future materials based on compounds in the nanometer range may eventually change the nature of the tissues around the implant and increase the clinical success of this approach [11]. Biopolymers are used to improve the above properties. One of them is chitosan [12]. It is an important biocompatible component of connective tissue. It dissolves and decomposes well [13].

The main objective of this study is to create a method for synthesizing chitosan-stabilized nanoscale magnesium carbonate and to study its properties. The material is considered as the basis for scaffold matrices for regenerative medicine.

Materials and Methods. Using chemical precipitation, magnesium carbonate nanoparticles were synthesized from a magnesium-containing precursor, magnesium acetate. The precipitant was ammonium carbonate, and the stabilizer was the polysaccharide chitosan. At the first stage, the required volume of 1% chitosan solution was added to the magnesium acetate solution. Then, using a dropping funnel, the precipitant solution was introduced into the precursor solution at a rate of 60 drops per minute with constant stirring. After the entire precipitant solution had been added, the resulting sol was stirred for another 10 minutes. The synthesized sol was centrifuged and then dried in a drying chamber. This is how magnesium carbonate powder samples were obtained. Their phase composition was studied using powder diffractometry on an Empyrean device (PANalytical, the Netherlands) with the following measurement parameters:

- copper cathode (radiation wavelength — 1.54 Å);
- measurement range — 10–90° 2θ;
- sampling rate — 0.01° 2θ.

The microstructure of magnesium carbonate samples was studied using a MIRA3-LMH scanning electron microscope (Tescan, Czech Republic).

To prepare the samples, carbon double-sided conductive tape was placed on the instrument table (12 mm), powder of the material under study and a carbon layer 10 nm thick were applied. Measurement parameters:

- accelerating voltage — 10 kV;
- focal length value — 4.9 mm;
- In-Beam SE detector.

For the computer quantum chemical modeling of magnesium carbonate in the interaction with chitosan, QChem software was used. The Hartree-Fock method and the basis set 6–31G¹ were selected for the research. The molecular editor IQmol [14] was used to configure the molecules. The samples were examined by infrared (IR) spectroscopy. For this purpose, an IR spectrometer with Fourier transform was used, FSM 1201 model (Russia).

¹ Here, 6–31G is the basis set used in this research. STO-nG is a family of Slater-type orbital basis sets.

Powders $MgCO_3$ and KBr were thoroughly mixed in a ratio of 1:300 and pressed into a tablet in a special press mold under a pressure of 500–1000 MPa. The resulting samples were placed in a spectrometer, and measurements were taken within the range of 400–4400 cm^{-1} .

The average hydrodynamic radius of chitosan-stabilized magnesium carbonate nanoparticles was studied using the dynamic light scattering method on a Photocor complex device (Russia). Their ζ -potential was estimated by the acoustic and electroacoustic spectroscopy method on a DT-1202 spectrometer (Dispersion Technology Inc., USA).

The method for obtaining magnesium carbonate nanoparticles was optimized through a multifactorial experiment. The following parameters were used:

- three variables (content of magnesium acetate, ammonium carbonate, and chitosan);
- two outputs (average hydrodynamic radius and zeta potential) [15].

The data were processed using the Statistica 10.0 program. The levels of variation are presented in Table 1.

Table 1

Levels of Variation of Variables

Name of parameters, designations	Levels of variation of variables		
Magnesium acetate content, mol	0.012	0.024	0.030
Ammonium carbonate content, mol	0.012	0.024	0.030
Mass of chitosan, g	0.150	0.300	0.450

Next, an experimental planning matrix was constructed (Table 2).

Table 2

Experimental Planning Matrix

No	Volume of 0.8 M acetate	Volume of 0.8 M carbonate solution	Volume of chitosan solution, ml
1	15	15	15
2	15	30	30
3	15	45	45
4	30	15	30
5	30	30	45
6	30	45	15
7	45	15	45
8	45	30	15
9	45	45	30

Research Results. At the first stage, the phase composition of the obtained samples was studied. The results are presented in Figure 1.

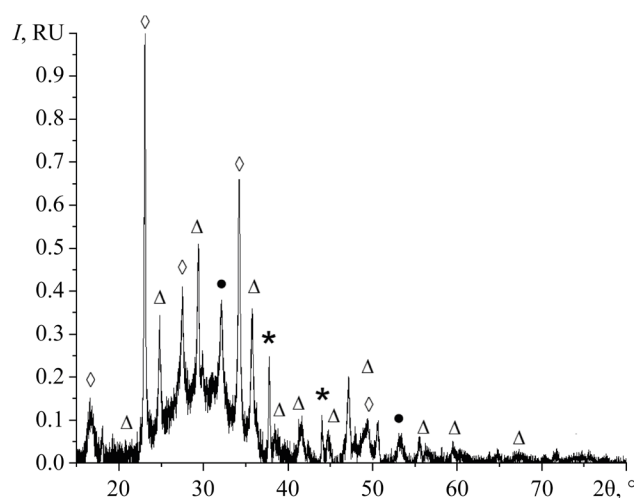


Fig. 1. Diffraction pattern of a sample of nanoscale magnesium carbonate stabilized with chitosan. Here, ● — $MgCO_3$, ◇ — $Mg_2(CO_3)(OH)_2 \cdot 3H_2O$, Δ — $MgCO_3 \cdot 5H_2O$, * — MgO

Next, the microstructure of the obtained samples of magnesium carbonate nanoparticles stabilized with chitosan was examined using a scanning electron microscope (SEM) (Fig. 2).

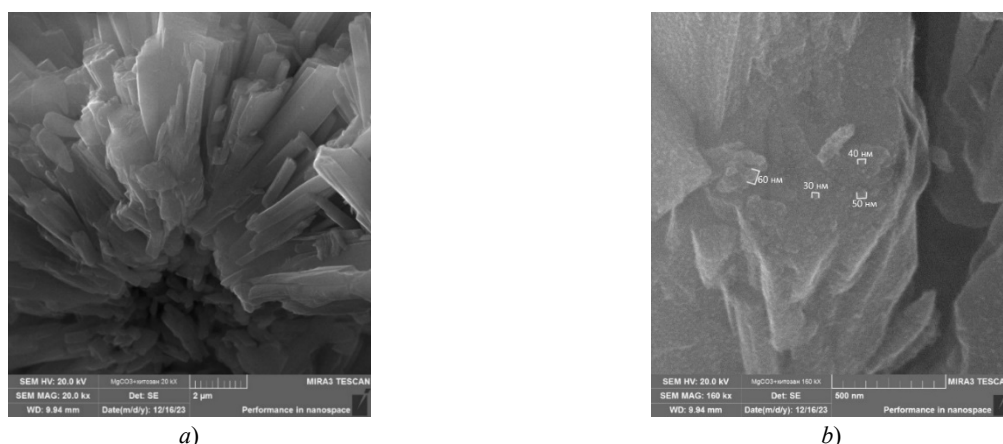


Fig. 2. SEM micrographs of a sample of magnesium carbonate nanoparticles stabilized with chitosan:
a — magnification 20,000 times; *b* — magnification 160,000 times

To study the method of coordination of magnesium carbonate nanoparticles with chitosan, the quantum chemical modeling of the molecular structures of magnesium carbonate with chitosan was performed. The results are shown in Table 3 and Figures 3, 4. Here, *HOMO* is the highest occupied molecular orbit, *LUMO* is the lowest unoccupied molecular orbital.

Table 3

Results of Quantum Chemical Calculations of Molecular Structures of Magnesium Carbonate and Basic Magnesium Carbonate with Chitosan

Interaction	Type of magnesium compound	E , kcal/mol	ΔE , kcal/mol	E_{HOMO} , eV	E_{LUMO} , eV	η , eV
Monomeric unit of chitosan	—	–1258.049	—	–0.225	0.030	0.128
Through hydroxyl group that is attached to C_6 residue of glucosamine	$MgCO_3$	–1720.436	462.387	–0.161	–0.037	0.062
	$Mg(OH)_2CO_3$	–1994.103	736.054	–0.179	–0.111	0.034
Through hydroxyl group that is attached to C_3 residue of glucosamine	$MgCO_3$	–1720.366	462.317	–0.167	–0.042	0.063
	$Mg(OH)_2CO_3$	–1994.273	736.224	–0.182	–0.064	0.059
Through amino group which is attached to C_2 residue of glucosamine	$MgCO_3$	–1720.418	462.369	–0.124	–0.019	0.053
	$Mg(OH)_2CO_3$	–1994.104	736.055	–0.156	–0.048	0.054

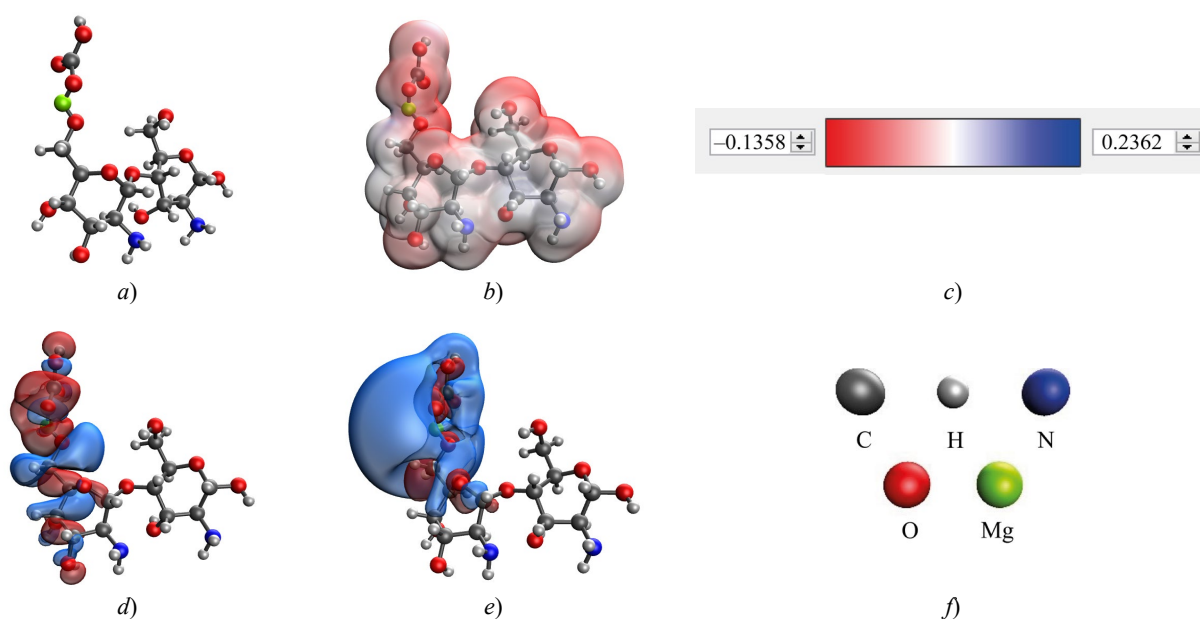


Fig. 3. Results of modeling the interaction of chitosan with magnesium carbonate through hydroxyl group attached to C_6 residue of glucosamine in chitosan: *a* — model of the complex; *b* — electron density distribution; *c* — gradient of electron density distribution; *d* — *HOMO*; *e* — *LUMO*; *f* — decoding of atoms

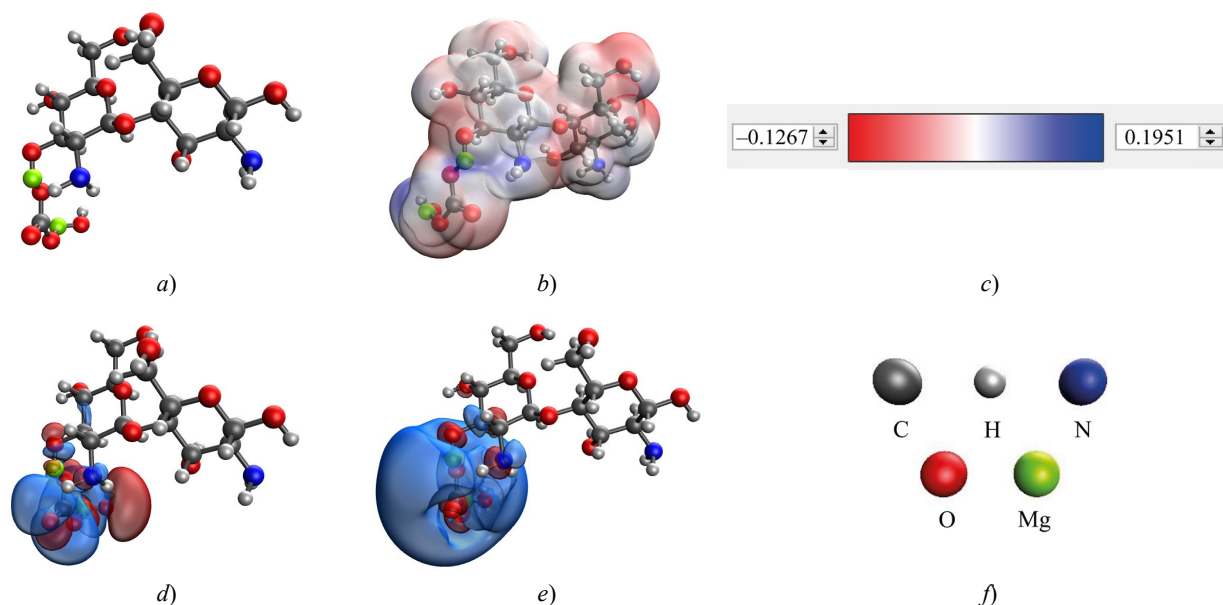


Fig. 4. Results of modeling the interaction of chitosan with basic magnesium carbonate through hydroxyl group attached to C_3 residue of glucosamine in chitosan: *a* — model of the complex; *b* — electron density distribution; *c* — gradient of electron density distribution; *d* — *HOMO*; *e* — *LUMO*; *f* — decoding of atoms

To validate the quantum chemical modeling data, the samples were examined using infrared spectroscopy. The results are shown in Figure 5.

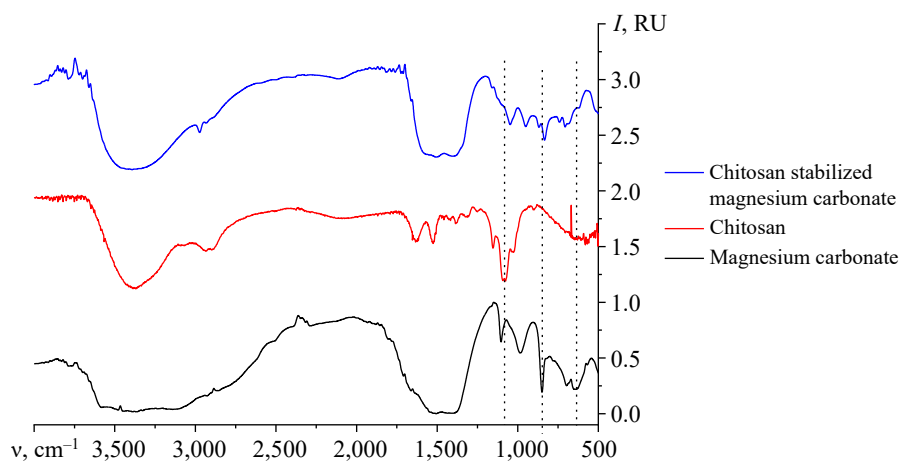
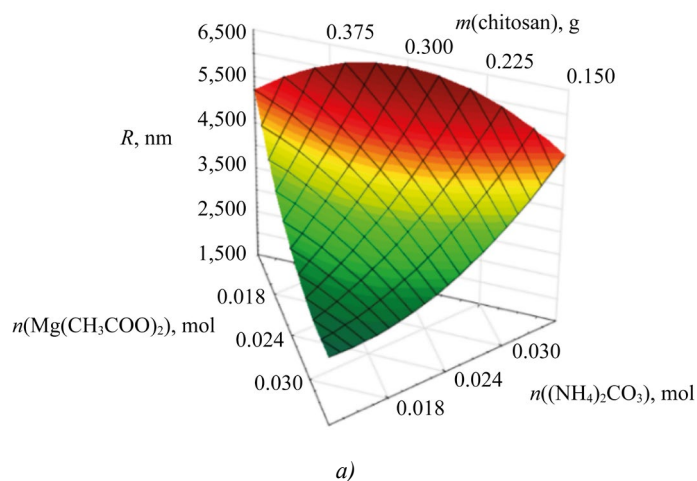


Fig. 5. IR spectrum of magnesium carbonate nanoparticles stabilized with chitosan

To study the influence of input parameters on the synthesis of nanoscale magnesium carbonate, ternary dependences were formed. Figure 6 shows the dependence of the average hydrodynamic radius of nanoparticles on the content of the initial reagents.



a)

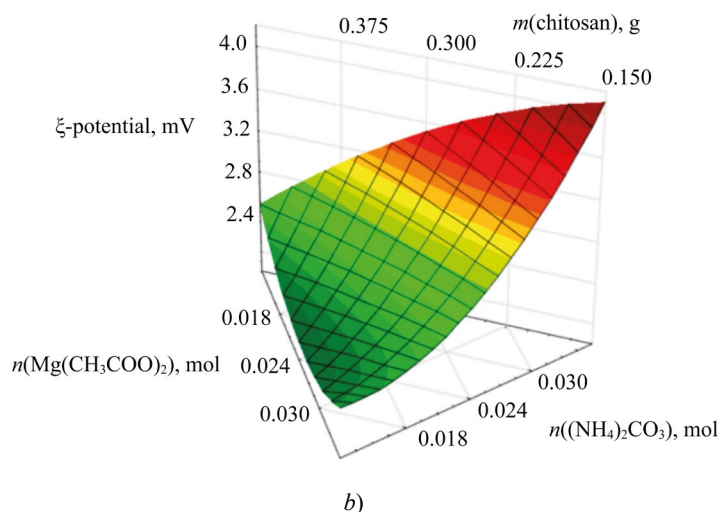


Fig. 6. Dependences of the change in average hydrodynamic radius and electrokinetic potential on concentrations of initial reagents: *a* — ternary surface describing the effect of initial reagents on particle size of magnesium carbonate; *b* — ternary surface describing the effect of initial reagents on electrokinetic potential of magnesium carbonate particles

Analysis of the phase composition of the samples has shown that there are phases of anhydrous magnesium carbonate ($MgCO_3$), two configurations of magnesium carbonate in the form of crystal hydrate ($MgCO_3 \cdot 5H_2O$), $Mg_2(CO_3)(OH)_2 \cdot 3H_2O$ and magnesium oxide (MgO).

When analyzing the surface microstructure of magnesium carbonate nanoparticles, it is found that the sample has an anisotropic shape. Magnesium carbonate is represented by rod-shaped particles from 2 to 10 μm in length, which consist of nanoparticles from 30 to 60 nm in size.

The computer quantum chemical modeling allowed us to compare the energy of interaction with the basic magnesium carbonate:

- chitosan with carbonate;
- a separate chitosan molecule.

In the first case, the energy value was lower than in the second. This indicates the chemical and energetic benefit of forming such complexes (for magnesium carbonate, the interaction energy is more than 462.00 kcal/mol, and for the basic carbonate — more than 736.00 kcal/mol).

In the optimal variant of coordination of magnesium carbonate with chitosan, the interaction occurred through the hydroxyl group of chitosan attached to C_6 residue of glucosamine. This interaction had the lowest energy $\Delta E = 462.387$ kcal/mol and chemical hardness $\eta = 0.062$ eV.

The position of the functional groups was determined by IR spectroscopy of chitosan-stabilized magnesium carbonate nanoparticles. Additionally, the spectra of pure chitosan and magnesium carbonate were recorded. The analysis of the IR spectrum of magnesium carbonate showed that in the region from 2200 to 3000 cm^{-1} there were the stretch vibrations of the groups NH_3^+ , NH_2^+ , NH^+ and CH_2 , $-CH_3$. The bands at 988 cm^{-1} , 1102 cm^{-1} , 1414 cm^{-1} and 1529 cm^{-1} were associated with vibrations of $C-O$ and $C=O$ in group CO_3^{2-} [16]. The band at 620 cm^{-1} corresponded to vibrations of the hydroxyl group, and the bands at 698 and 852 cm^{-1} were specified by vibrations of the bond $Mg-O$ [17].

The analysis of the IR spectra of chitosan showed that the region from 2500 to 3400 cm^{-1} was responsible for the stretching vibrations of the following functional groups: $-OH$, $-CH_3$, CH_2 [18]. The region from 1000 to 1900 cm^{-1} characterized the vibrations of bonds $C-O$, $C-O-C$, $-CH_2$, $-CH_3$, $C-N$, NH_2^+ [19]. The region of bands from 500 to 900 cm^{-1} referred to deformation vibrations: at 898 cm^{-1} — bonds $C-H$ [20], at 581, 652, 704 and 768 cm^{-1} — bonds $-CH$ and $-CH_2$.

As the analysis of the sample of magnesium carbonate nanoparticles stabilized with chitosan has shown, the range from 2100 to 3000 cm^{-1} contains stretching vibrations of the groups NH_3^+ , NH_2^+ , NH^+ , $-CH_3$, CH_2 , $O-H$. This is typical for the chitosan molecule. There are also bands at 1414 cm^{-1} and 1529 cm^{-1} , which correspond to vibrations $C-O$ and $C=O$ in group CO_3^{2-} , which confirms the presence of magnesium carbonate functional groups in the system [21]. The binding of magnesium is confirmed by the presence of deformation vibrations $C-O$ and $C=O$ in group CO_3^{2-} and bond vibrations $Mg-O$ and CO_3^{2-} in the range from 700 to 1100 cm^{-1} [22].

A decrease in the intensity of the peaks at 620 cm^{-1} and 1078 cm^{-1} , which correspond to the vibrations of groups $O-H$ and $C-O$, is noted. This indicates the interaction of magnesium carbonate and chitosan through hydroxyl groups and is consistent with the results of quantum chemical modeling.

The study on the ternary surfaces obtained suggests that the change in the ratio between magnesium acetate and ammonium carbonate affects significantly the size and zeta potential of magnesium carbonate particles [23]. The average hydrodynamic radius of the particles does not depend on the chitosan content. However, the change in zeta potential is related to the stabilizer content and precipitant concentration, which is important for assessing the stability of nanoscale systems. As a result, the parameters of the initial reagents are selected, at which the sample of magnesium carbonate nanoparticles has an optimal radius and zeta potential:

- 0.018 mol ammonium carbonate;
- 0.03 mol magnesium acetate;
- 0.15 g chitosan.

Discussion and Conclusion. Magnesium in magnesium carbonate is needed for the normal functioning of the body. In metabolic processes, it maintains the effective absorption of macronutrients. This allows us to talk about the urgency and potential demand for the method of obtaining nanoscale magnesium carbonate stabilized with chitosan. This approach is developed and optimized within the framework of the presented research. It has been established that magnesium carbonate nanoparticles are rod-shaped agglomerates with a length of 2 to 10 μm . These clusters consist of nanoparticles with a size of 30 to 60 nm. The optimal way of coordinating molecules is the interaction of magnesium carbonate through the hydroxyl group in C_6 residue of glucosamine in the chitosan molecule. The advantage is provided by significant indicators of energy and chemical rigidity.

IR spectroscopy of samples of magnesium carbonate nanoparticles stabilized with chitosan revealed a decrease in the intensity of the bands that characterize the vibrations of group O-H (for magnesium carbonate) and the vibrations of group C-O (for chitosan). It follows from this that the interaction occurs through the hydroxyl groups of chitosan.

The optimization of the method for synthesizing magnesium carbonate nanoparticles stabilized with chitosan, performed within the framework of the presented research, allows us to make a number of statements.

1. With increasing magnesium acetate content, the particle size and electrokinetic potential of nanoscale magnesium carbonate decrease.
2. With the growth of concentration of ammonium carbonate, the average hydrodynamic radius and surface charge of magnesium carbonate nanoparticles increase.
3. The concentration of chitosan has a slight effect on the radius of the particles, but as its content increases, the surface charge decreases.

References

1. Kanev AA, Kurakov FA, Cherchenko OV, Tsvetkova LA. The Development of Regenerative Medicine in Russia and in the World: Leading Researchers and Technological Drivers. *Economics of Science*. 2022;8(3–4):202–219. <https://doi.org/10.22394/2410-132X-2022-8-3-4-202-219>
2. Safronova TV. Inorganic Materials for Regenerative Medicine. *Inorganic Materials*. 2021;57(5):443–474. <https://doi.org/10.1134/S002016852105006X>
3. Agazade AR, Agazade RR, Gergieva TF, Amkhadov IS, Kadiev AA, Mamedov SE, et al. Evaluation of the Effectiveness of Treatment and Monitoring of Patients with Systemic Disorders of Bone Tissue during Dental Implantation. *Medical Alphabet*. 2023;1(1):44–49. <https://doi.org/10.33667/2078-5631-2023-1-44-49>
4. Golubeva AN. Proper Nutrition as the Main Component of a Healthy Lifestyle. *International Journal of Humanities and Natural Sciences*. 2023;76(1–4):40–42. <https://doi.org/10.24412/2500-1000-2023-1-4-40-42>
5. Pogozheva AV, Kodentsova VM, Sharafetdinov KhKh. The Role of Magnesium and Potassium in Preventive and Therapeutic Nutrition. *Problems of Nutrition*. 2022;91(5):29–42. <https://doi.org/10.33029/0042-8833-2022-91-5-29-42>
6. Kochneva EV. Magnesium Deficiency in Clinical Practice. *Nutrition*. 2018;8(1):37–51. <https://doi.org/10.20953/2224-5448-2018-1-37-51>
7. Evseeva GP, Suprun SV, Suprun EN, Rakitskaya EV, Kozlov VK, Lebed'ko OA. Influence of Trace Elements Imbalance on Immunity. *Trace Elements in Medicine*. 2021;22(S1):27–28. <https://doi.org/10.19112/2413-6174-2021-S1-12>
8. Hang Zhou, Bing Liang, Haitao Jiang, Zhongliang Deng, Kexiao Yu. Magnesium-Based Biomaterials as Emerging Agents for Bone Repair and Regeneration: From Mechanism to Application. *Journal of Magnesium and Alloys*. 2021;9(3): 779–804. URL: <https://www.jmamg.com/uploadfiles/2024/04/20240407095328708.pdf> (accessed: 25.06.2024).
9. Rubnikovich SP, Khomich IS. The Use of Bone Grafts and Bone Substitutes to Eliminate Defects and Augment Jaw Bones in Dental Implantology and Periodontology. *Dentist*. 2014;1(12):77–86. URL: <http://journal-stomatolog.by/wp-content/uploads/2018/05/2-13-2014.pdf> (accessed: 25.06.2024)
10. Monich SG, Khramkova AS, Bondarenko VA. The Use of Nanotechnology in Dental Implantology. In: *Proc. 16th International Science and Technology Conference "Instrumentation-2023"*. Minsk: BNTU Publ.; 2023. P. 288–289. (In Russ.) <https://rep.bntu.by/handle/data/138532>

11. Volova LT, Trunin DA, Ponomareva YuV, Popov NV. Study of Biocompatibility and Cytotoxicity of Personalized Bone Implants Using Cell Technologies. *Bulletin of REAVIZ: Rehabilitation, Doctor, and Health*. 2017;29(5):32–39.
12. Kou Sh(G), Peters L, Mucalo M. Chitosan: A Review of Molecular Structure, Bioactivities and Interactions with the Human Body and Micro-Organisms. *Carbohydrate Polymers*. 2022;282:119132. <https://doi.org/10.1016/j.carbpol.2022.119132>
13. Wenjie Wang, Changhu Xue, Xiangzhao Mao. Chitosan: Structural Modification, Biological Activity and Application. *International Journal of Biological Macromolecules*. 2020;164:4532–4546. <https://doi.org/10.1016/j.ijbiomac.2020.09.042>
14. Blinov AV, Pirogov MA, Gvozdenko AA, Golik AB, Rekhman ZA, Kolodkin MA. Computer Quantum-Chemical Modeling of the Interaction of Selenium Nanoparticles with Quaternary Ammonium Compounds. *Physical and Chemical Aspects of the Study of Clusters, Nanostructures and Nanomaterials*. 2023;15:357–366. <https://doi.org/10.26456/pcascnn/2023.15.357>
15. Anisimov AV. Experiment Planning as an Effective Method of Technological Process Optimization. In: *Proc. International Science and Technology Conference “Current Issues in Veterinary Medicine, Food and Biotechnology”*. Saratov: Saratov State Vavilov Agrarian University Publ.; 2022. P. 249–252. (In Russ.)
16. Frost RL. Raman Spectroscopic Study of the Magnesium Carbonate Mineral Hydromagnesite ($\text{Mg}_5[(\text{CO}_3)_4\text{OH}]_2 \cdot 4\text{H}_2\text{O}$). *Journal of Raman Spectroscopy*. 2011;42(8):1690–1694. <https://doi.org/10.1002/jrs.2917>
17. Kornprobst T, Plank J. Synthesis and Properties of Magnesium Carbonate Xerogels and Aerogels. *Journal of Non-Crystalline Solids*. 2013;361:100–105. <https://doi.org/10.1016/j.jnoncrysol.2012.10.023>
18. Aksay S. Effects of Al Dopant on XRD, FT-IR and UV–vis Properties of MgO Films. *Physica B: Condensed Matter*. 2019;570:280–284. <https://doi.org/10.1016/j.physb.2019.06.020>
19. Apfelbaum F, Mayer I, Rey C, Lebugle A. Magnesium in Maturing Synthetic Apatite: A Fourier Transform Infrared Analysis. *Journal of Crystal Growth*. 1994;144(3–4):304–310. [https://doi.org/10.1016/0022-0248\(94\)90471-5](https://doi.org/10.1016/0022-0248(94)90471-5)
20. Frost RL, Reddy BJ, Bahfenne S, Graham J. Mid-Infrared and Near-Infrared Spectroscopic Study of Selected Magnesium Carbonate Minerals Containing Ferric Iron – Implications for the Geosequestration of Greenhouse Gases. *Spectrochimica Acta. Part A: Molecular and Biomolecular Spectroscopy*. 2009;72(3):597–604. <https://doi.org/10.1016/j.saa.2008.10.043>
21. Zawadzki J, Kaczmarek H. Thermal Treatment of Chitosan in Various Conditions. *Carbohydrate Polymers*. 2010;80(2):394–400. <https://doi.org/10.1016/j.carbpol.2009.11.037>
22. Silva SML, Braga CRC, Fook MVL, Raposo CMO, Carvalho LH, Canedo EL. Application of infrared spectroscopy to analysis of chitosan/clay nanocomposites. In book: Th Theophanides (ed). *Infrared Spectroscopy — Materials Science, Engineering and Technology*. Ch. 3. London: IntechOpen Publ.; 2012. P. 43–62. <http://doi.org/10.13140/2.1.3806.5609>

About the Authors:

Andrey V. Blinov, Cand.Sci. (Eng.), Head of the Department of Physics and Technology of Nanostructures and Materials, North-Caucasus Federal University (1, Pushkin Str., Stavropol, 355017, Russian Federation), [SPIN-code](#), [ORCID](#), [ScopusID](#), blinov.a@mail.ru

Zafar A. Rekhman, Teaching Assistant of the Department of Physics and Technology of Nanostructures and Materials, North-Caucasus Federal University (1, Pushkin Str., Stavropol, 355017, Russian Federation), [SPIN-code](#), [ORCID](#), [ScopusID](#), zafrehman1027@gmail.com

Alexey A. Gvozdenko, Teaching Assistant of the Department of Physics and Technology of Nanostructures and Materials, North-Caucasus Federal University (1, Pushkin Str., Stavropol, 355017, Russian Federation), [SPIN-code](#), [ORCID](#), [ScopusID](#), [ResearcherID](#), gvozdenko.1999a@gmail.com

Maria A. Yasnaya, Cand.Sci. (Chemistry), Associate Professor, the Department of Physics and Technology of Nanostructures and Materials, North-Caucasus Federal University (1, Pushkin Str., Stavropol, 355017, Russian Federation), [SPIN-code](#), [ORCID](#), [ScopusID](#), [ResearcherID](#), iasnaia@ncfu.ru

Maxim A. Kolodkin, Head of the Laboratory Complex of the Department of Physics and Technology of Nanostructures and Materials, North-Caucasus Federal University (1, Pushkin Str., Stavropol, 355017, Russian Federation), [SPIN-code](#), mkolodkin@ncfu.ru

Maxim A. Taravanov, Assistant of the Department of Physics and Technology of Nanostructures and Materials, North-Caucasus Federal University (1, Pushkin Str., Stavropol, 355017, Russian Federation), [SPIN-code](#), [ORCID](#), [ScopusID](#), [ResearcherID](#), pronapro82@gmail.com

Claimed Contributorship:

AV Blinov: conceptualization.

ZA Rekhman: writing — review and editing.

AA Gvozdenko: validation.

MA Yasnaya: methodology.

MA Kolodkin: formal analysis.

MA Taravanov: investigation.

Conflict of Interest Statement: the authors declare no conflict of interest.

All the authors have read and approved the final version of the manuscript.

Об авторах:

Андрей Владимирович Блинов, кандидат технических наук, заведующий кафедрой физики и технологии наноструктур и материалов Северо-Кавказского федерального университета (355017, Российская Федерация, г. Ставрополь, ул. Пушкина, 1), [SPIN-код](#), [ORCID](#), [ScopusID](#), blinov.a@mail.ru

Зафар Абдулович Рехман, ассистент кафедры физики и технологии наноструктур и материалов Северо-Кавказского федерального университета (355017, Российская Федерация, г. Ставрополь, ул. Пушкина, 1), [SPIN-код](#), [ORCID](#), [ScopusID](#), zafrehman1027@gmail.com

Алексей Алексеевич Гвозденко, ассистент кафедры физики и технологии наноструктур и материалов Северо-Кавказского федерального университета (355017, Российская Федерация, г. Ставрополь, ул. Пушкина, 1), [SPIN-код](#), [ORCID](#), [ScopusID](#), [ResearcherID](#), gvozdenko.1999a@gmail.com

Мария Анатольевна Ясная, кандидат химических наук, доцент кафедры физики и технологии наноструктур и материалов Северо-Кавказского федерального университета (355017, Российская Федерация, г. Ставрополь, ул. Пушкина, 1), [SPIN-код](#), [ORCID](#), [ScopusID](#), [ResearcherID](#), iasnaia@ncfu.ru

Максим Андреевич Колодкин, заведующий лабораторным комплексом кафедры физики и технологии наноструктур и материалов Северо-Кавказского федерального университета (355017, Российская Федерация, г. Ставрополь, ул. Пушкина, 1) [SPIN-код](#), mkolodkin@ncfu.ru

Максим Александрович Тараванов, лаборант кафедры физики и технологии наноструктур и материалов Северо-Кавказского федерального университета (355017, Российская Федерация, г. Ставрополь, ул. Пушкина, 1), [SPIN-код](#), [ORCID](#), [ScopusID](#), [ResearcherID](#), pronapro82@gmail.com

Заявленный вклад авторов:

А.В. Блинов: разработка концепции.

З.А. Рехман: написание рукописи — рецензирование и редактирование.

А.А. Гвозденко: валидация результатов.

М.А. Ясная: разработка методологии.

М.А. Колодкин: формальный анализ.

М.А. Тараванов: проведение исследования.

Конфликт интересов: авторы заявляют об отсутствии конфликта интересов.

Все авторы прочитали и одобрили окончательный вариант рукописи.

Received / Поступила в редакцию 09.10.2024

Reviewed / Поступила после рецензирования 29.10.2024

Accepted / Принята к публикации 07.11.2024

MACHINE BUILDING AND MACHINE SCIENCE МАШИНОСТРОЕНИЕ И МАШИНОВЕДЕНИЕ



UDC 621.791.927.5

Original Theoretical Research

<https://doi.org/10.23947/2687-1653-2024-24-4-402-412>

Selection of the Process of Arc Welding of Sealing Surfaces of Power Valves with a Consumable Electrode in the Shielding Gas

Dmitrii V. Rogozin , Vyacheslav A. Lenivkin

Don State Technical University, Rostov-on-Don, Russian Federation

✉ dmrogozin@ya.ru

EDN: TKWDZL

Abstract

Introduction. One of the main requirements to the methods of weld overlay of sealing surfaces of power valve trim parts is to obtain a high-quality wear-resistant pad with minimal penetration and optimal process performance. Currently, arc, electrosag, plasma, beam, induction and other surfacing techniques have been developed and introduced into production. However, the influence of various arc welding processes with a consumable electrode in shielding gas on the geometric parameters of weld beads and metal hardness of sealing surfaces is understudied. The presented research is intended to fill this gap. The objective of its authors is to select such a process of arc welding of beads on parts of the power valve trim with a consumable electrode in shielding gases, which would provide the best workability of the deposited metal.

Materials and Methods. Arc surfacing with a consumable electrode in a mixture of gases was performed on steel plates. The welding torch was moved in a straight line, without transverse oscillations, using the FRC-9 mechanism (Fronius). A microprocessor-controlled inverter-type digital current source TransPulsSynergic 3200 CMT (Fronius) was used as the power supply. The following welding processes were analyzed: MIG/MAG process with self-regulation (Standard mode), synergic process of MIG/MAG method (Synergic mode), short arc process with mechanical separation of electrode metal droplets (CMT-ColdMetalTransfer), and synergic pulse-arc process (PulseSynergic). The short-cut process of bead surfacing was evaluated by the stability of the values of the energy parameters of the bead surfacing mode in time at the same electrode wire feed rates, which were recorded by oscilloscopes, as well as by comparing the geometric characteristics of the deposited beads and the hardness of the deposited metal.

Results. The analysis of experimental data of the geometries of the weld beads and their complex dimensional characteristics made it possible to establish that the welding engineering requirements for the welded beads are most fully met by long-arc surfacing by the PulseSynergic pulse-arc process.

Discussion and Conclusion. The study and the resulting data make a certain contribution to solving the problem of the influence of arc welding processes on the parameters of weld beads and on the hardness of the metal of sealing surfaces. A detailed analysis of the modes of arc surfacing of beads with a consumable electrode in shielding gases on the trim parts of power valves can be used in further research on this topic. The conclusions of the authors will not only provide considerable theoretical assistance to scientists, but will also make adjustments to the activities of practitioners.

Keywords: pulse arc surfacing, welding processes, short arc, long arc, consumable electrode, sealing surfaces

Acknowledgements. The authors would like to thank the Editorial board and the reviewers for their attentive attitude to the article and for the specified comments that improved the quality of the article.

For citation. Rogozin DV, Lenivkin VA. Selection of the Process of Arc Welding of Sealing Surfaces of Power Valves with a Consumable Electrode in the Shielding Gas. *Advanced Engineering Research (Rostov-on-Don)*. 2024;24(4):402–412. <https://doi.org/10.23947/2687-1653-2024-24-4-402-412>

Выбор процесса дуговой наплавки плавящимся электродом в защитном газе уплотнительных поверхностей энергетической арматуры

Д.В. Рогозин , В.А. Ленивкин 

Донской государственный технический университет, г. Ростов-на-Дону, Российская Федерация

 dmrogozin@ya.ru

Аннотация

Введение. Одно из главных требований к способам наплавки уплотнительных поверхностей деталей затвора энергетической арматуры заключается в получении качественного износостойкого наплавленного слоя металла при минимальном его проплавлении и оптимальной производительности процесса. В настоящее время разработаны и внедрены в производство дуговые, электрошлаковые, плазменные, лучевые, индукционные и другие способы наплавки. Однако влияние различных дуговых сварочных процессов плавящимся электродом в защитном газе на геометрические параметры наплавленных валиков и твердость металла уплотнительных поверхностей недостаточно изучено. Представленная научная работа призвана восполнить этот пробел. Целью ее авторов является выбор такого процесса дуговой наплавки валиков плавящимся электродом в защитных газах на детали затвора энергетической арматуры, который обеспечивал бы наилучшие сварочно-технологические свойства наплавленного металла.

Материалы и методы. Дуговую наплавку плавящимся электродом в смеси газов осуществляли на пластины из стали. Наплавочная горелка перемещалась прямолинейно, без поперечных колебаний, с помощью механизма FRC-9 (Fronius). В качестве источника питания использовали цифровой источник тока инверторного типа с микропроцессорным управлением TransPulsSynergic 3200 CMT (Fronius). Анализировались следующие сварочные процессы: процесс MIG/MAG с саморегулированием (режим Standard), синергетический процесс способа MIG/MAG (режим Synergic), процесс короткой дугой с механическим отрывом капель электродного металла (CMT-ColdMetalTransfer) и синергетический импульсно-дуговой процесс (PulseSynergic). Рациональный процесс наплавки валиков оценивался стабильностью величин энергетических параметров режима наплавки валиков во времени при одинаковых скоростях подачи электродной проволоки, которые фиксировались осциллографами, а также сравнение геометрических характеристик наплавленных валиков и твердости наплавленного металла.

Результаты исследования. Анализ экспериментальных данных геометрических размеров наплавленных валиков и их комплексных размерных характеристик позволил установить, что сварочно-технологическим требованиям, предъявляемым к наплавленным валикам, наиболее полно соответствует наплавка длинной дугой импульсно-дуговым процессом *PulseSynergic*.

Обсуждение и заключение. Проведенное исследование и полученные в результате его данные вносят определенный вклад в решение проблемы влияния дуговых сварочных процессов на параметры наплавленных валиков и на твердость металла уплотнительных поверхностей. Подробный анализ режимов дуговой наплавки валиков плавящимся электродом в защитных газах на детали затвора энергетической арматуры может быть использован в дальнейших исследованиях на эту тему. Выводы авторов не только окажут ощутимую теоретическую помощь ученым, но и внесут коррективы в деятельность специалистов-практиков.

Ключевые слова: импульсно-дуговая наплавка, сварочные процессы, короткая дуга, длинная дуга, плавящийся электрод, уплотнительные поверхности

Благодарности. Авторы выражают благодарность редакции и рецензентам за внимательное отношение к статье и замечания, которые позволили повысить ее качество.

Для цитирования. Рогозин Д.В., Ленивкин В.А. Выбор процесса дуговой наплавки плавящимся электродом в защитном газе уплотнительных поверхностей энергетической арматуры. *Advanced Engineering Research (Rostov-on-Don)*. 2024;24(4):402–412. <https://doi.org/10.23947/2687-1653-2024-24-4-402-412>

Introduction. One of the main results of the mechanized weld overlay of sealing surfaces of power valve trim parts in protective gases is the production of a high-quality wear-resistant weld layer of metal with minimal penetration [1]. The requirements for the metal of the weld layer are divided into three groups: welding and process, operational, and economic [2].

Welding and process requirements determine the absence of pores, cracks, areas with embrittled structure, and other welding defects that arise under surfacing. The deposited metal should be easily formed, have good slag separation in a

wide range of modes both in single-layer and multi-layer surfacing. Thermal expansion coefficients of the base and weld metal should be comparable. Otherwise, cold cracking may occur in the fusion zone with subsequent peeling of the weld metal. The content of various elements in the weld metal determines its structure, phase composition, hardness, and wear resistance [3].

The group of welding and process requirements also includes the productivity of arc surfacing in protective gases, which fluctuates up to 8 kg/h, and the layer thickness — up to 10 or more millimeters. Higher productivity can be achieved by using more powerful heat sources. However, when heating above a certain value, the proportion of the base metal in the deposited metal increases, harmful elements pass from it, the volume of liquid metal grows, and the primary structure of the deposited metal becomes larger [4]. In some cases, slow cooling of the deposited layer and its tempering reduce wear resistance and other quality indicators of the metal of the deposited layer. Contradictions often arise between the possibility of raising the productivity of deposition through increasing the power of the heat source and the quality of the deposited layer [5]. Therefore, technology factors determined by the method and mode of deposition affect the size and distribution of structural components in the deposited metal, its strength and quality.

The welding and process properties of the deposited bead are determined by the type of deposition process. One of the fundamental properties of the deposited metal of the sealing surfaces of power valves is its hardness [6]. Currently, arc, electroslog, plasma, beam, induction and other techniques of surfacing are widely used to form sealing surfaces on parts of energy valve trims [7, 8]. An effective and well-researched method of surfacing is arc surfacing with a consumable electrode in protective gases [9, 10].

The result of intensive development of power semiconductor devices (power transistors) in the last decades of the 20th century was the creation of new modern welding low-inertia, high-speed power sources (welding rectifiers), equipped with inverter converters capable of controlling process modes at the microcycle level. This expands significantly the scope of application of arc welding and surfacing due to the possibility of implementing specific welding processes with a short and long arc at the hardware level [11]. However, the influence of various arc welding processes with a consumable electrode in a protective gas on the geometric parameters of the deposited beads and the hardness of the deposited metal has not been sufficiently studied. In this regard, the objective of this research is to determine the process of arc surfacing of beads with a consumable electrode in protective gases on the parts of the trim of power valves, which would provide the best welding and process properties of the deposited metal.

Materials and Methods. The effect of various arc welding processes produced by a consumable electrode in protective gases on the geometric dimensions of the beads and on the hardness of the metal of the deposited surfaces was investigated under mechanized surfacing with a reverse polarity current of individual straight beads on plates (made of steel 20 GOST 1050 with a thickness of 10 mm, a length of 300 mm and a width of 150 mm) with electrode wire Sv-08G2S with a diameter of 1.2 mm in a mixture of protective gases (82% Ar + 18% CO_2). Protective gas consumption was 13–15 l/min, without transverse oscillations of the welding torch. The distance between the end of the contact tip and the surface of the welded plate was maintained constant — 20 mm.

The weld beads were arranged parallel at a distance of at least 20 mm from each other. Each subsequent bead was welded after the preceding one had been thoroughly cleaned of slag. The temperature of the metal of the preceding bead was no more than 100°C.

The surfacing speed was 30 cm/min (18 m/h) and was provided by the FRC-9 surfacing torch movement mechanism (Fronius).

The registration of electrical parameters during the entire process of bead surfacing (current value and voltage drop across the interelectrode gap) was performed by the IRSP-11 welding process measuring and recording device. Reading and viewing the registration results in the form of oscillograms was performed on a personal computer using the IRSP_Read software.

The hardness of the deposited metal was measured according to GOST 6996 on samples in the cross section after the application of attack-polishing method in a 4% alcohol solution of nitric acid according to Rockwell (HRC) on a Metrotest ITBRV-187.5-M hardness gauge. The hardness value was determined as the arithmetic mean at three points.

For surfacing the beads, a digital inverter-type current source with microprocessor control TransPulsSynergic 3200 CMT (Fronius) was used, which had a sufficient number of synergic programs for controlling the electrical parameters of the welding mode and provided 4 types of surfacing process:

- MIG/MAG process (*Standard* mode);
- synergistic process of the MIG/MAG method (*Synergic* mode);
- CMT process with a flexible software control system for the transfer of “cold metal” by a short arc (*CMT* mode);
- pulsed-arc process (*PulseSynergic* mode).

The rational process of bead surfacing was assessed by the stability of the values of the energy parameters of the bead surfacing mode over time at the same feed rates of the electrode wire, which were recorded by oscillograms (Fig. 1–4). The results are given in Tables 1–3.

Research Results. The energy parameters of the surfacing mode are:

- average value of the surfacing process current (I_{cp});
- voltage drop across the interelectrode gap (U_{np}).

For short arc surfacing:

- short-circuit current curve $i_{k3}(t_{k3})$;
- arc burning current curve $i_{гд}(t_{гд})$;
- peak current value (I_n), interrupting current of the liquid bridge between the drop immersed in the weld pool and the electrode;
- duration of short circuit t_{k3} , arc burning $t_{гд}$ and of the whole cycle $t_{ц}$;
- short circuit frequency f_{k3} .

The MIG/MAG (*Standard* mode) arc surfacing process was carried out with a constant feed rate of the electrode wire v_{mm} (hereinafter referred to as the electrode) with self-regulation of its melting, without the use of regulating devices, with a long arc (without short circuits) in an inert, active protective gas and their mixture, with a short arc (with short circuits of the inter-arc gap). The parameters of the MIG/MAG process surfacing mode are given in Table 1 (modes 1–3). A section of the MIG/MAG process oscillogram (*Standard* mode) is shown in Figure 1.

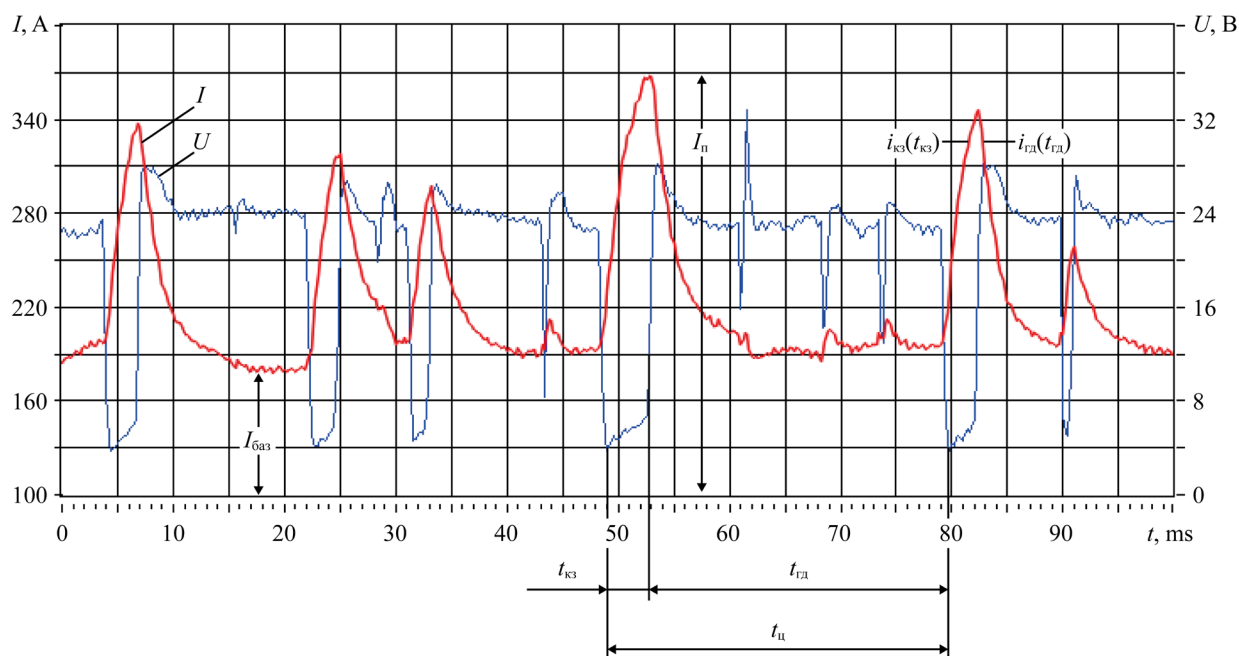


Fig. 1. Oscillogram of MIG/MAG process (*Standard* mode): surfacing mode 2 in Table 1

Table 1

Parameters of the Surfacing Modes by MIG/MAG Process and MIG/MAG (*Synergic* mode)

Mode No.	v_{mm} m/min	Process current value, A			Voltage, V	Duration, ms			Short circuit frequency, 1/s
		I_{cp}	I_{6a3}	I_n		t_{k3}	$t_{гд}$	$t_{ц}$	
1	5.0	$\frac{188-198}{194}$	$\frac{130-190}{160}$	$\frac{190-310}{250}$	19	$\frac{2-4}{3}$	$\frac{4-24}{14}$	$\frac{6-28}{17}$	59
2	6.5	$\frac{220-230}{225}$	$\frac{190-210}{190}$	$\frac{250-360}{310}$	21	$\frac{2-4}{3}$	$\frac{5-26}{15}$	$\frac{7-30}{18}$	51
3	8.0	$\frac{252-263}{256}$	$\frac{235-245}{240}$	$\frac{300-380}{340}$	25	$\frac{2-4}{3}$	$\frac{25-65}{45}$	$\frac{27-69}{48}$	21

4	5.0	$\frac{188-201}{193}$	$\frac{140-180}{160}$	$\frac{220-260}{240}$	19	$\frac{2-6}{3}$	$\frac{2-29}{16}$	$\frac{4-35}{19}$	52
5	6.5	$\frac{223-240}{234}$	$\frac{160-220}{190}$	$\frac{280-310}{290}$	19	$\frac{3-8}{5}$	$\frac{8-38}{23}$	$\frac{11-46}{28}$	35
6	8.0	$\frac{254-265}{258}$	$\frac{220-260}{240}$	$\frac{300-320}{310}$	24	$\frac{2-6}{4}$	$\frac{6-46}{26}$	$\frac{8-52}{30}$	33

Note. Numerator shows the smallest and largest values of the electrical and time parameters of the surfacing processes. Denominator shows the average value of the corresponding parameters during the bead surfacing time.

The synergistic process of the *MIG/MAG* method (*Synergic* mode) is a self-organizing system that automatically changes its process control structure by selecting the required synergistic program. In *Synergic* mode, setting one parameter of the surfacing mode leads to an automatic change in all other process parameters by switching to a new program that maintains a stable surfacing process (Table 1, modes 4–6). A section of the oscillogram of the synergic process of the *MIG/MAG* method (*Synergic* mode) is shown in Figure 2.

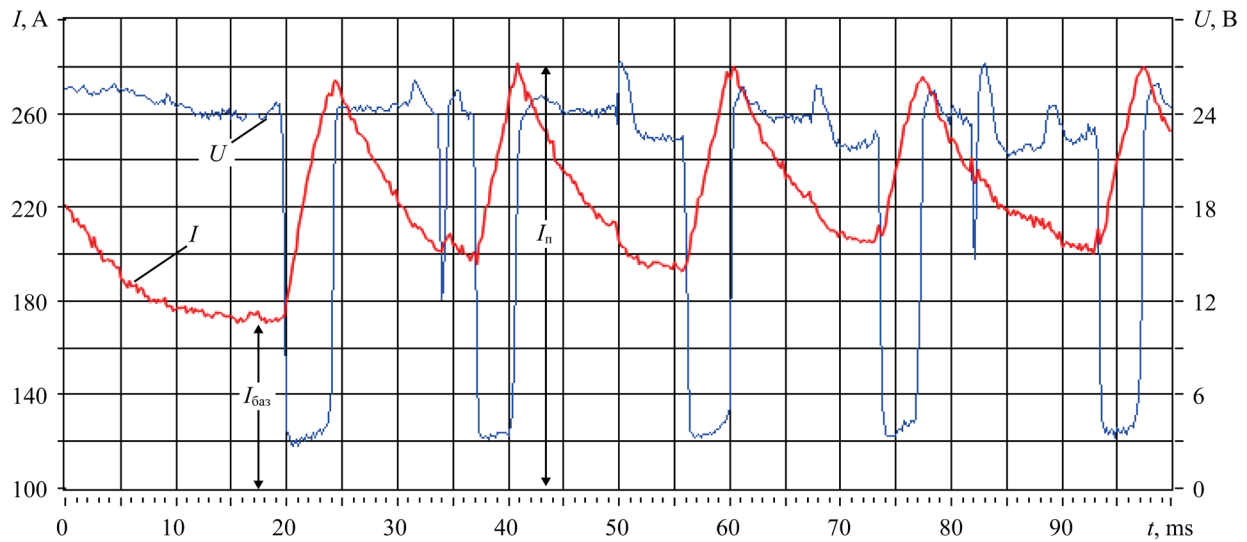


Fig. 2. Oscillogram of the synergistic process of the *MIG/MAG* method (*Synergic* mode): parameters of surfacing mode 5 in Table 2

Under short arc surfacing using the *MIG/MAG* method (*Standard* mode) and under the synergic process using the *MIG/MAG* method (*Synergic* mode), the current during a short circuit increases (short-circuit current curve $i_{k3}(t_{k3})$) according to the exponential law. When the bridge is interrupted, the arc burning current (arc burning current curve $i_{r3}(t_{r3})$) also decreases according to the exponential law, as in the case of surfacing from parametric welding rectifiers that do not have an inverter converter [12, 13].

A reliable interruption of the bridge in the specified surfacing processes occurs with a certain current reserve $I_n \leq 0.7I_0$, where I_n — peak current value at the moment of interruption of the liquid bridge between the electrode tip and the weld pool; $I_0 = U_{xx} / Z_n$ — steady-state short-circuit current; U_{xx} — voltage at the output of the power source; Z_n — complex electrical resistance of the surfacing circuit [12].

It is known that the nature of the process with frequent short circuits of the arc gap depends on the rate of increase of the current at the beginning of short circuit $i_{k3}(t_{k3})$ and at the interruption of the liquid bridge $i_{r3}(t_{r3})$ [14].

According to [14], when surfacing with an electrode of 1.2 diameter from welding rectifiers that do not have inverter converters, at a high rate of current increase, $i_{k3} > 200-300$ kA/s, the process is stable, but is accompanied by increased spatter. At low rates of current increase, $i_{k3} < 40$ kA/s, the process occurs with rare short circuits, unstable. At rates of 40–130 kA/s, the process is stable, with little spatter.

Welding power sources with inverter converters are equipped with step-down output transformers with low inductance, which provide low inertia of the source and the time constant of the circuit. The short duration of the time constant of the electric circuit provides a high rate of current increase at the moment of contact of the liquid metal of the electrode with the weld pool. This should worsen the reliable closure of the interelectrode gap and contribute to an increase in metal losses due to spattering from the pool and the electrode tip due to an increase in the axial component of the electrodynamic forces acting on the metal drop located at the electrode tip and the weld pool.

In this research, when surfacing beads using the processes in the modes specified in Tables 1 and 2, with short circuits of the arc gap from an inverter-type source with an electrode feed rate (v_{mm}) of 6.5 m/min, it was determined that the rate of current increase at the beginning of a short circuit during the MIG/MAG process (*Standard* mode) was 40–45 kA/s, in the *Synergic* mode — 20–25 kA/s, in the *CMT* mode — 25–30 kA/s.

The results of processing the oscillogram data presented in Table 1 (modes 1–6) show that MIG/MAG surfacing processes with short circuits (*Standard* mode and *Synergic* mode) are unstable in both electrical and time parameters. This contributes to the formation of droplets of uneven sizes and uneven frequency of their transfer. This circumstance is the reason for the unsatisfactory formation of the surface of the weld bead, which is manifested in the uneven, bumpy outline of its surface — scaling.

The control of the surfacing process in the *CMT* system is performed simultaneously by feedback signals on the instantaneous value of the welding current and voltage at various stages of the short circuit of the arc gap through acting on the low-inertia welding power source and on the feed rate of the electrode.

The *CMT* feeder uses a “push — pull” electrode feed system. A more powerful DC pusher motor feeds the electrode wire from the cassette into the flexible hose at a constant speed equal to the average speed of its melting. The reversible pulling servomotor installed in the torch body maintains the reciprocating movement of the electrode wire as it exits the current-supplying tip of the welding torch at a variable speed according to a given program.

The nature of the change in the electrical parameters of the process according to the *CMT* algorithm at an electrode feed rate of 6.5 m/min is shown in Figure 3.

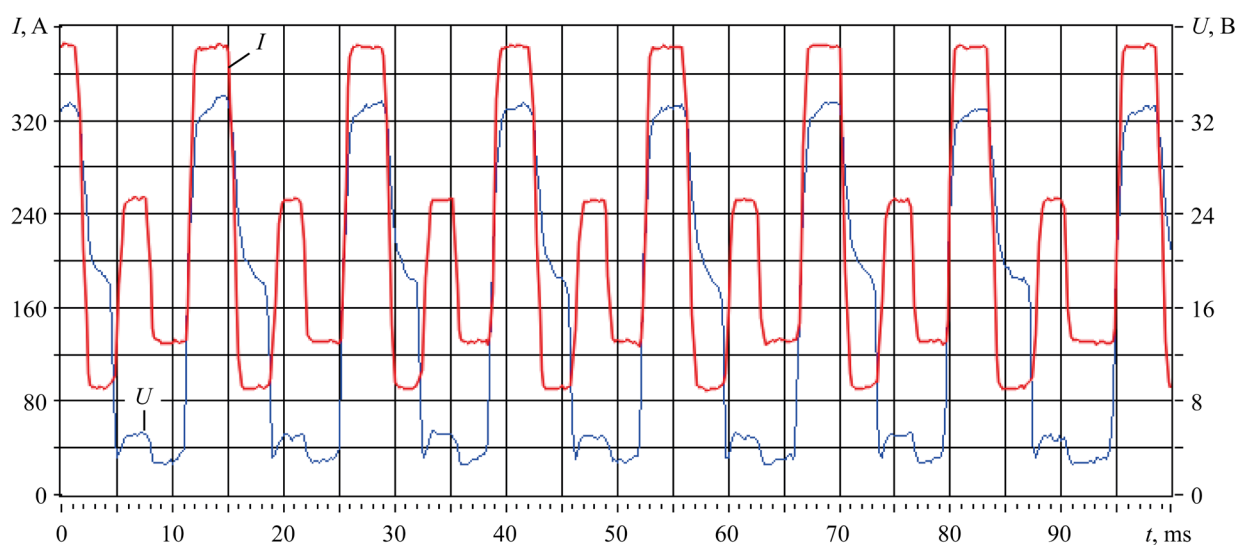


Fig. 3. Oscillogram of the *CMT* process: parameters of surfacing mode 8 in Table 2

Table 2

Parameters of Surfacing Modes by *CMT* Process

Mode no.	Feed speed, v_{mm} , m/min	Current value, A			Voltage, V	Duration, ms			Short circuit frequency, 1/s	Drop volume mm^3
		I_{cp}	$I_{\text{баз}}$	$I_{\text{п}}$		$t_{\text{кз}}$	$t_{\text{гд}}$	$t_{\text{ц}}$		
7	5.0	175	240	300	14	5	6	11	90	1.72
8	6.5	220	250	380	16	6	7	13	77	1.54

In order to explain the technological advantages of the *CMT* surfacing process, the feature of changing the electrical parameters of the algorithm in one cycle (Fig. 4), taken from the oscillogram in Figure 3, is considered.

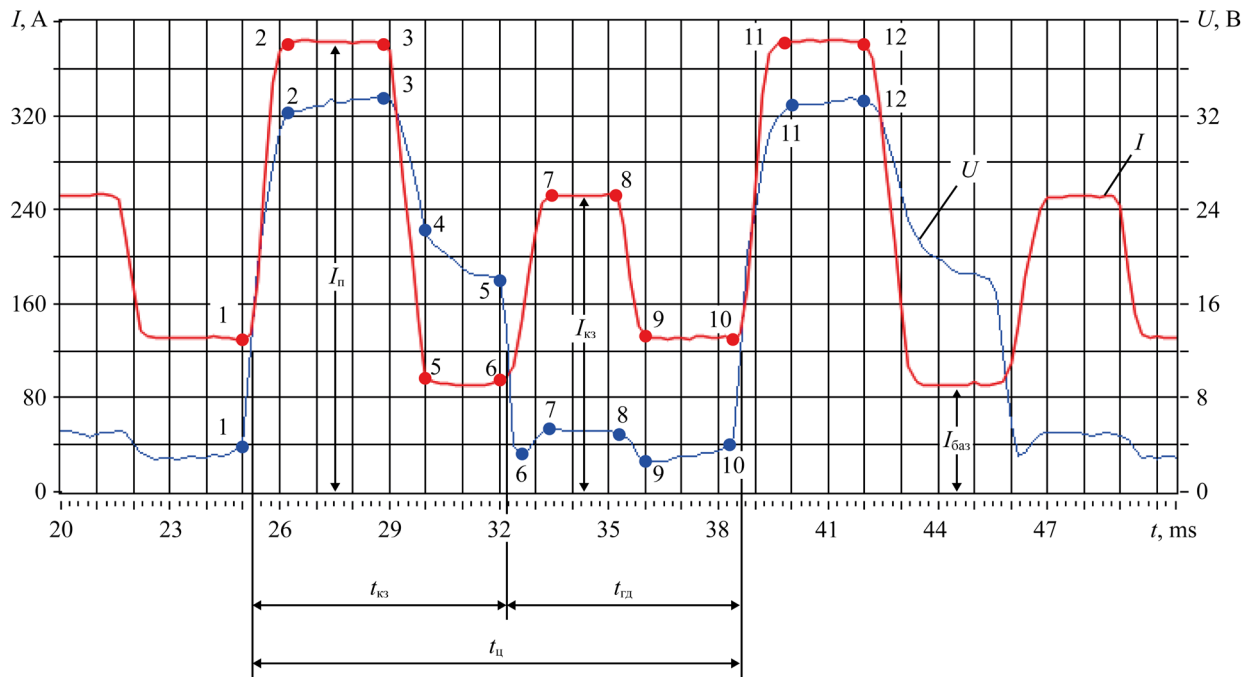


Fig. 4. Fragment of one cycle from the oscillogram of *CMT* process: mode parameters — in Figure 3

From the fragment of the oscillogram of one cycle (Fig. 4), it follows that at point (p.) 1, the process of interrupting the bridge starts at a relatively low current (135 A). This is much less than in the *MIG/MAG* process. The voltage drop on the interelectrode gap in 0.25 ms increases to the sum of the near-electrode voltage drops, and then, after 0.75 ms, increases to 32 V (p. 2), and the current increases to 380 A (p. 2) with a rate of increase of 250 kA/s.

The metal of the electrode wire, melted during the arc burning time in the time interval between p. 1 and p. 3 (about 4 ms) at a relatively high current value, is displaced from the electrode tip to its side surface. Then, within 1.0 ms, the current sharply decreases to the value of the base current (I_{0a3} — 90 A) at a rate of 290 kA/s, and the voltage decreases to 23 V. In the time interval of 2.0 ms (between p. 4 and p. 5), the length of the arc gap is reduced, and the voltage is decreased to 18 V. The value of the base current between p. 4 and p. 5 is automatically maintained constant by the source control system, the molten metal from the side surface of the electrode descends under its tip, takes the form of a spherical segment.

When the liquid metal of the spherical segment of the electrode comes into contact with the surface of the weld pool (p. 6 on the voltage curve), a reliable short circuit of the electric circuit occurs without splashing, which is observed during *MIG/MAG* surfacing, for 1 ms, and for 2 ms (between p. 7 and p. 8), the voltage drop on it is maintained constant (5 V), the current value is 250 A, respectively.

At p. 8, the servomotor is reversed, and the electrode starts moving in the opposite direction from the weld pool. The current value decreases to 130 A (p. 9) and remains unchanged for 2.5 ms (the interval between p. 9 and p. 10), and the voltage on the bridge increases by 1 V. At the same time, the bridge continues to be pulled out of the pool and narrows.

In p. 10, the bridge interrupts, the voltage on the arc gap becomes greater than the sum of its near-electrode drops, and the arc ignites. At the same time, the servomotor is reversed, and the electrode begins to flow toward the weld pool at an increased speed. Simultaneously, the voltage on the arc gap between p. 10 and p. 11 increases. This causes a high rate of current increase (480 kA/s) to a value of 380 A. In the time interval between p. 11 and p. 12, intensive melting of the electrode occurs, and the surfacing process cycle is repeated.

From the oscillogram data (Fig. 3 and Table 2), it follows that the *CMT* process is the most stable, since it has virtually no deviations — both in electrical and time parameters.

When surfacing a bead using the *CMT* process (Fig. 3), the current value during a short circuit of the arc gap, compared to the *MIG/MAG* process, at the same electrode feed rate, is lower, and the process is more stable and has a pronounced

cyclic nature. The frequency of short circuits is higher, and the duration of the arc and the cycle time are shorter (Table 2). This contributes to a finer metal transfer, satisfactory formation of the surface of the surfacing bead with uniform scaling.

In the process of pulse surfacing (*PulseSynergic*), along with the use of the *Synergic* process itself, it is possible to cyclically alternate the energy parameters of the surfacing process. Due to such a pulsed change in the process current and arc voltage, the heat input in the weld pool is regulated, which, in turn, affects the geometrics of the surfacing bead.

The major task of pulsed arc surfacing (welding) with a consumable electrode with a long arc is to provide controlled fine-droplet transfer of metal in the region of modes with natural large-droplet transfer. The best process properties here are manifested when using spatially stable arcs, which are observed in a protective environment of argon or in a mixture with more than 80% Ar and CO₂.

The section of the oscillogram of the *PulseSynergic* surfacing is shown in Figure 5. The parameters of the pulse surfacing process at different electrode feed rates are shown in Table 3, and the parameters of the rollers are shown in Table 4 (modes 9–11).

The current pulse has a trapezoidal shape, the amplitude of which is determined as $I_{\Pi} = I_{\Pi} - I_{\text{баз}}$.

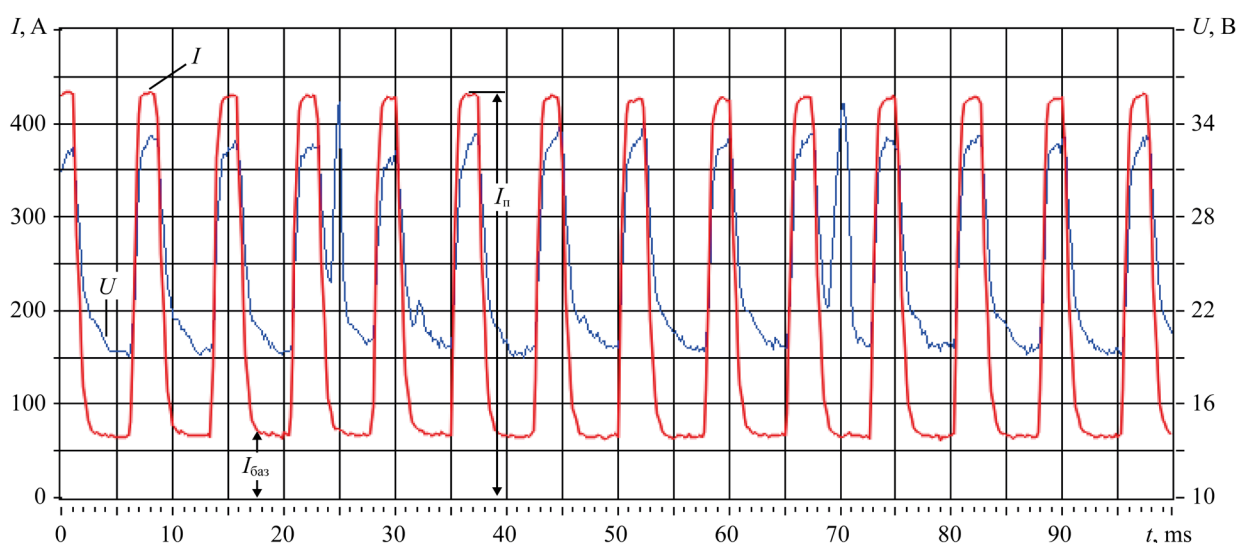


Fig. 5. Oscillogram of the pulse-arc process (*PulseSynergic* mode): surfacing mode parameter 10 in Table 3

Table 3

Parameters of Surfacing Modes by *PulseSynergic* Process

Mode no.	Feed speed, v_{mm} , m/min	Process current value, A			Voltage, V	Duration, ms			Current pulse frequency, 1/s	Drop volume, mm ³
		I_{cp}	$I_{\text{баз}}$	I_{Π}		t_{IM}	t_{Π}	t_{II}		
9	5.0	157	45	430	24	3	7	10	100	1.19
10	6.5	192	70	430	24	3	5	8	125	1.11
11	8.0	233	100	430	26	3	3	6	166	1.15

The characteristic feature of the control algorithm of the surfacing process of the *PulseSynergic* mode is that the average process current (I_{cp}) and its base current ($I_{\text{баз}}$) are set by the electrode feed rate, and their values increase with an increase in the electrode feed rate. At the same time, the peak pulse current (I_{Π}) and its duration (t_{IM}) remain unchanged, and the pause duration (t_{Π}) is reduced with a simultaneous increase in the pulse repetition frequency ($f_{\text{ИМП}}$), the volume of drops remains almost the same, fine-droplet (Table 3). Under such conditions, the surface of the deposited bead has a fine uniform scaly texture.

Table 4

Parameters of Beads Deposited by Different Processes

Mode no.	Surfacing process	Depth of penetration, a , mm	Bead width e , mm	Height of convexity, g , mm	Penetration area, mm ²	Surfacing area mm ² (calculation)	Welding shape coefficient	Form factor fusion	Hardness HRC
1	MIG/MAG	2.4	8.8	3.2	10.0	20.0	2.8	3.7	21.0
2		3.0	10.7	3.2	15.0	24.5	3.3	3.6	24.0
3		3.3	14.5	2.9	21.0	29.4	5.0	4.4	18.5
4	Synergic	2.3	9.2	2.9	9.2	18.2	3.2	4.0	29.0
5		1.2	10.1	3.6	4.0	26.0	2.8	8.4	24.0
6		4.0	14.4	3.0	22.0	30.0	4.8	3.6	19.0
7	CMT	1.5	7.0	3.7	3.8	20.3	1.9	4.7	25.0
8		2.2	10.2	3.7	7.0	27.8	2.8	4.6	24.5
9	Pulse Synergic	2.3	11.4	2.6	10.4	20.0	4.4	5.0	20.0
10		3.2	12.6	2.9	17.0	25.0	4.3	3.9	22.0
11		3.6	14.4	3.0	22.3	32.3	4.8	4.0	19.0

Note. The hardness of the plates made of steel 20 GOST 1050 was 10–12 HRC.

Table 4 shows the data on the geometric parameters of the beads deposited under the same conditions, at the same electrode feed rates. Based on these data, the dimensional characteristics of the beads were calculated (deposition shape coefficient $k_{\Phi} = e/g$, penetration shape coefficient $k_{\Phi} = e/a$, and deposition completeness coefficients $\mu_{\text{m}} = F_w/(eg)$), which characterize the completeness of filling a rectangle with the weld with dimensions e and g [8, 15]. Based on these indicators, it can be concluded that it is advisable to weld the beads to create sealing surfaces for power engineering valves using a long arc through the *PulseSynergic* surfacing process, which provides stable electrical and time parameters that meet the welding and process properties of the surfaces under weld overlay.

Discussion and Conclusion. As a result of the conducted research, data were obtained that are of great importance for studying the influence of arc welding processes on the dimensions of deposited beads, on the hardness of sealing surfaces. The revealed patterns of changes in time of energy parameters of the surfacing mode with a short and long arc in the process of transferring electrode metal in the inter-arc gap can be taken into account when using low-inertia welding inverter power sources by specialists in their practical activities. The analysis of the modes of arc surfacing of beads with a consumable electrode in protective gases on the parts of the trim of power valves and the specific data obtained during it can be used in the further development of arc surfacing technologies and in future research on this topic. The selection of the gas-shielded arc welding process for sealing surfaces of power valves in favor of the *PulseSynergic* long arc welding process provides an opportunity to validate the minimization of electrical and time parameters of the welding process.

References

1. Losev AS, Eremin EN, Gurzhiy AS, Vasenko OYu. Wear-Resistant Facing of the Sealing Surfaces of the Stop Valve Wedge. *Rossiya molodaya: peredovye tekhnologii — v promyshlennost'*. 2013;(1):073–076. (In Russ.)
2. Sokolov GN, Lysak VI. *Surfacing of Wear-Resistant Alloys on Press Dies and Tools for Hot Deformation of Steels*. Volgograd: VolgGTU; 2005. 284 p. (In Russ.)
3. Stepin VS, Starchenko EG, Volobuev YuS, Egorov MYu. Modern Facing Materials for Sealing Surfaces of NPP and TPP Valves. *Valve Industry*. 2006;41(2):55–56. (In Russ.)

4. Erofeev VA, Zakharov SK, Kuznetsov OV. Features of Technology of Arc Surfacing Layers on the Steel Substrate. *Izvestiya Tula State University*. 2014;(11–1):132–138.
5. Sokolov GN, Zorin IV, Artem'ev AA, Elsukov SK, Dubtsov YuN, Lysak VI. Thermal- and Wear-Resistant Alloy Arc Welding Depositions Using Composite and Flux-Cored Wires with TiN, TiCN, and WC Nanoparticles. *Journal of Materials Processing Technology*. 2019;272:100–110. <https://doi.org/10.1016/j.jmatprotec.2019.05.014>
6. Eremin EN, Filippov YuO, Pokrovskiy DG, Losev AS, Eremin AE. Wear-Resistant Surfacing of Hot-Cutting Knives for Rolled Metal Products. *Zagotovitel'nye proizvodstva v mashinostroenii*. 2008;(4):17–19. (In Russ.)
7. Poloskov SS. Problems of Weld Overlay of Sealing Surfaces of Pipe Fitting and Solutions. *Vestnik of Don State Technical University*. 2019;19(4):349–356. <https://doi.org/10.23947/1992-5980-2019-19-4-349-356>
8. Elsukov SK. *Improving the Efficiency of Two-Electrode Surfacing in Shielding Gases of Chromium-Nickel Austenitic Steels on Petrochemical Equipment Parts*. Cand.Sci. (Eng.), diss. Volgograd; 2023. 143 p. (In Russ.)
9. Eremin AE, Filippov YuO, Matalasova AE, Kats VS. Structure and Properties of High Chromium Metal Valves Overlaid by Serially Produced Welding Wires *Omsk Scientific Bulletin*. 2014;127(1):55–58.
10. Rogozin DV, Lenivkin VA. Formation of a Technological Narrow-Band Weld Layer. *Welding and Diagnostics*. 2023;(5):49–54.
11. Kah P, Suoranta R, Martikainen J. Advanced Gas Metal Arc Welding Processes. *International Journal of Advanced Manufacturing Technology*. 2013;67:665–674. <http://doi.org/10.1007/s00170-012-4513-5>
12. Lenivkin VA, Dyurgerov NG, Sagirov KhN. *Process Properties of Welding Arc in Shielding Gases*. 2nd ed., enl. Moscow: NAKS; 2011. 368 p. (In Russ.)
13. Lenivkin VA, Rogozin DV. Types of Self-Regulation of Consumable Arc Welding Processes. *Welding and Diagnostics*. 2021;(1):53–60. (In Russ.) https://doi.org/10.52177/2071-5234_2021_01_53
14. Potap'evskii AG. *Gas-Shielded Welding with a Consumable Electrode*. Part 1. *Active Gas Welding*. 2nd rev. ed. Kiev: Ekotekhnologiya; 2007. 192 p. (In Russ.)
15. Milyutin VS, Kataev RF. *Welding Properties of Arc Welding Equipment*. Moscow: NAKS media; 2016. 457 p. (In Russ.)

About the Authors:

Dmitrii V. Rogozin, Cand.Sci. (Eng.), Associate Professor of the Welding Fabrication Machines and Automation Department, Don State Technical University (1, Gagarin Sq., Rostov-on-Don, 344003, Russian Federation), [SPIN-code](#), [ORCID](#), [ScopusID](#), dmrogozin@ya.ru

Vyacheslav A. Lenivkin, Dr.Sci. (Eng.), Leading Researcher at the Scientific Competence Center, Don State Technological University Don State Technical University (1, Gagarin Sq., Rostov-on-Don, 344003, Russian Federation), [SPIN-code](#), [ORCID](#)

Claimed Contributorship:

DV Rogozin: conducting experiments, processing experimental data, preparation of the text, formulation of conclusions.

V.A. Lenivkin: academic advising, basic concept formulation, research objectives and tasks, revision of the text, correction of the conclusions.

Conflict of Interest Statement: the authors do not have any conflict of interest.

All authors have read and approved the final manuscript.

Об авторах:

Дмитрий Викторович Рогозин, кандидат технических наук, доцент кафедры машин и автоматизации сварочного производства Донского государственного технического университета (344003, Российская Федерация, г. Ростов-на-Дону, пл. Гагарина, 1), [SPIN-код](#), [ORCID](#), [ScopusID](#), dmrogozin@ya.ru

Вячеслав Андреевич Ленивкин, доктор технических наук, ведущий научный сотрудник центра научных компетенций Донского государственного технического университета (344003, Российская Федерация, г. Ростов-на-Дону, пл. Гагарина, 1), [SPIN-код](#), [ORCID](#)

Заявленный вклад авторов:

Д.В. Рогозин: проведение экспериментов, обработка экспериментальных данных, подготовка текста, формирование выводов.

В.А. Ленивкин: научное руководство, формирование основной концепции, цели и задачи исследования, доработка текста, корректировка выводов.

Конфликт интересов: авторы заявляют об отсутствии конфликта интересов.

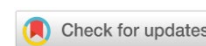
Все авторы прочитали и одобрили окончательный вариант рукописи.

Received / Поступила в редакцию 31.10.2024

Reviewed / Поступила после рецензирования 22.11.2024

Accepted / Принята к публикации 27.11.2024

INFORMATION TECHNOLOGY, COMPUTER SCIENCE AND MANAGEMENT ИНФОРМАТИКА, ВЫЧИСЛИТЕЛЬНАЯ ТЕХНИКА И УПРАВЛЕНИЕ






UDC 519.688

Original Empirical Research

<https://doi.org/10.23947/2687-1653-2024-24-4-413-423>

Algorithm for Constructing the Hazard Function of the Extended Cox Model and its Application to the Prostate Cancer Patient Database

Ilya I. Mikulik¹ , Gennadiy M. Zharinov² , Aleksei Y. Kneev² 

¹ Emperor Alexander I St. Petersburg State Transport University, St. Petersburg, Russian Federation

² Granov's Russian Research Center for Radiology and Surgical Technologies, St. Petersburg, Russian Federation

✉ mikulik.ilia@gmail.com



EDN: LNZDKF

Abstract

Introduction. In medicine and related industries, bioinspired approaches are used for the survival analysis, among which the Cox regression model holds a specific place. The practice of its application is described in the theoretical and applied literature. However, a significant drawback of this method requires careful study. The fact is that the features correlate with the hazard function linearly, and the model does not use more complex dependences. This causes some difficulties in studying survival analysis. The presented work is aimed at solving this problem. The object of study is the extended Cox model, in which the hazard function includes a nonlinear combination of features.

Materials and Methods. A database of prostate cancer patients was used, since this was a common diagnosis in global oncology. A class of extended Cox models with an additive/multiplicative hazard function was defined. To solve the problem using the optimization method, a fitness function was constructed that evaluated the results of prognosis, the number of features, and the degree of overtraining of the model — the complexity and load of the compiled hazard function. An algorithm of pollinating ants has been developed to optimize the fitness function. It simulates the reproduction of flowering plants using pollinating insects and consists of three parts: an ant colony algorithm, a genetic algorithm, and an ant pollinator algorithm. The quality of training of the Cox model was assessed by C-index.

Results. A metaheuristic algorithm for ant pollinator optimizing was proposed, providing for the construction of hazard functions of the extended Cox model. The set of parameters for training the standard Cox model was the entire set of features used: TNM, prostate-specific antigen doubling time (PSADT), Gleason score, serum PSA concentration at diagnosis, patient age and education, Rh factor. C-index value of the trained model was 0.853691. The extended Cox model with the found additive/multiplicative hazard function had a higher C-index value — 0.856241 with a smaller number of features used (TNM, PSADT, and Gleason score). In terms of quality, this approach is not inferior to or superior to the classical Cox model. Reducing the number of features involved should improve the efficiency of medical decisions and speed up the start of treatment.

Discussion and Conclusion. The presented algorithm for constructing survival analysis models increased the accuracy of predicting the occurrence of a terminal event, and reduced the number of features used for this purpose. The difference in accuracy for the studied data set seemed insignificant — C-index increased from 0.853691 to 0.856241 (by 0.3%). At this, the number of features taken into account was reduced from 7 to 3 (by 57.1%). Consequently, the proposed method solves effectively the problem of feature selection, and can be applied to improve the quality of prognostication.





Keywords: prostate cancer, survival prediction, terminal event probability, Cox regression model, ant pollinator algorithm

Acknowledgements. The authors would like to thank E.A. Blagoveshchenskaya, Dr.Sci. (Phys.-Math.), Professor, for consulting on issues of the graph theory and optimization algorithms.

For Citation. Mikulik II, Zharinov GM, Kneev AY. Algorithm for Constructing the Hazard Function of the Extended Cox Model and its Application to the Prostate Cancer Patient Database. *Advanced Engineering Research (Rostov-on-Don)*. 2024;24(4):413–423. <https://doi.org/10.23947/2687-1653-2024-24-4-413-423>

Оригинальное эмпирическое исследование

Алгоритм построения функции риска расширенной модели Кокса и его применение на базе данных больных раком предстательной железы

И.И. Микулик¹  , Г.М. Жаринов² , А.Ю. Кнеев² 

¹ Петербургский государственный университет путей сообщения Императора Александра I,
г. Санкт-Петербург, Российская Федерация

² Российский научный центр радиологии и хирургических технологий имени академика А.М. Гранова Минздрава России,
г. Санкт-Петербург, Российская Федерация

 mikulik.ilia@gmail.com

Аннотация

Введение. В медицине и связанных с ней отраслях для анализа выживаемости используются биоинспирированные подходы, среди которых особое место занимает регрессионная модель Кокса. Практика ее применения описана в теоретической и прикладной литературе. Однако требует тщательной проработки существенный недостаток данного метода. Дело в том, что признаки коррелируют с функцией риска линейно, и модель не задействует более сложные зависимости. Это создает трудности при исследовании анализа выживаемости. Представленная работа нацелена на решение данной проблемы. Объект изучения — расширенная модель Кокса, в которой функция риска включает нелинейную комбинацию признаков.

Материалы и методы. Использовалась база данных больных раком предстательной железы, так как в мировой онкологии это широко распространенный диагноз. Определен класс расширенных моделей Кокса с аддитивно-мультипликативной функцией риска. Для решения задачи методом оптимизации построена функция приспособленности, которая оценивает результаты прогнозов, количество признаков, а также степень переобучения модели — сложность и нагруженность составленной функции риска. Для оптимизации функции приспособленности разработан алгоритм муравьев-опылителей. Он имитирует размножение цветковых растений с помощью насекомых-опылителей и состоит из трех частей: муравьиный алгоритм, генетический алгоритм и алгоритм опыления. Качество обучения модели Кокса оценивали по С-индексу.

Результаты исследования. Предложен метаэвристический алгоритм оптимизации муравьев-опылителей, позволяющий строить функции риска расширенной модели Кокса. Набор параметров для обучения стандартной модели Кокса — весь используемый комплекс признаков: распространенность опухолевого процесса, время удвоения простатспецифического антигена (ПСА), сумма баллов по шкале Глисона, сывороточная концентрация ПСА на момент постановки диагноза, возраст и образование пациента, резус-фактор. Значение с-индекса обученной модели — 0,853691. Расширенная модель Кокса с найденной аддитивно-мультипликативной функцией риска имеет более высокий показатель С-индекса — 0,856241 с меньшим количеством используемых признаков (распространенность опухолевого процесса, время удвоения ПСА и сумма баллов по Глисон). По качеству этот подход не уступает классической модели Кокса или превосходит ее. Сокращение числа задействованных признаков должно повысить оперативность врачебного решения и ускорить начало лечения.

Обсуждение и заключение. Представленный алгоритм построения моделей анализа выживаемости повысил точность предсказания наступления терминального события и уменьшил количество используемых для этой цели признаков. Разница в точности для исследуемого набора данных представляется несущественной — С-индекс возрос с 0,853691 до 0,856241 (на 0,3 %). При этом количество принимаемых во внимание признаков сократилось с 7 до 3 (на 57,1 %). Следовательно, предложенный метод эффективно решает задачу выбора признаков и может быть применен для повышения качества прогнозирования.

Ключевые слова: рак предстательной железы, прогнозирование выживаемости, вероятность наступления терминального события, регрессионная модель Кокса, алгоритм муравьев-опылителей

Благодарности. Авторы благодарят Благовещенскую Е.А., доктора физико-математических наук, профессора, за консультацию в области теории графов и алгоритмов оптимизации.

Для цитирования. Микулик И.И., Жаринов Г.М., Кнеев А.Ю. Алгоритм построения функции риска расширенной модели Кокса и его применение на базе данных больных раком предстательной железы. *Advanced Engineering Research (Rostov-on-Don)*. 2024;24(4):413–423. <https://doi.org/10.23947/2687-1653-2024-24-4-413-423>

Introduction. Survival analysis is a set of statistical methods that provide the estimation of the probability of a terminal event, after which the object goes out of control. The methods involve working with data that has a time characteristic. This is the time from the beginning of observation to the occurrence of a terminal event or the exit of an object from observation. The possibility of working with objects that have been no longer under observation is of interest to applied areas of science, including medicine [1].

One of the classic models of survival analysis is Cox regression model [2]. Its hazard function uses a linear combination of features, which in general may not be entirely correct, since the influence of features on the hazard function value can be expressed by a nonlinear correlation. For each problem, the contribution of features and the hazard function can correlate differently. This is determined by the data used and requires special approaches to finding forms of dependences. Various methods for determining dependences of features in the hazard function are considered in [3]. This paper proposes to use the extended Cox model, whose hazard function establishes not only an additive, but also a multiplicative combination of features. Aside from that, a method for constructing such models is described depending on the data used and the set of features.

Building a model involves solving the problem of feature selection, one of the key problems in data analysis [4]. It consists of finding the optimal set of features sufficient to build a forecast. The solution gives an idea of which features have greater prognostic significance. The problem can be formulated in terms of optimization and solved using optimization methods. The proposed ant pollinator algorithm for its solution refers to metaheuristic hybrid optimization methods. It uses ant colony and genetic optimization algorithms, as well as the first developed model of flower crossing.

The algorithm is implemented on the basis of data of patients with prostate cancer. In the world medical practice, this is one of the most common malignant neoplasms in men [5]. The introduction of screening based on the assessment of serum concentration of prostate-specific antigen (PSA) has significantly changed the structure of newly diagnosed cases of prostate cancer. If previously most of them were locally advanced and metastatic forms of tumor, now localized forms dominate. Due to this, the frequency of radical interventions has increased, and the ten-year survival rates of certain groups of patients who have undergone radical prostatectomy or combined hormonal radiation therapy have approached 100%.

Despite the obvious success in the diagnosis and treatment of prostate cancer, several important issues remain unresolved and require research.

Modern methods for predicting survival in prostate cancer are based on a combination of factors: age, tumor grade and histological differentiation, serum PSA concentration, its doubling time [6] and density [7]. The Cox and other models of survival analysis provide a general idea of fate, but their accuracy in predicting outcomes for individual patients can vary. Moreover, a prognosis based on a set of features does not provide an indication of the significance of each feature. This limits the ability of clinicians to adapt treatment recommendations to the needs of an individual patient.

Improving approaches to assessing cancer patient survival is a key aspect of scientific research in oncology. More and more attention is being paid to the accuracy of prediction, which is critical for selecting a therapeutic strategy. A high-quality prognostic model more accurately determines the risk for the patient and allows for adapting treatment approaches depending on the expected outcome. This can improve both treatment outcomes and the patient's quality of life.

Under conditions of high workload for medical personnel, limiting the number of features in the forecast model is of significant practical value, as it shortens the time spent on making medical decisions. Simplifying the model allows focusing on key aspects of the clinical picture, which reduces the likelihood of incorrect interpretations of data. In addition, the use of a limited set of features increases the reproducibility and stability of the forecast results, i.e., its reliability.

The objective of this research is to develop an algorithm for constructing survival analysis models with the selection of key features. The accuracy of the new approach should be no lower than that of the Cox model. Note that various methods for constructing hazard functions of the Cox model define not one extended Cox model, but a whole class of algorithms with different hazard functions. This approach to adapting the hazard function to the set of available data and features is selected as a way to achieve the stated goal.

The tasks solved in this research are listed below.

1. A class of extended Cox models with an additive-multiplicative hazard function is defined.
2. A fitness function that evaluates the results of forecasts of the extended Cox model is constructed.
3. An optimization method that solves the problem is created.
4. A program that implements the proposed algorithm is developed.
5. The result of the program's operation on a database of patients with prostate cancer is obtained, and the effectiveness of the developed algorithm is shown.

Materials and Methods. In the survival analysis, survival and hazard functions are used to estimate the risk of the event under consideration. The first function is a stochastic characteristic that determines the probability of survival (absence of a terminal event) over a given time. In other words, survival function $S(t)$ is defined as the probability that the terminal event does not occur before time t :

$$S(t) = P(T > t),$$

where T — time of the terminal event occurrence.

Survival analysis models construct survival curves for each data sample based on its features. The models are often specified using a hazard function, which defines the probability of a terminal event occurring in an infinitesimal time interval between t and Δt , given that it has not occurred before t :

$$\lambda(t) = \lim_{\Delta t \rightarrow 0} \frac{P(t \leq T < t + \Delta t | T \geq t)}{\Delta t}.$$

The Cox proportional hazards model computes the hazard function for a single instance as a linear combination of its features, establishing a relationship between the instance features and the hazard function.

On the one hand, the explicit assignment of the hazard function makes the model transparent and convenient for interpreting forecasts. On the other hand, the assumption of a linear relationship between features and forecast is a limitation and cannot be fulfilled for all practical problems.

Research Results. Let S be the training dataset. The hazard function in the classical Cox model is:

$$\lambda(t | X_i) = \lambda_0 \exp(\beta_1 X_{i1} + \dots + \beta_p X_{ip}) = \lambda_0 \exp(\beta \cdot X_i),$$

where β — vector of influence of features; $X_i \in S$ — data instance.

In [3], the hazard function of the Cox model is considered in a generalized form $\lambda(t | X_i) = \lambda_0 \exp(g(\beta \cdot X_i))$, where $g(\beta \cdot X_i)$ is the function that establishes the relationship between the features of the instances. In this paper, function g is a polynomial of a special form.

Let $F = \{f_1, f_2, \dots, f_n\}$ be a set of all features. $|F| = p$. F_t — a subset of features: $F_t \subset F$. $P_q(F_t)$ — polynomial composed of features $f \in F_t$:

$$P_q(F_t) = \sum_{i=1}^{|\xi|} \varphi_i \sum_{j=1}^{|F_t|} f_i^{\xi_{ij}},$$

where $\xi = \{(\xi_1, \xi_2, \dots, \xi_{|F_t|})\}$, $\xi_i \in \{0; 1\}$ — a set of indicators of the occurrence of the i -th feature in the term of the polynomial; $\varphi_i \in \{0, 1\}$ — marker indicating the occurrence of the i -th monomial in P_q .

Thus, polynomial $P_q(F_t)$ is the sum of monomials, each of which is a product of features. In this case, the degree of a feature in a monomial is no more than one. Hazard function $\lambda(t | X_i) = \lambda_0 \exp(g(\beta \cdot X_i))$, where $g(\beta \cdot X_i) = P_q(F_t, \beta \cdot X_i)$, is called additive-multiplicative, since the value of each feature in it can be included either in the sum or in the product.

To obtain and process the results, it is required to evaluate the quality of the constructed model. In [8], the quality of the model is evaluated using the loss function, and this is a general approach for any learning model. The most commonly used evaluation indicator is the Concordance index (C-index). It was also selected to evaluate the extended Cox model. The C-index takes into account both observed events and censored cases [9]. Here, the rank correlation between the actual survival time and the model predictions is quantitatively determined. The C-index shows the ratio of correctly ordered (concordant) and comparable pairs [10].

The paper considers the hypothesis of an extended Cox model with prediction accuracy no lower than that of the classical Cox model.

Let $c(S, P_q(F_t))$ be the C-index of the extended Cox model trained on data S , with an additive-multiplicative hazard function constructed using polynomial $P_q(F_t)$, and $c(S, P_\Sigma(F))$ — C-index of the classical Cox model trained on the same data S . The hypothesis can be formulated as:

$$\exists P_q(F_t), F_t \subset F: c(S, P_q(F_t)) \geq c(S, P_\Sigma(F)). \quad (1)$$

To find non-trivial examples of the hypothesis, a problem was set and an algorithm was developed. The problem can be formulated in terms of the optimization theory. It is necessary to construct polynomial $P_q(F_t)$ on subset F with the largest value $c(S, P_q(F_t))$ with a minimum set of features F_t . Thus, two optimization conditions are introduced $c(S, P_q(F_t)) \rightarrow \max$ and $|F_t| \rightarrow \min$. Another problem of constructing a polynomial should be taken into account. As the number of possible features increases, the number of possible polynomials, including those constructed due to overfitting,

grows exponentially. Typically, such polynomials consist of the sum of a relatively large number of monomials, and the monomials themselves consist of a large number of factors. Such polynomials increase the accuracy of the model only on trained data and do not readily lend themselves to analysis.

To get rid of the problem of overtraining, the paper proposes optimization by two additional criteria: the number of monomials in $P_q(F_t)$ and the loading of polynomial $P_q(F_t)$, which reflects the number of multiplicative connections in the polynomial.

The number of monomials is defined as $\sum_i^{|\xi|} \varphi_i$. However, to construct a correct condition, it is necessary to take into account the nonlinearity of the contribution of the number of features to the objective function. With a small number of incoming features, a more significant change in the indicator is expected than with a large one. Therefore, the paper proposes the indicator:

$$K_q = \frac{\log_2 \left(\sum_i^{|\xi|} \varphi_i \right)}{p}.$$

Note that value K_q does not exceed 1.

$\sum_i^{|\xi|} \varphi_i \rightarrow \max$ at $\forall \varphi_i = 1$, hence:

$$\begin{aligned} \sum_i^{|\xi|} \varphi_i &= |\xi| = 2^p - 1, \\ \log_2 (2^p - 1) &< \log_2 2^p = p, \\ K_q &< 1. \end{aligned}$$

It is not entirely correct to define the polynomial loading as the number of multiplicative bonds. In this case, the real assessment of the polynomial complexity is not reflected with a different number of monomials included in it. The indicator should demonstrate the loading of each incoming monomial; therefore, the following value is introduced in the work, not exceeding 1:

$$B_q = \frac{\sum_{i, \varphi_i \neq 0} \sum_{j=1}^{|F_t|} \xi_{ij}}{\sum_i^{|\xi|} \varphi_i \cdot |F_t|}.$$

Given the introduced characteristics, the optimization problem consists of finding $P_q(F_t)$ under the conditions:

$$\begin{cases} c(S, P_q(F_t)) \rightarrow \max, \\ F_t \rightarrow \min, \\ K_q \rightarrow \min, \\ B_q \rightarrow \min. \end{cases} \quad (2)$$

Let us move on to one-dimensional optimization by introducing balancing coefficients ω :

$$f = \omega_1 c(S, P_q(F_t)) - \omega_2 \frac{F_t}{p} - \omega_3 K_q - \omega_4 B_q \rightarrow \max.$$

Or it is represented as a sum:

$$f = \omega_1 \cdot c(S, P_q(F_t)) + \omega_2 \cdot \left(1 - \frac{F_t}{p} \right) + \omega_3 \cdot (1 - K_q) + \omega_4 \cdot (1 - B_q) \rightarrow \max. \quad (3)$$

The last form of recording, if necessary, allows us to fix the value of the objective function f by introducing an explicit relationship between the balancing coefficients:

$$\begin{aligned} \omega_1 &= \frac{\gamma_1}{1 + \gamma_2 + \gamma_3}, \\ \omega_2 &= \frac{\gamma_2}{1 + \gamma_1 + \gamma_3}, \\ \omega_3 &= \frac{\gamma_3}{1 + \gamma_1 + \gamma_2}, \\ \omega_4 &= 1 - \omega_1 - \omega_2 - \omega_3. \end{aligned}$$

For any $\gamma_1, \gamma_2, \gamma_3 \in (0; 1)$. Thus, by selecting the required γ_i or directly ω_i , it is possible to strengthen or weaken the corresponding conditions of system (2). The task is to find the maximum of the objective function $f(3)$ under certain ω_i .

To solve the optimization problem, the article presents the developed ant pollinator algorithm. It is based on the model of an ant colony adapted to the task. The algorithm transforms a set of graph vertices representing features or their product into a model. The process of pollination and reproduction of flowering plants using pollinating insects is simulated. The solution includes three algorithms:

- ant colony algorithm is used to build the model;
- genetic algorithm improves the performance of ant colony algorithm;
- pollination algorithm provides selecting properties or their product.

The result of the algorithm is polynomial $P_q(F_i)$, which maximizes function $f(3)$. Each monomial included in the sum of the polynomial is represented by a flower. The set of flowers forms a graph. The pollinating ants build a path along it. Each ant determines a set of flowers, and the sum of the corresponding monomials forms polynomial $P_q(F_i)$. The estimate of the path built by the ant is the value of function $f(3)$ for the extended Cox model with $g = P_q(F_i)$.

The ant stage of the algorithm is a simple ant colony algorithm adapted to the problem [11]. Each ant k has a different set of parameters α_k, β_k, Q_k . The sensitivity of ants to pheromones α_k determines the degree to which ants exploit the solutions found. The heuristic sensitivity β_k sets the level of exploitation of heuristic information. The pheromone intensity Q_k determines the amount of pheromone that an ant deposits on a flower during the search for a solution. The static parameters of the algorithm are: number of ants n , evaporation rate ρ , initial level of pheromones τ_0 .

Each ant chooses a vertex stochastically according to the rule:

$$p_v^k(t) = \frac{\tau_v^{\alpha_k}(t) \eta_v^{\beta_k}}{\sum_u \tau_u^{\alpha_k}(t) \eta_u^{\beta_k}}, \quad (4)$$

where $p_v^k(t)$ — probability of choosing flower v by ant k at iteration t ; $\tau_v(t)$ — amount of pheromone deposited on flower v at iteration t ; η_v — heuristic information, which is calculated as $\eta_v = c(S, P_i \equiv v)$. The second part of this equality is the C-index of the extended Cox model trained on one monomial of flower v .

Each ant deposits pheromone according to the rule:

$$\Delta\tau_v = \frac{Q_k}{f(P_q(F_i))}, \quad (5)$$

where $P_q(F_i)$ — polynomial constructed by ant k ; f — objective function.

The second stage is the application of the genetic algorithm. It modifies parameters of the ant colony algorithm taking into account the efficiency of the solutions found [12]. The algorithm sequentially applies three operators to the ant population (their parameters): selection, crossing over, mutation. The roulette wheel method is used as the selection operator. An ant gets into a new population with the probability:

$$p_i = \frac{f(P_i(F_i))}{\sum_j f(P_j(F_i))}. \quad (5)$$

The crossover operator is the bitwise sum of the bit representations of the parameters of the selected individuals. The mutation operator is the inversion of a random bit in the bit representation of the parameter of the individual.

Pheromones left on vertices-flowers are also used at the pollination stage. This stage employs the population idea. Four operators are applied to the flower population: selection, crossbreeding, linebreeding, and aging. Each flower, in addition to the stored value of the vertex-monomial, has a parameter — age. The selection operator chooses flowers with the highest concentration of pheromones. The crossbreeding operator introduces new flowers with some probability, the monomial of which is the product of the combination of features from the monomials of the parent flowers:

$$v_i = (e_i, \tau_i, \eta_i, o_i),$$

$$v_i \times v_j = v_k, v_k = \left(e_k = \prod f_q \in e_i \cup e_j f_q, \tau_k = \frac{\tau_i + \tau_j}{2}, \eta_k = c(S, P \equiv e_k), o_k = o_{max} \right),$$

where e — monomial of a new flower; τ — random amount of pheromone not exceeding τ_0 , deposited on the flower; η — heuristic component; o — age of the flower; o_{max} — established lifetime of the flower.

If the transformation results in flowers already in the population, then new flowers are not created, but the age of the existing ones is updated. The linebreeding operator is unlikely to add a new flower with a single feature to the population. This operator is used to leave the opportunity for displaced traits to participate in the algorithm. The aging operator decreases the age indicator for each flower. If the aging indicator becomes zero, the flower is eliminated from the population.

Thus, the configurable parameters of the algorithm are: $n, \tau_0, \rho, o_{max}, \alpha_0, \beta_0, Q_0, p_{kross}, p_{mut}$. The selection of their values depends on the current application task and affects the convergence rate of the algorithm. Note that the parameters α_0, β_0, Q_0 are adapted under the operation of the genetic algorithm; therefore, their initial values do not have a large effect on the convergence rate of the algorithm, especially with a significant number of iterations of the algorithm presented below.

Start

1. Define parameters $n, \tau_0, \rho, o_{max}, \alpha_0, \beta_0, Q_0, p_{kross}, p_{mut}$
2. Set $c = 0, P = \emptyset$
3. Place a set of flowers $V = \{v_i = (e_i = f_i, \tau_i = rand(0, \tau_0), \eta_i = c(S, P_i \equiv f_i), o_i = o_{max}) \mid \forall f_i \in F\}$
4. Place a set of ants $A = \{\alpha_k = (\alpha_k = \alpha_0, \beta_k = \beta_0, Q_k = Q_0)\}$
5. Until the stop criterion is reached
 - 5.1. For every ant $\alpha_k \in A$
 - 5.1.1. $E_k(t) = \{v_{random}\}$
 - 5.1.2. $c_k(t-1)$
 - 5.1.3. $c_k(t) = \eta_i$
 - 5.1.4. Until $c_k(t) > c_k(t-1)$
 - 5.1.4.1. Select v in accordance with rule (4)
 - 5.1.4.2. $E_k(t) = \cup \{v\}$
 - 5.1.4.3. $c_k(t-1) = c_k(t)$
 - 5.1.4.4. $P_k = \sum_{i, v_i \in E_k(t)} e_i$
 - 5.1.4.5. $c_k(t) = f(S, P_k)$
 - 5.1.5. If $c_k(t) > c$
 - 5.1.5.1. $c = c_k(t)$
 - 5.1.5.2. $P = P_k$
 - 5.1.6. For each $v_i \in E_k(t)$, calculate $\Delta\tau_v$ according to rule (5)
- 5.2. Apply the selection operator $A = S_{selection}(A)$
- 5.3. Apply the crossover operator $A = S_{crossover}(A)$
- 5.4. Apply the mutation operator $A = S_{mutation}(A)$
- 5.5. Apply the flower selection operator $V = S_{selection}(V)$
- 5.6. Apply the crossbreeding operator $V = S_{crossbreeding}(V)$
- 5.7. Apply the linebreeding operator $V = S_{linebreeding}(V)$
- 5.8. Apply the aging operator $V = S_{aging}(V)$
6. Return values c, P

The algorithm's stop criterion can be the number of iterations or the convergence of solutions to a single value. Thus, the presented method of optimizing pollinating ants solves the problem of constructing a hazard function and selecting features for the extended Cox model. If there are non-trivial examples for hypothesis (1), they can be found by the described method.

The algorithm was tested on a database of patients with prostate cancer. They were treated or observed from January 1996 to December 2016 at the Russian Scientific Center of Radiology and Surgical Technologies named after Academician A.M. Granov, Ministry of Health of the Russian Federation [13]. The study included anonymized data on the prevalence of the tumor process in 5,073 patients.

The list of features used in the research, with the description and the number of non-zero entries, is presented in Table 1.

Table 1

Dataset Features

Name of the feature		Description	Value	Number of completed records
short	full			
'TS'	Type of tumor spread	Damage to adjacent organs and structures, presence of regional and distant metastases	1 — localized 2 — locally advanced 3 — metastatic	5073
'DT'	PSA doubling time	Doubling of serum PSA concentration indicating possible doubling of tumor cell count	Floating point number	2423
'GS'	Gleason score	Ordinal variable. Reflects the histological differentiation of the tumor	1 — $GS < 7$ 2 — $GS = 7$ 3 — $GS > 7$	3968
'PSA'	Serum PSA concentration that prompted biopsy	Prostate-specific antigen. Glycoprotein, serine protease normally produced by the secretory epithelium of the prostate gland. Liquefies ejaculate, improves sperm motility. Concentration above 4 ng/ml may be grounds for biopsy.	Floating point number	4760
'Education'	Patient's education level	Completed patient's education at time of diagnosis	0 — secondary general 1 — secondary special 2 — higher 3 — academic degree	4622
'Age'	Age of the patient	Patient's age at diagnosis	Integer	5073
'Rhesus'	Rhesus factor	The presence or absence of the protein responsible for the Rh factor	1 — positive 2 — negative	399

Not all the features presented in Table 1 are essential for the survival study. There are also insignificant ones (e.g., 'Education', 'Rhesus'). They are needed to demonstrate the correct operation of the algorithm that solves the problem of feature selection. The presence of correlated and not very important features shows the practical possibility of using the algorithm under conditions when neither the dependence of features nor their significance are known in advance.

The algorithm is implemented in the Python programming language in the CoxPHFitter package from the Lifelines library. The Pandas software library was used to store and process the data.

Before running the algorithm, the data was preprocessed. This is due to the fact that the prostate cancer patient database has gaps in a number of values for some patients. To eliminate the problem, two methods of processing the database were used — deleting observations and replacing them taking into account other values in the column [14]. The features 'TS', 'DT' and 'age' are important and play a role in the consistency of the data; therefore, observations without these features were removed. The Gleason score was ranked. Each observation was assigned one of three values: 1 — $GS < 7$ (1281 observations), 2 — $GS = 7$ (1479 observations), 3 — $GS > 7$ (1208 observations).

For the remaining features, missing values are filled using the weighted k -nearest neighbors method. This missing value imputation is based on the assumption that the proximity of samples by measured features indicates their proximity by unmeasured features [15]. The weighted k -nearest neighbors method is preferable due to the low time costs of missing value imputation [16], although there are more efficient approaches [17].

The algorithm is implemented with the following set of parameters: $n = 12$; $\tau_0 = 0.01$; $p = 0.8$; $\sigma_{max} = 3$; $\alpha_0 = 0.5$; $\beta_0 = 2$; $Q_0 = 25$; $p_{kross} = 0.9$; $p_{mut} = 0.2$. The given list of parameter values is recommended for the initial configuration of the algorithm. However, it can be modified to solve a specific problem. Table 2 presents the results of the proposed algorithm.

Table 2

Values of C-index and Fitness Function f Depending on Polynomial of Hazard Function of Extended Cox Model, Found for Given Balancing Coefficients

Polynomial of additive-multiplicative hazard function of extended Cox model	C-index	Fitness function	Balancing coefficients $\omega_1; \omega_2; \omega_3; \omega_4$
'TS' + 'DT'	0.836789	0.782894	0.91;0.05;0.05;0.05
'TS' \times 'GS' + 'DT'	0.840516	0.842814	0.99;0.05;0.05;0.05
'TS' + 'DT' + 'GS'	0.849790	0.746328	0.9;0.0;0.05;0.05
'TS' + 'DT' + 'GS' + 'TS' \times 'DT'	0.849828	0.827410	0.94;0.05;0.0;0.0
'TS' + 'GS' + 'TS' \times 'DT' \times 'GS'	0.849830	0.841567	0.97;0.05;0.05;0.0
'TS' + 'GS' + 'DT' \times 'GS'	0.850000	0.787661	0.94; 0.0;0.05;0.0
'TS' + 'DT' + 'GS' + 'PSA' + 'Education' + 'Age' + 'Rh'	0.853691	0.838012	0.99; 0.0;0.0;0.05
'TS' + 'DT' + 'GS' + 'TS' \times 'GS'	0.855292	0.809308	0.94;0.05;0.0;0.05
'TS' + 'TS' \times 'GS' + 'GS' + 'TP' \times 'DT'	0.856241	0.764870	0.91;0.0;0.05;0.0
'TS' + 'TS' \times 'GS' \times 'PSA' + 'IIF' + 'PSA' + 'GS' \times 'PSA' + 'DT' + 'TS' \times 'GS' + 'TS' \times 'PSA'	0.861085	0.839459	0.95;0.05;0.0;0.0
'TS' + 'DT' + 'GS' + 'PSA' + 'Education' + 'Age' + 'Rh' + 'TS' \times 'GS' + 'TS' \times 'PSA' + 'GS' \times 'PSA'	0.861643	0.826508	0.97;0.0;0.0;0.05
'TS' + 'DT' + 'GS' + 'PSA' + 'Education' + 'Rh' + 'TS' \times 'GS' + 'TS' \times 'PSA' + 'GS' \times 'PSA' + 'PSA' \times 'Age'	0.862345	0.845098	0.98;0.0;0.0;0.0

In Table 2, the variations of the occurrence of features in the hazard function are ranked in ascending order of the C-index. The values of the balancing coefficients of fitness function (3), for which the presented solution was found, and the value of the function itself are also indicated here. The last rows of the table contain the hazard functions with the highest concordance index. They are quite complex for analysis due to the loading associated with the low values of the corresponding balancing coefficients.

Discussion and Conclusion. The best set of features for training the standard (non-extended) Cox model is the entire set of features presented, i.e., function 'TS' + 'DT' + 'GS' + 'PSA' + 'Education' + 'Age' + 'Rh' with the C-index value of 0.853691. At the same time, the extended Cox model with the found hazard function 'TS' + 'TS' \times 'GS' + 'GS' + 'TS' \times 'DT' has the higher C-index value of 0.856241 with a smaller number of features used.

The results of this research allow us to draw certain conclusions. If we keep in mind the presented database, then the parameters 'TS', 'DT', 'GS' are sufficient to build a high-quality survival analysis model. Thus, the result of the study is the possibility of building a survival model with a smaller number of features used. Moreover, the proposed solution is not inferior to or exceeds the effectiveness of the classical Cox model, for the training of which numerous features are used.

The algorithm created within the framework of this work is capable of solving the problem of finding the best combination of features in an acceptable number of iterations (30). A set of regularizing coefficients provides setting a certain configuration for the algorithm. Thus, an application engineer can make a choice in favor of improving the quality of prediction, reducing the number of features or eliminating the problem of overfitting.

Thus, the class of metaheuristic algorithms is acceptable for solving the problem. At the pollination stage, monomials are constructed in a polynomial, i.e., the search for multiplicative dependences of features is performed. At the stage of the ant colony algorithm, a polynomial is constructed from monomials, i.e., the search for additive dependences of features is carried out. The genetic stage is required to improve the convergence and stability of the ant colony algorithm.

For the data set considered, the proposed algorithm increased the prediction accuracy. Yet, only slightly. C-index increased by only 0.3%, from 0.853691 to 0.856241. However, the number of features considered decreased by 57.1%, from 7 to 3. Fewer features in the predictive model make the work of doctors easier, allow them to gain time when making decisions, and can reduce the likelihood of errors in interpreting data.

References

1. Archetti A, Lomurno E, Lattari F, Martin A, Matteucci M. Heterogeneous Datasets for Federated Survival Analysis Simulation. In: *Proc. Companion of the 2023 ACM/SPEC International Conference on Performance Engineering*. New York: Association for Computing Machinery; 2023. P. 173–180. <http://doi.org/10.1145/3578245.3584935>
2. Atlam M, Torkey H, El-Fishawy N, Salem H. Coronavirus Disease 2019 (COVID-19): Survival Analysis Using Deep Learning and Cox Regression Model. *Pattern Analysis and Applications*. 2021;24:993–1005. <http://doi.org/10.1007/s10044-021-00958-0>
3. Govindarajulu US, Malloy EJ, Ganguli B, Spiegelman D, Eisen EA. The Comparison of Alternative Smoothing Methods for Fitting Non-Linear Exposure-Response Relationships with Cox Models in a Simulation Study. *The International Journal of Biostatistics*. 2009;5(1):2. <http://doi.org/10.2202/1557-4679.1104>
4. Miren Hayet-Otero, Fernando García-García, Dae-Jin Lee, Joaquín Martínez-Minaya, Pedro Pablo España Yandiola, Isabel Urrutia Landa, et al. Extracting Relevant Predictive Variables for COVID-19 Severity Prognosis: An Exhaustive Comparison of Feature Selection Techniques. *PLoS One*. 2023;18(4):e0284150. <https://doi.org/10.1371/journal.pone.0284150>
5. Berenguer CV, Pereira F, Câmara JS, Pereira JA. Underlying Features of Prostate Cancer — Statistics, Risk Factors, and Emerging Methods for Its Diagnosis. *Current Oncology*. 2023;30(2):2300–2321. <https://doi.org/10.3390/curroncol30020178>
6. Zharinov GM, Bogomolov OA. The Pretreatment Prostate-Specific Antigen Doubling Time: Clinical and Prognostic Values in Patients with Prostate Cancer. *Cancer Urology*. 2014;(1):44–48.
7. Kneev AY, Shkol'nik MI, Bogomolov OA, Zharinov GM. Prostate Specific Antigen Density as a Prognostic Factor in Patients with Prostate Cancer Treated with Combined Hormonal Radiation Therapy. *Siberian Journal of Oncology*. 2022;21(3):12–23. <https://doi.org/10.21294/1814-4861-2022-21-3-12-23>
8. Ewees AA, Al-qaness MA Abualigah L, Oliva D, Algamal ZY, Anter AM, et al. Boosting Arithmetic Optimization Algorithm with Genetic Algorithm Operators for Feature Selection: Case Study on Cox Proportional Hazards Model. *Mathematics*. 2021;9(18):2321. <https://doi.org/10.3390/math9182321>
9. Alabdallah A, Ohlsson M, Pashami S, Rögnvaldsson Th. The Concordance Index Decomposition: A Measure for a Deeper Understanding of Survival Prediction Models. *Artificial Intelligence in Medicine*. 2024;148:102781. <https://doi.org/10.48550/ARXIV.2203.00144>
10. Cavalcante Th, Ospina R, Leiva V, Cabezas X, Martin-Barreiro C. Weibull Regression and Machine Learning Survival Models: Methodology, Comparison, and Application to Biomedical Data Related to Cardiac Surgery. *Biology*. 2023;12(3):442. <https://doi.org/10.3390/biology12030442>
11. Guangyu Liu, Yuwei Bai, Ling Zhu, Qingyun Wang, Wei Zhang. A Sequential Excitation and Simplified Ant Colony Optimization Based Global Extreme Seeking Control Method for Performance Improvement. *Swarm and Evolutionary Computation*. 2024;86:101522. <https://doi.org/10.1016/j.swevo.2024.101522>
12. Blagoveshchenskaya EA, Mikulik II, Strüngmann LH. Ant Colony Optimization with Parameter Update Using a Genetic Algorithm for Travelling Salesman Problem. In: *Proc. Workshop "Models and Methods for Researching Information Systems in Transport"*. 2020;2803:20–25. URL: <https://ceur-ws.org/Vol-2803/paper3.pdf> (accessed: 17.09.2024).
13. Zharinov GM. Prostate Cancer Patients Database. RF Database, no. 2016620331. 2016. 1 p. (in Russ.) URL: https://www1.fips.ru/fips_servl/fips_servlet?DB=DB&DocNumber=2016620331&TypeFile=html (accessed: 17.09.2024).
14. Ghannad-Rezaie M, Soltanian-Zadeh H, Hao Ying, Ming Dong. Selection-Fusion Approach for Classification of Datasets with Missing Values. *Pattern Recognition*. 2010;43(6):2340–2350. <https://doi.org/10.1016/j.patcog.2009.12.003>
15. Troyanskaya O, Cantor M, Sherlock G, Brown P, Hastie T, Tibshirani R, et al. Missing Value Estimation Methods for DNA Microarrays. *Bioinformatics*. 2001;17(6):520–525. <https://doi.org/10.1093/bioinformatics/17.6.520>
16. Koshechkin AA, Andryushchenko VS, Zamyatin AV. A New Method to Missing Value Imputation for Immunosignature Data. *CTM (Sovremennye tehnologii v medicine)*. 2019;11(2):19–24. <https://doi.org/10.17691/stm2019.11.2.03>
17. Eunseo Oh, Hyunsoo Lee. Quantum Mechanics-Based Missing Value Estimation Framework for Industrial Data. *Expert Systems with Applications*. 2024;236:121385. <https://doi.org/10.1016/j.eswa.2023.121385>

About the Authors:

Ilya I. Mikulik, Postgraduate student of the Higher Mathematics Department, Emperor Alexander I St. Petersburg State Transport University (9, Moskovsky Pr., St. Petersburg, 190031, Russian Federation), [SPIN-code](#), [ORCID](#), [ScopusID](#), [ResearcherID](#), mikulik.ilia@gmail.com

Gennadiy M. Zharinov, Dr.Sci.(Medicine), Professor, Chief Researcher of the Department of Radiation and Combined Methods of Treatment, Granov's Russian Research Center for Radiology and Surgical Technologies (70, Leningradskaya Str., v. Pesochny, St. Petersburg, 197758, Russian Federation), [SPIN-code](#), [ORCID](#)

Aleksei Yu. Kneev, Cand.Sci.(Medicine), Senior Lecturer of the Department of Radiology, Surgery and Oncology, Oncologist of the Department of Oncourology, Granov's Russian Research Center for Radiology and Surgical Technologies (70, Leningradskaya Str., v. Pesochny, St. Petersburg, 197758, Russian Federation), [SPIN-code](#), [ORCID](#), [ScopusID](#)

Claimed Contributorship:

И Mikulik: development and implementation of the research method — the ant pollinator algorithm.

GM Zharinov: setting the research objective, providing a database for research, describing the characteristics of the database, describing the applied task.

AY Kneev: description of the urgency of the study and the research results.

Conflict of Interest Statement: the authors declare no conflict of interest.

All authors have read and approved the final manuscript.

Об авторах:

Илья Игоревич Микулик, аспирант кафедры высшей математики Петербургского государственного университета путей сообщения Императора Александра I (190031, Российская Федерация, г. Санкт-Петербург, Московский пр., 9), [SPIN-код](#), [ORCID](#), [ScopusID](#), [ResearcherID](#), mikulik.ilia@gmail.com

Геннадий Михайлович Жаринов, доктор медицинских наук, профессор, главный научный сотрудник отдела лучевых и комбинированных методов лечения РНЦРХТ им. акад. А.М. Гранова Минздрава России (197758, Российская Федерация, г. Санкт-Петербург, пос. Песочный, ул. Ленинградская, 70), [SPIN-код](#), [ORCID](#)

Алексей Юрьевич Кнеев, кандидат медицинских наук, старший преподаватель кафедры радиологии, хирургии и онкологии, врач-онколог отделения онкоурологии РНЦРХТ им. акад. А.М. Гранова Минздрава России (197758, Российская Федерация, г. Санкт-Петербург, пос. Песочный, ул. Ленинградская, 70), [SPIN-код](#), [ORCID](#), [ScopusID](#)

Заявленный вклад авторов:

И.И. Микулик: разработка и реализация метода исследования — алгоритма муравьев-опылителей.

Г.М. Жаринов: постановка цели исследования, предоставление базы данных для исследования, описание характеристик базы данных, описание прикладной задачи.

А.Ю. Кнеев: описание актуальности и результатов исследования.

Конфликт интересов: авторы заявляют об отсутствии конфликта интересов.

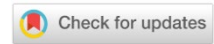
Все авторы прочитали и одобрили окончательный вариант рукописи.

Received / Поступила в редакцию 28.10.2024

Reviewed / Поступила после рецензирования 22.11.2024

Accepted / Принята к публикации 02.12.2024

INFORMATION TECHNOLOGY, COMPUTER SCIENCE AND MANAGEMENT ИНФОРМАТИКА, ВЫЧИСЛИТЕЛЬНАЯ ТЕХНИКА И УПРАВЛЕНИЕ






UDC 621.372

Original Theoretical Research

<https://doi.org/10.23947/2687-1653-2024-24-4-424-432>

Optimization Problem for Probabilistic Time Intervals of Quasi-Deterministic Output and Self-Similar Input Data Packet Flow in Telecommunication Networks

Gennadii I. Linets , Roman A. Voronkin , Gennadii V. Slyusarev ,
Svetlana V. Govorova 

North-Caucasus Federal University, Stavropol, Russian Federation

✉ kbytw@mail.ru

EDN: MCOGWO

Abstract

Introduction. When managing traffic at the packet level in modern telecommunication networks, it is proposed to use methods that transform a self-similar stochastic packet flow into a quasi-deterministic one. To do this, it is required to apply complex probabilistic laws of distribution of self-similar flows. From the literature, methods of balancing the network load are known, which, with the problem indicated above, contribute to increasing the efficiency of telecommunication systems. However, there is no strictly mathematical solution to find out the optimal probabilistic characteristics of the output flow, based on the input flow. The presented research is intended to fill this gap. Its objective is to create a method for determining the optimal probabilistic characteristics of the packet flow, using the minimum value of the measure closeness of the self-similar input and quasi-deterministic output flows.

Materials and Methods. To solve the research problem, the parameters of the output flow distribution were selected so that the approximation function was close to δ -function. The Kullback-Leibler divergence was used as a measure closeness of the input and output distributions of time intervals. Methods of set theory, metric spaces, multidimensional optimization, and teletraffic were used. The solution algorithm included minimization of the Kullback-Leibler divergence and the limit passage to δ -function.

Results. A probability distribution was shown — an approximation of δ -function, which maintained the equality of time intervals of a quasi-deterministic output packet flow. A method for transforming a self-similar input flow into a quasi-deterministic output flow was presented. The Kullback–Leibler divergence was used as a measure of their closeness. The minimum of the Kullback-Leibler divergence between the input and output flows with a normal distribution was achieved in the case of equality of the mathematical expectations of these flows. Using the passage to the limit, it was established that time interval T between packets of the quasi-deterministic output flow should be equal to the mathematical expectation of the time intervals between packets of the input self-similar flow. To obtain a quasi-deterministic flow, the passage to the limit was performed for the found value of the mathematical expectation at $\sigma \rightarrow 0$.

Discussion and Conclusion. The application of this method will reduce the negative impact of self-similarity of network traffic on the efficiency of the telecommunication network. The use of quasi-deterministic flows makes it possible to predict the load of network resources, which can be the basis for improving the quality of user service. Two difficulties associated with calculations and practical implementation of the solution are eliminated. Firstly, it is difficult to use the delta function as a function of the output flow distribution density. Secondly, there are no ideal deterministic flows in the operation of telecommunication networks. The proposed method has great potential in the design and optimization of communication networks.

Keywords: self-similar packet flow, quasi-deterministic packet flow, packet arrival time intervals, Kullback-Leibler divergence

Acknowledgements. The authors would like to thank the Editorial board and the reviewers for their attentive attitude to the article and for the specified comments that improved the quality of the article.

For Citation. Linets GI, Voronkin RA, Slyusarev GV, Govorova SV. Optimization Problem for Probabilistic Time Intervals of Quasi-Deterministic Output and Self-Similar Input Data Packet Flow in Telecommunication Networks. *Advanced Engineering Research (Rostov-on-Don)*. 2024;24(4):424–432. <https://doi.org/10.23947/2687-1653-2024-24-4-424-432>

Оригинальное теоретическое исследование

Оптимизационная задача для вероятностных временных интервалов квазидетерминированного выходного и самоподобного входного потока пакетов данных в телекоммуникационных сетях

Г.И. Линец , Р.А. Воронкин , Г.В. Слюсарев , С.В. Говорова 

Северо-Кавказский федеральный университет, г. Ставрополь, Российская Федерация

✉ kbytw@mail.ru

Аннотация

Введение. При управлении трафиком на уровне пакетов в современных телекоммуникационных сетях связи предлагается задействовать методы, преобразующие самоподобный стохастический поток пакетов в квазидетерминированный. Для этого нужно применить сложные вероятностные законы распределения самоподобных потоков. Из литературы известны методы балансировки сетевой нагрузки, которые при обозначенной выше проблеме способствуют повышению эффективности телекоммуникационных систем связи. Однако нет строго математического решения, позволяющего узнать оптимальные вероятностные характеристики выходного потока, ориентируясь на входной. Представленная научная работа призвана восполнить этот пробел. Ее цель — создать метод определения оптимальных вероятностных характеристик потока пакетов, используя минимальное значение меры близости самоподобного входного и квазидетерминированного выходного потоков.

Материалы и методы. Для решения задачи исследования параметры распределения выходного потока выбирались так, чтобы функция аппроксимации была близка к δ -функции. В качестве меры близости входных и выходных распределений временных интервалов использовали дивергенцию Кульбака – Лейблера. Задействовали методы теорий множеств, метрических пространств, многомерной оптимизации и телетрафика. В алгоритм решения включили минимизацию дивергенции Кульбака – Лейблера и предельный переход к δ -функции.

Результаты исследования. Показано вероятностное распределение — приближение δ -функции, обеспечивающей равенство временных интервалов квазидетерминированного выходного потока пакетов. Представлен метод преобразования самоподобного входного потока в квазидетерминированный выходной. В качестве меры их близости использовали дивергенцию Кульбака – Лейблера. Минимум дивергенции Кульбака – Лейблера между входным и выходным потоками с нормальным распределением достигается в случае равенства математических ожиданий этих потоков. С помощью предельного перехода установлено, что интервал времени T между пакетами квазидетерминированного выходного потока должен быть равен математическому ожиданию интервалов времени между пакетами входного самоподобного потока. С целью получения квазидетерминированного потока выполняется предельный переход для найденного значения математического ожидания при $\sigma \rightarrow 0$.

Обсуждение и заключение. Применение данного метода уменьшит негативное влияние самоподобия сетевого трафика на эффективность телекоммуникационной сети. Использование квазидетерминированных потоков дает возможность прогнозировать нагрузку сетевых ресурсов, что может быть базой для повышения качества обслуживания пользователей. Устраняются две сложности, связанные с расчетами и практической реализацией решения. Во-первых, затруднительно использовать дельта-функцию в качестве функции плотности распределения выходного потока. Во-вторых, при эксплуатации телекоммуникационных сетей не бывает идеальных детерминированных потоков. Предложенный метод обладает большим потенциалом при проектировании и оптимизации сетей связи.

Ключевые слова: самоподобный поток пакетов, квазидетерминированный поток пакетов, временные интервалы поступления пакетов, дивергенция Кульбака – Лейблера

Благодарности. Авторы выражают благодарность редакции и рецензентам за внимательное отношение к статье и замечания, которые позволили повысить ее качество.

Для цитирования. Линец Г.И., Воронкин Р.А., Слюсарев Г.В., Говорова С.В. Оптимизационная задача для вероятностных временных интервалов квазидетерминированного выходного и самоподобного входного потока пакетов данных в телекоммуникационных сетях. *Advanced Engineering Research (Rostov-on-Don)*. 2024;24(4):424–432. <https://doi.org/10.23947/2687-1653-2024-24-4-424-432>

Introduction. Telecommunication networks operate under conditions of increasing loads and traffic growth, which is subject to complex probabilistic distribution laws and cannot be accurately predicted. Self-similarity of the packet flow creates stable dependences, which limits the volume of information exchange between users [1]. In [2], methods were proposed that met the requirements of quality of service (QoS) of the communication. The authors of the mentioned work believed that it was necessary to focus on the priority traffic of new generation networks. However, their solution did not eliminate the problem of self-similarity of packet flows. Millán G. and Lefranc G. proposed a model for managing network flows taking into account the channel capacity, without considering the fractal characteristics of traffic [3]. In [4], techniques for load balancing taking into account the multifractal properties of traffic were developed. However, they did not solve the problem of self-similarity and structural optimization of output flows. Ushanev K.V. and Makarenko S.I. [5], having analyzed methods for increasing the stability of networks taking into account complex traffic characteristics, proposed models for transforming self-similar input flows [6]. In this case, strict mathematical analysis allowed minimizing the differences between the distributions of input and output flows and, consequently, eliminating self-similarity. However, in [6], this solution is absent.

High-quality regular data transmission involves the use of a constant bitrate (CBR) traffic source model [4]. In this model, a node transmits fixed-size packets at equal time intervals T . If the time between sending packets is significantly greater than the transmission time of one packet, then the packet size may be insignificant. As noted in [4], under conditions of the limited bandwidth, this model can be used to maintain traffic stationarity and minimize delays. Paper [7] shows the advantages of CBR for networks with strict requirements for transmission time characteristics, and [8] emphasizes its effectiveness under conditions of high sensor density. According to [9], the predictability of traffic in this model makes it more effective in terms of energy savings, which is critical for energy-constrained devices.

As shown in [10], the CBR model is traditionally associated with wireless sensor networks, but it can also be useful in general purpose networks [11]. It is useful for solving load balancing problems in telecommunication systems [12].

Thus, to ensure predictability and stability of network operation, it is important to consider quasi-deterministic packet flows. They need to be integrated into applications with high quality of service and performance requirements [13].

Researchers have repeatedly addressed the problem of limiting the impact of fractal characteristics of network load [14]. It is known, for example, that it is possible to control traffic at the packet level. This reduces the number of retransmissions of packets and structural similarities between them [15].

The necessity of determining the optimal time intervals between packet downloads is worth mentioning separately. This is of particular importance for traffic management and involves transforming a self-similar stochastic packet flow into a quasi-deterministic one.

The approach described in [16] provides the transformation of the input packet flow with a gamma distribution into a quasi-deterministic output flow based on the solution to the Lindley equation system. However, [16] does not provide recommendations for reducing the impact of long-term dependences on QoS for other self-similar distributions.

The objective of the presented research is to create a method for obtaining optimal probabilistic characteristics of the output packet flow. The solution is based on the use of the minimum value of the measure of closeness of two flows: self-similar input and quasi-deterministic output.

Materials and Methods. Parameters of the output flow distribution were selected so that the approximation function was close to δ -function (the Dirac delta function, also known as the distribution function of the quasi-deterministic output flow). The measure of closeness of the input and output distributions of the time intervals of packet flows is the Kullback–Leibler divergence. Methods of the set theory, metric spaces, multidimensional optimization and teletraffic were used. The algorithm for solving the problem included a passage to the limit of δ -function, which allows restoring the quasi-deterministic flow, as well as minimization of the Kullback-Leibler divergence. To do this, partial derivatives were found and equated to zero.

We assume that the characteristics of the probability distribution of intervals between input traffic packets $f(\tau; \theta_1, \theta_2, \dots, \theta_n)$ are known. Here, $\theta_1, \theta_2, \dots, \theta_n$ — distribution parameters; τ — time distance between packets. Hurst exponent $0.5 < H < 1$, $\theta_1(H)$ [17]; $g(\tau; \eta_1, \eta_2, \dots, \eta_n)$ — probability distribution of the values of intervals between packets in the output flow without self-similarity with parameters $\eta_1, \eta_2, \dots, \eta_n$.

The conditions for using premetrics are known from [17]:

- 1) $\rho(f, g) \geq 0$;
- 2) $\rho(f, g) \geq 0 \leftrightarrow f \equiv g$.

It is necessary to determine:

1. probability distribution $g(\tau; \eta_1, \eta_2, \dots, \eta_n)$ based on its approximation to δ -function (Dirac function), providing the equality of time intervals of the quasi-deterministic output packet flow;

2. method that provides obtaining optimal probabilistic characteristics of the output packet flow.

The decision is based on the minimum value of the measure of closeness of the self-similar input and quasi-deterministic output flows.

We take into account three restrictions:

1. minimal value of premetrics $\rho(f, g) \rightarrow \min$;
2. functions $f(\tau; \theta_1, \theta_2, \dots, \theta_n)$ and $g(\tau; \eta_1, \eta_2, \dots, \eta_m)$ — piecewise continuous;
3. function $\rho(f, g)$ — differentiable with respect to variables $\eta_1, \eta_2, \dots, \eta_m$ in the entire domain of definition:

$$\forall \eta_j \left| \frac{\partial \rho(f, g)}{\partial \eta_j} \right| < \infty, \text{ where: } j = 1, 2, \dots, m.$$

Research Results. We assume that the probability distribution of the quasi-deterministic output flow is described by the Dirac function [18]:

$$g(\tau; \eta_1, \eta_2, \dots, \eta_m) = \delta(\tau - T).$$

There are two reasons why we use this same function (or δ -function) as the probability distribution function.

1. It takes non-negative values:

$$\delta(\tau - T) \geq 0.$$

2. The integral over the entire number axis is determined by the expression:

$$\int_{-\infty}^{+\infty} \delta(\tau - T) d\tau = 0.$$

Note that when calculating the premetric value $\rho(f, g)$, it is difficult to use the delta function as the output flow distribution density function. In addition, ideal deterministic flows do not exist under the operating conditions of telecommunication networks. Therefore, it makes sense to use a quasi-deterministic flow instead of a deterministic one. In this case, when changing one parameter of the distribution density function, it tends to the Dirac delta function in the limit.

Let us consider a uniform distribution with a mathematical expectation equal to T , and a range of values equal to ΔT . The distribution density function in this case will have the form:

$$\rho(\tau) = \begin{cases} \frac{1}{\Delta T}, & \text{if } T - \frac{\Delta T}{2} \leq \tau \leq T + \frac{\Delta T}{2} \\ 0, & \text{otherwise} \end{cases}.$$

At $\Delta T \rightarrow 0$, the distribution density of this flow $\rho(\tau) \rightarrow \delta(\tau - T)$.

In practice, jitter makes it impossible to maintain uniform intervals between packets. Most often, mathematical models of telecommunication processes are built on the assumption that the jitter value obeys the normal distribution law [19]. For a deterministic packet flow, the time intervals between them are distributed normally with mathematical expectation $\mu = T$ and standard deviation that must satisfy the three-sigma rule [20]: $0 < 3\sigma \leq J_0$, where J_0 — normative value of jitter.

In [18], it is established that a jitter-induced quasi-deterministic flow with a normal distribution converges weakly to $\delta(\tau - T)$ at $\delta \rightarrow 0$.

This means that the best approximation to a deterministic flow is a quasi-deterministic packet flow with a normal distribution. Its mathematical expectation coincides with a constant time interval between packets $\mu = T$ and standard deviation σ , limited by jitter level J_0 :

$$g(\tau; \eta_1, \eta_2, \dots, \eta_m) = g(\tau, \mu, \sigma) = \frac{1}{\sigma\sqrt{2\pi}} e^{-\frac{1}{2}\left(\frac{\tau - \mu}{\sigma}\right)^2}.$$

To achieve the research objective, we use the Kullback-Leibler divergence as premetrics [17] $D_{KL}(f||g)$. Taking into account its properties and the adopted assumptions, we formulate the lemma.

Lemma. Let $f(\tau; \theta_1, \theta_2, \dots, \theta_n)$ be piecewise continuous function:

$$f(\tau; \theta_1, \theta_2, \dots, \theta_n) = \begin{cases} \varphi(\tau; \theta_1, \theta_2, \dots, \theta_n), & \tau \geq t, \\ 0, & \tau < t. \end{cases} \quad (1)$$

Here, $t \geq 0$ — some threshold value, and $\varphi(\tau; \theta_1, \theta_2, \dots, \theta_n) > 0$ — continuous function on interval $(t, +\infty)$.

Output flow $g(\tau; \mu, \sigma)$ obeys the normal distribution of time intervals between packets without self-similarity with parameters μ and $\sigma > 0$.

It is required to prove that $D_{KL}(f||g)$ reaches a minimum when the mathematical expectations f and g are equal.

Proof. We use the approach described in [17].

Cross entropy $H(f, g)$ can be defined in two ways.

The first:

$$\begin{aligned} H(f) &= - \int_{-\infty}^{+\infty} f(\tau; \theta_1, \theta_2, \dots, \theta_n) \ln[f(\tau; \theta_1, \theta_2, \dots, \theta_n)] d\tau = \\ &= - \int_{\max\{t, 0\}}^{+\infty} f(\tau; \theta_1, \theta_2, \dots, \theta_n) \ln \left[\frac{1}{\sigma\sqrt{2\pi}} e^{-\frac{1}{2} \left(\frac{\tau - \mu}{\sigma} \right)^2} \right] d\tau. \end{aligned} \quad (2)$$

The second:

$$\begin{aligned} H(f, g) &= - \int_t^{+\infty} \varphi(\tau; \theta_1, \theta_2, \dots, \theta_n) \left[\ln(\sigma\sqrt{2\pi}) - \frac{1}{2} \left(\frac{\tau - \mu}{\sigma} \right)^2 \right] d\tau = \\ &= \ln(\sigma\sqrt{2\pi}) \int_t^{+\infty} \varphi(\tau; \theta_1, \theta_2, \dots, \theta_n) d\tau + \frac{1}{2\sigma^2} \int_t^{+\infty} (\tau - \mu)^2 \varphi(\tau; \theta_1, \theta_2, \dots, \theta_n) d\tau. \end{aligned} \quad (3)$$

For the density function of the input packet flow:

$$\int_t^{+\infty} \phi\varphi(\tau; \theta_1, \theta_2, \dots, \theta_n) d\tau = 1.$$

Hence:

$$\begin{aligned} H(f, g) &= \ln(\sigma\sqrt{2\pi}) + \frac{1}{2\sigma^2} \int_t^{+\infty} (\tau - \mu)^2 \phi(\tau; \theta_1, \theta_2, \dots, \theta_n) d\tau = \\ &= \ln(\sigma\sqrt{2\pi}) + \frac{1}{2\sigma^2} \int_t^{+\infty} (\tau^2 - 2\tau\mu + \mu^2) \phi(\tau; \theta_1, \theta_2, \dots, \theta_n) d\tau = \\ &= \ln(\sigma\sqrt{2\pi}) + \frac{1}{2\sigma^2} \int_t^{+\infty} (\tau^2 - 2\tau\mu) \phi(\tau; \theta_1, \theta_2, \dots, \theta_n) d\tau + \frac{\mu^2}{2\sigma^2} \int_t^{+\infty} \phi(\tau; \theta_1, \theta_2, \dots, \theta_n) d\tau = \\ &= \ln(\sigma\sqrt{2\pi}) + \frac{\mu^2}{2\sigma^2} + \frac{1}{2\sigma^2} \int_t^{+\infty} \tau^2 \phi(\tau; \theta_1, \theta_2, \dots, \theta_n) d\tau - \frac{\mu}{\sigma^2} \int_t^{+\infty} \tau \phi(\tau; \theta_1, \theta_2, \dots, \theta_n) d\tau. \end{aligned} \quad (4)$$

It is also known:

$$\begin{aligned} \int_t^{+\infty} \tau \phi(\tau; \theta_1, \theta_2, \dots, \theta_n) d\tau &= E(\theta_1, \theta_2, \dots, \theta_n), \\ \int_t^{+\infty} \tau^2 \phi(\tau; \theta_1, \theta_2, \dots, \theta_n) d\tau &= v_2(\theta_1, \theta_2, \dots, \theta_n), \end{aligned}$$

where E — function that provides determining the mathematical expectation of an input self-similar packet stream.

Thus,

$$H(f, g) = \ln(\sigma\sqrt{2\pi}) + \frac{\mu^2}{2\sigma^2} + \frac{1}{2\sigma^2} v_2(\theta_1, \theta_2, \dots, \theta_n) - \frac{\mu}{\sigma^2} E(\theta_1, \theta_2, \dots, \theta_n). \quad (5)$$

Then:

$$\begin{aligned} D_{KL}(f \parallel g) &= H(f, g) - H(f) = \\ &= \ln(\sigma\sqrt{2\pi}) + \frac{\mu^2}{2\sigma^2} + \frac{1}{2\sigma^2} v_2(\theta_1, \theta_2, \dots, \theta_n) - \frac{\mu}{\sigma^2} E(\theta_1, \theta_2, \dots, \theta_n) - H(\theta_1, \theta_2, \dots, \theta_n). \end{aligned} \quad (6)$$

Let us solve the problem of multidimensional optimization:

$$\frac{\partial D_{KL}(f \parallel g)}{\partial \mu} = \frac{\mu}{\sigma^2} - \frac{1}{\sigma^2} E(\theta_1, \theta_2, \dots, \theta_n). \quad (7)$$

It means:

$$\mu = E(\theta_1, \theta_2, \dots, \theta_n).$$

For normal distribution:

$$E(g) = \mu,$$

consequently,

$$E(g) = E(\theta_1, \theta_2, \dots, \theta_n),$$

$$E(f) = E(g).$$

Let us use Sylvester's criterion:

$$\frac{\partial^2 D_{KL}(f \| g)}{\partial \mu^2} = \frac{1}{\sigma^2}. \quad (8)$$

A necessary and sufficient condition for the minimum $D_{KL}(f \| g)$ is the equality of the mathematical expectations of the input and output packet flows.

For a deterministic flow, time interval T between packets can be determined by the limit transition as $\sigma \rightarrow 0$, that is:

$$T = \lim_{\sigma \rightarrow 0} E(\theta_1, \theta_2, \dots, \theta_n) = E(\theta_1, \theta_2, \dots, \theta_n). \quad (9)$$

The last equality is possible because expression $E(\theta_1, \theta_2, \dots, \theta_n)$ does not explicitly contain σ . Therefore, within the framework of this method, for a quasi-deterministic output flow, the time interval between packets is equal to the mathematical expectation of the time intervals of a self-similar stochastic flow.

The sequence of implementation of the developed method is given below.

1. The normal law with the standard deviation limited by jitter value J_0 should be used as the law of distribution of time intervals between packets of the output flow.

2. It is necessary to find the mathematical expectation of the input self-similar packet flow $E(\theta_1, \theta_2, \dots, \theta_n)$ and determine the value of mathematical expectation μ of the output flow, which has a normal distribution. For this, the statement of the previously proven lemma is used.

3. For the found value μ , time interval $\mu = T$ of the quasi-deterministic output packet flow is determined.

As an example, consider a self-similar flow with the Pareto distribution:

$$f(\tau; \alpha; \tau_m) = \begin{cases} \frac{\alpha \tau_m^\alpha}{\tau^{\alpha+1}}, & \tau \geq \tau_m \\ 0, & \tau < \tau_m. \end{cases} \quad (10)$$

It is required to determine value $\mu = \psi(\alpha, \tau_m)$ that minimizes $D_{KL}(f \| g)$.

For the Pareto distribution:

$$H(f(\tau)) = - \int_{\tau_m}^{\infty} \tau^{-b-2} \tau_m^{b+1} (b+1) \log(\tau^{-b-2} \tau_m^{b+1} (b+1)) d\tau. \quad (11)$$

The cross entropy of the laws under study is equal to:

$$M(f(\tau), g(\tau)) = - \int_{\tau_m}^{\infty} \alpha \tau^{-\alpha-1} \tau_m^\alpha \ln \left(\frac{e^{\frac{(\mu-\tau)^2}{2\sigma^2}}}{\sqrt{2\pi\sigma}} \right) d\tau. \quad (12)$$

We reason in the same way as when proving the lemma. We obtain:

$$\mu = \frac{\alpha \tau_m}{\alpha - 1}. \quad (13)$$

This expression corresponds to the mathematical expectation of the Pareto distribution.

Let us find the second derivative, and then value μ minimizes value $D_{KL}(f \| g)$.

To obtain a quasi-deterministic flow, we perform the limit transition for the found value of the mathematical expectation at $\sigma \rightarrow 0$:

$$T = \lim_{\sigma \rightarrow 0} \mu = \lim_{\sigma \rightarrow 0} \frac{\alpha \tau_m}{\alpha - 1} = \frac{\alpha \tau_m}{\alpha - 1}. \quad (14)$$

Thus, when transforming a self-similar input packet stream into a quasi-deterministic output stream, the value of the time intervals of the quasi-deterministic flow T coincides with the mathematical expectation of the input flow [21].

Discussion and Conclusion. The conducted research opens up new possibilities for providing telecommunications under conditions of limited network resources. The authors used mathematical methods and obtained optimal probabilistic characteristics of the output packet flow using the minimum value of the measure of closeness of the self-similar input and quasi-deterministic output flows. According to the lemma proved in this paper, for a normal distribution for the output flow, the minimum value of the Kullback-Leibler divergence is achieved if the mathematical expectations of the input and output flows are equal. The solution to the multidimensional optimization problem verified the adequacy of the proposed method. Its capabilities should be taken into account when working with telecommunication networks. The use of this approach can limit the negative impact of flow self-similarity and thus improve the quality of user service while maintaining the volume of information exchange.

In the future, the authors plan to develop methods for reducing the self-similarity of network traffic. Such an approach will presumably be based on the Jensen-Shannon divergence. This measure of closeness differs from the Kullback-Leibler distribution in that it is a complete metric and is bounded from above [22].

References

1. Hausdorff F. *Set Theory*. Moscow: Lenand; 2023. 304 p. (In Russ.)
2. Karmeshu Shachi Sharma. *Long Tail Behavior of Queue Lengths in Broadband Networks: Tsallis Entropy Framework*. URL: <https://arxiv.org/abs/1012.2464> (accessed: 16.09.2024).
3. Millán G, Lefranc G. *A Simplified Multifractal Model for Self-Similar Traffic Flows in High-Speed Computer Networks Revisited*. URL: <https://arxiv.org/abs/2103.05183> (accessed: 16.09.2024).
4. Astakhova T, Verzun N, Kasatkin V, Kolbanev M, Shamin AA. Sensor Network Connectivity Models. *Information and Control Systems*. 2019;(5):38–50. <https://doi.org/10.31799/1684-8853-2019-5-38-50>
5. Ushanev KV, Makarenko SI. Analytical-Simulation Model of Functional Conversion of Complex Traffic. *Systems of Control, Communication and Security*. 2015;(2):26–44.
6. Ushanev KV, Makarenko SI. Traffic Structure Conversion with Requirements for the Traffic Service Quality. *Radio Engineering and Telecommunications Systems*. 2015;(2):74–84.
7. Tchuitcheu WC, Bobda C, Pantho MJ. H. Internet of Smart-Cameras for Traffic Lights Optimization in Smart Cities. *Internet of Things*. 2020;11:100207. <https://doi.org/10.1016/j.iot.2020.100207>
8. Dutta H, Bhuyan AK, Biswas S. *Reinforcement Learning for Protocol Synthesis in Resource-Constrained Wireless Sensor and IoT Networks*. URL: <https://arxiv.org/abs/2302.05300> (accessed: 16.09.2024).
9. Pasandi HB, Haqiqat A, Moradbeikie A, Keshavarz A, Rostami H, Paiva S, et al. Low-Cost Traffic Sensing System Based on LoRaWAN for Urban Areas. In: *Proc. 1st International Workshop on Emerging Topics in Wireless*. New York, NY: Association for Computing Machinery; 2022. P. 6–11. URL: <https://dl.acm.org/doi/10.1145/3565474.3569069> (accessed: 16.09.2024).
10. Qiong Liu, Chehao Wang, Ce Zheng. *Distributed Decisions on Optimal Load Balancing in Loss Networks*. URL: <https://arxiv.org/abs/2307.04506> (accessed: 16.09.2024).
11. Shenoy N. A Deterministic Quantised Rate Based Flow Control Scheme for ABR Type Traffic in ATM Networks. In: *Proc. Second IEEE Symposium on Computer and Communications*. New York City: IEEE; 1997. P. 73–79. URL: <https://ieeexplore.ieee.org/document/615974> (accessed: 16.09.2024).
12. Müller-Clostermann B. Employing Deterministic and Stochastic Petri Nets for the Analysis of Usage Parameter Control in ATM-Networks. In: *Workshop on High Performance Computing and Gigabit Local Area Networks*. Springer: Berlin, Heidelberg; 2006. P. 101–121. URL: https://link.springer.com/chapter/10.1007/3540761691_8 (accessed: 16.09.2024).
13. Daryalal M, Bodur M. Stochastic RWA and Lightpath Rerouting in WDM Networks. *Inform Journal on Computing*. 2022;34(5):2383–2865. <https://doi.org/10.1287/ijoc.2022.1179>
14. Shelukhin OI, Tenyakshev AM, Osin AV. *Fractal Processes in Telecommunications*. Moscow: Radiotekhnika; 2003. 479 p. (In Russ.)
15. Millán G, Lefranc G, Osorio-Comparán R. *The Associative Multifractal Process: A Novel Model for Computer Network Traffic Flows*. URL: <https://arxiv.org/abs/2106.14666> (accessed: 16.09.2024).
16. Kartashevsky IV. *Processing of Correlated Traffic in Infocommunication Networks*. Moscow: Goryachaya liniya — Telekom; 2023. 200 p. (In Russ.)

17. Linets GI, Voronkin RA, Govorova SV. Functional Transformation of the Self-Similar Network Teletraffic Based on the Multidimensional Measure of Similarity between Probability Parameters of Input and Output Packet Flows. *Systems of Control, Communication and Security*. 2022;(4):38–63.
18. Chakraborty S. Some Applications of Dirac's Delta Function in Statistics for More Than One Random Variable. *Applications and Applied Mathematics*. 2008;3(1):42–54.
19. Blagov A. Modeling a Jitter in Telecommunication Data Networks for Studying Adequacy of Traffic Patterns. *Modern Applied Science*. 2015;9(4):254–263. <https://pdfs.semanticscholar.org/7ef0/611d69fb4fcfd467b7d909b74de8eab47f55.pdf>
20. Slyusar VI, Bondarenko M. Methods for Estimating the ADC Jitter in Noncoherent Systems. *Journal of the Russian Universities. Radioelectronics*. 2011;54(10):19–28.
21. Linets GI. *Methods of Structural-Parametric Synthesis, Identification and Management of Transport Telecommunication Networks to Achieve Maximum Performance*. Stavropol: Fabula; 2014. 384 p. (In Russ.)
22. Nielsen F. On the Jensen–Shannon Symmetrization of Distances Relying on Abstract Means. *Entropy*. 2019;21(5):485.

About the Authors:

Gennady I. Linets, Dr.Sci. (Eng.), Professor of the Digital, Robotic Systems and Electronics Department, Institute of Engineering, North-Caucasus Federal University (2, Kulakova Ave., Stavropol, 355000, Russian Federation), [SPIN-code](#), [ORCID](#), [ScopusID](#), kbytw@mail.ru

Roman A. Voronkin, Cand.Sci. (Eng.), Associate Professor of the Department of Digital, Robotic Systems and Electronics, Institute of Engineering, North-Caucasus Federal University (2, Kulakova Ave., Stavropol, 355000, Russian Federation), [SPIN-code](#), [ORCID](#), [ScopusID](#), roman.voronkin@gmail.com

Gennadii V. Slyusarev, Dr.Sci. (Eng.), Professor of the Civil Engineering and Prototyping Department, Institute of Engineering, North-Caucasus Federal University (2, Kulakova Ave., Stavropol, 355000, Russian Federation), [SPIN-code](#), [ORCID](#), gslyusarev@ncfu.ru

Svetlana V. Govorova, Senior Lecturer of the Department of Digital, Robotic Systems and Electronics, Institute of Engineering, North-Caucasus Federal University (2, Kulakova Ave., Stavropol, 355000, Russian Federation), [SPIN-code](#), [ORCID](#), [ScopusID](#), mitnik2@yandex.ru

Claimed Contributorship:

GI Linets: conceptualization, supervision.

RA Voronkin: formal analysis, investigation, writing – review and editing.

GV Slyusarev: validation.

SV Govorova: writing – original draft preparation.

Conflict of Interest Statement: the authors declare no conflict of interest.

All the authors have read and approved the final version of the manuscript.

Об авторах:

Геннадий Иванович Линец, доктор технических наук, профессор, профессор департамента цифровых, робототехнических систем и электроники, Институт перспективной инженерии, СКФУ (355000, Российская Федерация, г. Ставрополь, пр. Кулакова, 2, корп. 9), [SPIN-код](#), [ORCID](#), [ScopusID](#), kbytw@mail.ru

Роман Александрович Воронкин, кандидат технических наук, доцент, доцент департамента цифровых, робототехнических систем и электроники, института перспективной инженерии, СКФУ (355000, Российская Федерация, г. Ставрополь, пр. Кулакова, 2, корп. 9), [SPIN-код](#), [ORCID](#), [ScopusID](#), roman.voronkin@gmail.com

Геннадий Васильевич Слюсарев, доктор технических наук, профессор, профессор департамента строительной инженерии и прототипирования института перспективной инженерии, СКФУ (355000, Российская Федерация, г. Ставрополь, пр. Кулакова, 2, корп. 9), [SPIN-код](#), [ORCID](#), gslyusarev@ncfu.ru

Светлана Владимировна Говорова, старший преподаватель департамента цифровых, робототехнических систем и электроники института перспективной инженерии, СКФУ (355000, Российская Федерация, г. Ставрополь, пр. Кулакова, 2, корп. 9), [SPIN-код](#), [ORCID](#), [ScopusID](#), mitnik2@yandex.ru

Заявленный вклад авторов:

Г.И. Линец: разработка концепции, научное руководство.

Р.А. Воронкин: формальный анализ, проведение исследования, написание, рецензирование и редактирование текста.

Г.В. Слюсарев: валидация результатов.

С.В. Говорова: написание черновика рукописи.

Конфликт интересов. Авторы заявляют об отсутствии конфликта интересов.

Все авторы прочитали и одобрили окончательный вариант рукописи.

Received / Поступила в редакцию 20.09.2024

Reviewed / Поступила после рецензирования 16.10.2024

Accepted / Принята к публикации 24.10.2024